

Climate Trends and Projections for the Pacific Large Aquatic Basin

Editors

J.R. Christian and M.G.G. Foreman

Fisheries and Oceans Canada
Science Branch
Pacific Region
Institute of Ocean Sciences
P.O. Box 6000
Sidney, B.C. V8L 4B2

2013

Canadian Technical Report of
Fisheries and Aquatic Sciences 3032



Fisheries
and Oceans

Pêches
et Océans

Canada 

Canadian Technical Report of Fisheries and Aquatic Sciences

Technical reports contain scientific and technical information that contributes to existing knowledge but which is not normally appropriate for primary literature. Technical reports are directed primarily toward a worldwide audience and have an international distribution. No restriction is placed on subject matter and the series reflects the broad interests and policies of Fisheries and Oceans Canada, namely, fisheries and aquatic sciences.

Technical reports may be cited as full publications. The correct citation appears above the abstract of each report. Each report is abstracted in the data base *Aquatic Sciences and Fisheries Abstracts*.

Technical reports are produced regionally but are numbered nationally. Requests for individual reports will be filled by the issuing establishment listed on the front cover and title page.

Numbers 1-456 in this series were issued as Technical Reports of the Fisheries Research Board of Canada. Numbers 457-714 were issued as Department of the Environment, Fisheries and Marine Service, Research and Development Directorate Technical Reports. Numbers 715-924 were issued as Department of Fisheries and Environment, Fisheries and Marine Service Technical Reports. The current series name was changed with report number 925.

Rapport technique canadien des sciences halieutiques et aquatiques

Les rapports techniques contiennent des renseignements scientifiques et techniques qui constituent une contribution aux connaissances actuelles, mais qui ne sont pas normalement appropriés pour la publication dans un journal scientifique. Les rapports techniques sont destinés essentiellement à un public international et ils sont distribués à cet échelon. Il n'y a aucune restriction quant au sujet; de fait, la série reflète la vaste gamme des intérêts et des politiques de Pêches et Océans Canada, c'est-à-dire les sciences halieutiques et aquatiques.

Les rapports techniques peuvent être cités comme des publications à part entière. Le titre exact figure au-dessus du résumé de chaque rapport. Les rapports techniques sont résumés dans la base de données *Résumés des sciences aquatiques et halieutiques*.

Les rapports techniques sont produits à l'échelon régional, mais numérotés à l'échelon national. Les demandes de rapports seront satisfaites par l'établissement auteur dont le nom figure sur la couverture et la page du titre.

Les numéros 1 à 456 de cette série ont été publiés à titre de Rapports techniques de l'Office des recherches sur les pêcheries du Canada. Les numéros 457 à 714 sont parus à titre de Rapports techniques de la Direction générale de la recherche et du développement, Service des pêches et de la mer, ministère de l'Environnement. Les numéros 715 à 924 ont été publiés à titre de Rapports techniques du Service des pêches et de la mer, ministère des Pêches et de l'Environnement. Le nom actuel de la série a été établi lors de la parution du numéro 925.

Canadian Technical Report of
Fisheries and Aquatic Sciences 3032

2013

CLIMATE TRENDS AND PROJECTIONS FOR THE PACIFIC LARGE AQUATIC BASIN

Editors

J. R. Christian and M.G.G. Foreman

Institute of Ocean Sciences
Fisheries and Oceans Canada
P.O. Box 6000
Sidney, B.C. V8L 4B2

© Her Majesty the Queen in Right of Canada, 2013
Cat. No. Fs 97-6/3032 E ISSN 0706-6457 (print version)
Cat. No. Fs 97-6/2873E-PDF ISSN 1488-5379 (online version)

Correct citation for this publication:

Christian, J. R. and Foreman, M.G.G. 2013. Climate trends and projections for the Pacific Large Aquatic Basin. Can. Tech. Rep. Fish. Aquat. Sci. 3032: xi + 113 p.

TABLE OF CONTENTS

TABLE OF CONTENTS.....	iii
LIST OF TABLES.....	v
LIST OF FIGURES	vi
ABSTRACT.....	x
INTRODUCTION	1
GEOGRAPHICAL SCOPE OF THE PACIFIC LARGE AQUATIC BASIN	1
OCEANOGRAPHIC CONDITIONS.....	2
CLIMATE VARIABILITY	2
TRENDS AND PROJECTIONS	3
TRENDS	4
TRENDS IN SEA SURFACE TEMPERATURE AND SALINITY	4
Analysis of lighthouse data.....	5
Variability	5
TRENDS IN SALINITY AND TEMPERATURE OFF THE WEST COAST OF VANCOUVER ISLAND.....	10
Introduction.....	10
The analysis approach.....	12
Results.....	12
Discussion and Summary.....	17
TRENDS IN TEMPERATURE, SALINITY, WATER COLUMN STABILITY AND MIXING DEPTH IN THE OPEN GULF OF ALASKA	18
Introduction.....	18
British Columbia Shorestations	19
Line-P Trends in Temperature, Salinity and Density	20
Line P trends in mid-winter mixed layer depth	24
Discussion and Summary.....	25
TRENDS IN SEA LEVEL.....	26
Pacific Sea Level Trends	26
Northeast Pacific Projections.....	33
Information Gaps and Future Work.....	38
TRENDS IN UPWELLING AND DOWNWELLING WINDS ALONG THE BRITISH COLUMBIA CONTINENTAL SHELF.....	40
Summary	40
TRENDS IN OXYGEN CONCENTRATION ON THE CONTINENTAL SHELF OF BRITISH COLUMBIA.....	46
Introduction.....	46
Spatial Distribution	47
Temporal changes	49
Summary	52

TRENDS IN NUTRIENT CONCENTRATION IN THE NORTHEAST SUBARCTIC PACIFIC	53
Introduction.....	53
Open Ocean.....	54
British Columbia continental Shelf.....	56
THE INCREASE IN CARBON ALONG THE CANADIAN PACIFIC COAST	57
Introduction.....	57
Physical circulation and its impact on carbon states.....	59
Annual carbon cycles.....	60
Anticipated trends.....	65
Conclusions.....	65
PROJECTIONS	67
PROJECTIONS FOR THE OPEN GULF OF ALASKA.....	67
Introduction.....	67
Projections of ocean surface temperature, salinity, and stratification	68
Changes in ocean carbon chemistry.....	71
Changes in ocean oxygen content.....	73
Changes in ocean productivity.....	75
Summary and Conclusion.....	77
GLOBAL CLIMATE MODEL WIND PROJECTIONS ALONG THE BRITISH COLUMBIA CONTINENTAL SHELF	77
Summary	77
CANADIAN REGIONAL CLIMATE MODEL PROJECTIONS AFFECTING BRITISH COLUMBIA COASTAL WATERS	81
Introduction.....	81
Strategy and Wind Stress Anomalies.....	83
Precipitation, Air Temperature, Short Wave Radiation and Cloud Cover Anomalies	85
Freshwater Discharge.....	87
Ocean Conditions.....	90
Summary and Future Work.....	91
RESULTS FROM REGIONAL OCEAN MODEL SIMULATION FOR THE BRITISH COLUMBIA CONTINENTAL SHELF	92
Introduction.....	92
Changes in Water Properties.....	94
Changes in Sea Surface Elevation	95
Changes in the Flow Fields.....	97
Summary and Future Work.....	101
ACKNOWLEDGEMENTS.....	102
REFERENCES	103

LIST OF TABLES

Table 1: Leading mode EOF amplitudes (loadings)	7
Table 2: Long term secular trends at different lighthouse stations	9
Table 3: Temperature (top panel) salinity (middle panel) and density (bottom panel) trends at three lighthouse stations well exposed to the open ocean. F90 and F97 are the trends reported in the previously cited studies.....	19
Table 4: Estimates of thermosteric sea level rise from various sources (U.S. National Research Council 2012).	34
Table 5: Projected relative sea levels for year 2100 compared to 2000, for the Strait of Georgia, the Fraser Delta and the west coast of Vancouver Island (modified after Thomson et al. 2008).....	36
Table 6: Sea level rise at the end of the 21 st Century relative to 2000 for various British Columbia communities based on mean, low and high projected eustatic changes of 1.1, 0.7 and 1.4 m by 2100. Regional changes are derived using observed trends in both tide gauge and GPS data series.....	37
Table 7: Decadal average start (1 st number, Julian day number) and end dates (2 nd number) of the upwelling season at the six weather buoys..	42
Table 8: TUMI and TDMI decadal averages (m^3s^{-1} per 100m of coastline), linear trends (m^3s^{-1} per 100m per year), and associated percentage wind increase over forty years at the six weather buoys. * and # denote trends that are significantly different from zero at the 90% and 95% levels.	44
Table 9. List of global Earth System models used and their horizontal and vertical resolution (number of grid points in x/y/z directions).....	67
Table 10: Climate Models Used in This Study and Their Atmospheric Resolutions.....	78
Table 11: List of Buoys and Their Positions	79

LIST OF FIGURES

Figure 1: The four spatial sub-divisions of the Pacific LAB: Strait of Georgia (SOG), West Coast of Vancouver Island (WVCI), North Coast (NC), and Gulf of Alaska (GOA).	1
Figure 2: Lighthouse stations are indicated by red dots. This represents a subset of the stations with the longest records.	4
Figure 3: PC1 for lighthouse SST provides an index of SST variability for coastal BC waters. Note the variability occurring on decadal time scales.	5
Figure 4: PC1 for lighthouse SSS. This also shows variability over a wide range of time scales. PC1 for salinity is not correlated ($r = -0.1$) with PC1 for SST.	6
Figure 5: Autocorrelation for PC1 of lighthouse SST (top panel) and SSS (lower panel).	6
Figure 6: PC1 of lighthouse SST vs. the PDO. A 9-month triangular filter has been applied to both records.	7
Figure 7: Cross-correlation of PC1 and PDO time series in Figure 6. Red line indicates no smoothing. .	7
Figure 8: Depth-averaged temperature anomalies in the Strait of Georgia (blue curve) and for 10-50 m along Line P (red curve), normalized by the standard deviation for each region.	8
Figure 9: Running 20-year SST trends for four lighthouse stations. Note that the long term trend has not been removed from the SST anomalies for this calculation.	9
Figure 10: Average histograms for running SST trends of different lengths	10
Figure 11: West coast Vancouver Island water property stations used in this analysis.	11
Figure 12: a) Observed summer temperatures and fitted linear trend at 10 m depth at station 11 in Line-B, b) monthly PDO values, and linear trend, for 1979-2011.	12
Figure 13: Trends in a) temperature ($^{\circ}\text{C}/365$ days) and b) salinity (PSU/365 days) along Line-B. Station numbers are given along the x-axis, depths are along the y-axis, and land below the shelf bathymetry is shaded.	13
Figure 14: As in Figure 13 but for Line-C.	14
Figure 15: As in Figure 13 but for Line-D.	15
Figure 16: As in Figure 13 but for Line-G.	16
Figure 17: As in Figure 13 but for Line-BP.	17
Figure 18: This map shows the principal locations used in the report. Amphitrite Point, Kains Island and Langara Island are lighthouses where sea-surface temperature and salinity have been observed daily since the mid 1930s.	20
Figure 19: Sampling at Ocean Station Papa (P26).	21
Figure 20: Trends in scalar properties computed at station P26 versus depth.	22
Figure 21: Monthly density trends (averaged over the interval 0-80 dbar) at station P26.	23
Figure 22: Density anomaly trends ($\text{kg m}^{-3} \text{ century}^{-1}$) along Line-P averaged over all months of the year, the symbols above the top axis indicate the location of the stations used.	23
Figure 23: The mid-winter mixed-layer depths at station P26 (Ocean Station Papa) in the upper panel and a parameter proportional to the potential energy of the water column.	25
Figure 24: Post-glacial eustatic sea level rise.	27
Figure 25: Global mean sea level change since the end of the 19 th Century based on tide gauge records. Superimposed on the tide gauge curve is a shorter sea level curve (red line) beginning in 1993	28
Figure 26: Global mean sea level change between 1993 and 2006 based on satellite altimetry.	28

Figure 27: Continuing uplift (mm per year) of Vancouver Island and the adjacent British Columbia mainland resulting from the melting of glaciers during the last Ice Age.....	29
Figure 28: Annual rates of uplift (mm per year) of the land along coastal British Columbia.	30
Figure 29: Map of Vancouver and the Fraser Delta showing areas of documented subsidence (sinking) (blue areas) on the Fraser Delta and more stable surrounding areas (yellow areas).....	31
Figure 30: Changes in relative sea level along the British Columbia coast as measured by tide gauges between 1910 and 2004.	31
Figure 31: Comparison of global mean sea level rise estimates from various sources based on data from Rahmstorf (2010) and U.S. Army Corps of Engineers (2011).	35
Figure 32: Projected mean global sea level change during the 21 st Century presented as low, medium and high scenarios relative to 1992.....	36
Figure 33: Frequency of 100-year extreme sea level (storm surge) events in 2050. Note that in Juan de Fuca Strait today's 100-year storm surge will occur every 20 years in 2050. (Tebaldi et al. 2012).	38
Figure 34: Storm surge amplitudes and frequencies for today (green), 2030 (blue) and 2050 (red) in Juan de Fuca Strait (Tebaldi et al. 2012). Amplitudes are metres above Mean High Water at the time, taking into account regional relative sea level rise.	38
Figure 35: Locations of 13 weather buoys off the Canadian west coast. Only observations from those shown in blue are discussed in this analysis.	41
Figure 36: Decadal-average CUIs for 1959-2008 at weather buoys a) 205, b) 208, c) 147, d) 207, e) 132, f) 206.....	43
Figure 37: a) TUMI and b) TDMI values (dots) and linear trends over the past five decades at the six weather buoys..	45
Figure 38: Historical observations of oxygen concentration (ml/l^{-1}) within 20 m of the ocean bottom plotted on maps of the BC shelf and inlets, for the months of June to September. (a) northern BC; (b) southern BC.	48
Figure 39: Oxygen and σ_t at stations LB08 (left) and P4 (right) observed in late summer and early autumn. (a, d) Oxygen versus year of observation. (b, e) σ_t versus year of observation. (c, e) Oxygen versus σ_t	49
Figure 40: Oxygen concentration interpolated onto the 26.7 σ_θ surface for observations over the continental slope of the south coast of Vancouver Island.	
Figure 41: Oxygen concentration interpolated onto the 26.7 σ_θ surface for observations over Dixon Entrance and west of Haida Gwaii.....	51
Figure 42: (a) Hovmöller plot of upper mixed-layer nitrate concentration anomalies ($\mu\text{mol/L}$) along Line P from 1969 to 1981 and from 1988 to 2012. (b) Comparison of upper mixed-layer nitrate concentration anomalies averaged along Line P (west of 128°W) with the NPGO climate index.	54
Figure 43: (a) Map of the NE subarctic Pacific showing the Line P transect and the location of the five main stations, (b) surface nitrate concentration along Line P during the summer in selected years, and (c) time-series of nitrate depletion and two climate indices (ONI and NPGO).	55
Figure 44: Time-series of nitrate concentration in the surface layer in winter (magenta triangles) and at 150 m (blue diamond) at (a) stations P4 and (b) OSP. (c) Comparison of nitrate and oxygen concentration at OSP.....	55
Figure 45: Composite contours of nitrate concentration at the surface and at 100m in the British Columbia shelf from historical observations at IOS and WOD05 data for the years 1960-2006.	56
Figure 46: Near bottom nitrate (a) and oxygen (b) concentrations versus day of year at LB08 during 1979 to 2011. Comparison of nitrate and oxygen concentrations (c). The black line has a slope of 9. ...	57

Figure 47: Modelled annual (bottom axis - Julian Day, top axis - months of the year) cycles of surface pCO ₂ (thin solid line), surface average total inorganic carbon (DIC) concentrations (bold line) and lower layer average DIC (bold dashed line) over the outer shelf (bottom panel) and slope (top panel) of the WCVI for a typical year in upwelling and downwelling forcing.	61
Figure 48: Modelled annual (bottom axis - Julian Day, top axis - months of the year) cycles of pH in the surface layer (bold green curve) and lower layer (black dashed curve) over the shelf (bottom panel) and slope (top panel) of the WCVI for a typical year in upwelling and downwelling forcing.	61
Figure 49: The probability of undersaturation with respect to aragonite along the BC coast as determined by an empirical model (A) over the shelf (inshore of the 200 m isobath) and (B) immediately adjacent to the shelf over the slope and offshore waters during the four oceanographic seasons	63
Figure 50: Modelled annual pH cycles in the Southern Strait of Georgia for 2010, which is a typical year, in the top 40 m of the water column.	64
Figure 51: Maps of Gulf of Alaska sea surface temperature for 1966-1985, 2006-2025 (RCP 4.5) and 2046-2065 (RCPs 4.5 and 8.5). Ensemble mean of six models.....	68
Figure 52: Maps of Gulf of Alaska sea surface salinity for 1966-1985, 2006-2025 (RCP 4.5) and 2046-2065 (RCPs 4.5 and 8.5). Ensemble mean of six models.....	69
Figure 53: Time series of sea surface temperature in the vicinity of Ocean Station Papa (50°N, 145°W) from historical plus RCP 4.5 or 8.5 simulations. Ensemble mean ± one standard deviation (dashed lines) of six models.....	69
Figure 54: Maps of Gulf of Alaska mixed layer depth for 1966-1985, 2006-2025 (RCP 4.5) and 2046-2065 (RCPs 4.5 and 8.5). Ensemble mean of five models.	70
Figure 55: Time series of mixed layer depth in the vicinity of Ocean Station Papa (50°N, 145°W) from historical plus RCP 4.5 or 8.5 simulations.	70
Figure 56: Maps of Gulf of Alaska surface pH for 1966-1985, 2006-2025 (RCP 4.5) and 2046-2065 (RCPs 4.5 and 8.5). Ensemble mean of six models.....	71
Figure 57: Depth-time plots of seawater saturation state with respect to aragonite (Ω_A) and calcite (Ω_C) in the vicinity of Ocean Station Papa (50°N, 145°W) using RCP 4.5.....	72
Figure 58: Maps of seawater saturation state with respect to aragonite (Ω_A) on the 1026.6 kg m ⁻³ density surface for 1966-1985, 2006-2025 (RCP 4.5) and 2046-2065 (RCPs 4.5 and 8.5). Ensemble mean of six models.....	73
Figure 59: Depth-time plot of oxygen concentration in the vicinity of Ocean Station Papa (50°N, 145°W), for historical and RCP 4.5 simulations.....	74
Figure 60: Maps of oxygen concentration on the 1026.6 kg m ⁻³ density surface for 1966-1985, 2006-2025 (RCP 4.5) and 2046-2065 (RCPs 4.5 and 8.5). Ensemble mean of four models.....	74
Figure 61: Time series of oxygen concentration at the 1026.6 kg m ⁻³ density horizon in the vicinity of Ocean Station Papa (50°N, 145°W) from historical plus RCP 4.5 or 8.5 simulations.....	75
Figure 62: Maps of primary production for 1966-1985, 2006-2025 (RCP 4.5), and 2046-2065 (RCPs 4.5 and 8.5). Ensemble mean of five models.....	76
Figure 63: Time series of integrated primary production in the vicinity of Ocean Station Papa (50°N, 145°W) from historical plus RCP 4.5 or 8.5 simulations..	76
Figure 64: Locations of 13 weather buoys off the Canadian west coast. Colours denote the four categories described in Table 11.....	77
Figure 65: Summer (June-August) 1976-95 mean surface winds from buoy observations (vectors), individual GCMs (alphabetical codes from Table 10), and multi-model mean (large circles), for our regional groupings of the buoys.....	79

Figure 66: Future changes in January-March (left) and June-August (right) surface winds, averaged at the near-offshore buoy locations, between the 1976-95 base period and 2030-49 (upper panels) and 2080-99 (lower panels).	80
Figure 67: Map of the British Columbia continental shelf showing bathymetric contours, place names, and major offshore currents	82
Figure 68: a) Mean monthly winds at the six EC buoys shown in Figure 67: observed and re-constructed (Foreman et al. 2011) means over the period of 1971-2000 (black), NARCCAP CRCM/CGCM means for the same period interpolated to these buoy locations (green), interpolated NARCCAP CRCM/CGCM means for 2041-2070 (red); b) monthly ratios of future versus contemporary wind stresses (red versus green in (a) for buoys 132 and 208.	83
Figure 69: NARCCAP CRCM/CGCM3 monthly-averaged precipitation anomalies (mm/day) for the period of 2041-2070 minus 1971-2000.	85
Figure 70: NARCCAP CRCM/CGCM3 monthly-averaged surface air temperature anomalies ($^{\circ}\text{C}$) for the period of 2041-2070 minus 1971-2000.	86
Figure 71: NARCCAP CRCM/CGCM3 monthly-averaged short wave radiation anomalies (W/m^2) for the period of 2041-2070 minus 1971-2000. Values following the month name within each panel are monthly average values (W/m^2) for the 1971-2000 period.	87
Figure 72: Drainage basins whose major rivers discharge into the model domain.	88
Figure 73: a) Monthly-average contemporary and future freshwater discharges for the twenty-one watersheds (Figure 73) impacting coastal BC waters as estimated by output from CRCM output, b) monthly-average total discharge for the entire coast, c) monthly-average discharge temperatures.	89
Figure 74: Seasonal temperature (blue lines), salinity (red lines) and perpendicular velocity anomalies (colour contours, difference of means for 2040-2070 and 1970-2000) for the western boundary as computed from CGCM3 (specifically CGCM3.1 T47 SRES A2 run #4). Positive velocities denote flow into the ROMS model domain.	90
Figure 75: Temperature and salinity anomalies applied to the MF12 initial (January) conditions as functions of latitude and depth, and as computed from CGCM3.	91
Figure 76: Map of the British Columbia continental shelf showing bathymetric contours, place names, and average positions of major offshore currents.	93
Figure 77: Seasonally-averaged sea surface temperature anomalies ($^{\circ}\text{C}$).	94
Figure 78: Seasonally-averaged sea surface salinity anomalies (psu).	95
Figure 79: Seasonally-averaged sea surface height anomalies (cm).	96
Figure 80: Annually-averaged eddy kinetic energy (cm^2/s^2) for the contemporary (from MF12) and future (2040-2070) simulations.	98
Figure 81: Contemporary, future and differences in seasonally-averaged currents at 20 m depth in Queen Charlotte Sound. Note the colour scale change for the anomaly column.	98
Figure 82: Contemporary, future and differences in seasonally-averaged currents at 20 m depth in the Salish Sea and southwest Vancouver Island shelf.	99
Figure 83: Along-shelf currents crossing, and temperature (blue) and salinity (red) contours along, a transect off the mid Vancouver Island shelf (see Figure 76)	100

ABSTRACT

Christian, J. R. and Foreman, M.G.G. 2013. Climate trends and projections for the Pacific Large Aquatic Basin. Can. Tech. Rep. Fish. Aquat. Sci. 3032: xi + 113 p.

The Pacific Large Aquatic Basin (LAB) includes all marine waters along the west coast of Canada as well as rivers, lakes and streams bearing anadromous fishes that live in the Pacific Ocean for part of their lifespan. There are four spatial sub-divisions of the Pacific LAB: Strait of Georgia (SOG), West Coast of Vancouver Island (WVCI), North Coast (NC), and Gulf of Alaska (GOA). The Gulf of Alaska includes all oceanic waters beyond the continental shelf. Within these domains there are a variety of sources of data on trends in and projections of climatic and ocean states. Some data sets collected by DFO go back more than half a century while others are much more recent. In this report we document trends in temperature, salinity and stratification, coastal sea level, the carbon system, oxygen, and nutrients, and projections of these quantities using Global Climate Models (GCMs) and future greenhouse gas forcing scenarios. A *trend* is based on past observations; the length of the observational records varies and in many cases is too short to detect long-term trends against the background of natural variability. A *projection* is estimated from climate model output based on scenarios for future anthropogenic greenhouse gas emissions. For the coastal domains, GCM output was downscaled using regional atmosphere and ocean models with greatly enhanced resolution relative to the GCMs. Trends and projections show a coherent picture of an ocean becoming warmer, fresher and more stratified, resulting in reduced entrainment of nutrients into the euphotic zone and declining subsurface oxygen concentration. In some cases these trends are modulated by opposing tendencies in certain regions and seasons, e.g., through the enhancement of upwelling-favourable winds. Global sea level rise and ocean acidification are monotonic trends superimposed on background natural variability. Sea level rise is mitigated somewhat on the BC coast by tectonic uplift of the land; extreme states associated e.g. with El Niño events become more serious risks as mean sea level increases. In the freshwater habitats of Pacific salmon, air temperatures are projected to increase with regional and seasonal variation in the magnitude, while precipitation changes may be positive or negative depending on region and season. Warmer, drier summers will pose risks to stocks in some areas.

RESUMÉ

Christian, J. R. and Foreman, M.G.G. 2013. Climate trends and projections for the Pacific Large Aquatic Basin. Can. Tech. Rep. Fish. Aquat. Sci. 3032: xi + 113 p.

Le grand bassin du Pacifique inclut toutes les eaux marines le long de la côte ouest du Canada ainsi que les rivières, lacs et cours d'eau abritant des poissons anadromes qui vivent dans l'océan Pacifique pour une partie de leur vie. Le grand bassin du Pacifique se divise en quatre sections spatiales: le détroit de Géorgie, la côte ouest de l'île de Vancouver, la côte Nord et le golfe d'Alaska. Le golfe d'Alaska comprend toutes les eaux océaniques au-delà du plateau continental. Il existe diverses sources de données sur les tendances et les projections des conditions climatiques et océaniques pour ces régions. Quelques ensembles de données ont été recueillis par le MPO depuis plus d'un demi siècle tandis que d'autres sont beaucoup plus récents. Dans le cadre de ce rapport, nous documentons les tendances de la température, salinité et stratification, niveau côtier de la mer, le système de carbone, oxygène et éléments nutritifs ainsi que les projections de ces variables dérivées de modèles climatiques globaux (MCGs) et de scénarios futurs de forçage des gaz à effet de serre. Une tendance est fondée sur des observations antérieures; le nombre d'observations réalisées varie mais souvent le nombre limité ne permet pas de révéler des tendances à long terme dans le contexte de la variabilité naturelle. Une projection est obtenue à partir des résultats de modèles climatiques qui s'appuient sur des scénarios d'émissions futures de gaz de serre d'origine anthropique. Pour les domaines côtiers, les données produites à partir de MCGs ont été converties à une échelle plus fine à l'aide de modèles régionaux atmosphérique et océanique offrant une résolution nettement améliorée par rapport au MCGs. Les tendances et projections dressent un tableau cohérent d'un océan qui devient plus chaud, doux et stratifié; ce qui réduit l'entraînement des éléments nutritifs vers la zone euphotique et la concentration de l'oxygène en profondeur. Dans certains cas, ces tendances sont mitigées par des tendances opposées dans certaines régions et saisons; par ex. par l'intensification des vents favorables à la remontée. La hausse du niveau de mer global et l'acidification de l'océan sont des tendances monotones qui s'ajoutent à la variabilité naturelle fondamentale. La hausse du niveau de mer est atténuée sur la côte de la C.-B. en partie par le soulèvement tectonique des régions côtières; conditions extrêmes associées par ex. avec les événements El Niño posent des risques plus grands avec la montée du niveau moyen de la mer. Les températures de l'air devraient augmenter dans les habitats d'eau douce du saumon du Pacifique, avec des variations régionales et saisonnières en magnitude, tandis que les changements de précipitation seront soit positifs ou soit négatifs selon la région et la saison. Des étés plus chauds et secs poseront des risques aux stocks dans certaines régions.

INTRODUCTION

J. R. Christian, Institute of Ocean Sciences, Fisheries and Oceans Canada

GEOGRAPHICAL SCOPE OF THE PACIFIC LARGE AQUATIC BASIN

The geographical scope of the Pacific Large Aquatic Basin (LAB) is the marine waters along the west coast of Canada, as well as rivers, lakes and streams bearing anadromous fishes that live in the Pacific Ocean for part of their lifespan. The characteristics of both marine and freshwater environments differ considerably across the region. The Pacific LAB consists of the open ocean ecosystems of the Gulf of Alaska, the Canadian portion of the North Pacific continental shelf (from the Strait of Juan de Fuca to Dixon Entrance), the Canadian portions of the Salish Sea (Straits of Georgia and Juan de Fuca), the numerous fjords and inlets of the BC coast, and the rivers where salmon and other anadromous fish spawn. The various domains are connected by the migrations of the salmon (which are present in all five domains), by the influence of freshwater inflow on coastal circulation, and by the upwelling of nutrient rich but oxygen and carbonate poor waters from the oceanic thermocline onto the continental shelf.

There are four spatial sub-divisions of the Pacific LAB: Strait of Georgia (SOG), West Coast of Vancouver Island (WVCI), North Coast (NC), and Gulf of Alaska (GOA) (Figure 1). The Gulf of Alaska includes all oceanic waters beyond the continental shelf (as defined e.g., by the 300 m depth contour). The SOG subdomain includes all Canadian waters of the Salish Sea (which includes the Strait of Juan de Fuca and Puget Sound as well as the Strait of Georgia proper). The North Coast region roughly overlaps the Pacific North Coast Integrated Management Area (PNCIMA). While there may be biophysical justifications for further subdividing this region, it is aggregated here for primarily practical rather than conceptual reasons (e.g. lack of data).

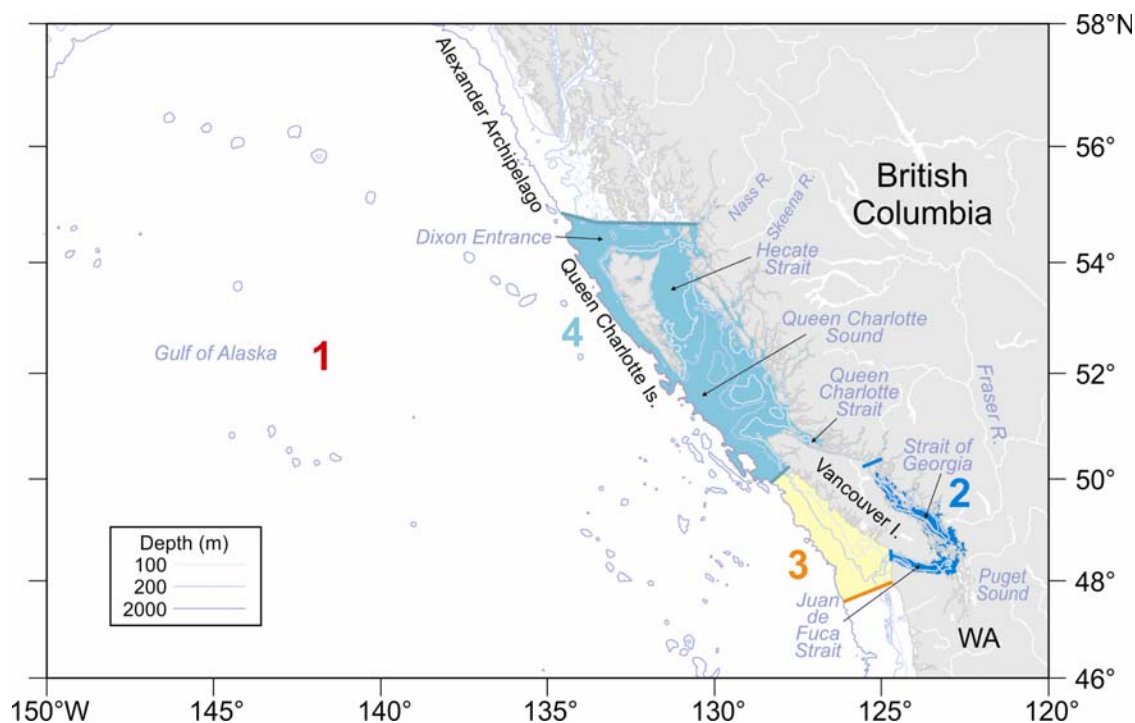


Figure 1: The four spatial sub-divisions of the Pacific LAB: Strait of Georgia (SOG), West Coast of Vancouver Island (WVCI), North Coast (NC), and Gulf of Alaska (GOA).

OCEANOGRAPHIC CONDITIONS

Among the three marine LABs (Atlantic, Arctic, and Pacific), the Pacific is unique in that it lacks sea ice, at least within Canadian waters. Another unique oceanographic characteristic is the extremely low oxygen concentrations and low CaCO_3 saturation states found at very shallow depths of the oceanic thermocline. Finally, the economic importance of anadromous fish is much larger than in the other LABs (the wild Atlantic salmon fishery being of relatively minor importance), so the impacts of terrestrial climate changes are more directly experienced by marine fisheries.

The seasonal cycle of wind stress varies greatly along the coast. The west coast of Vancouver Island (WCVI) is part of the California Current large marine ecosystem, characterized by seasonal upwelling that exists throughout the US west coast from Washington to California. The winds are upwelling favourable (Ekman transport offshore) in summer, with downwelling (transport onshore) in winter. Further north the prevailing winds induce onshore transport (downwelling) year round, although the mean wind is relatively small compared to the variance in winter (i.e., storm-induced mixing and mesoscale currents are more important than the mean flow). The BC coast is characterized by large amounts of freshwater input, which affects coastal circulation both by enhancing near-surface stratification and via currents induced directly by the flux of 'excess' water.

The large freshwater flux (along with the mineralogy of the drainage basins) also regulates productivity via the mixture of nutrients available to phytoplankton. For example, BC coastal waters are rich in silicate, and the principal limiting nutrient is nitrogen (Whitney et al. 2005). It is important to note that river borne nutrients play a relatively small role in regulating phytoplankton production: enormous amounts of nitrogen are dissolved in subsurface ocean water and marine phytoplankton growth is mostly determined by physical ocean processes such as seasonal stratification and mixing and upwelling of nutrients into the near-surface layers. Open ocean waters of the Gulf of Alaska are mostly iron-limited, but the boundary between the iron and nitrogen-limited domains is not well characterized and is likely an ever-changing mosaic. Mesoscale eddies that are characteristically generated at specific locations along the coast are an important mechanism for transport of iron from the shelf to iron-deficient offshore waters (Johnson et al., 2005). Diatoms and dinoflagellates dominate the phytoplankton of the shelf and coastal domains but give way to the smaller ($<10\ \mu\text{m}$) flagellates in the open Gulf.

CLIMATE VARIABILITY

Northeast Pacific climate has an extremely large amount of year-to-year variability. This is usually known as interannual to interdecadal variability, interannual being variations such as the El Niño – Southern Oscillation (ENSO), with a characteristic timescale of 3-7 years, and interdecadal the longer time scale variations associated with the Pacific Decadal Oscillation (PDO). These terms refer to variations in climate at the same phase of the seasonal cycle in successive years. They are smaller in amplitude than the seasonal cycle, but large relative to the more gradual long-term trends associated with anthropogenic warming. So on a time scale of e.g. 10-20 years, the anthropogenic component will be small (although its relative magnitude may increase, depending on future emissions).

It is important to note that while the term 'oscillation' may seem to imply a regular, cyclic process, the PDO is neither. It is simply a term that came into use with the observation that the system tends to 'oscillate' between two apparently distinct states: colder (warmer) than usual in the Northeast Pacific and the eastern tropical Pacific when it is warmer (colder) than usual in the west-central Pacific. This is partly an artefact of the statistical methods used to characterize the phenomenon, but even to the extent that these 'reversals' are a real phenomenon, they do not occur at regular intervals. Nor are they demonstrably cyclic in the way that ENSO is (despite its irregular period). The year-to-year variability

is thus for all practical purposes “noise” (every frequency contributes about equally) with a slight bias towards lower frequencies (i.e., warmer and colder years tend to come in clusters so if one year is unusually cold there is a better-than-even chance that the next one will be as well).

Skill at predicting climate variations more than a season ahead is limited and may not improve much in the coming decades, as it is limited by the inherent unpredictability of the climate system and not simply by our technology and ingenuity. Much of the coherence and predictability in coastal BC climate derives from ENSO. El Niño events are rarely predictable more than a season ahead (although this could conceivably improve), but often their genesis can be clearly seen a few months prior to the peak, and there are predictable consequences for coastal BC climate and sea level. The state of the tropical Pacific is now well observed in real time, so the effects of ENSO on the Pacific LAB can be 'predicted' from these observations even if they can not be forecast ahead of time. However, one of the largest unsolved problems in climate science is whether anthropogenic warming will 'project' onto the ENSO 'mode' (i.e., will manifest as a shift towards greater prevalence of one extreme of the existing mode), whether it will be a uniform warming across an unchanged 'background' ENSO, or something in between (e.g. Vecchi and Wittenberg 2010). The implications of this for the Pacific LAB are mostly in the frequency of extreme years at either end of the spectrum (e.g. El Niño winters with warm temperatures and little snow, La Niña winters with heavy snow).

TRENDS AND PROJECTIONS

A trend is based on past observations, and the length of the observational records varies. A projection is estimated from climate model output based on assumptions about future anthropogenic greenhouse gas emissions. We make projections only for the 50 year timescale.

In the North Pacific, natural climate variability is large relative to the long-term anthropogenic trend. Climate model projections are not meaningful on the 10-year time scale, and trends based on less than 20-30 years of data can not be assumed to represent long-term trends. Ten year projections are best estimated as linear extrapolations of past trends, with the caveats that (a) only those based on relatively long time series are robust trends, and (b) even these are only our best estimate of the long-term trend on which unpredictable short-term variability is superimposed, and not the total signal.

The uncertainty associated with extrapolation of a trend depends of the length of the data record used to estimate the trend, and on how far out we extrapolate. Extrapolating an observed trend 50 years out would be extremely speculative. On a ten year time scale, it is possible to extrapolate present trends if the data record is sufficiently long, but as noted above, the natural variability will tend to overwhelm the anthropogenic component at this time scale.

The 50 year projections are based on climate model output, and uncertainty derives from three sources: (1) the forcing scenario (the greenhouse gas emissions used to force the model), (2) model error, and (3) model internal variability. The latter is analogous to the natural (e.g., PDO) variability discussed above. A good model reproduces the general characteristics of this variability (i.e. it will reproduce the frequency and magnitude of events), but climate models can never reproduce the timing of specific events exactly. Therefore model projections are only useful when averaged over fairly long periods (20 years has been used routinely in ACCASP). We also minimize model error by averaging over multiple models. While it is possible that there are systematic biases common to most or all models, it is well established that the average of an ensemble of models developed (mostly) independently will generally be a better predictor of the actual state than any individual model (Lambert and Boer 2001).

Scope of this report

This report represents a summary of our best available knowledge at this time about trends in and projections of the oceanography and climate of the Pacific LAB. It consists of a number of largely independent reports on specific topics. In most cases if a topic is not covered it is because there is no information available. This report does not consider trends in abundance of fish or other "macro" organisms, which will be covered in separate publications by the by the Impacts, Vulnerabilities and Opportunities (IVO) group.

TRENDS

TRENDS IN SEA SURFACE TEMPERATURE AND SALINITY

P. Cummins and D. Masson. Institute of Ocean Sciences, Fisheries and Oceans Canada

Introduction

Anthropogenic global warming is a phenomena taking place on a century-long time scale. However, ecosystem-based management of coastal waters must consider not only such long term secular changes but also variability in the marine environment occurring over range of time scales, from seasonal out to the medium term, say 20 to 30 years. Both long term global warming, as well as natural variability on ENSO to decadal time scales, can contribute importantly to variability over the middle-term. While it is reasonable to expect secular warming trends to dominate over the long term, what can be expected over the middle term? To address such a question, we have characterized trends and variability of the coastal waters of BC. For this purpose, use is made of data collected at lighthouse stations (Figure 2), in part because they represent some of the longest records available.

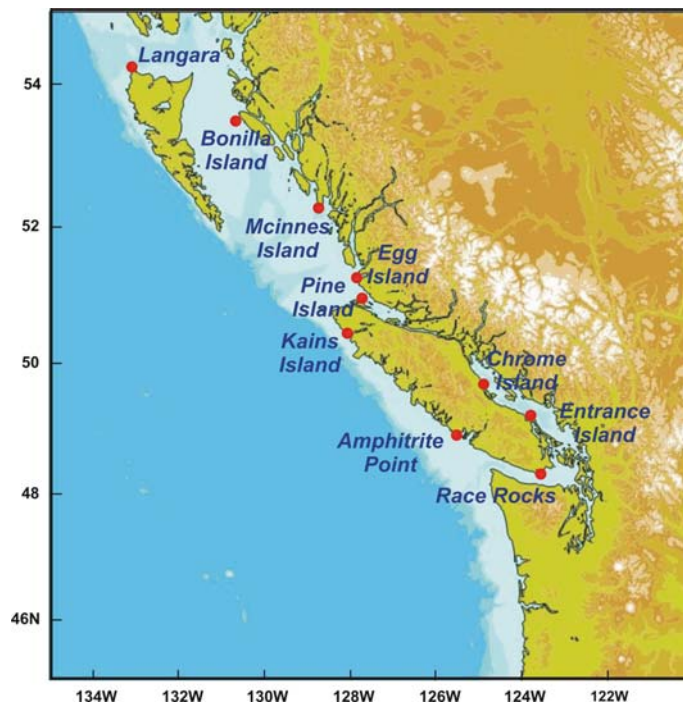


Figure 2: Lighthouse stations are indicated by red dots. This represents a subset of the stations with the longest records.

Six stations with long, near-continuous records to 2010 are considered:

- Entrance Island – 74 yrs
- Race Rocks – 69 yrs

- Amphitrite Pt. – 76 yrs
- Kains Is. – 76 yrs
- Langara Is. – 74 yrs
- Pine Is. – 74 yrs

Additional sites considered are:

- Bonilla Is. – 51 yrs
- Chrome Is. – 48 yrs

Analysis of lighthouse data

Temperature and salinity anomalies are formed by removing monthly means for 1971-2000 from the data. Except where noted, no smoothing of data is done. Anomalies are de-trended by removing long term linear trends. Empirical Orthogonal Functions (EOFs) of the longest records are used to characterize regional variability. Time series analysis techniques were applied to leading Principal Components (PCs). The extent to which the leading PCs are related to other indices or forcing was examined. The influence of decadal variability on trends of varying duration was also examined.

Variability

An EOF analysis on the SST and SSS records is used to characterize the variability. The leading principal components of SST and SSS and given in Figure 3 and Figure 4.

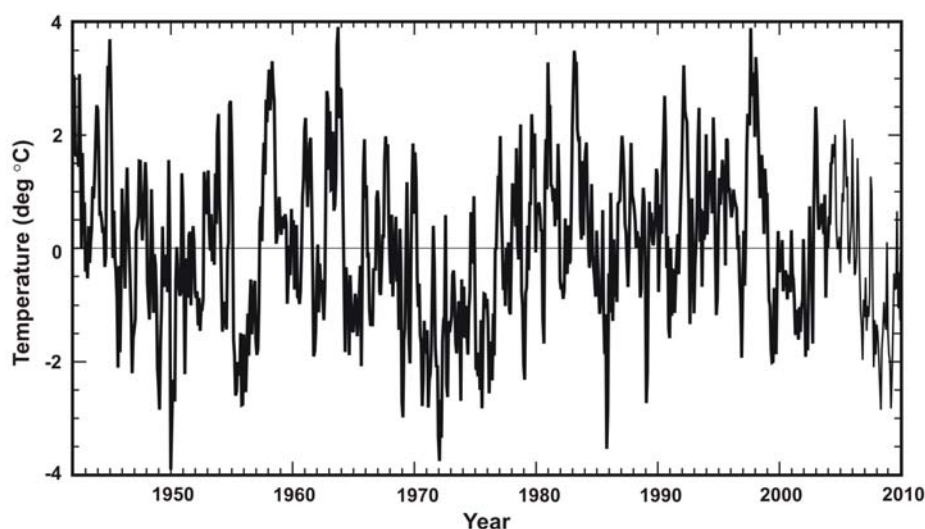


Figure 3: PC1 for lighthouse SST provides an index of SST variability for coastal BC waters. Note the variability occurring on decadal time scales.

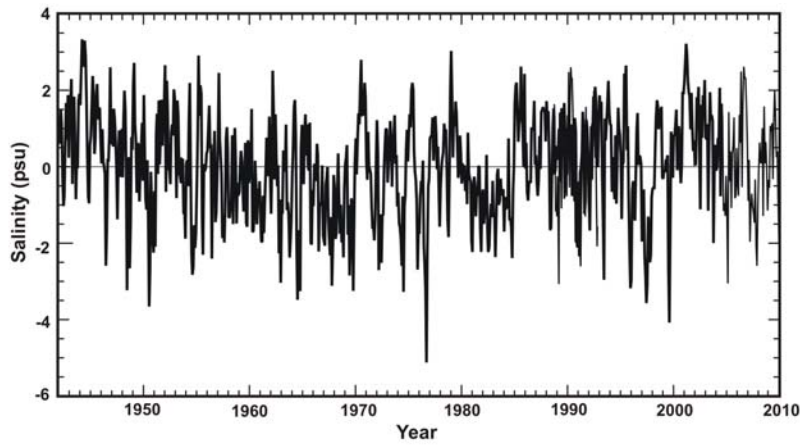


Figure 4: PC1 for lighthouse SSS. This also shows variability over a wide range of time scales. PC1 for salinity is not correlated ($r = -0.1$) with PC1 for SST.

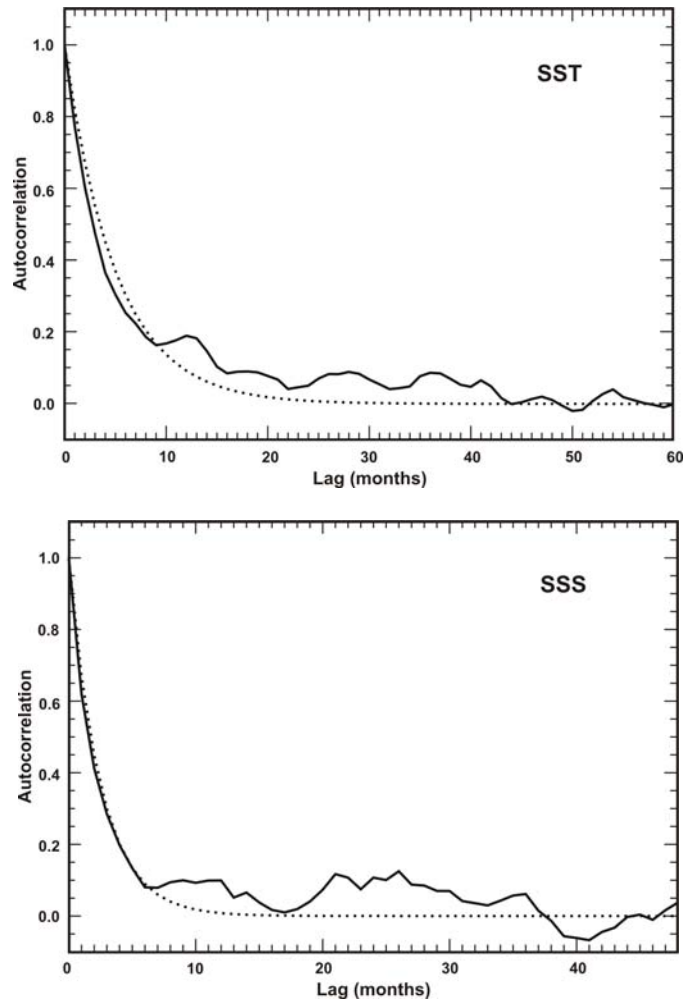


Figure 5: Autocorrelation for PC1 of lighthouse SST (top panel and SSS (lower panel).

The autocorrelation function the leading principal component of the lighthouse SST and SSS data are shown in Figure 5. The dotted lines indicate an exponential decay of autocorrelation which provides a reasonable fit for lags out to 6 months. The integral time scale for the SST principal component is 10 months, whereas it is only 5 months for the SSS principal, indicating that SSS is subject to greater short

term variability than SST. All entries in Table 1 are of the same sign, implying in-phase co-variability over the entire coast. The non-stationary Langara salinity record is omitted.

Table 1: Leading mode EOF amplitudes (loadings).

	SST mode 1 (68% variance)	SSS mode 1 (59% variance)
Amphitrite Pt.	0.46	0.47
Kains Is.	0.50	0.44
Langara Is.	0.44	—
Pine Is.	0.37	0.13
Entrance Is.	0.36	0.75
Race Rocks	0.28	0.11

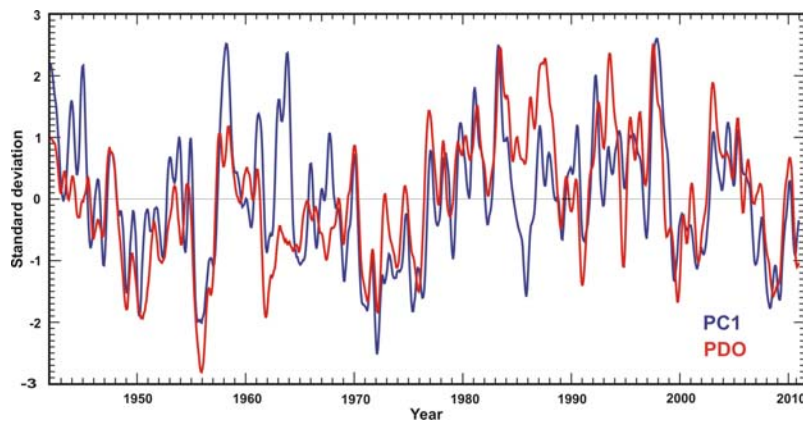


Figure 6: PC1 of lighthouse SST vs. the PDO. A 9-month triangular filter has been applied to both records.

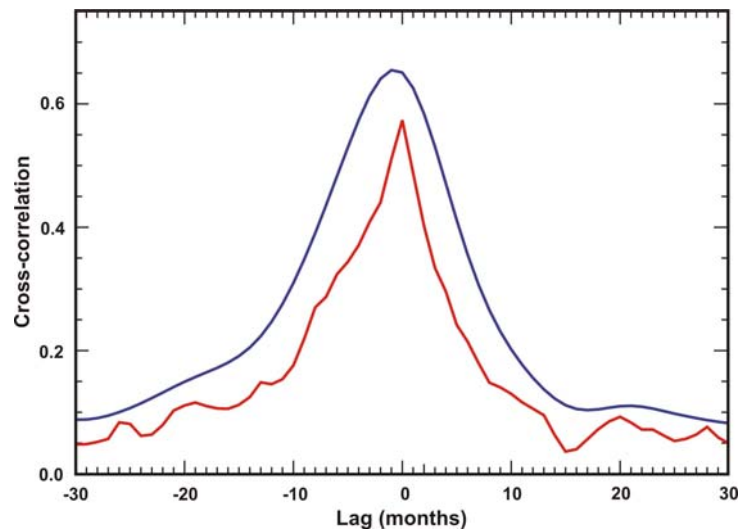


Figure 7: Cross-correlation of PC1 and PDO time series in Figure 6. Red line indicates no smoothing.

The time history of PC1 of lighthouse SST is compared with that of the Pacific Decadal Oscillation in Figure 6. Note the generally close agreement on decadal times scale. The cross-correlation between the two time series is given in Figure 7 and indicates that the two records are most correlated at zero time

lag. The implication is that the leading mode of BC coastal SST co-varies with the large scale variability over the Pacific. This is consistent with the earlier finding of Masson and Cummins (2007) that low frequency variability in the Strait of Georgia water column temperature reflect northeast Pacific variability as measured along Line P (Figure 8).

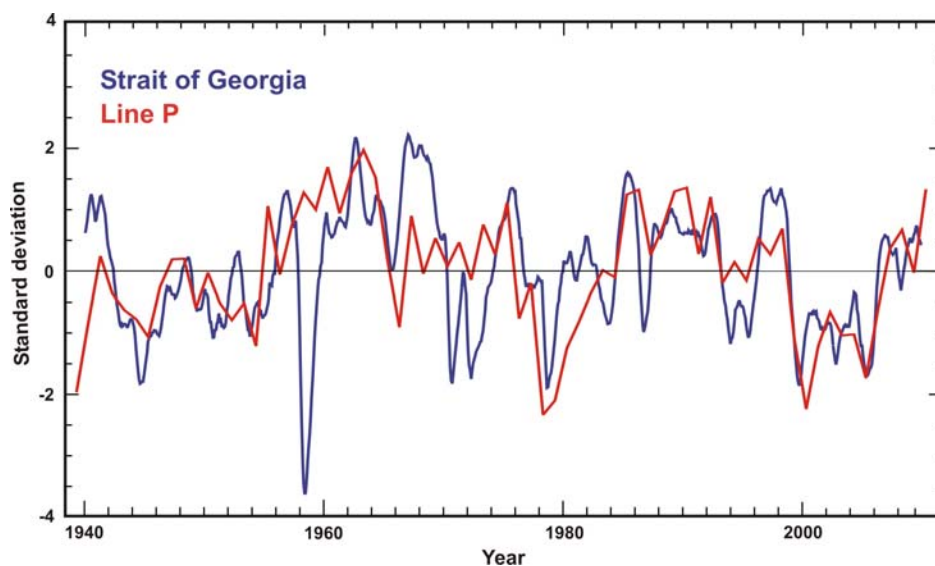


Figure 8: Depth-averaged temperature anomalies in the Strait of Georgia (blue curve) and for 10-50 m along Line P (red curve), normalized by the standard deviation for each region. Figure is adapted from Masson and Cummins (2007).

The leading principal component (PC1) of SST variability represents an index of variability for coastal BC waters. This PC1 is strongly correlated with the PDO index, which is the leading principal component of SST variability over the entire extratropical North Pacific. We can not say that local SST variability is driven by the PDO. Rather, they co-vary on interannual to decadal time scales. They may be driven by common forcing. SSS anomalies have shorter time scales than SST and appear to be locally driven as they are not related to any large scale climate index. The results presented here are consistent with an earlier study (Masson and Cummins 2007) that showed water column temperatures in the SoG covary with Line P temperatures.

Long term and decadal trends

Long term trends, calculated over the full length of each record, are given in Table 2, along with 95% confidence intervals. These intervals were computed according to an exponential fit to the autocorrelation of each record, as in Masson and Cummins (2007). All of the stations display varying degrees of warming over the long term, presumably reflecting the global warming signal. These results are largely consistent with the SST trends identified in the shorter lighthouse records analysed by Freeland (1990). The SSS data also indicate a tendency for freshening of the offshore coastal waters (see subsequent chapter on Trends In Temperature, Salinity, Water Column Stability And Mixing Depth In The Open Gulf Of Alaska).

Trends over the middle term, say over 20-40 years, are also of interest and will reflect both long term secular trends, as well as variability on decadal time scales. Figure 9 illustrates 20-year running trends for SST based on records at four representative lighthouse stations.

Table 2: Long term secular trends at different lighthouse stations.

	Duration (yrs)	dof (T)	Temp trend (°C century ⁻¹)	dof (S)	Salinity trend (century ⁻¹)
Amphitrite Pt.	76	140	0.77 ± 0.60	228	-0.78 ± 0.54
Kains Is.	76	96	0.57 ± 0.74	223	-0.45 ± 0.50
Entrance Is.	74	198	1.48 ± 0.53	192	1.09 ± 0.79
Race Rocks	69	78	1.52 ± 0.57	56	-0.33 ± 0.51
Pine Is.	74	51	0.86 ± 0.80	86	-0.67 ± 0.33
Langara Is.	71	104	0.85 ± 0.75	73	-1.36 ± 0.31
Bonilla Is.	51	89	0.86 ± 1.05	77	0.50 ± 0.60
Chrome Is.	48	144	3.60 ± 1.86	61	0.46 ± 1.35

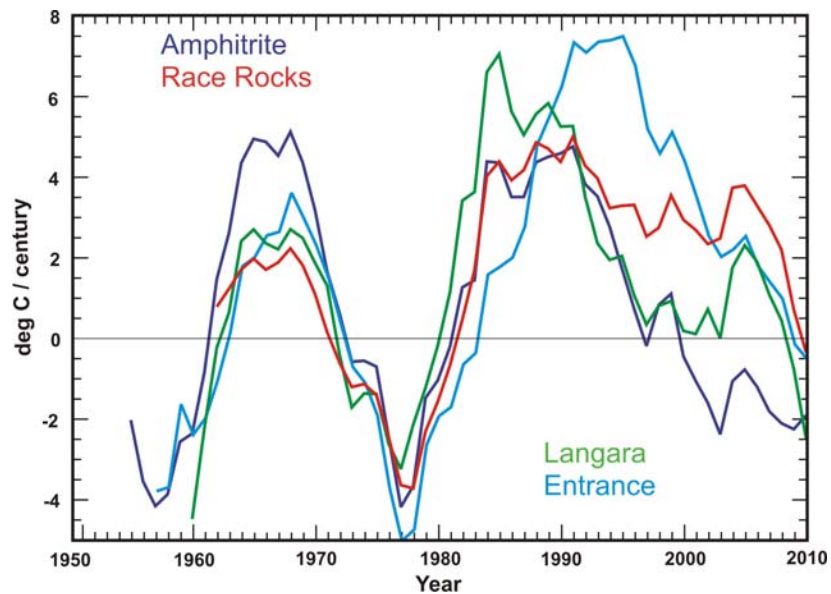


Figure 9: Running 20-year SST trends for four lighthouse stations. Note that the long term trend has not been removed from the SST anomalies for this calculation.

Average histograms for the running SST trends of varying length are presented in Figure 10. The average is based on the four stations presented in Figure 9. The results show that as the period over which trends are determined becomes longer, the histogram becomes narrower and shifts toward positive values reflecting to the long term warming over the region. A similar change is seen in results from global climate models (Easterling and Wehner 2009). For shorter periods, the spread of the histogram is greater due to decadal variability. The probability of a negative (i.e., cooling) trend decreases as the length of the running trends increases.

The probability of the trend ≤ 0 :

- 20-year running trends: 39%
- 30-year running trends: 34%
- 40-year running trends: 17%

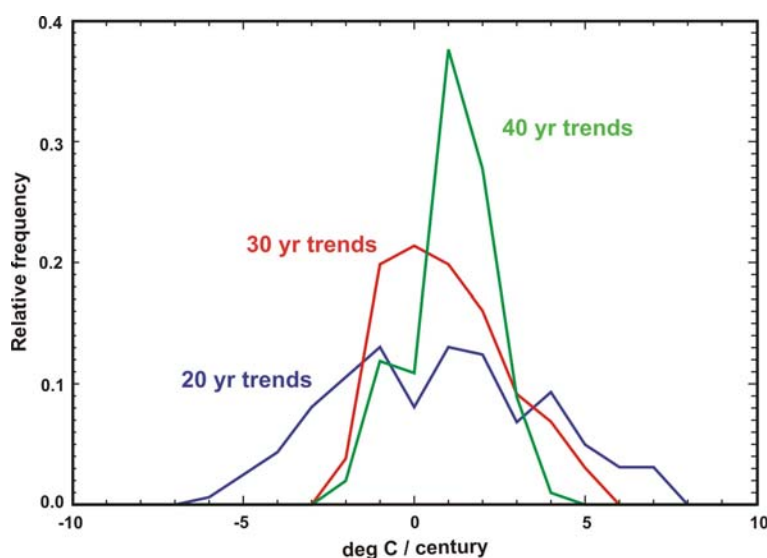


Figure 10: Average histograms for running SST trends of different lengths

Summary

The first Principal Component (PC1) for the lighthouse SST observations provides an index of the dominant SST variability over BC coastal waters. It is closely related to the PDO; hence it reflects large-scale variability occurring on decadal time scales over the Pacific. This is not the case for SSS which appears to be closely linked to regional forcing. To varying degrees, all of the lighthouse stations display long term warming tendencies. The stations on the open west coast also show a freshening tendency which appears to be a phenomena extending over the northeast Pacific. Tendencies determined on time scales of 20-30 years are dominated by decadal variability, although the long term warming signal is also manifest. On a time scale of 20 years, the historical record at BC lighthouse indicates that there is a fairly significant probability (nearly 40%) for either no net tendency, or cooling of SSTs. This is a consequence of the strong decadal variability. However, over periods greater than 40 years duration, the probability of seeing a warming tendency is much greater.

TRENDS IN SALINITY AND TEMPERATURE OFF THE WEST COAST OF VANCOUVER ISLAND

M.G.G. Foreman¹ and J. Galbraith². ¹Institute of Ocean Sciences, Fisheries and Oceans Canada, ²560 Wildwood Crescent, Gabriola, BC V0R 1X4

Introduction

Water temperature and salinity observations have been taken off the west coast of Vancouver Island for several decades. Early observations were with bottles but since 1979 conductivity-temperature-depth (CTD) measurements have been taken at stations along several lines crossing the shelf (http://maps.waterproperties.ca/wcvi_stations.php) at least two to three times a year. These observations were at the standard depths of 0 m, 5 m, 10 m, and every 10 m thereafter down to the bottom or 2400 m. Though the stratification and internal tide patterns do change seasonally, it is feasible to restrict each station/depth time series to one season and analyze for tidal variations in salinity and temperature. Here we restrict the observations to the summer period of June through September, inclusive, and the five lines shown in Figure 11. As the stations were seldom visited at exactly at the same location, for the purpose of this analysis any observations taken within 2km of the “standard” locations were assumed to be at that station.

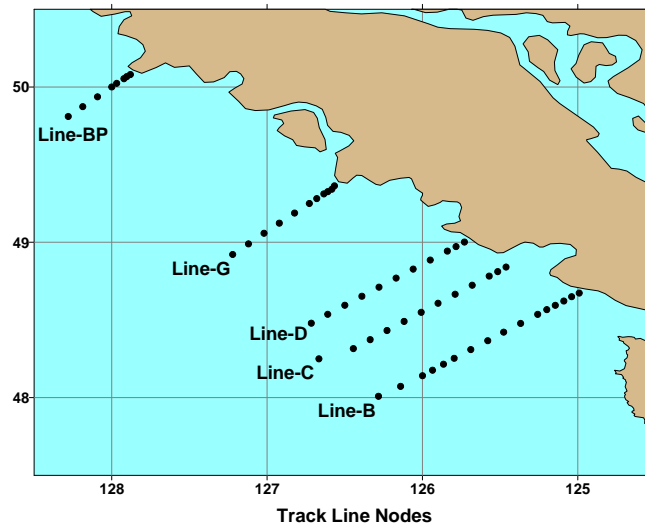
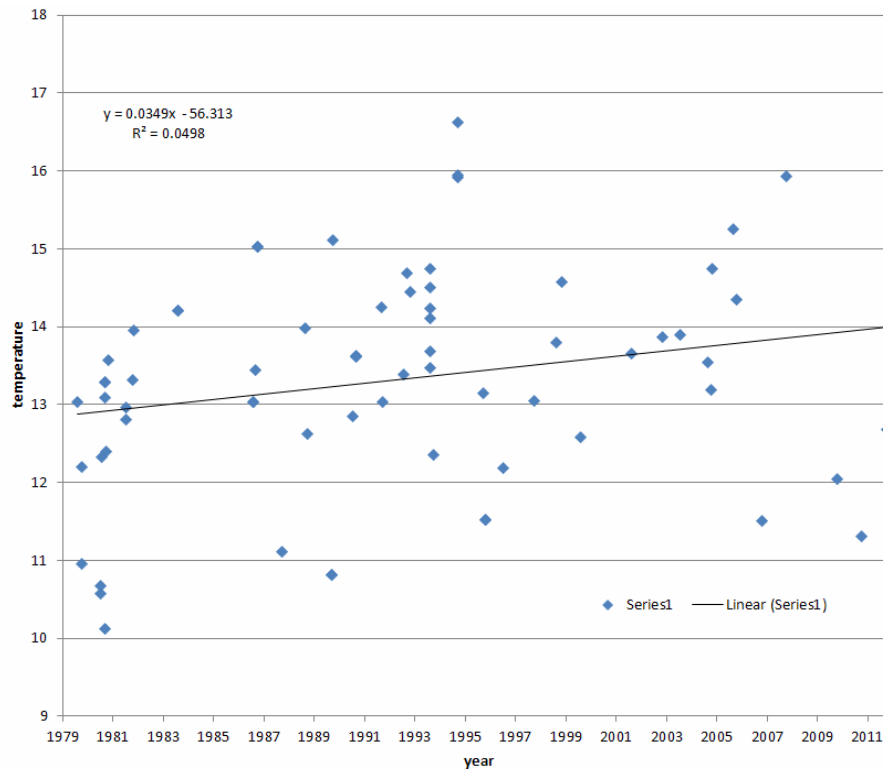


Figure 11: West coast Vancouver Island water property stations used in this analysis.

Figure 12a shows the 10 m summer temperatures observed at station 11 (numbers increase from the shore) in Line-B over the period of 1979 to 2011. An increasing linear trend and R^2 value obtained via regression are also shown. Given the relatively short length of this time series it is likely that the trend is highly influenced by variability arising from features like El Niño and the Pacific Decadal Oscillation (PDO, Mantua et al. 1997). In fact, monthly PDO values (<http://jisao.washington.edu/pdo/PDO.latest>) for the same time period (Figure 12b) show a decreasing trend in temperature over this period, suggesting that if the PDO influence were somehow removed from the station 11 temperatures, the latter would show an even stronger increase. This has not been done for the present analysis but is being considered for the future.



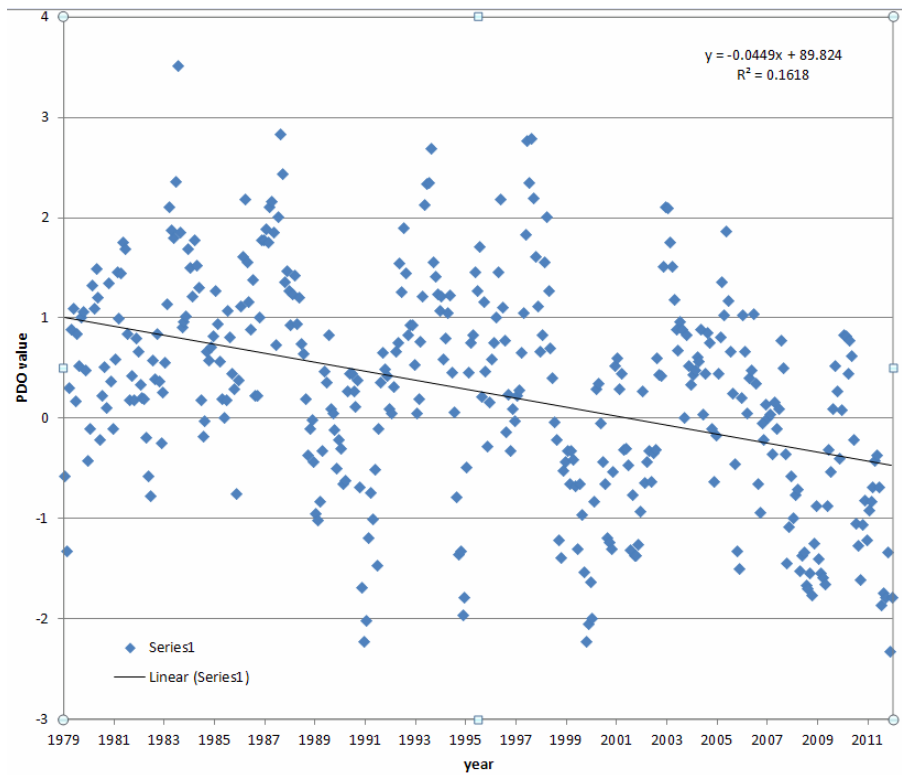


Figure 12: a) Observed summer temperatures and fitted linear trend at 10 m depth at station 11 in Line-B, b) monthly PDO values, and linear trend, for 1979-2011.

The analysis approach

At each station and depth, the salinity and temperature time series were assumed to have the form $y_i = a_0 + a_1 * t_i$ where t_i is the time in 365 day increments from an arbitrary origin, y_i is the temperature or salinity observation at time t_i , and a_0 and a_1 are parameters found from a least squares fit using a Singular Value Decomposition algorithm (Press et al. 1992). Though initial analyses also included tidal harmonics in the fit (Foreman et al. 2009), their presence was not found to make much difference to the solutions for (a_0, a_1) . No analyses were performed with fewer than twenty-one observations and the maximum number of observations at one station was 79. A *t*-test (<http://stattrek.com/regression/slope-test.aspx>) was applied to determine if the slope, a_1 , was significantly different from zero, and the number of degrees of freedom was taken to be $N-2$, where N is the number of observations at a particular station and depth.

Results

Figure 13a shows smoothed temperature trends along Line-B (Figure 11). Average summer seasonal currents crossing this line include a near-surface, wind-driven, Shelf Break Current (SBC) flowing to the southeast; a near-surface Vancouver Island Coastal Current (VICC, Thomson et al. 1989) flowing to the northwest, and a California Undercurrent (CUC) flowing to the northwest along the continental slope and centered at about 200 m depth (Freeland et al. 1984; Thomson and Krassovski 2010). Similar to the analysis in Foreman et al. (2009), a warming of up to $0.047^\circ\text{C}/\text{year}$ is seen in the SBC, a cooling of up to $0.037^\circ\text{C}/\text{year}$ is seen in the VICC, and a slight warming is evident in the CUC. However a cooling pattern that extends from underneath the SBC upward and onto the shelf is also evident and may indicate increased upwelling. However when a *t*-test is applied to determine if these (and other) trend values are different from zero, relatively few are found to be statistically significant. Apart from a

slightly saltier trend in the near surface portion of the SBC, the associated salinity trends (Figure 13b) show only a weak tendency to fresher values.

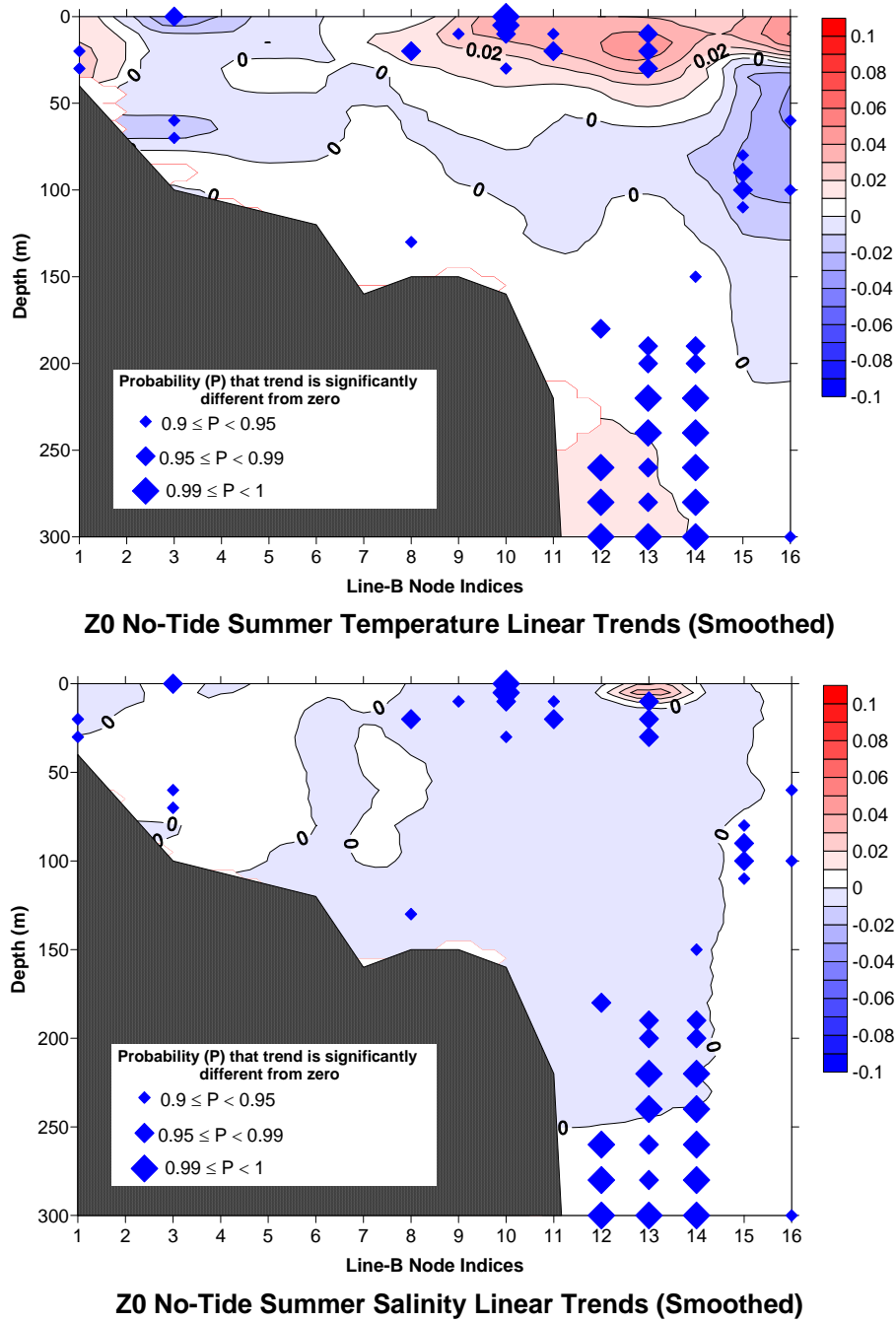


Figure 13: Trends in a) temperature ($^{\circ}\text{C}/365$ days) and b) salinity ($\text{PSU}/365$ days) along Line-B. Station numbers are given along the x-axis, depths are along the y-axis, and land below the shelf bathymetry is shaded. *t*-test probabilities indicating if particular trend values are significantly different from zero are indicated by the different sized diamonds. “Z0 No-Tide” indicates that only a constant term, a_0 , and linear trend, a_1 , were included in the least squares analyses.

Trends in temperature and salinity along Line-C are shown in Figure 14. Warming down to approximately 50 m is seen to extend eastward from station 12 to station 4 with cooler waters extending below that to approximately 150m. As with Line-B, this suggests a warmer SBC and the upwelling of

cooler waters. However, in this case the cooling upwelled waters do not reach the surface. The pattern near the coast is a little more complex. The warming waters below the surface could be the VICC and the slightly cooler water right at the surface could reflect fresher (and more buoyant) water leaving Barkley Sound. The associated salinity trends show a small to zero freshening everywhere except at station 3 where a saltier trend is evident near the surface. This latter feature needs more investigation; it may indicate more upwelling off Amphitrite Point.

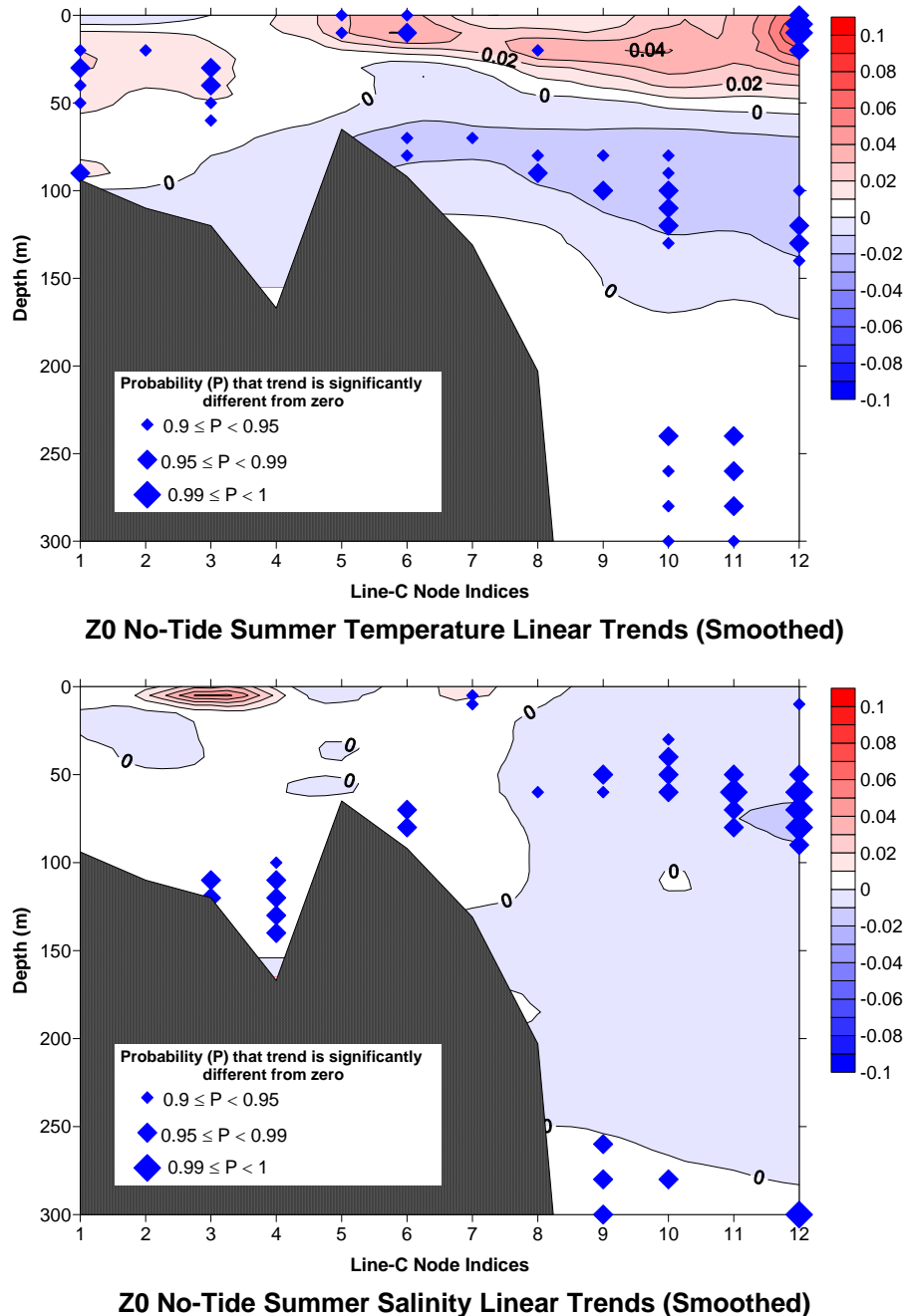


Figure 14: As in Figure 13 but for Line-C.

Trends in temperature and salinity along Line-D are shown in Figure 15. The temperature patterns are similar to those for Line-B with warming down to about 30 m off the shelf break and a cooling pattern underneath that, in this case, extends up onto the shelf and to the coast. A slightly warmer VICC lies underneath the cooler coastal waters and there is also the suggestion of a slightly warmer CUC, though

only some of the trend values are statistically significant. Apart from slightly saltier waters at about 100m depth at stations 8 and 9, the associated salinity trends suggest slight freshening.

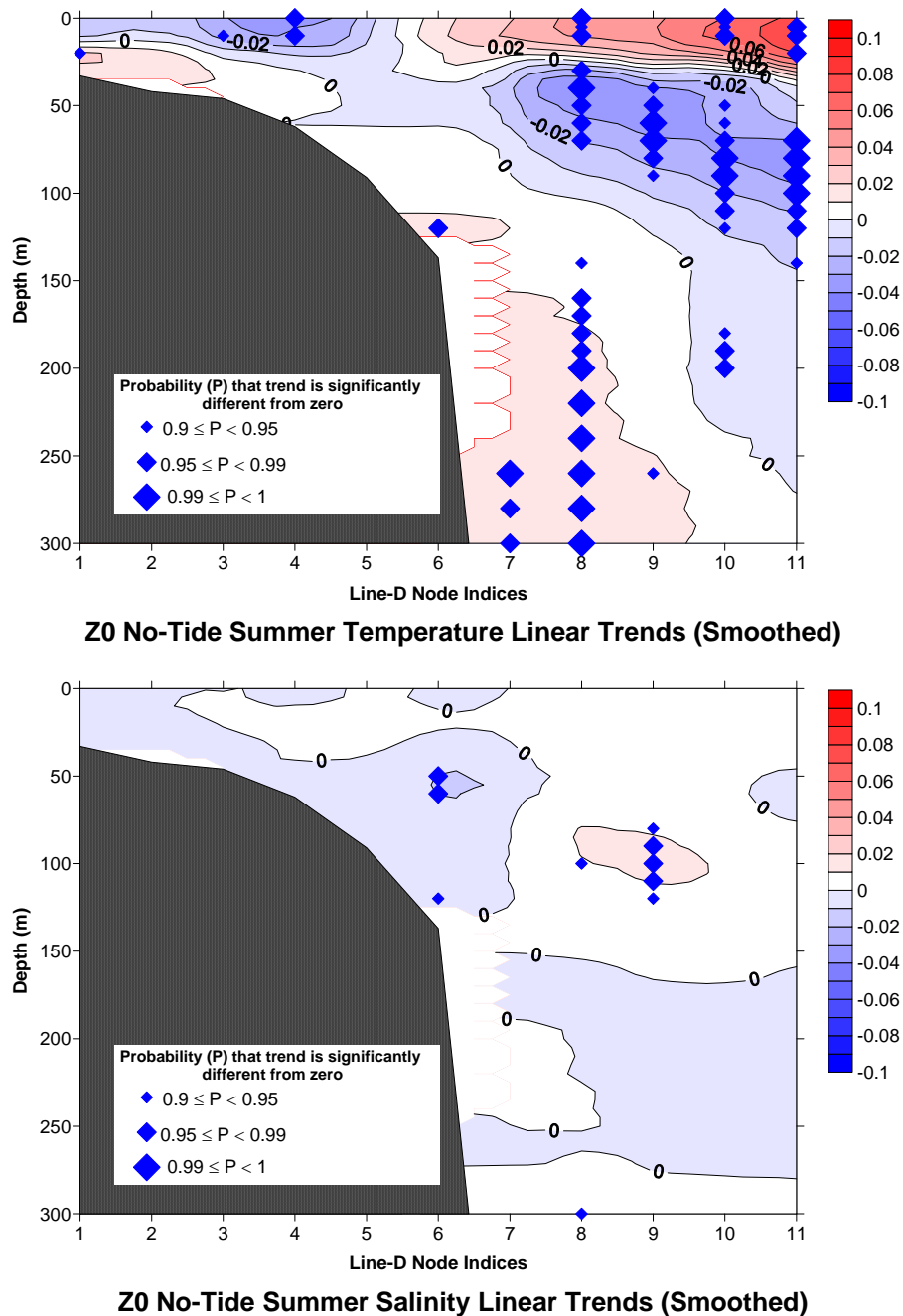


Figure 15: As in Figure 13 but for Line-D.

Trends in temperature and salinity along Line-G off Estevan Point (Figure 16) show similar patterns to those along Lines B and D; namely, warming waters down to about 30m off the shelf, cooling waters underneath that extend onto the shelf and reach the surface, and a warmer surface waters at the coast that may be associated with the VICC. A slightly (in some cases statistically significant) warmer CUC is also evident. In this case the associated salinity trends suggest the SBC is becoming slightly saltier and everywhere else there is no change or slight freshening.

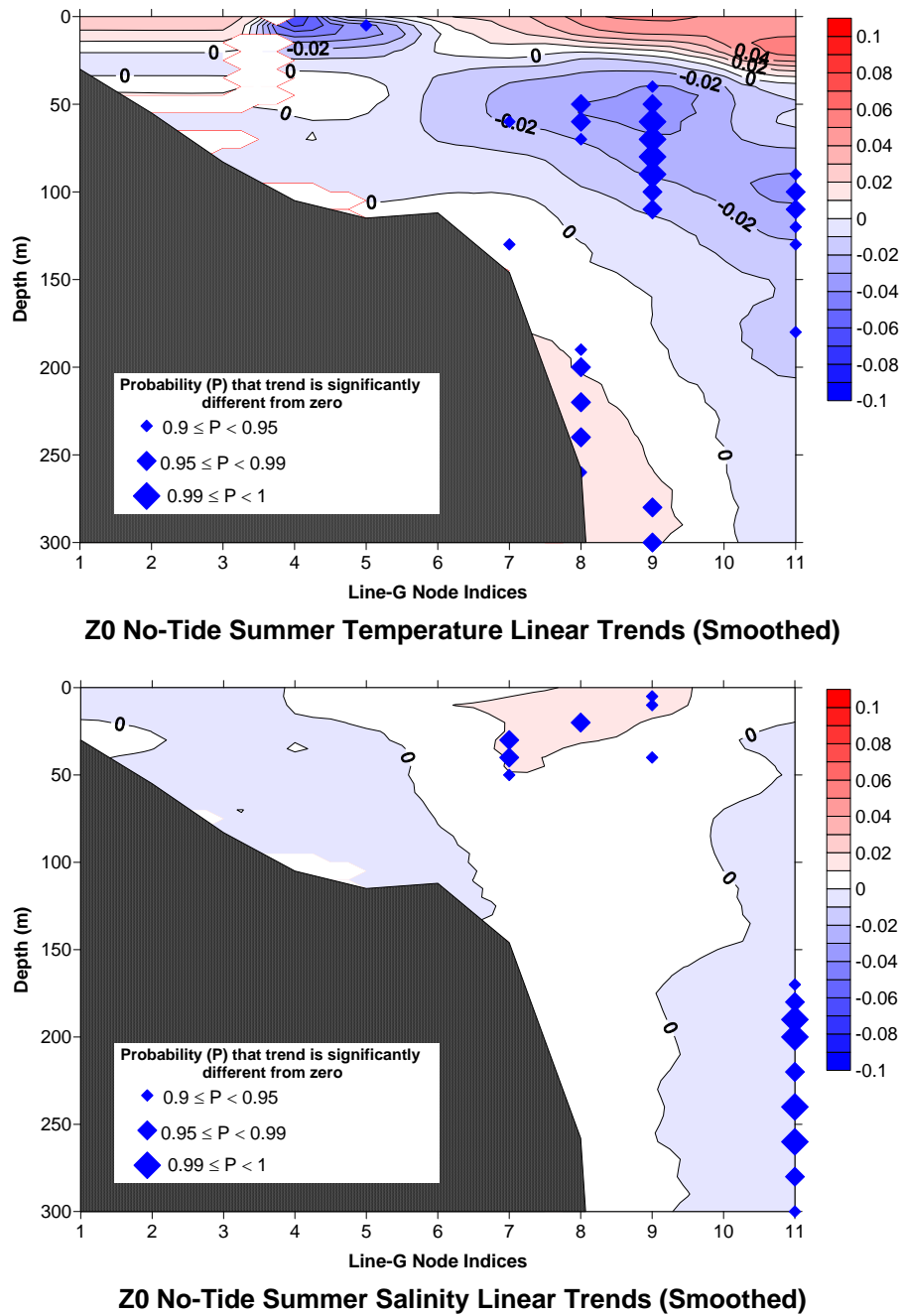
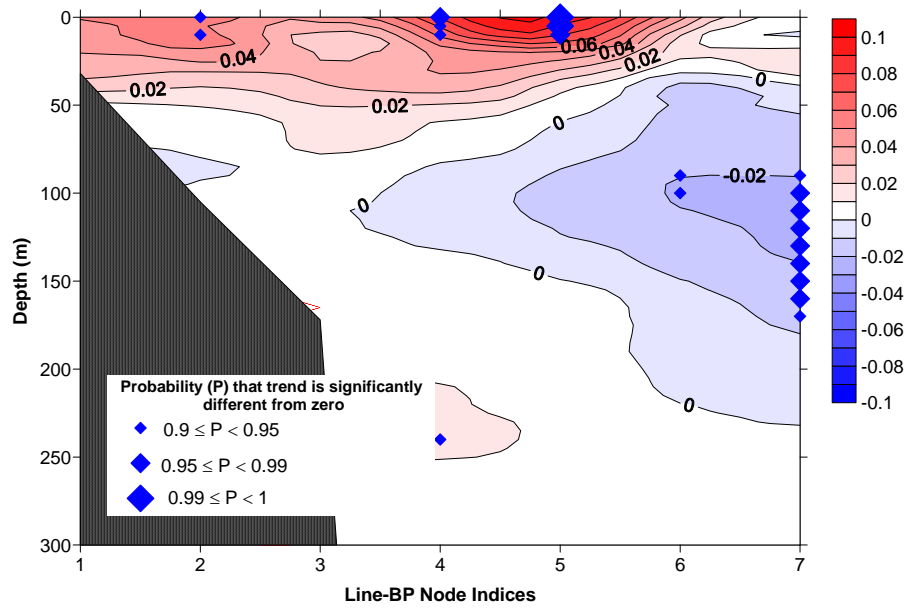
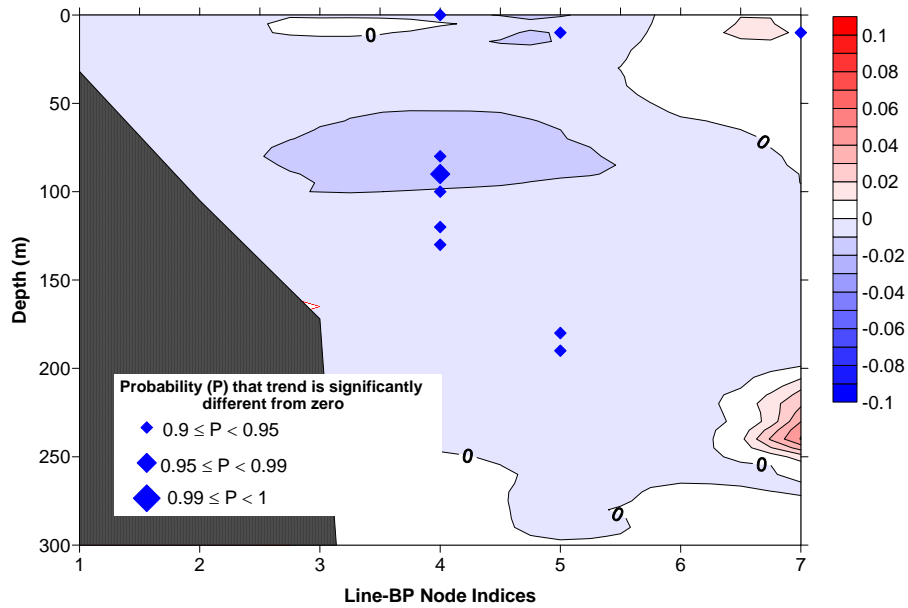


Figure 16: As in Figure 13 but for Line-G.

Results of the trend analysis along line BP off Brooks Peninsula are shown in Figure 17. In this case, significant warming in the SBC extends eastward for all near-surface waters, albeit with smaller values over most of the shelf and then attains larger values in what could be the VICC, though it is not clear that this current always extends past Brooks. Slight cooling trends are seen under this surface warming feature and again extend eastward, though unlike the patterns for Line-B, do not reach the surface. The associated salinity trends indicate a slight freshening almost everywhere, though at only a few locations and depths are the values significant.



Z0 No-Tide Summer Temperature Linear Trends (Smoothed)



Z0 No-Tide Summer Salinity Linear Trends (Smoothed)

Figure 17: As in Figure 13 but for Line-BP.

Discussion and Summary

The preceding presentation describes a preliminary trend analysis of summer (June to September) temperatures and salinities at stations along five sampling lines crossing the west coast of Vancouver Island. Though the time series span the relatively short period of 1979 to 2011 and the trends will be aliased with interannual and interdecadal variability from features like El Nino and the PDO, some statistically significant linear trends were found (particularly with the temperatures) that might be attributable to climate change. The predominant summer currents in the region (SBC, VICC, and CUC) are generally evident in the temperature trend contours and show consistent warming trends for all five lines. A subsurface tongue of cooling water that extends from offshore (under the SBC and over the

CUC) onto the shelf is also found consistently and may indicate increased upwelling of cooler waters. The salinity trends are less definitive and generally indicate fresher waters.

Clearly further analyses need to be done. They could include attempts to remove the PDO component from the time series, analyses over more lines, correlations with trends from nearby coastal lighthouses, a more careful examination of apparent anomalous features (e.g., the near surface salinity trend at station 3 in Line-C), and attempts to explain (or at least link) the trends with associated changes in fields that force the main currents (e.g., winds for the SBC, freshwater discharge for the VICC). Of course, similar analyses could be carried out for other seasons and waiting a few years until there are more data might help the statistical significance of the results (assuming the trends continue).

TRENDS IN TEMPERATURE, SALINITY, WATER COLUMN STABILITY AND MIXING DEPTH IN THE OPEN GULF OF ALASKA

H. Freeland, Institute of Ocean Sciences, Fisheries and Oceans Canada

Introduction

Freeland (1990), hereinafter F90, showed evidence, based on daily observations of sea-surface temperature at lighthouse stations around the coast of British Columbia, that the coastal ocean was warming. Seven years later, this problem was revisited by Freeland et al. (1997), hereinafter F97. In F97 the warming problem was re-examined with longer time series and it was shown that though some changes had occurred the essential story had remained unchanged. F97 also examined trends in salinity and included Ocean Station Papa in the analysis. It was shown that significant freshening trends existed, in addition to the warming trends, with both of these contributing to decreasing sea-surface density. Assuming that trends in deeper waters were weak this must imply steadily increasing barriers to mid-winter mixing. The F97 paper then examined the mid-winter mixed layer depths at Ocean Station Papa and showed that indeed the mid-winter mixed layer was getting shallower at the surprisingly large rate of 58 ± 28 metres per century. It was recognised that this was a very large rate of decline that simply could not be sustained for a long time. In two centuries such a trend would completely eliminate the mid-winter mixed layers, an option that must be extremely unlikely. F97 also made use of data from a few profiling floats that had been launched near Ocean Station Papa.

A detailed reanalysis of coastal stations to review the results of the F90 is difficult because so many of the coastal sampling stations have been terminated. However, a significant number remain and we will re-examine three of those stations. Further, the sampling frequency along the line of oceanographic stations known as Line-P, extending from the mouth of the Juan de Fuca Strait to Ocean Station Papa at 50°N and 145°W , has also decreased and that makes a direct comparison with F97 also problematic. Fortunately, a large array of floats has been maintained in the Gulf of Alaska as part of the Argo project since 2002, and this can be used to make up the recent deficits in shipboard sampling along Line-P, especially at Ocean Station Papa.

This report re-examines the temperature and salinity trends reported in F90 and F97. It will be shown that though the specific numbers have changed the basic story has not. The paper will then examine the variation in trends with depth and show that, with 15 years more data, the conclusions in F97 concerning the increasing stability of the water column remain valid. Finally, the time series of mixed-layer depths will be extended to the present time. We will see that a statistically significant shallowing trend remains, though the trend is smaller than the 58 metres/century reported in F97.

British Columbia Shorestations

Sea-surface temperature and salinity have been sampled daily along the Pacific Coast of Canada since 1935. At a few locations in inside waters sampling began much earlier, but these stations will not be discussed here. The paper F90 reported temperature trends at 19 lighthouse stations and since that time 6 of those stations have been terminated as the lighthouses have been automated. F97 was mainly concerned with the effects of changes on the formation of ocean mixed layers and so focused on only three of the lighthouse stations that were well exposed to the open sea. Here we will re-examine those three stations. 95% confidence intervals are quoted and the method for allowing for autocorrelation in the time series is described in Masson and Cummins (2007) which is itself based on the methods outlined by von Storch and Zwiers (1999).

Table 3: Temperature (top panel) salinity (middle panel) and density (bottom panel) trends at three lighthouse stations well exposed to the open ocean. F90 and F97 are the trends reported in the previously cited studies.

Temperature Trends ($^{\circ}\text{C}$)			
Site	F90 ($\text{century}^{-1} \pm 95\%$)	F97 ($\text{century}^{-1} \pm 95\%$)	This Study ($\text{century}^{-1} \pm 95\%$)
Amphitrite Point	0.87 ± 0.68	1.01 ± 0.69	0.75 ± 0.53
Kains Island	0.19 ± 0.67	0.61 ± 0.77	0.52 ± 0.57
Langara Island	0.53 ± 0.78	0.95 ± 1.15	0.78 ± 0.59

Salinity Trends (pss)			
Site	F90 ($\text{century}^{-1} \pm 95\%$)	F97 ($\text{century}^{-1} \pm 95\%$)	This Study ($\text{century}^{-1} \pm 95\%$)
Amphitrite Point	Not reported	-1.00 ± 0.51	-0.71 ± 0.41
Kains Island	Not reported	-0.91 ± 0.61	-0.48 ± 0.44
Langara Island	Not reported	-0.82 ± 1.15	-1.40 ± 0.32

Density Trends (σ_t , kg.m^{-3})			
Site	F90 ($\text{century}^{-1} \pm 95\%$)	F97 ($\text{century}^{-1} \pm 95\%$)	This Study ($\text{century}^{-1} \pm 95\%$)
Amphitrite Point	Not reported	-0.95 ± 0.19	-0.67 ± 0.34
Kains Island	Not reported	-0.81 ± 0.24	-0.46 ± 0.38
Langara Island	Not reported	-0.78 ± 0.42	-1.21 ± 0.29

Table 3 illustrates the trends observed at three lighthouse stations well exposed to the open Pacific Ocean. The F90 study only examined temperature trends but also reported trends for a large number of other stations. Other stations have also been examined recently both by this author and also as part of a paper by Cummins and Masson (unpublished data). The new trends shown here are consistent with those shown by Cummins and Masson. One significant change is the rather large trend in salinity that has developed at Langara Island. When the salinity started to decline rapidly samples were obtained to check that the sampling protocols were being observed and no problem was detected. Further the onset of a rapid decline is also occurring at another nearby light station at Bonilla Point.

The data shown in Table 3 indicate that the temperature trends shown in 1990 continued through the 1997 report without significant change, and are continuing through the end of 2011. We see consistently around the coast of British Columbia trends towards warmer and fresher waters. Warming and freshening trends both contribute to decreasing surface density and so it is not surprising that the trends

in density and salinity show higher significance levels than temperature (Figure 20). There is also a tendency for short-term variations in temperature to be anti-correlated with short-term variations in salinity and so are density-compensating. The result is that the time series of density has a lower background noise level than do either temperature or salinity. This also results in higher significance levels.

The observations of the freshening trends shown in Table 3 are also broadly consistent with the trends in the Gulf of Alaska shown by Durack and Wijffels (2010) and Durack et al. (2012) in their global analyses.

Line-P Trends in Temperature, Salinity and Density

Before we examine trends along Line-P it is necessary to understand some of the history of sampling along that line. Systematic ocean observations at Ocean Station Papa itself began in 1949, but these were largely observations using mechanical bathythermographs and the data are not very useful. In 1956 systematic sampling began using the regular trips completed by the Weatherships CCGS Vancouver and CCGS Quadra between the mouth of the Juan de Fuca Strait and Ocean Station Papa at 50°N and 145°W, producing surveys at approximately 6-week intervals. In the early years sampling was restricted to a set of 13 stations shown by the large dots in Figure 18. In 1980 the Weathership program was terminated and sampling was continued using various research vessels. As part of this change the number of stations was increased to 27 but sampling was significantly less frequent. Gradually, funding cuts have resulted in fewer and fewer surveys per year. At present, research vessels complete surveys along Line-P three times per year, typically in February, June and September. After 1981 sampling was carried out at 27 stations of which the original 13 stations were a sub-set (Ocean Station Papa was designated as P26 rather than P13).

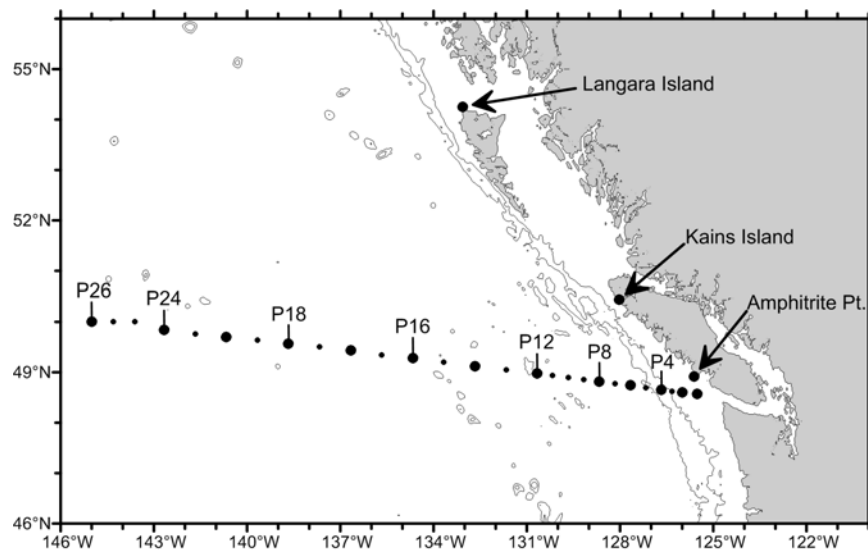


Figure 18: This map shows the principal locations used in the report. Amphitrite Point, Kains Island and Langara Island are lighthouses where sea-surface temperature and salinity have been observed daily since the mid 1930s. The dots in the offshore regions show the locations of stations comprising Line-P. Station P26 is more commonly known as Ocean Station Papa.

The various changes in sampling strategies are clearly evident in the upper panel of Figure 19. The dots on Figure 19 show only when sampling has been carried out in any month/year combination at Ocean Station Papa. Some of the other stations are sampled better than is P26, for example the inshore stations

P1 and P2 are very well sampled in most months, and some stations, P14 being a good example, are not sampled as well as P26 is sampled. This makes it difficult to estimate trends uniformly as the data coverage varies so much from station to station and especially from one month to the next. However, since 2001 the international Argo program has been supplying a wealth of data in the upper 2000 metres of the Gulf of Alaska. For the purposes of this paper we will view the start of the Argo era in January 2002, continuing to the present time. For any particular station along Line-P we can draw a large circle around that station and accept, for any month, all Argo profiles falling inside that circle, then use those observations to interpolate onto the Line-P station using objective analysis as described by Bretherton et al. (1976). For this particular application data were accepted into the interpolation process that lay within 800 km of the interpolation location and interpolation was carried out using a Gaussian autocovariance function with a decay scale of 400 km. This allows us to simulate Line-P stations for every month of each year starting in 2002 as shown in the lower panel of Figure 19. The data selection process provides a large range in the number of profiles within 800 km, varying from a low of 20 to a maximum of about 70. Sections of temperature and salinity anomalies have been computed and compare well with those computed directly from shipboard surveys. This interpolation process was completed for 11 of the 13 original Line-P stations only; the two neglected being the two stations closest to the coast, since including these would require extrapolating beyond the Argo array. The sampling at the two innermost stations was judged to be excellent without the assistance of Argo. All of the following results will be based on analyses at the original 13 stations only because the time series for the other stations (the small circles on Figure 18) are substantially shorter.

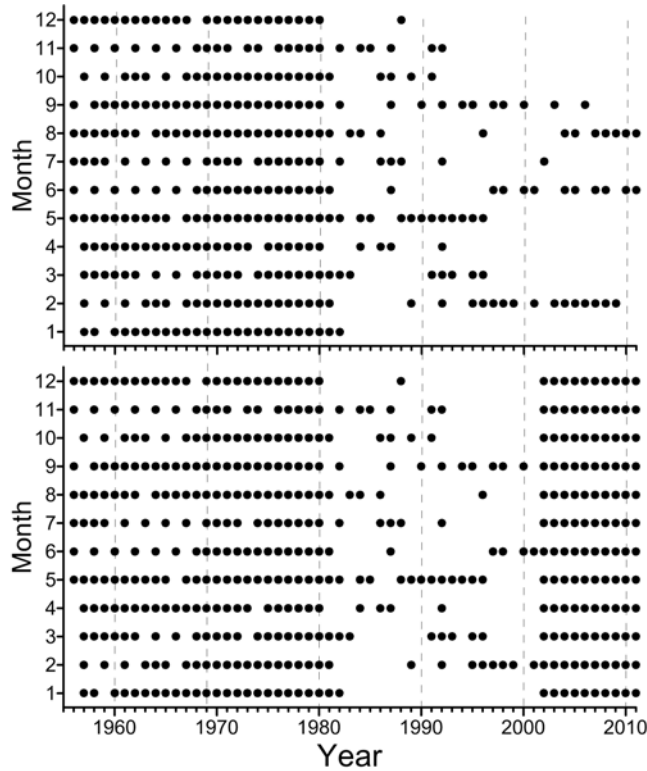


Figure 19: Sampling at Ocean Station Papa (P26) in the upper panel. In the lower panel the distribution of samples as shown after the sampling along Line-P is augmented with interpolations using Argo data.

Figure 20 shows the distribution of trends in temperature, salinity and σ_t plotted against depth in the top 200 metres of the water column and listed as the appropriate units per century.

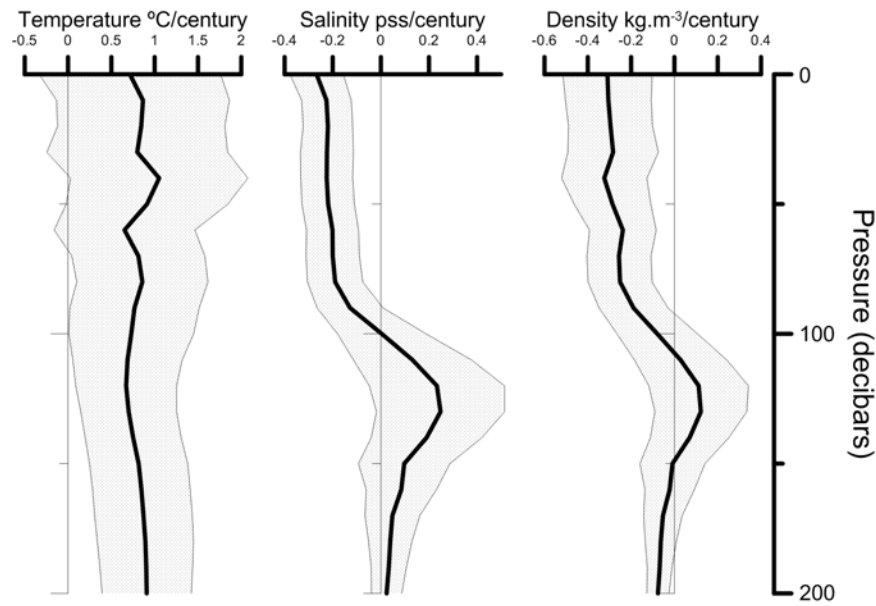


Figure 20: Trends in scalar properties computed at station P26 versus depth.

The shaded bands show the 95% confidence bounds and it is interesting that though the warming trend is persistent, in the top 100 metres it is generally not significant at the 95% confidence level. The salinity trends by contrast are highly significant in the top 100 metres and so are the density trends. Below 100 metres the density trend is smaller and not significantly different from zero and hence we conclude that the density contrast between the surface waters and water below 100 metres is increasing. Another way of stating this is that the potential energy of the water column is decreasing. It follows from this that we require an increasing work rate from mid-winter winds to produce any given mixed-layer depth. Or, if the rate of working by the winds remains unchanged, then we require that mixed layers are getting shallower. This was the important result from the paper F97, and inevitably must result from this paper. The important remaining questions are, by how much are mixed layers changing and how are the changes distributed?

To compute the trends in Figure 21, σ_t was computed for each month for which data exist at station P26, i.e. at each of the dots in Figure 19. The trend was then computed for each month. The number of years for which data exist varies from one month to another; also, the amount of variability is significantly variable from one season to another. Given the observations shown in Figure 20 that the density trend is fairly constant between the surface and a depth of about 80 metres, then decreases to zero between 80m and 100m, the density was averaged over the top 80 m of the water column before the trends in Figure 21 were computed. The shaded bands again are 95% confidence levels. We see that the trend towards decreasing density is evident in all months of the year, though not always passing the significance test. The wider confidence bands in the late summer months are due primarily to an increase in natural variability. The plot suggests that the observed trends are significantly different from zero in 8 of the 12 months, but some of these carry very marginal significance. The trends are most clearly distinguishable from zero in the winter months, November through March, when the surface mixed layer is always deeper than the base of the layer (80 metres) used for averaging the density trends in Figure 21.

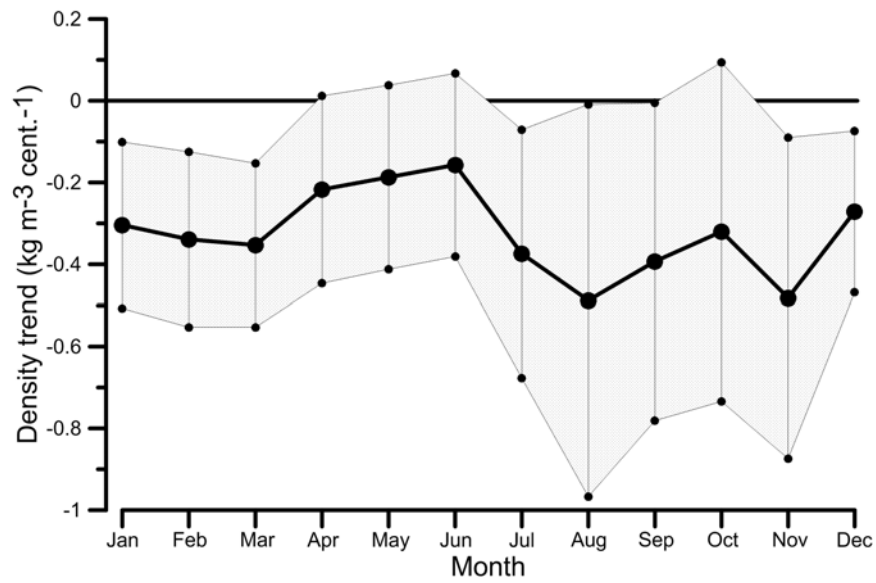


Figure 21: Monthly density trends (averaged over the interval 0-80 dbar) at station P26.

Figure 22 shows the distribution of the trend in σ_t versus depth and distance along Line-P. For this display data are used irrespective of month, which is sensible given the observations in Figure 21 that the density trends are present in each month. For this computation we used only the data from the original 13 stations, shown by the large circles in Figure 18. The data from the other stations has a significantly shorter duration and in particular miss the early period of frequent sampling which is a deficit that Argo cannot correct.

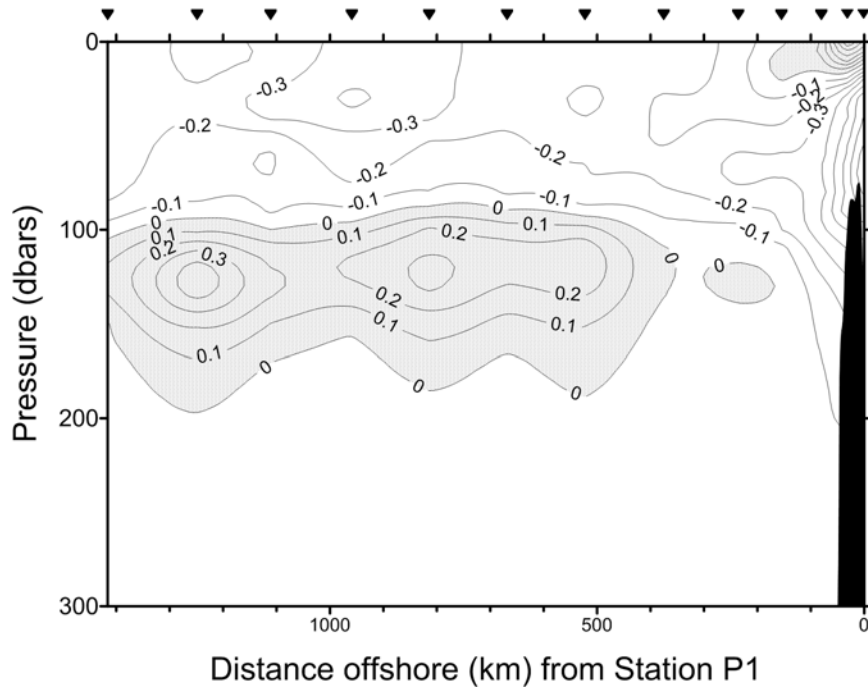


Figure 22: Density anomaly trends ($\text{kg m}^{-3} \text{ century}^{-1}$) along Line-P averaged over all months of the year, the symbols above the top axis indicate the location of the stations used.

In Figure 22 we see essentially the same behaviour at all stations as is illustrated at Ocean Station Papa (a.k.a. P26) in Figure 20. Thus we conclude in general from our survey of trends seen by the lighthouse stations and the Line-P observations that warming and freshening are continuing along all of Line-P and in the surface waters along the outside coasts of British Columbia. The freshening, in particular, is the dominant driver towards less dense near-surface waters, but this tendency does not persist below about 100 metres depth. Thus we conclude that, in at least the bulk of the Gulf of Alaska, the density contrast between near-surface waters and deeper waters is increasing. In other words the potential energy of the water column is decreasing everywhere in the Gulf of Alaska. This is in agreement with the observations made recently by Durack and Wijffels (2010) and Durack et al. (2012). In the latter paper Durack et al. make a strong case for the driving force of this change being a strong intensification of the global hydrological cycle yielding freshening of surface waters at high latitudes and increasing salinity at low latitudes.

It remains now to examine the effect of these changes on the development of the mixed layers in the Gulf of Alaska and the effects on the potential energy of the water column.

Line P trends in mid-winter mixed layer depth

There are a very great many papers written describing different methods of representing the continuous vertical profiles we see in the ocean as a two-layer system. For example, Li et al. (2005) use a method first described by Kara et al. (2000) which claims to be an objective method. It is similar to many other methods in that it requires the specification of a threshold change that is used to detect the depth of the mixed layer. A different approach was described by Thomson and Fine (2003) which uses neither a threshold nor conservation of integral properties of the water column. In this case we note that certain properties of the ocean need to be conserved when we make the transition from a continuous profile to a two-layer system. Specifically, when a representative layer depth, h , is determined then the potential energy and total mass of the 2-layer representation must equal that of the continuous profile. So with that in mind let us explore how we would take a continuous profile of the density anomaly $\sigma_t(z)$ and reduce it to a two-layer system where shallow and deep values of σ_t , call them σ_s and σ_d respectively are separated by a mixed layer of depth h . All computations are made relative to a deep reference level $H = 250$ decibars.

Following Ladd and Stabeno (2012) we define a parameter χ proportional to the potential energy of the water column as:-

$$\chi = \int_{-H}^0 (\sigma_t(z) - \langle \sigma \rangle) z dz$$

where

$$\langle \sigma \rangle = \frac{1}{H} \int_{-H}^0 \sigma_t(z) dz.$$

If we then set these two integral values equal to the values that would be obtained in the 2-layer representation then:-

$$\langle \sigma \rangle = [h\sigma_s + (H-h)\sigma_d] / H$$

and

$$\chi = [h^2(\sigma_s - \langle \sigma \rangle) + (H^2 - h^2)(\sigma_d - \langle \sigma \rangle)] / 2.$$

Substituting between these two equations we obtain an expression for the mixed layer depth of:-

$$h = \frac{2\chi}{H(\langle \sigma \rangle - \sigma_s)}.$$

Evidently we need one more constraint to determine the mixed-layer depths from the integral constraints and, somewhat arbitrarily, we choose to set σ_s , the surface value of σ_t , equal to the average value over the top 60 metres of the water column. This is selected because the depth of 60m is about the greatest depth one can choose without ever coming close to the shallowest mixed-layer depth ever observed in winter months, which is about 90 metres. This will not work well during the summer months when the mixed-layer depths can become as shallow as 20 metres, so in all that follows it will be assumed that this method applies only to mid-winter mixed layer depths.

Figure 23 shows the results of this computation. In the upper panel the mid-winter mixed-layer depths are plotted where “mid-winter” is defined as an average over the months November to March inclusive. As part of the computation of the mixed-layer depth an integral quantity that is proportional to the potential energy of the water column is computed, and that is plotted in the lower panel. The dashed lines show the regression slopes. For the MLD the slope indicated a shallowing trend of 15.4 ± 15.2 decibars/century and the PE-like parameter shows a declining trend of 410 ± 342 units/century. The error bars listed here are the 95% confidence levels, each of the parameters just barely being significant at that level. Both are significant at the 90% confidence level (± 12.7 and ± 286 respectively).

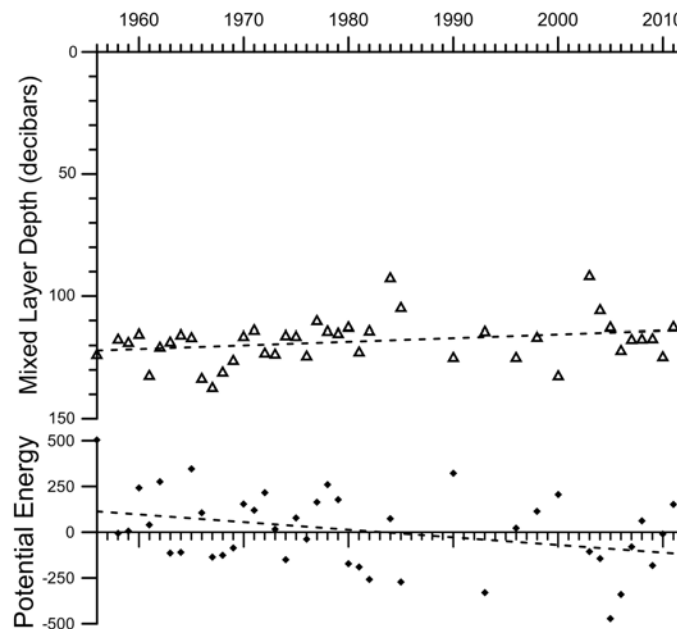


Figure 23: The mid-winter mixed-layer depths at station P26 (Ocean Station Papa) in the upper panel and a parameter proportional to the potential energy of the water column.

Discussion and Summary

This paper has compared trends in temperature and salinity in several long time-series around the coast of British Columbia and into the Gulf of Alaska with computations published 15 and 22 years ago. The original conclusion in earlier papers, that the waters of the Gulf of Alaska are both warming and freshening, remains valid. The temperature trend is weak and generally does not pass significance tests, but the salinity trend in the upper ocean is robust and does pass 95% significance tests. The specific trends computed have changed from the earlier papers, but not sufficiently to change the essential conclusions. Additional to the conclusions of the earlier papers we now conclude that the surface freshening extends over almost all of the length of the Line-P series of oceanographic stations into the centre of the Gulf of Alaska.

It is clear from the trends computed that the changes in potential energy of the water column in the Gulf of Alaska are primarily being driven by changes in salinity rather than changes in temperature. That conclusion was also reached in F97, but that paper could only speculate rather vaguely about the possible cause. Durack and Wijffels (2010) look at a global analysis of salinity in the upper ocean and come to the same conclusion in the Gulf of Alaska. The centre panel of Figure 5b in Durack and Wijffels shows a contour of -0.2 pss/50 years passing close to Ocean Station Papa. This is not far from the value of -0.3 pss/century shown in Figure 20 of this paper. The Durack and Wijffels (2010) paper shows a clear pattern of changing salinity that is close to the distribution of actual salinity. Essentially, all low-salinity areas of the oceans are getting fresher and the high-salinity areas are getting saltier, a scenario described by the authors as “the rich get richer”. In Durack et al. (2012) modelling studies are used to show that this is completely consistent with an acceleration of the global water cycle between 1950 and 2000, an idea that was only vaguely speculated about in F97.

A simple box model is enlightening as it shows how little additional freshwater is needed to change the Gulf of Alaska in the way we describe. Consider a vertical column of water at Ocean Station Papa of height $H = 700$ decibars. At Station Papa we compute a trend in salinity, averaged over the top 700 decibars of the water column of -3.9×10^{-4} pss/year. If we ignore horizontal advection the rate of change of total salt in the water column is given by $H \frac{dS_0}{dt} = w(S_B - S_0) - S_0 R$, where S_0 is the average salinity of the water column, S_B is the salinity at the base of the column, w is a deep upwelling velocity and R is the excess of precipitation over evaporation. So in steady state we must have $w(S_B - S_0) - S_0 R_0 = 0$. Now let us keep the deep vertical velocity constant and perturb this steady state by increasing R , so $H \frac{dS_0}{dt} = w_0(S_B - S_0) - S_0(R_0 + \delta R)$ and so $H \frac{dS_0}{dt} = -S_0 \delta R$. Setting $H = 700$ metres, S_0 at Station Papa is 33.77 pss and the rate of change in salinity at -3.9×10^{-4} pss/year we find a needed value of $\delta R = 0.81$ cm/year. This is not a very large change in total rainfall and is not measurable by any available technique except inference from salinity changes.

The results of a persistently shallowing mixed layer are potentially profound, leading to changes in the ocean environment that can have effects on organisms. Two effects spring to mind immediately. If we assume that phytoplankton is cycled between the surface and the base of the mixed layer by turbulent motions, then as the mid-winter mixed layer shallows it will spend a larger fraction of its time in the photic zone and able to use nutrients as we approach spring. However, as the base of the mid-winter mixed layer becomes shallower we must also expect the supply of nutrients to decrease. It seems important, therefore, that we continue to monitor the evolution of the upper ocean in response to global climate change.

TRENDS IN SEA LEVEL

B. D. Bornhold¹ and R. E. Thomson². ¹Coastal and Ocean Resources Inc., ²Institute of Ocean Sciences, Fisheries and Oceans Canada

Pacific Sea Level Trends

The four main mechanisms which determine relative sea level – the local or regional position of the ocean surface with respect to the land - are:

- changes in global ocean volume due to the melting of mountain glaciers, grounded polar ice caps and continental ice sheets;
- changes in ocean volume resulting from temperature and salinity effects on water density;

- regional volume redistribution due to changes in atmospheric and oceanic circulation, such as shifting locations of major atmospheric pressure systems and ocean gyres; and,
- local changes due to vertical land motions associated with recovery from glacial loading and regional gravitational enhancement during the last Ice Age, compaction (sinking) of deltaic areas, and tectonic processes resulting from interactions among the earth's crustal plates.

While the general nature of these mechanisms is well-understood, many details are not. There has been considerable examination of these mechanisms over the past few years, with particular attention focused on the contribution from the melting of large continental ice sheets, a significant element in determining mean global (eustatic) sea level rise.

Thomson et al. (2008) presented an in-depth examination of the trends in sea levels along the British Columbia coast and made projections regarding possible future sea level scenarios for the end of the 21st Century. Using the best available information at the time, they provided sea level trend analyses for many British Columbia coastal communities and estimates of high, medium and low sea level rise by 2100. We shall not repeat the detailed discussions in that report but have updated some of the estimates to reflect the scientific advances which have taken place over the past four years.

Over the course of geologic time, the earth has witnessed sea level changes of several hundred metres, mostly in response to the growth and retreat of continental glaciers (with time scales of many thousands of years) and to varying rates of plate tectonic processes (for example, episodes of increased or decreased volcanic activity on mid-ocean ridges and deformation of continental margins as they cool or undergo compression related to subduction). Large tectonically induced sea level changes typically occur over time scales of tens of millions of years.

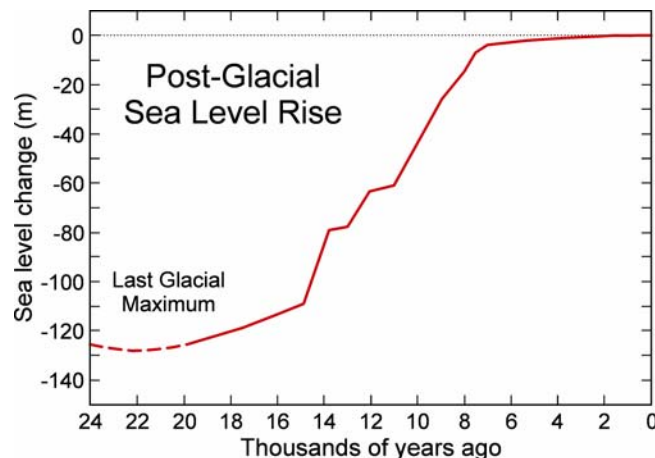


Figure 24: Post-glacial eustatic sea level rise.

During the last Ice Age, which reached a maximum about 21,000 years ago and started to rapidly warm about 18,000 years ago, sea levels globally were approximately 120 m lower than they are today. This is because a significant portion of the globe's water was moved from the oceans into continental glaciers. Between 15,000 and 7,000 years ago, sea levels around the world rose, on average between 13 and 14 mm per year, or about 75 cm during a person's lifetime (Figure 24). About 2,000 to 3,000 years ago globally averaged sea levels stabilized at about their present position.

Based on tide gauge measurements from around the world, we know that sea level globally has risen more than 20 cm since the late 19th century (Figure 25), equivalent to an annual sea level rise of about 1

mm per year in the early part of this period and more than 3 mm per year over the past two decades. These findings are supported by more precise satellite (altimetry) measurements that have collected since 1993 (Figure 26).

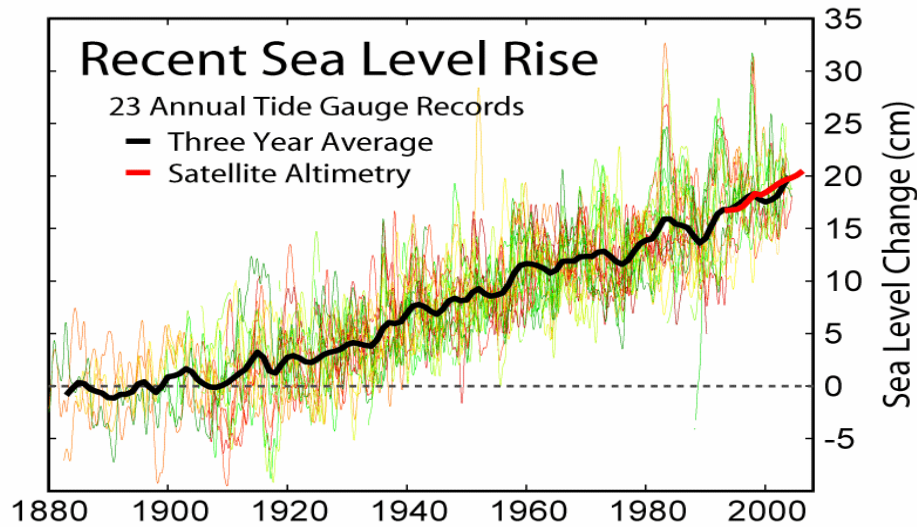


Figure 25: Global mean sea level change since the end of the 19th Century based on tide gauge records. Superimposed on the tide gauge curve is a shorter sea level curve (red line) beginning in 1993 that is based solely on satellite altimetry data (see Figure 26).

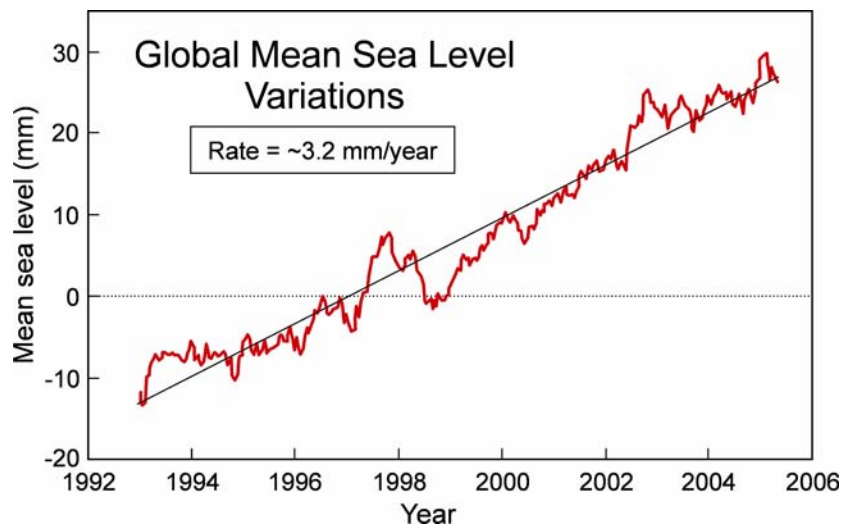


Figure 26: Global mean sea level change between 1993 and 2006 based on satellite altimetry (also plotted in Figure 25).

According to the IPCC (2007) report, more than half of the present 3.2 mm/year rise in globally averaged sea levels is the result of changes in volume due to heating of the upper ocean. Most of the remaining increase (about 1.2-1.6 mm per year) is the result of melting of glaciers in Antarctica, Greenland and mountain areas.

Superimposed on these global mean trends are regional and local influences resulting from changing ocean temperature and salinity, subsidence of land areas (e.g., the Fraser Delta), remnant glacial adjustment (uplift) Figure 27), and tectonically driven uplift (e.g., west coast of Vancouver Island).

These regional or local trends can effect quite different sea level rise trends over relatively short distances.

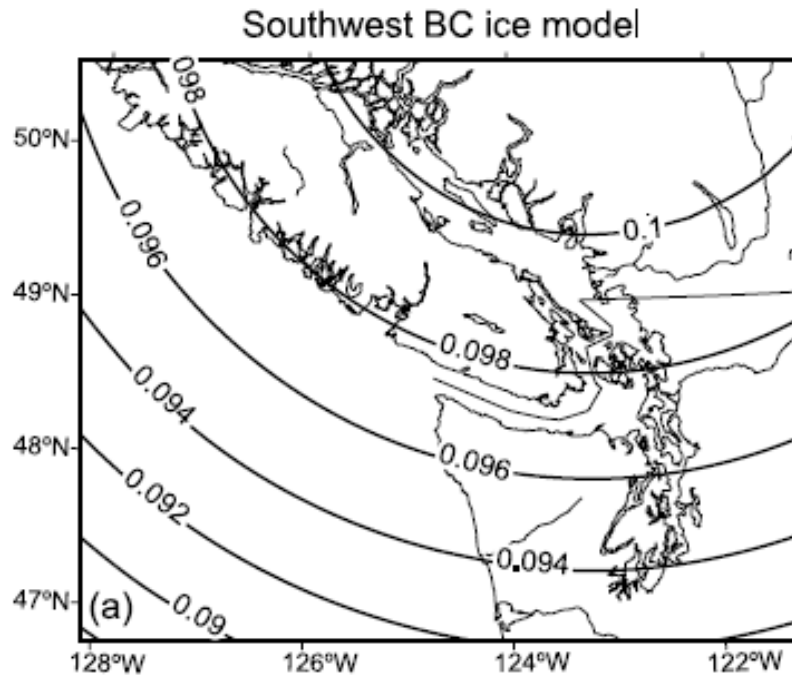


Figure 27: Continuing uplift (mm per year) of Vancouver Island and the adjacent British Columbia mainland resulting from the melting of glaciers during the last Ice Age (James et al. 2009).

In coastal British Columbia there remains a small effect of relative sea level fall resulting from the disappearance and unloading of glaciers from the landscape after about 18,000 ago (Glacial Isostatic Adjustment or GIA). Because of the generally low mantle viscosity in the region (Hyndman et al. 2005; James et al. 2009 and references therein), response to glacial unloading has been rapid. Today, rebound velocities are expected to be everywhere low (less than about 0.1 mm per year) along the British Columbia coast (Figure 27). In addition to the change in land level (uplift) due to the unloading of the crust with the removal of glacial ice, sea levels are affected by the gravitational effects of continental ice sheets on the adjacent sea water. This spatially varying “sea level fingerprinting” occurs because, as the ice disappears, relative sea levels fall at decreasing rates from highly glaciated areas to less glaciated areas (Mitrovica et al. 2001; Riva et al. 2010; U.S. National Research Council, 2012). Continued investigations of the spatial variability in this effect are taking place for the BC coast by the Geological Survey of Canada (T. James, pers. comm., June, 2012).

Coastal British Columbia is also affected by major, but spatially varying, tectonic forces which have a significant effect on relative sea levels. Along western Vancouver Island, for example, continued stress caused by the Juan de Fuca tectonic plate as it descends beneath North America results in annual uplift of the land (or fall in relative sea level) of about 2 to 3 mm per year (Mazzotti et al. 2008a, b) (Figure 28). This effect diminishes across Vancouver Island and the Strait of Georgia to near zero on bedrock areas near Vancouver. Similar rates of 2 to 3 mm per year have also been measured on parts of Haida Gwaii. The uplift of Vancouver Island is largely reversed during great (larger than Magnitude 9) earthquakes along the Cascadia subduction zone with subsidence of the land by 0.5 m to 2 m. These events occur approximately every 500 to 600 years with the last being on January 26, 1700.

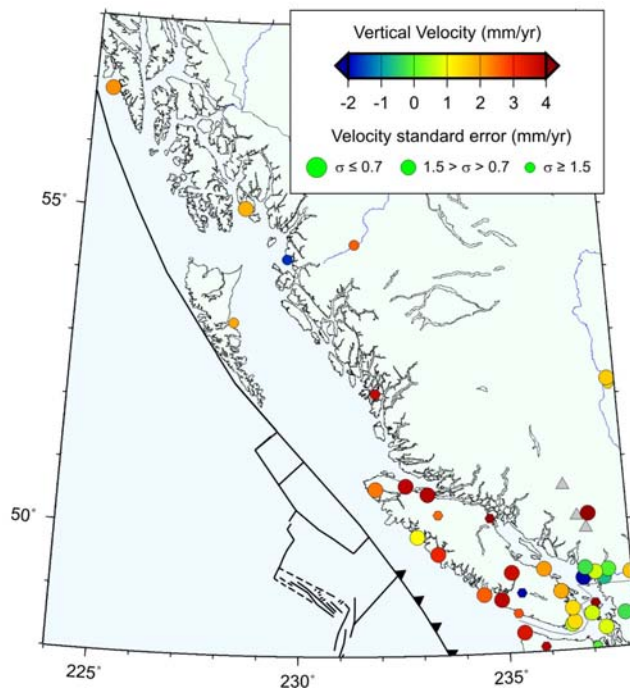


Figure 28: Annual rates of uplift (mm per year) of the land along coastal British Columbia. Note the high rates on southwestern Vancouver Island which diminish rapidly to the east to zero near Vancouver (Mazzotti et al. 2008a, b).

Mazzotti et al. (2008b) undertook a combined GPS-tide gauge study of relative and absolute sea level change in British Columbia and the northwestern U.S. Their careful and thorough analysis showed that mean absolute sea level (ASL) increased at 1.8 ± 0.2 mm/year in the region during the 20th Century, a value very close to other global mean sea level rise estimates. Between 1993 and 2003, however, ASL rates in the study area were found to be -4.4 ± 0.5 mm/year, in contrast to global estimates of +3.2 mm/year, reflecting regional decadal-scale climatic and oceanographic effects such as El Niño-Southern Oscillation (ENSO) and Pacific Decadal Oscillation (PDO).

On the Fraser Delta, on the other hand, the load of sediment is causing the delta to sink (or a rise in relative sea level) at rates of 1 to 2 mm per year (Mazzotti et al. 2008) (Figure 28, Figure 29). Although all major deltas in the world are compacting, the tendency for the land to sink is, under natural conditions, countered by new river-borne sediments being added to the surface of the delta. In the case of developed deltaic areas, such as those of the Fraser and Mississippi Rivers, human intervention (dredging, construction of training walls and dikes) results in the diversion of these sediments into deeper water away from the delta. Because of the slow response of the deltas to sediment loading, the deltas continue to sink long after the supply of sediment to their surface has been cut off. The rate of sinking observed for the Fraser Delta is further increased locally (to more than 3 mm per year) by very large construction projects, such as ferry terminals, airports or other port facilities, which add a further load and serve to further compact the sediments below; these higher rates decline over time and eventually reach the background levels of the rest of the delta region.

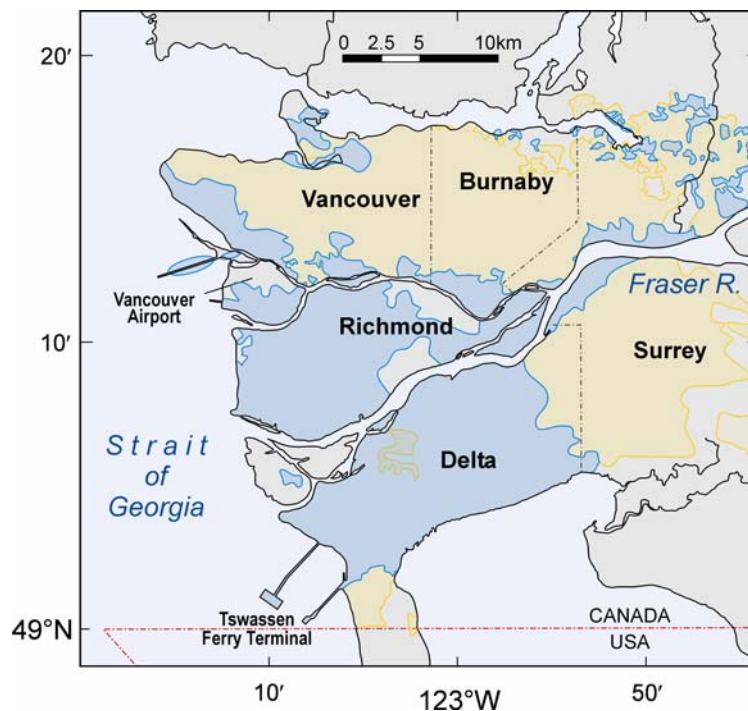
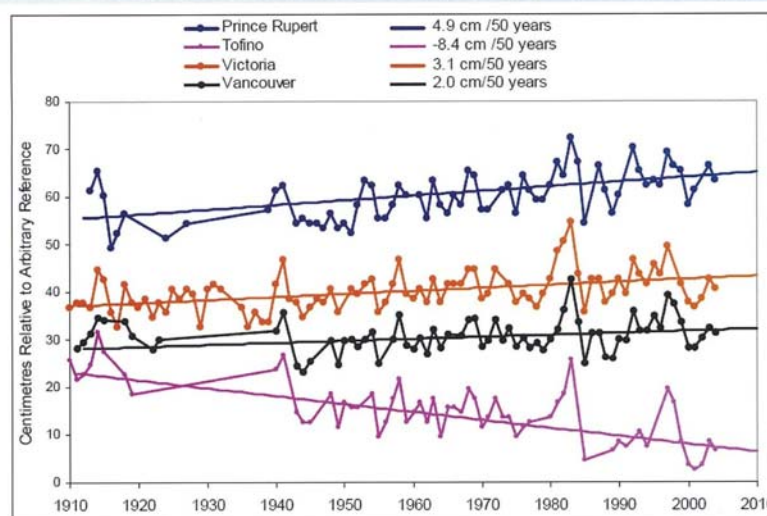


Figure 29: Map of Vancouver and the Fraser Delta showing areas of documented subsidence (sinking) (blue areas) on the Fraser Delta and more stable surrounding areas (yellow areas).

While there have been few studies of the steric effects on sea levels in the northeast Pacific, one investigation based on an extensive time series of water property profiles at Station “P” (50° N, 145° W) has revealed that between 1956 and 1986 there was an average 1.1 mm/year sea level rise, of which 67 % was due to increased upper ocean temperature and 33 % to decreased upper ocean salinity (Thomson and Tabata 1989). Since that time, further analysis to 2007 has shown an accelerated rate of steric sea level rise in the northeast Pacific, consistent with the globally accelerating sea level rise observed since 1993 in satellite altimetry data.

Historic Sea Level Change along BC coast to 2004



Source: Marine Environmental Data Service, Fisheries and Oceans Canada.

Figure 30: Changes in relative sea level along the British Columbia coast as measured by tide gauges between 1910 and 2004. (Kangasniemi 2009)

Figure 30 summarizes the relative sea level history at four locations on the British Columbia coast between 1910 and 2004 (Kangasniemi 2009). In contrast to Tofino, where sea level has been falling because of tectonic processes, sea levels at Victoria, Vancouver and Prince Rupert rose between 2 and 4.9 cm over 50 years. These rates are significantly less than long-term global sea level rise over the same period because of residual glacial isostatic and tectonic effects on the British Columbia coast.

Sea levels also vary on shorter time scales of days to decades (Abeysirigunawardena, unpublished data; Tinis, unpublished data). While past trends in the frequency and magnitude of short-term variability are not well known, it is expected that these trends will be altered as mean global and regional oceanographic conditions are altered. Atmospheric conditions can affect relative sea levels on daily to seasonal time scales, with amplitudes of 0.1 to 0.5 m arising from passing atmospheric low pressure systems and associated winds. Prevailing southeasterly winds in winter, combined with low atmospheric pressure, increase sea levels along the British Columbia coast by 0.1 to 0.3 m. Prevailing northwesterly (equatorward) alongshore winds in summer, combined with high atmospheric pressure and equatorward coastal currents, normally lower coastal sea levels by ~ 0.1 m.

Decadal-scale variability in regional sea level along the British Columbia coast associated with changes in alongshore currents, coastal water temperature and atmospheric wind and pressure conditions are primarily linked to El Niño-Southern Oscillation (ENSO) and Pacific Decadal Oscillation (PDO) fluctuations. Longer-term trends are linked to climate-induced changes in ice melt and steric effects arising from changes in upper ocean temperature and salinity. El Niño events occur every 2 and 7 years in the tropical Pacific region and last from 6 to 18 months. However, only major events (such as those in 1982/83 and 1997/98) have a pronounced impact on the British Columbia coast. The PDO and ENSO interact to intensify or diminish oceanographic effects in coastal areas. Since about 1976, ENSO events have become more intense and frequent with their effects lasting longer (Trenberth and Hurrell 1995; Timmermann 1999). Off the coast of Oregon, Washington and British Columbia, documented sea level changes related to ENSO can be in the range of 0.30 to 0.40 m above the monthly mean values. In the 1997-98 ENSO event, Hecate Strait had sea levels ~ 0.4 m higher than normal (Barrie and Conway 2002; Walker et al. 2007); it was even greater during the 1982-83 El Niño period (Figure 30).

Bromirski et al. (2012) point out that relative sea level rise along the west coast of the continental U.S. since 1980 has actually been less than global mean sea level rise. This is in contrast to the western tropical Pacific where relative sea level rise has been much higher than global mean rates. They attribute this departure from global mean values to "... a dramatic change in eastern boundary and basin-wide wind stress patterns after the mid-1970s climate regime shift". These changes suppressed sea level along western North America in an absolute sense and in relation to what would be expected during a warm phase of the Pacific Decadal Oscillation (PDO). Bromirski et al. (2012) state that "... future regional sea level changes across the North Pacific will depend on the magnitude of changes in the PDO and the trade wind mode, as well as other regional and basin-wide anomalies in wind forcing".

Annual changes in upper ocean temperature and salinity off British Columbia give rise to thermosteric and halosteric sea level changes of about 0.2 m. Clearly, as future run-off from coastal rivers changes and the temperature in the upper ocean increases, the magnitude and timing of these steric sea level cycles are also expected to change. These cycles are set against a broader regional sea level rise driven by more widespread warming and salinity changes. In the Strait of Georgia, salinity effects account for about 63 % of the observed sea level change and temperature about 37 %, reflecting the greater role of coastal run-off (R.E. Thomson, unpublished data).

Extreme sea level events that occur during the passage of intense storms have resulted in sea level up to one metre above the predicted high tide levels off western Canada. These elevations do not take into account run-up effects, which are controlled by local coastal and seafloor morphology, which can add significantly to the actual sea level heights experienced at a particular location. Since these extreme events are added to the sea level conditions at the time, clearly the most hazardous situation would be a major storm system occurring at high spring tide during an El Niño year when sea levels are elevated due to temperature effects. Some research has indicated that the frequency and intensity of major storms along the British Columbia coast have been increasing over the several decades. Some studies suggest that North Pacific storm intensities between 1940 and 1998 have increased (Graham and Diaz 2001) while others have shown that storm surge-related winds have increased in frequency since the 1970s (Abeyirigunawardena 2010); both of these changes are coincident with a regime shift in the Pacific Decadal Oscillation around 1976 and a possible ENSO regime shift during the 1970s.

Abeyirigunawardena (2010) examines the relationships among extreme events, climate change, climate variability and overall sea level rise in British Columbia. The following are some of her conclusions regarding the present and future trends in sea levels:

- Since the mid-20th Century, annual maximum sea level amplitudes at Prince Rupert have been increasing at about 3.4 mm/year, about twice the measured mean sea level rise in the area. This is attributed to enhanced storm conditions and to the influence of major ENSO events, particularly since the mid-1970s, in agreement with the observations of other researchers (e.g. Graham and Diaz 2001).
- Mean sea levels show highly significant correlations (both positive and negative) with many climate variability indices (e.g., PDO, ALPI, NOI, MEI) for the northern coastal waters of BC.
- Major regime shifts, as reflected by large simultaneous changes in the principal climate variability indices, are reflected in long-term changes in sea level in northern coastal BC. Eight out of 9 of the highest mean sea level events examined occurred after the mid 1970s PDO regime shift while 7 out of 9 of the lowest sea level events preceded it.
- Climate variability indices from preceding seasons cannot be reliably used to predict mean or extreme sea levels into the future.
- Decadal to interdecadal climatic variability is important in explaining the frequency and amplitude of extreme sea levels in southern coastal BC.
- Extreme winds are more frequent during ENSO cold phases (La Niña) than during warm phases on BC's inner coast. Regional sea levels are lower during these periods than during El Niño periods due to steric effects.

We question the last conclusion because changes in the alongshore wind strength and direction along the BC coast in winter change from markedly poleward during moderate to strong El Niño events to weaker poleward-prevailing winds during moderate to strong La Niña events. Because of the Coriolis effect, prevailing wind-driven poleward currents along the coast are balanced by an upward cross-shore tilt of the sea surface (prevailing equatorward currents are balanced by a downward cross-shore tilt). The weaker the poleward winds (cold phase) in winter, the lower the sea level set-up at the coast while the stronger the poleward winds (warm phase) in winter the greater the sea level set-up.

Northeast Pacific Projections

Projections of regional relative sea level change are the sum of the various factors identified above. Fundamentally they are based on global mean sea level projections upon which are superimposed:

- local and regional anticipated changes in land level due to residual glacial influences, tectonic uplift and subsidence;

- steric effects arising from changes in upper ocean temperature and salinity;
- anticipated trends in the frequency and magnitude of mid latitude storminess, ENSO, PDO, and other ocean-atmosphere phenomena.

Table 4: Estimates of thermosteric sea level rise from various sources (U.S. National Research Council 2012).

Source	Period	Depth Range (m)	Instrument Bias Corrections	Thermosteric Sea-Level Rise (mm yr ⁻¹)
IPCC (2007)	1961–2003	0–700 0–3,000	None	0.32 ± 0.12 0.42 ± 0.12
Domingues et al. (2008)	1961–2003	0–700 Full depth	XBT fall-rate bias	0.52 ± 0.08 0.72 ± 0.13
Ishii and Kimoto (2009)	1951–2005	0–700	XBT and MBT depth bias	0.29 ± 0.06
Kuo and Shum (personal communication, 2011) ^a	1955–2009	0–700	XBT and MBT depth bias	0.33 ± 0.01
Ishii (personal communication, 2011) ^b	1961–2008	0–700	XBT and MBT depth bias	0.39 ± 0.05
IPCC (2007)	1993–2003	0–700 0–3,000	None	1.5 ± 0.5 1.6 ± 0.5
Domingues et al. (2008)	1993–2003	0–700 Full depth	XBT fall-rate bias	0.79 ± 0.39 1.0 ± 0.40
Ishii and Kimoto (2009)	1993–2005	0–700	XBT and MBT depth bias	1.23 ± 0.30
Ishii (personal communication, 2011) ^b	1993–2009	0–700	XBT and MBT depth bias	0.80 ± 0.16
Church et al. (2011) ^c	1993–2008	0–700 Full depth	XBT fall-rate bias, ARGO pressure bias	0.71 ± 0.31 0.88 ± 0.33
Willis (personal communication, 2011) ^d	2005–2011	0–900	Biased ARGO data removed	0.48 ± 0.15

Since publication of the Thomson et al. (2008) report, there have been changes in global sea level projections related to the contribution of meltwater from the Antarctic and Greenland ice sheets. It is generally agreed that these contributions had been substantially underestimated in projections of the IPCC (2007) (Figure 31). IPCC estimated that land ice melting accounted for about 40 % of sea level rise whereas more recent estimates suggest that it probably accounts for about 65 % of the rise (U.S. National Research Council 2012).

In addition to the IPCC's underestimation of glacial ice's current volumetric contribution to sea level rise, it also now appears, due to instrumental biases, that it also overestimated the thermosteric contribution; it had previously been concluded that recent rates of thermosteric sea level rise were significantly higher than the long-term average rate. Recent corrections show that the two rates are actually similar (U.S. National Research Council 2012). As shown in Table 4, IPCC (2007) indicates nearly a five-fold difference between the long-term thermosteric contribution and the recent thermosteric contribution; other estimates, with appropriate corrections, show a much closer agreement between the two values.

Since 2008 there have also been relatively small modifications to our understanding of other sea level contributions such as impoundment of water behind dams, extraction of groundwater, and various post-glacial rebound effects such as sea level “fingerprinting” (see above). In particular, Wada (2012) has

shown that changes in groundwater extraction and reservoir storage since 1990 has led to a net 0.25 mm/yr rise in global mean sea level; if the trends for greater exploitation of groundwater and reduction in dam construction and water storage continue, this contribution to global sea level rise could increase during the 21st Century (U.S. National Research Council 2012).

Projections of sea level change fall into two broad approaches – semi-empirical and model-based. The model-based approach of the IPCC (which was based on an imperfect understanding of ice and precipitation dynamics) yielded much lower projections of sea level rise for the 21st Century than empirical estimates based on actual observations of conditions in Greenland and Antarctica.

Depending on the model used and the greenhouse gas emission scenario assumed, there are presently several different estimates of projected global mean sea level change. The following is a summary of these based on 2011-2012 publications from several sources.

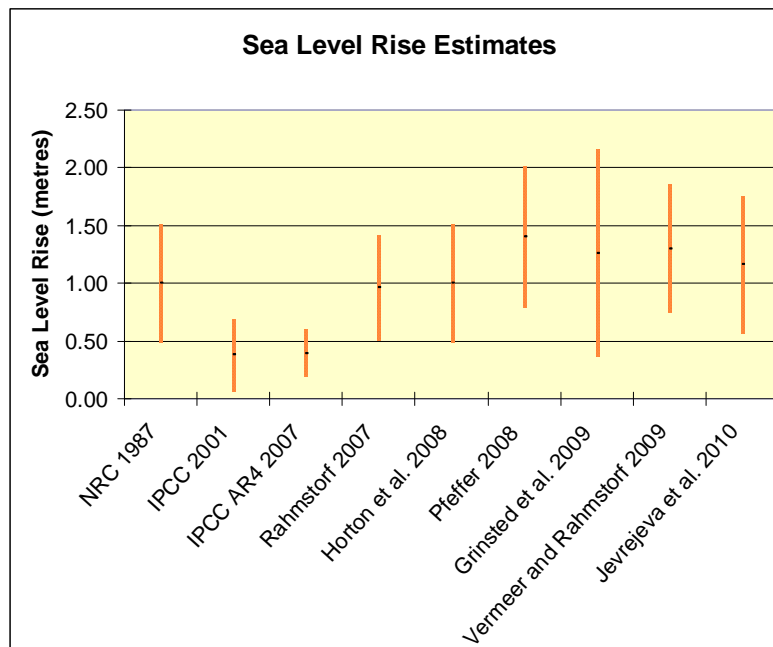


Figure 31: Comparison of global mean sea level rise estimates from various sources based on data from Rahmstorf (2010) and U.S. Army Corps of Engineers (2011).

Jevrejeva et al. (2012) state that the most likely estimates for 2100 global sea level rise (referenced to 2000) fall into the range 0.57 to 1.10 m (the 5 % and 95 % limits are 0.36 and 1.65 m). The authors point out that these estimates are lower than their previous estimates (Jevrejeva et al. 2010) presented in Figure 31. Rahmstorf (2012) references several other studies and their projections: specifically, the Delta Commission of the Dutch government gives an upper limit of 1.10 m (Vellinga et al. 2009); the Scientific Committee on Antarctic Research (SCAR 2009) cites 1.4 m as a maximum; the Arctic Monitoring and Assessment Programme (AMAP) presents a range from 0.90 to 1.60 m (AMAP 2011); and the U.S. Army Corps of Engineers (2011) presents “low”, “medium” and “high” scenarios of 0.5, 1.0 and 1.5 m for civil works planning purposes relative to 1992 levels (Figure 32) (note that sea levels in 2000 were about 0.026 m higher on average than in 1992). In the U.S. National Research Council’s (2012) report on sea level rise for California, Oregon and Washington, they assume global mean eustatic sea level rise by 2100 of 0.50 to 1.40 m (mean 0.827 ± 0.016 m).

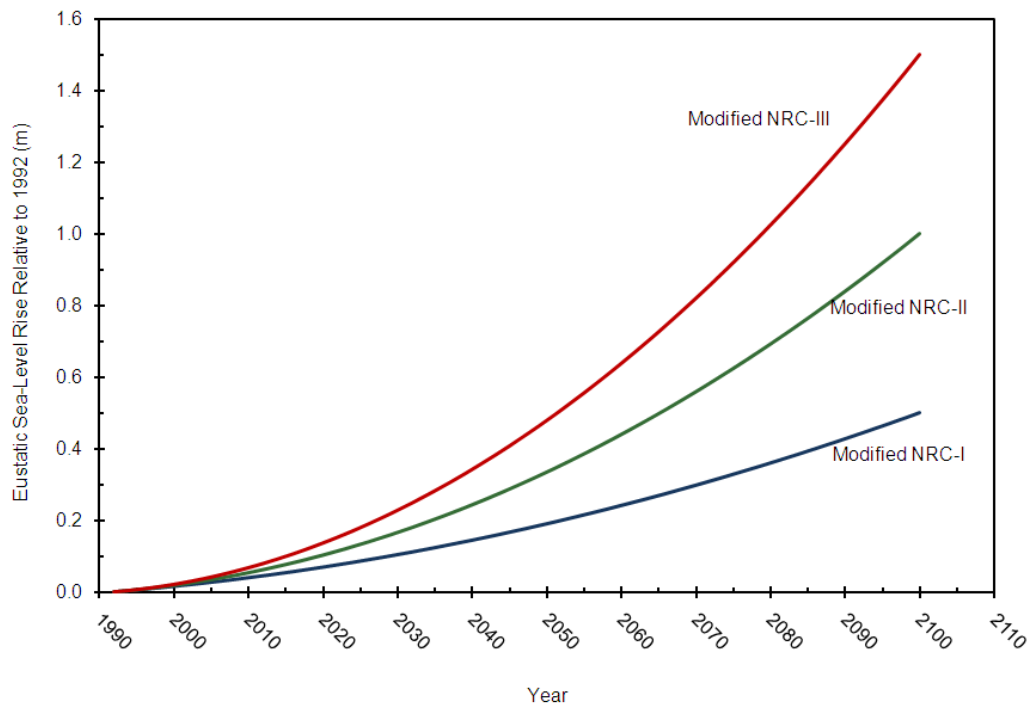


Figure 32: Projected mean global sea level change during the 21st Century presented as low, medium and high scenarios relative to 1992 (U.S. Army Corps of Engineers 2011).

While there remain many uncertainties with the above projections, it would appear that reasonable estimates for “low”, “medium” and “high” sea level rise relative to 2000 levels are 0.7 m, 1.1 m and 1.4 m. Using these revised values for global mean sea level rise at the end of the 21st Century, we have re-calculated the projections of relative sea level change for the British Columbia coast using the 2008 methodology of Thomson et al. (2008). Table 5 presents the results for the Strait of Georgia, the Fraser Delta and western Vancouver Island, including the western entrance to Juan de Fuca Strait. We note that the U.S. National Research Council (2012) report concludes that expected relative sea level rise by 2100 at the mouth of Juan de Fuca Strait would be about 0.65 m, compared to our estimated mean of 0.83 m.

Table 5: Projected relative sea levels for year 2100 compared to 2000, for the Strait of Georgia, the Fraser Delta and the west coast of Vancouver Island (modified after Thomson et al. 2008).

Source	Mean (m)	Low (m)	High (m)
<i>Long-term global and regional trends</i>			
Global Eustatic	1.10	0.70	1.40
Steric (Strait of Georgia)	0.076	0.063	0.088
Steric (northeast Pacific)	0.034	0.028	0.040
<i>Vertical Land Motion – Str. of Georgia</i>			
Tectonic	0.0	-0.05	0.05
Subsidence – Fraser Delta	0.30	0.23	0.37
<i>Vertical Land Motion – West Coast Vancouver Island</i>			
Tectonic	-0.30	-0.23	-0.37

TOTAL – Strait of Georgia	1.18	0.76	1.49
TOTAL – Fraser Delta	1.48	0.99	1.86
TOTAL – West Coast Vancouver Is.	0.83	0.50	1.07
<i>Amplitudes of Variation about Trend</i>			
Seasonal steric height	0.15	0.10	0.25
Seasonal atmospheric pressure	0.15	0.05	0.50
Seasonal winds and currents	0.15	0.10	0.25
Storm surges	0.40	0.10	1.00
Major ENSO steric height	0.50	0.30	1.00
Major ENSO atmospheric pressure	0.10	0.0	0.30

Table 6 presents a summary of anticipated sea level changes at various British Columbia communities for a revised mean, low and high projected eustatic change of 1.1, 0.7 and 1.4 m by 2100. The non-eustatic components used in the table are derived from local trends obtained using regional tide gauge and GPS time series.

Table 6: Sea level rise at the end of the 21st Century relative to 2000 for various British Columbia communities based on mean, low and high projected eustatic changes of 1.1, 0.7 and 1.4 m by 2100. Regional changes are derived using observed trends in both tide gauge and GPS data series.

Location	Mean (m)	Low (m)	High (m)
Prince Rupert – tide gauge	1.05	0.65	1.35
Prince Rupert - GPS	1.26	0.86	1.56
Nanaimo - GPS	0.91	0.51	1.21
Victoria – Tide gauge	0.99	0.59	1.29
Victoria - GPS	0.97	0.57	1.27
Vancouver – Tide Gauge	0.99	0.59	1.29
Vancouver - GPS	1.13	0.73	1.43

Thus, under these new estimates of mean eustatic sea level rise, all locations in British Columbia will experience sea level rise during the 21st Century. Sea level rise will range from a possible low of **0.50 m** along western Vancouver Island to a high of **1.86 m** on the Fraser Delta.

An area of research which is only now receiving greater attention relates to climatically induced circulation changes in the North Pacific and their consequences for regional sea levels. Bromirski et al. (2012) indicate that sea levels in the North Pacific will depend to a great extent on the magnitude of changes in the Pacific Decadal Oscillation as well as basin-wide and regional wind forcing anomalies. They suggest that the anticipated weakening and poleward expansion of Hadley Cell circulation, which is expected to accompany global warming, will lead to reduced trade wind strengths and higher sea levels along the West Coast of North America.

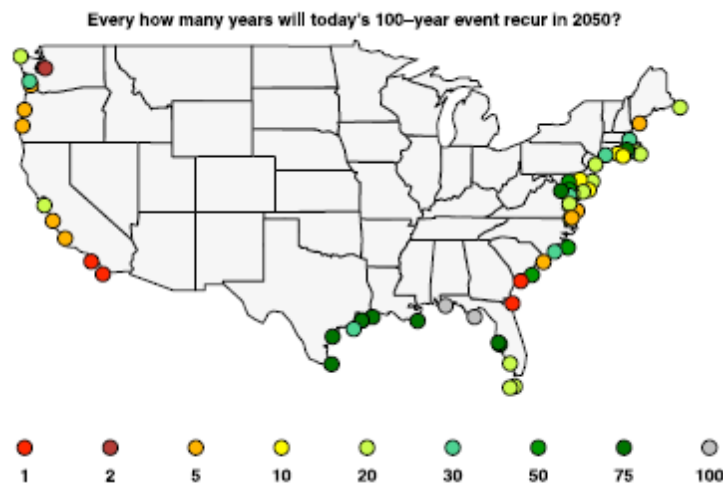


Figure 33: Frequency of 100-year extreme sea level (storm surge) events in 2050. Note that in Juan de Fuca Strait today's 100-year storm surge will occur every 20 years in 2050. (Tebaldi et al. 2012).

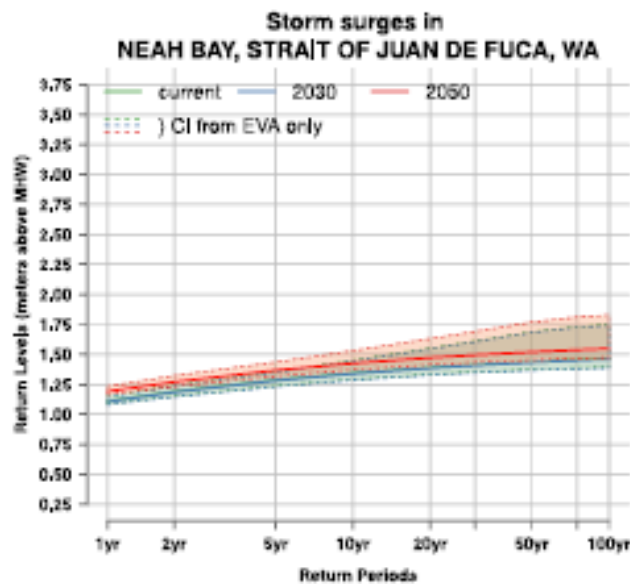


Figure 34: Storm surge amplitudes and frequencies for today (green), 2030 (blue) and 2050 (red) in Juan de Fuca Strait (Tebaldi et al. 2012). Amplitudes are metres above Mean High Water at the time, taking into account regional relative sea level rise.

Extreme sea level events (storm surges) are predicted to increase in frequency during the 21st Century, including in coastal British Columbia (e.g. Abeyirigunawardena 2010). Tebaldi et al. (2012) examine the probable change in return periods for major storm surges around the U.S. (Figure 33). For the entrance to Juan de Fuca Strait they show that what today is a 1 in 100 year event (1 % annual probability) will occur every 20 years (5 % annual probability). At Neah Bay at the entrance to Juan de Fuca Strait, the “100 year” event in 2050 will have a mean amplitude of about 1.55 m above Mean High Water at the time, with the a 5 % probability that it could reach about 1.8 m (Figure 34).

Information Gaps and Future Work

Most of the information gaps identified by Thomson et al. (2008) remain today. Because of the marked regional differences in the rate of sea level rise along the British Columbia coast, there is a requirement

for the continuation, and expansion, in long-term physical oceanic measurements from both offshore and coastal regions of the province. Primary focus should be on the maintenance of long-term observations of sea level variations using coastal tide gauges, offshore bottom pressure recorders (BPRs), and land-based GPS installations. Coincident measurement of upper ocean temperature and salinity continue to be critical to determining the contribution of steric effects on long-term sea level trends. New observational sites are needed if we are to resolve the pronounced regional differences in sea level rise arising from tectonic, oceanic, atmospheric, and hydrological changes within coastal BC. Moreover, these regional changes need to be considered within the broader global context of sea level change processes and projections. Specifically, the following are seen as important areas on which to focus future observations and research:

(1) *Glacial and Ice Cap Contributions.* Understanding the contributions to sea level change from major ice sheets on Antarctica and Greenland, as well as from mountain glaciers, is, and will continue to be, a major focus of international research over at least the next decade. This is a critical area of uncertainty which is being addressed both by those investigating processes and by those involved in the analysis of a growing observational dataset from satellite altimetry and tide gauges. In Canada, particular attention could be focused on a better understanding of the processes and rates of mountain glacier retreat and the consequences in terms of freshwater delivery to coastal waters and regional SLR.

(2) *Coupling of regional sea level change to climate-scale changes in ocean circulation and steric effects.* The atmospheric and oceanic circulation systems are complexly coupled through complex feedback mechanisms. Long-term repositioning of the basin-scale North Pacific High and Aleutian Low atmospheric pressure systems in the North Pacific could conceivably give rise to long-term changes in sea level associated with the corresponding changes in the dynamical contributions from oceanic wind regimes and circulation. Modeling is required, on a regional scale, to understand better possible scenarios in the northeast Pacific for atmospheric/oceanic circulation in relation to anticipated global climate change, and the implications for sea level elevations at the coast (mean, seasonal and extreme events). Interactions among climatic phenomena such as the Pacific Decadal Oscillations and Hadley cell intensity dynamics are expected to have important consequences for regional sea levels but are as yet poorly understood.

(3) *Hydrologic modeling of coastal British Columbia watersheds.* The volume of freshwater entering coastal waters of British Columbia will have an impact on coastal circulation and, through dynamic and steric effects, sea levels. As regional climate modeling improves, research is required to focus particularly on: (a) rivers entering the central and North Coast of British Columbia (especially the Skeena); (b) glacier-fed coastal rivers primarily on mainland British Columbia (see 1., above); and, (c) rainfall-dominated watersheds mainly on Vancouver Island. It will be important to understand the nature of regime shifts from glacier-dominated to rainfall-dominated systems and the possible redistribution of flow throughout the year.

(4) *Storm surge frequency and magnitude.* As global sea level continues to rise, there will be an increasing impact of storm surges on the low lying regions of British Columbia. Further research and numerical modeling is needed to improve the forecast and predictions of storm surges in British Columbia, including changes in frequency, intensity and direction of future major storm events.

(5) *ENSO frequency and magnitude.* Major El Niño events also lead to anomalously high sea levels along the coast of British Columbia. Present coupled atmosphere/ocean models are beginning to deal with ENSO phenomena but are not yet particularly sophisticated. It will be important to understand whether global climate change in the tropical Pacific will be El Niño- or La Niña-like and, if El Niño-

like, how it will affect the frequency and magnitude of ENSO events on coast of British Columbia. Changes in these events will, in turn, have implications for mean regional sea levels and the frequency and amplitudes of extreme sea levels associated with storms.

(6) *Steric effects in the North Pacific and coastal waters.* Steric contributions rival the volume contributions from melting ice in terms of long-term increases in global sea level. Establishing the rate of sea level change from increased global heating and advective redistribution of heat and salt in the ocean presently lays with a determination of steric sea level changes from oceanic temperature-salinity profile observations. Estimates will improve with ever growing time series of oceanic CTD profile data from repeat shipboard survey lines, moored buoy instrumentation, cabled observatory instrumentation, and the International Argo program. Eventually, coupled ocean-atmosphere GCMs, with realistic ocean circulation and surface mixing dynamics will be capable of determining the contributions of halosteric and thermosteric effects on global and regional sea level rise.

(7) *Long term measurements by tide gauges, GPS and CTD profiling.* Ongoing time series measurements (including tide gauge, GPS, meteorological, and CTD programs), as well as new tide series for poorly sampled coastal regions and highly vulnerable shorelines, are critical in coastal areas of British Columbia where there is a complex suite of geological and oceanographic processes which determine relative sea level rise. In particular, the CTD profiling series at the Nanoose Bay site, on the west coast of Vancouver Island and at Station “P” need to be maintained and upgraded if we are to understand the steric changes which affect regional sea levels along the coast and in the Northeast Pacific. More measurements are needed in poorly sampled northern BC coastal areas (e.g., Hecate Strait/Dixon Entrance) where freshwater influences, especially from the Skeen River, are expected to change during this century. As well, there appear to be some anomalous tectonic effects on some parts of the BC coast (e.g., Vancouver, Prince Rupert) which require longer GPS time series as well as further geophysical modelling.

TRENDS IN UPWELLING AND DOWNWELLING WINDS ALONG THE BRITISH COLUMBIA CONTINENTAL SHELF

M.G.G. Foreman¹, W.J. Merryfield² and B. Pal². ¹Institute of Ocean Sciences, Fisheries and Oceans Canada, ²Canadian Centre for Climate Modelling and Analysis, Environment Canada, University of Victoria.

Summary

As this section summarizes Foreman et al. (2011) (henceforth FPM11), the interested reader is referred to that manuscript for more details.

Using the Bakun (1973) upwelling index to approximate the amount of water drawn upward from the base of the Ekman layer at six equally spaced sites between 33°N and 48°N, Bograd et al. 2009 (henceforth B09) estimated trends and variability in coastal upwelling along the California Current System (CCS) over the period of 1967 to 2007. Cumulative upwelling indices (CUI, Schwing et al. 2006; henceforth S06) computed for each year and at each site were used to quantify the timing of the spring transition, the length of the upwelling season, and cumulative upwelling and downwelling strength. Among various statistically significant trends, they found that in the northern CCS the spring transition was becoming later and the upwelling season was becoming shorter at the respective rates of 1.0 day/yr and 1.1 day/yr.

FPM11 extended the B09 analysis northward to the waters off British Columbia (BC) where the North Pacific Current bifurcates into the California and Alaska Currents (Dodimead et al. 1963). Though upwelling is generally considered to be a characteristic of CCS and roughly extends from Vancouver Island to Baja California (Thomson 1981), the latitude of the bifurcation and positions of the Aleutian Low and North Pacific High pressure systems all exhibit interannual variability so that northern BC waters can have a short upwelling season (Hsieh et al. 1995; Freeland 2006). It is therefore useful not only to determine if the trends found by B09 extend to southern BC, but also how far upwelling extends to the north and whether or not its timing and magnitudes have changed.

As Faucher et al. (1999) extended the Environment Canada network (Figure 35) of weather buoys off the BC coast back to 1958, the winds from the six stations closest to the shelf break (206, 132, 207, 147, 208, 205), rather than those derived from atmospheric pressure fields (Bakun 1973), were used to compute our BC CUIs. Specifically, the Faucher et al. (1999) version of these winds were used up to 1997 while for 1998 to 2007, gaps in the buoy observations were filled using the NASA archive of cross-calibrated, multi-platform (CCMP) ocean surface winds (Ardizzone et al. 2009; http://podaac.jpl.nasa.gov/DATA_CATALOG/ccmpinfo.html). See FPM11 for analyses of the differences between these data sets and the expected impact of combining them on the subsequent trend analyses.

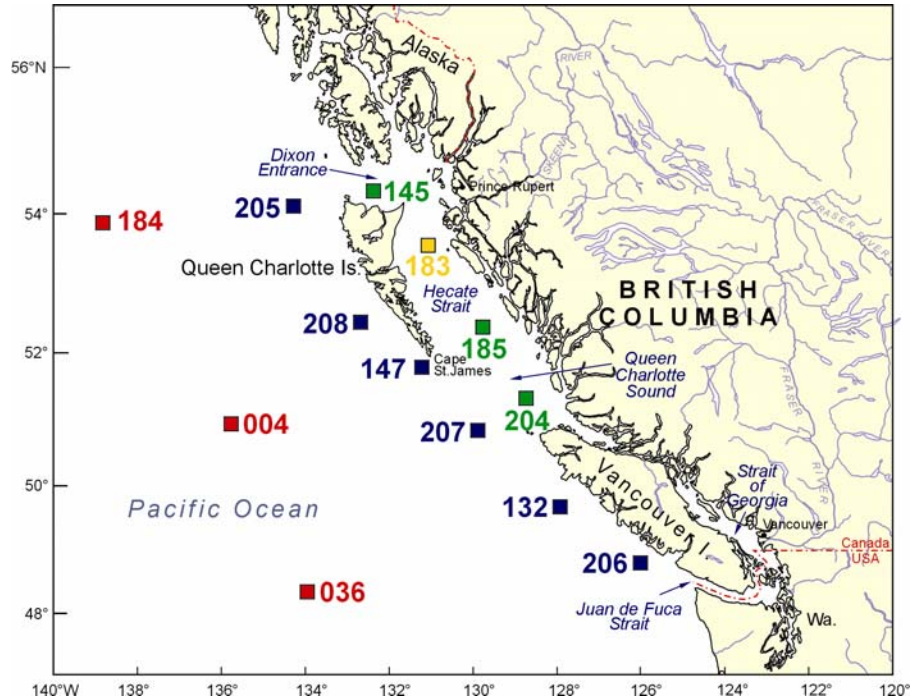


Figure 35: Locations of 13 weather buoys off the Canadian west coast. Only observations from those shown in blue are discussed in this analysis.

Once all gaps were filled in the wind time series, the associated wind stresses, τ , were calculated using the bulk formula (Gill 1982).

$$\tau = \rho_a * C_d * |\mathbf{v}| \mathbf{v}$$

where ρ_a is the air density (1.2kg/m^3), C_d is a constant drag coefficient (0.0013) and \mathbf{v} is the wind vector with magnitude $|\mathbf{v}|$. These stresses were then resolved into their alongshore and cross-shore components, where, consistent with alongshore bathymetry and coastline orientations (Figure 35), 30° counterclockwise from north was chosen as the alongshore direction for the three northern buoys while

45° counterclockwise from north was chosen for the southern ones. Offshore/onshore Ekman transports per 100m of coastline were then estimated by dividing these alongshore stresses by the Coriolis parameter and density of seawater (S06). At each buoy location, the CUI was calculated (S06) by integrating the daily upwelling indices over the duration of the upwelling season and for each year, the spring and fall transitions were determined as the dates when the gradient of the CUI changed sign from negative to positive (spring) and vice-versa (fall). For each buoy location, decadal (or climatological) means were then computed by simply averaging the CUIs over ten consecutive years and filtering with a fifteen-day running average to remove any remaining high frequency variability. Consistent with B09, the total upwelling magnitude index (TUMI) was computed as the difference between the CUI at the end of the upwelling period and at the beginning; and somewhat differently from B09, the total downwelling magnitude index (TDMI) was defined as the CUI on December 31 minus the TUMI.

Decadally-averaged CUIs were computed for the F99 and observed+CCMP data sets are shown in Figure 36. The associated upwelling start and end dates are given in Table 7 and also shown in Figure 36. The estimation of confidence limits associated with these dates is complicated by numerous wiggles in the yearly CUIs, even after the application of a fifteen-day moving average filter. Though careful analysis of local versus global minima/maxima might permit the definition of start/end dates for each year, FPM11 used a bootstrap approach to estimate 90% confidence intervals for the values listed in Table 7. These limits are usually less than about 20 days and comparable to those listed in Table 7 of B09, but in some instances they can be much larger. The interested reader is referred to FPM11 for further details.

Table 7: Decadal average start (1st number, Julian day number) and end dates (2nd number) of the upwelling season at the six weather buoys.

Buoy	1959- 1968 (F99)	1969- 1978 (F99)	1979- 1988 (F99)	1989- 1998 (F99)	1999-2008 (obs+CCMP)
206	89 275	78 283	105 272	118 277	113 271
132	94 275	118 274	127 272	119 279	113 280
207	97 251	153 264	144 270	122 276	151 276
147	169 249	158 231	149 266	125 271	151 263
208	100 251	154 262	144 267	122 264	151 270
205	174 245	159 232	190 236	128 244	209 225

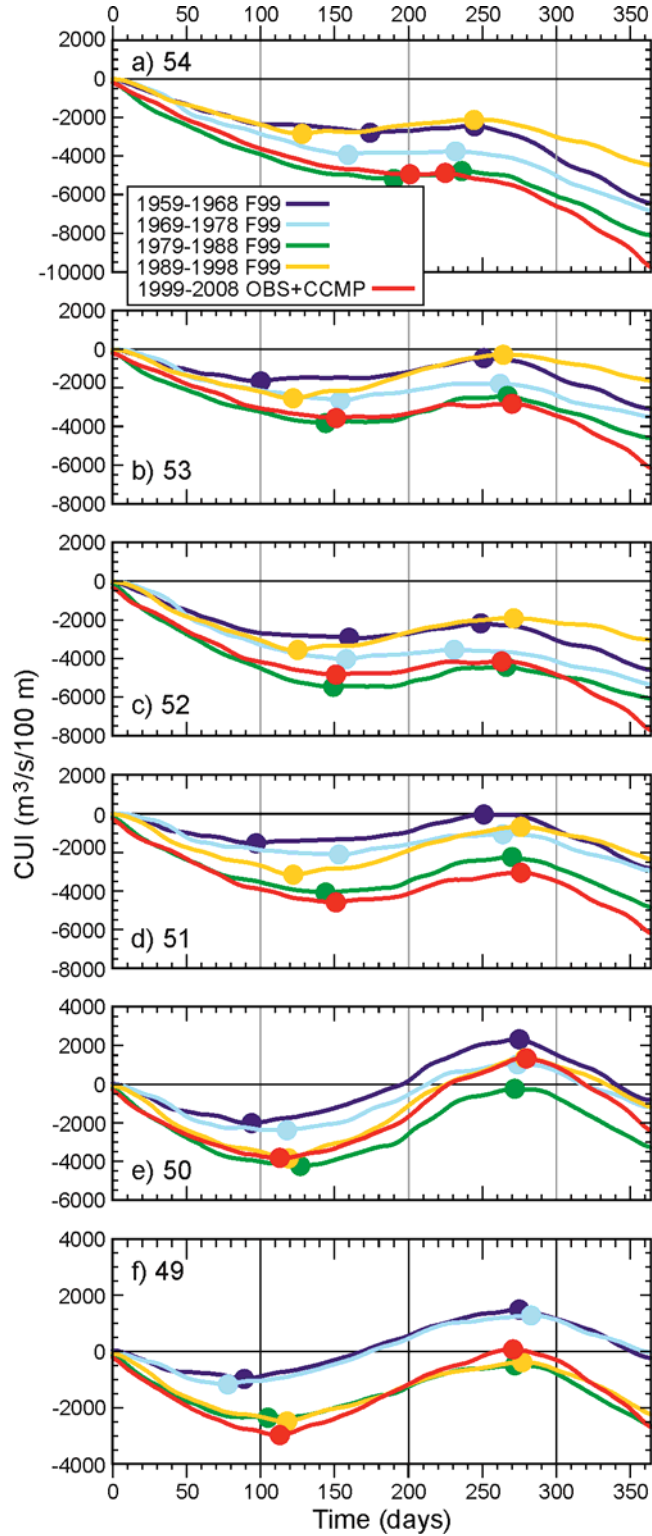


Figure 36: Decadal-average CUIs for 1959-2008 at weather buoys a) 205, b) 208, c) 147, d) 207, e) 132, f) 206. CUIs for the first four decades were computed from the F99 time series while those for the last decade used observed buoy winds with gaps filled from the CCMP data set. Dots denote the start and end of the upwelling season. Labels 49-54 denote buoy latitudes ($^{\circ}$ N) rounded to the nearest degree.

Visual inspection of the upwelling start dates shown in Figure 36 suggests that despite some interdecadal variability, there may be trends towards later onsets at all buoys except 147. In fact there are, and FPM11 compute them to be 0.88, 0.39, 0.77, -0.69, 0.70, and 0.23 days per year for buoys 206, 132, 207, 147, 208, and 205 respectively. All are significantly different from zero at the 95% level and at all buoys except 147, upwelling is becoming later, a trend consistent with, though smaller than, the 1.0 days/year value that B09 found at their 48°N site. A similar analysis was carried out for the upwelling season durations and again at all buoys except 147, the trend was toward shorter upwelling duration. In this case, all trends except that for buoy 207 were significantly different from zero at the 95% level and the value for buoy 206 was -1.02 days/year, very close to the -1.1 days/year that B09 found at their 48°N site. The contrary trends toward an earlier spring transition and longer upwelling season at buoy 147 are interesting and may arise from changes in the seasonal winds in Hecate Strait and Queen Charlotte Sound, even though opposite trends were found at buoy 207 which should also be affected similarly. As seen in Figure 35, Environment Canada has three buoys in this region (204, 185, 183) and F99 also extended their time series back to 1958. Analyses of trends in these are ongoing but the results are not reported here.

Table 8 lists five decades of TUMI and TDMI associated with the CUI shown in Figure 36, while Figure 37 displays these data in graphical form, along with linear trends that have been fit via least squares. Note that the TUMIs do not decrease monotonically from south to north. The largest TUMIs are at the second most southerly buoy (132) while the fifth buoy (208) displays more upwelling than the fourth (147). Although there is considerable interdecadal variability and a notable decline in upwelling over the last decade at all but buoy 206, all TUMIs except 205 show an overall increase over the past five decades with the largest trends (Table 8) being at buoys 132 and 207. The trends at buoys 206, 132, 207, and 147 are significantly different than zero at the 95% confidence level while that for buoy 208 is significant at the 90% level. Transforming these trends into forty-year changes in the associated upwelling-favourable winds, the last column in Table 8 shows increases ranging between 0.9% (205) and 25.7% (147).

Table 8: TUMI and TDMI decadal averages (m^3s^{-1} per 100m of coastline), linear trends (m^3s^{-1} per 100m per year), and associated percentage wind increase over forty years at the six weather buoys. * and # denote trends that are significantly different from zero at the 90% and 95% levels.

Buoy	1959- 1968 (F99)	1969- 1978 (F99)	1979- 1988 (F99)	1989- 1998 (F99)	1999- 2008 (obs+ CCMP)	Mean (F99 + obs/CCMP)	Linear trend	% wind speed increase
206	2457 -2647	2453 -2478	1859 -4563	2093 -4445	3041 -5826	2381 -3992	8.1 [#] -83.3 [#]	7.0 55.9
132	4344 -5095	3420 -4627	4000 -7367	5189 -6531	5168 -7661	4424 -6256	34.2 [#] -70.4 [#]	16.9 25.7
207	1489 -4228	1050 -4008	1845 -6808	2470 -4946	1542 -7817	1679 -5561	15.3 [#] -81.2 [#]	20.2 35.1
147	754 -5362	482 -5870	1030 -7177	1655 -4718	686 -8582	921 -6341	10.4 [#] -52.9 [#]	25.7 18.3
208	1204 -4232	849 -4412	1411 -6096	2259 -3947	737 -7085	1292 -5154	4.8 [#] -52.4 [#]	7.7 20.9
205	342 -6782	167 -7073	406 -8646	730 -5246	91 -10054	343 -7556	0.2* -46.7 [#]	0.9 13.2

Although the largest and smallest (negative) TDMI values (Figure 37b) arise at the most northerly and southerly buoys, namely 205 and 206, TDMI values at the buoys in between do not display a monotonic progression from north to south. The second smallest TDMI is at the second most northerly buoy (208) and the third largest is at the second most southerly buoy (132). Though all TDMI values show a 1989-98 decrease in downwelling that becomes progressively stronger to the north, all linear trends show increased downwelling with particularly strong increases over 1999-2008. All trends are significantly different from zero at the 95% level with the largest being at buoys 206 and 207. The associated forty-year increases in downwelling-favourable winds range between 13.2% (205) and 55.9% (206).

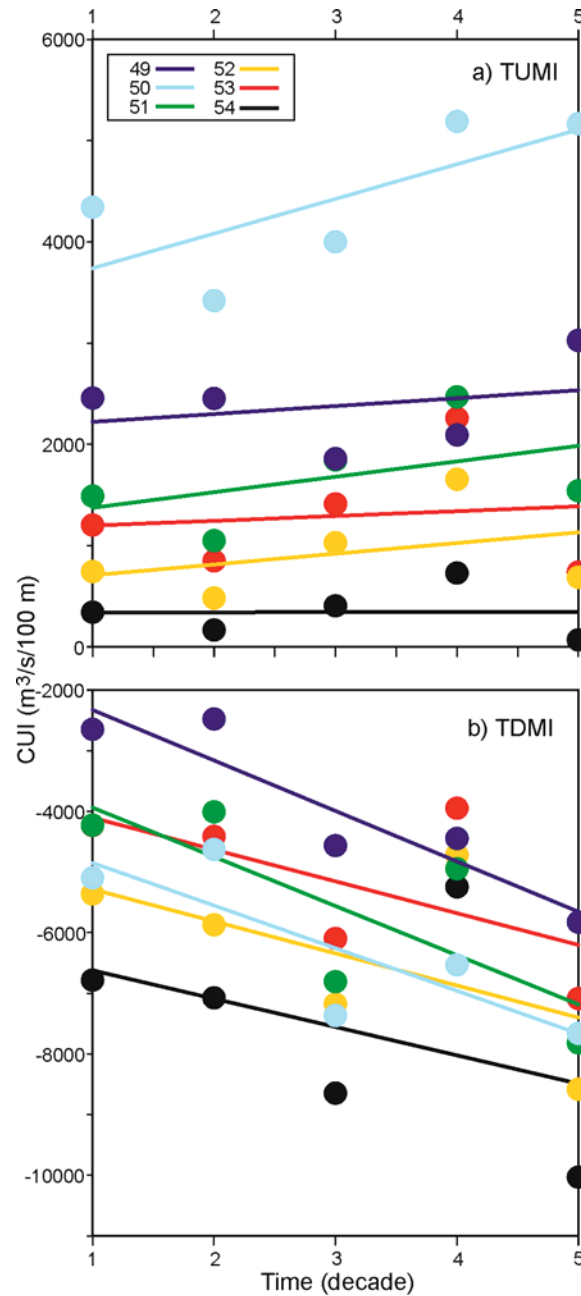


Figure 37: a) TUMI and b) TDMI values (dots) and linear trends over the past five decades at the six weather buoys. Labels 49, 50, 51, 52, 53, 54 denote buoy latitudes rounded to the nearest degree and correspond to buoys 206, 132, 207, 147, 208, and 205, respectively.

An intensification of TUMI and TDMI along the BC shelf over the last fifty years leaves open the question of whether these trends might continue in the future. As summarized in another section of this report, Merryfield et al. (2009) showed that ensemble mean summer winds along the BC shelf in the late 21st century were projected to increase in speed by 5–10% and rotate clockwise by $\approx 5^\circ$, both statistically significant changes, while the associated model ensemble winter winds showed no statistically significant changes. Though these changes are considerably less than the historical upwelling- and downwelling-favourable wind changes found here, both Yin (2005) and Salathé (2006) found a deepening and northward shift of the Aleutian Low accompanied by a northward shift in North Pacific storm tracks that would be a consistent continuation of our TDMI trends. Perhaps more importantly, Gillett et al. (2003) not only found trends in December-February Northeast Pacific sea level pressures over 1948-98 that are consistent with stronger downwelling-favourable winds in the California Current region, but they also demonstrated that anthropogenic greenhouse gases and sulphate aerosols have had a detectable influence on sea level pressures over the second half of the 20th century.

Though Global Climate Models (GCMs) have been used to project future changes in the seasonality and magnitude of winds and river discharges (Morrison et al. 2002), further study with regional models that have much finer horizontal resolution than the $>1^\circ$ that is common to most GCMs will be necessary to provide more credibility and spatial detail. A 3 km regional ocean model has been developed for the British Columbia continental shelf and results from one simulation are presented in the subsequent chapter "Results from Regional Climate Model Simulation for the British Columbia Continental Shelf".

TRENDS IN OXYGEN CONCENTRATION ON THE CONTINENTAL SHELF OF BRITISH COLUMBIA.

Bill Crawford¹ and Angelica Peña². ¹Fisheries and Oceans Canada, retired, ²Institute of Ocean Sciences, Fisheries and Oceans Canada.

Introduction

This report describes the typical oxygen concentrations on the British Columbia continental shelf, based on almost 80 years of measurements by oceanographers and fisheries scientists, evaluates past changes in these concentrations, and offers insight into future changes. For records of oxygen concentration, we rely on observations archived by the Ocean Sciences Division of Fisheries and Ocean Canada at the Institute of Ocean Sciences, as well as those of the US National Ocean Data Center. This chapter summarizes results by Crawford and Peña (2013), henceforth CP13, and also include more recent calculations not yet submitted for publication in a scientific journal.

Subsurface waters of the continental margin of the west coast of the Americas are chronically low in dissolved oxygen. Whereas ocean surface waters everywhere are usually saturated with oxygen, with concentration close to 300 micromoles per kilogram ($\mu\text{mol kg}^{-1}$), the oxygen concentration declines with increasing depth below the ocean surface mixed layer. This decline with depth is significantly greater along the North American west coast than is typical of the ocean in general. On the British Columbia continental margin the oxygen concentration declines to almost zero at depths of 700 to 1000 m below the ocean surface. The low concentration is attributed to low oxygen in the California Undercurrent that flows northward at depths of 200 to 300 m along the North American margin from Central America, as well as to oxidation of organic material on the continental margin itself. Upwelling-favourable winds along the west coast, especially in summer, advect low-oxygen waters across the slope and shelf, decreasing the near-bottom oxygen concentration. This same upwelling also injects nutrients into surface waters that accelerate plankton growth and increase biomass of species higher up the food chain.

The continual fallout of detritus from this biomass leads to increased oxidation rates in summer and additional declines in local oxygen concentration on the shelf.

The waters of the California Current originate in the Eastern Tropical North Pacific (ETNP) off Central America where oxygen concentration is near zero, but along the route there is significant exchange with adjacent more oxygenated waters. By the time they reach British Columbia, the ETNP waters are diluted by about 50% (Thomson and Krassovski 2010). Therefore, multi-year changes in oxygen concentration in bottom waters off BC are due to changes in these two source waters, as well as to changes in the mixing of these waters and in upwelling winds along the west coast.

Local ecosystems have adapted to these low concentrations, but changing oxygen concentration will lead to ecosystem changes. In 2002 a significant decline in oxygen concentration on the bottom of the Oregon continental shelf at depths less than 100 m in summer led to mortality of shellfish, an event not recorded in previous years (Grantham et al. 2004). Similar events followed in later summers, and the low-oxygen bottom water reached its greatest extent to the north in the summer of 2006, reaching Canadian waters (Connolly et al. 2010).

Spatial Distribution

As noted above, the oxygen concentration decreases with increasing depth below the ocean surface mixed layer. This decrease is due to slow mixing of oxygen from the ocean surface and to local oxidation of organic material. Because in shelf and slope waters the lowest oxygen concentration is usually near the ocean bottom, we first examine the spatial distribution of oxygen along the bottom on the British Columbia continental shelf.

Figure 38 presents a summary of observations of oxygen within 20 m of the ocean bottom by plotting symbols to represent past observations. Only observations from months of June to September are included, since winter concentrations are almost always higher. Concentration is expressed in millilitres per litre (ml L^{-1}), where $1 \text{ ml L}^{-1} \sim 44 \mu\text{mol kg}^{-1}$. The term hypoxia is often used for waters with low oxygen concentration. For example, Connolly et al. (2010) define hypoxia as $<1.4 \text{ ml L}^{-1}$ ($61 \mu\text{mol kg}^{-1}$). Chan et al. (2008) define extreme hypoxia as $<0.5 \text{ ml L}^{-1}$ ($<22 \mu\text{mol kg}^{-1}$).

The two panels of Figure 38 reveal the decrease of oxygen concentration with increasing depth. Severe hypoxia ($<0.5 \text{ ml L}^{-1}$) is observed only deeper than 500 metres, or in some inlets. The bottoms of these inlets exchange deep water very slowly with outside oceanic waters, and do not mix oxygen down to the bottom, so their oxygen concentration can go to zero in some inlets. This is a natural feature. Changes in oxygen in these inlets are outside the scope of this paper.

Hypoxic bottom water ($<1.4 \text{ ml L}^{-1}$) is rarely found along the inner continental shelf of British Columbia, inside the 100 m contour. In contrast, hypoxia, and even extreme hypoxia have been observed in summer on the Oregon and Washington shelves well inside the 100 m contour (Grantham et al. 2004). We do not expect to see similar hypoxia along the BC coast. We attribute this fundamental difference to the outflow of seawater from Juan de Fuca Strait that flows to the northwest along the Vancouver Island coast, forming the Vancouver Island Coastal Current. This outflow is well oxygenated due to intense tidal mixing in Juan de Fuca Strait, and is about 100 m deep. When winds blow from the northwest in summer and upwell nearshore water, this upwelled water is replaced by oxygenated water of the Vancouver Island Coastal Current. By contrast, the Oregon and Washington coasts have no comparable alongshore current, so upwelling winds there bring low-oxygen water toward shore along the ocean bottom.

A comparison of Figure 38a and b reveals that at most depths the oxygen concentration is lower off southern British Columbia than in northern BC. Almost all the hypoxic shelf water inside the 200 m contour is at mid-shelf off southwest Vancouver Island (Figure 38b), where there is a broad shelf between 100 and 200 m depth (CP13). Concentration below 1.4 ml L^{-1} on the continental shelf is rarely observed inside the 200 m contour in samples north of 49.5°N (CP13). Concentration below 1 ml L^{-1} is rarely observed in summer inside the 100 m contour north of this same latitude.

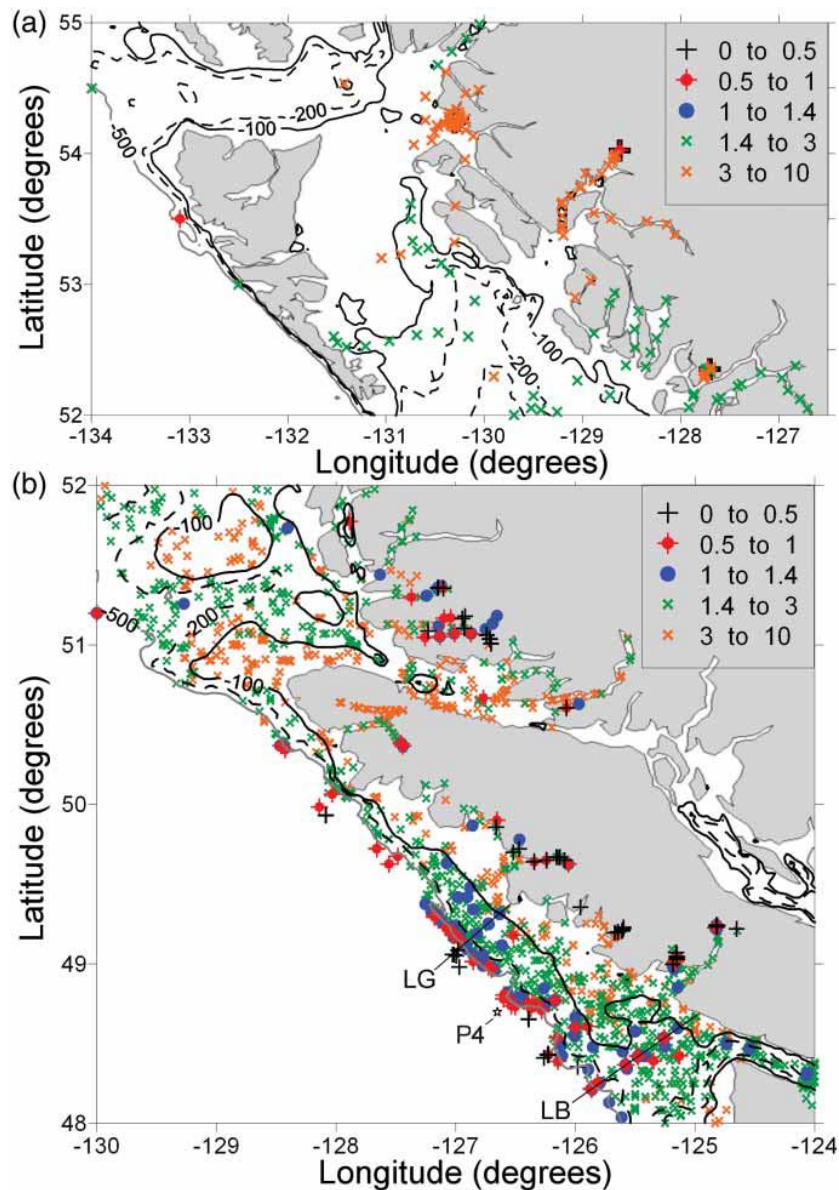


Figure 38: Historical observations of oxygen concentration (ml l^{-1}) within 20 m of the ocean bottom plotted on maps of the BC shelf and inlets, for the months of June to September. (a) northern BC; (b) southern BC. Depth contours are in metres. Straight black lines pass along the LB and LG lines. Station P4 is marked by a star. (Source: Crawford and Peña 2013).

There is a broad shelf section off southwest Vancouver Island with hypoxia extending well across the continental shelf. Sampling line LB (Figure 38b) lies in this region. We attribute this extensive hypoxic region to the presence of the Juan de Fuca Eddy (CP13). This eddy carries seawater cyclonically (counterclockwise) over the shelf, with its northern arc passing directly over the LB line of stations.

Bottom water with lower oxygen concentration upwells into the centre of this eddy from deeper regions, bringing low oxygen water. A numerical simulation of this eddy reveals that both upwelling of low-oxygen water and local oxidation inside this eddy in summer contribute to hypoxia in summer near bottom (CP13).

Temporal changes

We focus on stations of the southern British Columbia shelf where hypoxia is most frequent in summer. There are two stations with sampling in almost all summers for three decades. LB08 is on the continental shelf at 48°25.3N, 125°28.66W in 145 m of water. Station P4 is on the continental slope at 48°39.0N, 126°40.0W in 1300 m of water. Figure 39 presents time series of changes in summer oxygen concentration at these stations. The symbol sigma-t (σ_t) refers to the density of water, whereby σ_t of 26.4 indicates a water density of 1026.4 kg m⁻³.

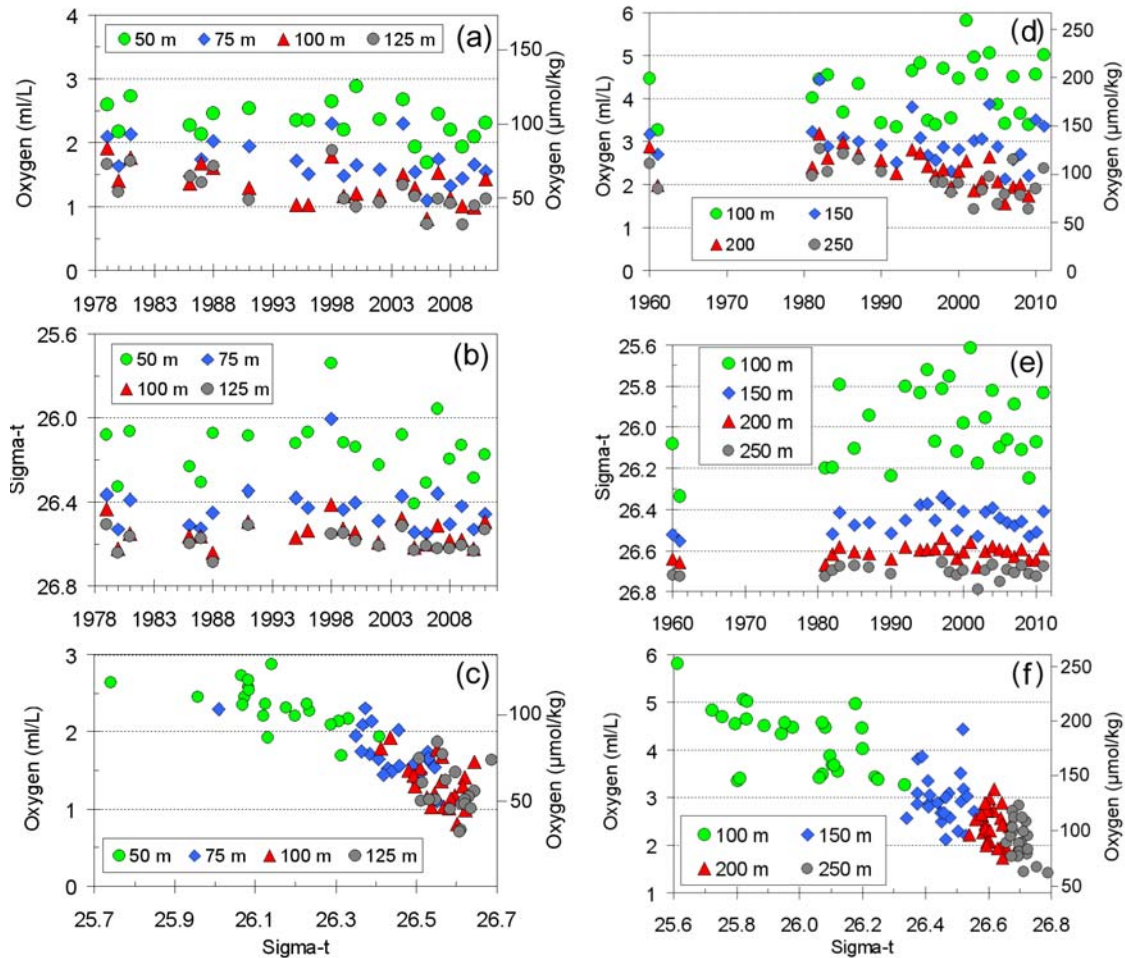


Figure 39: Oxygen and σ_t at stations LB08 (left) and P4 (right) observed in late summer and early autumn. (a, d) Oxygen versus year of observation. (b, e) σ_t versus year of observation. (c, e) Oxygen versus σ_t . Observations were averaged within each year prior to plotting. Colours denote depth of observation. (Source: Crawford and Peña 2013)

The time series of oxygen (Figure 39a-c) shows a decline for the period 1979 to 2011 at both 125 and 100 m, with linear slopes of 0.019 and 0.017 ml L⁻¹ y⁻¹ (0.83 and 0.74 μmol kg⁻¹ y⁻¹), respectively, and an R² of 0.44 and 0.33 and P < 0.01 and 0.001 respectively (data were assumed independent from one

year to the next). A smaller linear decline of $0.013 \text{ ml L}^{-1} \text{ y}^{-1}$ ($0.57 \text{ } \mu\text{mol kg}^{-1} \text{ y}^{-1}$) per year at 75 m is significant only at $p < 0.1$. There is even less statistical significance to the linear trend at 50 m and no decrease at shallower depths. Similar trends in σ_t from 1978 to 2011 (Figure 39b) were not observed at the four depths from 50 to 125 m. However, rather large year-to-year variability might mask the tendency for σ_t to have been greater from 2004 to 2010, when oxygen also tended to be lower. Figure 39c presents the co-variability of σ_t and oxygen in the same data. At 50 and 75 m there is clear co-variability in these two properties, with lower oxygen on higher σ_t surfaces. The outliers with the lowest density occur in 1998. At both 100 and 125 m it is more difficult to see a relationship between σ_t and oxygen. The years with the lowest oxygen at 125 m (2006 and 2009) have a σ_t of about 26.61, with seven other years experiencing higher density but also higher oxygen. From Figure 39b and c we conclude that the co-variability of σ_t and oxygen might explain some of the interannual variability of oxygen between 1979 and 2011 but not the general decline of oxygen at 100 and 125 m over this period (CP13).

A longer time series of oxygen on density surfaces is available on the continental slope along Line P at Station P4 (Figure 40d-f). This station lies in 1300 m of water off southwest Vancouver Island. Oxygen concentration has been measured here during almost every Line P cruise since the early 1980s and on several cruises in the early 1960s. We averaged August to September observations in each year, plotting one value per year. As shown in Figure 39d, there is a decrease in oxygen from the 1980s to present at three of the depths. The lowest oxygen concentrations occurred in 2002, 2005, and 2009. The linear declines are 0.017 , 0.025 , and $0.024 \text{ ml L}^{-1} \text{ y}^{-1}$ (0.74 , 1.1 , $1.0 \text{ } \mu\text{mol kg}^{-1} \text{ y}^{-1}$) at 150, 200 and 250 m depths, respectively, with corresponding R^2 of 0.083, 0.32 and 0.36. Trends at 200 and 250 m are significantly different from zero at $P < 0.01$, while the trend at 150 m is not significant. Concentration at 100 m does not have a trend over this same interval. Although calculations indicate that oxygen has been decreasing at P4 more rapidly than at LB08 since 1980, the differences are not statistically significant. When observations from the 1960s are included in the calculation of trend, the linear rates of decline are $0.012 \text{ ml L}^{-1} \text{ y}^{-1}$ at both 250 and 200 m, with R^2 of 0.20 and 0.15, respectively ($P > 0.07$). There is no significant linear trend in σ_t in Figure 39e. However, at 150 m depth there is a minimum in σ_t from 1997 to 1998, corresponding to the prolonged El Niño impacts on local waters. We plotted σ_t versus oxygen concentrations at four depths in 22f to investigate any tendency for low oxygen concentrations to be caused by shoaling of isopycnal surfaces. The three years 2002, 2005, and 2009 stand out from other data points at 250 m. These are the three years that provide the lowest recent oxygen concentrations to the time series of Figure 39d. However, even excluding these three years, a decrease in oxygen at 250 m is still present in this time series. A separate analysis revealed a decline of $0.022 \text{ ml L}^{-1} \text{ y}^{-1}$ ($0.96 \text{ } \mu\text{mol kg}^{-1} \text{ y}^{-1}$) in oxygen on the 26.6 σ_t surface near P4, not significantly different from the rate of decrease at 200 m depth, close to this density surface (CP13).

To examine changes in subsurface oxygen concentration prior to about 1980, we cannot rely on repeat sampling at one or two fixed location stations. Instead, we examined all observations and averaged over general shelf regions where there have been many samples in most decades. We decided to examine changes in oxygen on constant density surfaces of the ocean, since CP13 showed at LB08 and P4 that decadal declines in oxygen were not due to uplifting of the density structure, but instead to changes in oxygen on these constant density surfaces. We computed oxygen concentration on several constant density surfaces for each profile in the archives, this time using sigma-theta (σ_θ) rather than sigma-t (σ_t). The numerical difference between these two parameters is very small at depths we examine, and the actual difference is related to effects of subsurface water pressure on water temperature. Since the waters of the continental slope are source waters for the bottom of the continental shelf in summer, we examined changes in oxygen over the continental slope.

We found that the archives hold many observations of oxygen in the continental slope of the west coast between latitude 48N and 49N. From these observations we prepared a time series of oxygen on several σ_θ surfaces. Results on the 26.7 surface are shown in Figure 41 below. Each blue symbol represents a sample collected over past decades between latitude 48°N and 49°N, where the total water depth was between 200 and 1500 m. The red line is a least-squares-fit cubic polynomial to the blue symbols. We found little change if a fourth order polynomial was plotted.

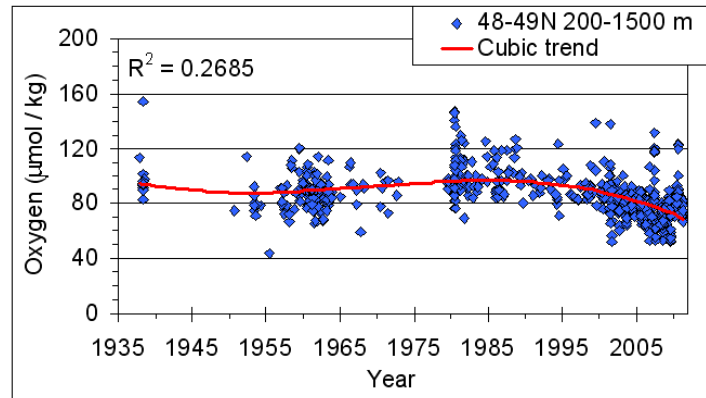


Figure 40: Oxygen concentration interpolated onto the 26.7 σ_θ surface for observations over the continental slope of the south coast of Vancouver Island. Blue symbols show individual observations; red line is a cubic least-squares polynomial.

Figure 40 clearly shows decadal variability, with increasing oxygen concentration for 1950s to 1980s, and declining concentration through the 1990s and 2000s. Therefore the declines observed since 1980 are not part of a longer period decline in oxygen. A second feature of Figure 40 is a slight increase in oxygen after 2009.

We found similar decadal variability on the continental margin to south, as far as 32°N. Off Central America, Deutsch et al (2011) observed similar decadal variability in the spatial extent of the eastern tropical Pacific oxygen minimum zone. Therefore the decadal changes presented in Figure 40 might be due to changes in oxygen content on the source waters of the California Undercurrent.

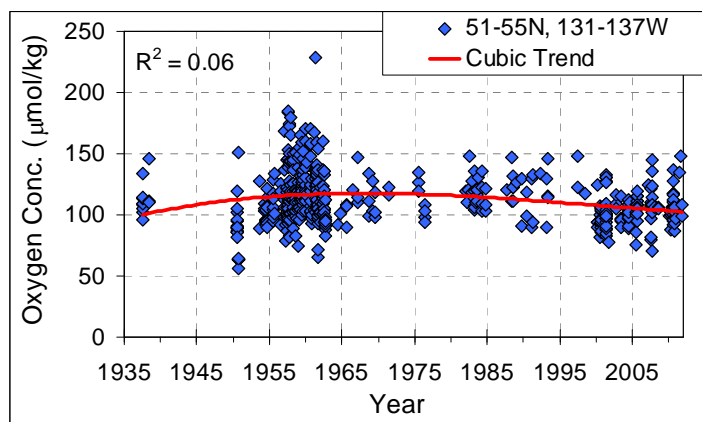


Figure 41: Oxygen concentration interpolated onto the 26.7 σ_θ surface for observations over Dixon Entrance and west of Haida Gwaii. Blue symbols show individual observations; red line is a cubic least-squares polynomial.

There are few samples on the central and northern BC continental margin, so we examined observations there over a larger range from 51°N to 55°N, and 131°W to 137°W. These observations extend through Dixon Entrance and west of Haida Gwaii, and are not confined to the continental margin. Results are presented in Figure 41.

Figure 41 reveals a broad maximum in oxygen concentration from the 1950s to the 1980s, and declines after then until 2003. The low correlation coefficient of $R^2 = 0.06$ suggests the decadal variability represented by the red line is not significant.

Whitney et al. (2007) and Falkowski et al. (2011) have examined changes in oxygen on constant density surface at Ocean Station P at 50°N, 145°W in the Gulf of Alaska. They document a half-century of decadal variability and declining oxygen concentration on the 26.7 σ_θ surface, and on other similar-density surfaces. A minimum in oxygen was observed in 2003. Our own analysis of all data collected in the Gulf of Alaska as well as at Ocean Station P reveals considerable variability and the most dominant and widespread change is a drop in oxygen concentration from mid 1990s to mid 2000s, not only in deep ocean waters, but also along the continental margin of USA and Canada.

These findings of decadal variability from 1940s to 2011 suggest that future declines in oxygen concentration along the North American West coast will be modulated by decadal variability, and that the rate of decline between 1980 and 2010 might have been stronger than expected for an average over then next 50 years or so (see subsequent chapter on "Projections For The Open Gulf Of Alaska").

Summary

Over the British Columbia continental shelf and in adjacent oceanic waters the ocean surface waters are saturated with oxygen. However, as one descends through the ocean the concentration decreases, reaching almost zero at 700 to 1000 metres depth. The decline is most significant at depths below the ocean surface mixed layer, which can be 10 to 100 metres deep. Most of the continental shelf has bottom depths less than 200 m, and in some shelf regions the oxygen concentration is sufficiently low to impact marine life near the ocean bottom.

The lowest near-bottom oxygen concentration on the continental shelf is found in late summer and early autumn in some regions off southwest Vancouver Island, where a concentration of 1 millilitre per litre (ml L^{-1}) is typical at depths of 145 m ($1 \text{ ml L}^{-1} \sim 44 \mu\text{mol kg}^{-1}$). Higher concentrations are observed in other seasons and elsewhere on the British Columbia continental shelf.

Off southwest Vancouver Island, oxygen concentration declined to 0.7 ml L^{-1} in the late summer of 2006 and again in 2009. On average, near-bottom oxygen concentration there declined at a rate of $0.019 \text{ ml L}^{-1} \text{ y}^{-1}$ ($0.83 \mu\text{mol kg}^{-1} \text{ y}^{-1}$) from 1979 to 2011. This decline is based on repeated observations at a single station, LB08 (48° 25.3'N, 125° 28.66'W in 145 m of water) in almost every summer since 1979. Station P4 (48°39.0N, 126°40.0W in 1300 m of water) on the nearby continental slope has also been sampled regularly for several decades. The decline in concentration of oxygen there at 200 m depth is $0.025 \text{ ml L}^{-1} \text{ y}^{-1}$ ($1.1 \mu\text{mol kg}^{-1} \text{ y}^{-1}$) from 1981 to 2011. Because regular sampling does not extend back past 1979 at these two stations, we cannot determine earlier trends.

However, by searching through DFO and American databases of oxygen measurements since the 1930s, we have been able to determine longer-period trends and decadal variability of oxygen concentration for several general regions of the British Columbia continental slope, as well as along the USA continental slope. This search reveals that from the 1960s to 1980s oxygen concentration increased at depths of 200 to 300 m along the continental slope of California to southwest Vancouver Island. In British Columbia,

oxygen concentration increased somewhat after 2009. Because the water near 200 m depth upwells onto the continental shelf in summer and influences the minimum oxygen concentration at shelf-bottom in late summer, we believe that the rate of decline at LB08 and at P4 noted above for the past three decades was greater than the average over a longer period. A future decline in oxygen concentration off southwest Vancouver Island will likely continue at a smaller rate than observed for the period of 1979 to 2011, and will be influenced by decadal variability.

TRENDS IN NUTRIENT CONCENTRATION IN THE NORTHEAST SUBARCTIC PACIFIC

Angelica Peña, Institute of Ocean Sciences, Fisheries and Oceans Canada

Introduction

This report describes variations in nutrient concentrations on the continental shelf and open ocean of the northeast subarctic Pacific, based mostly on almost 40 years of measurements along Line P, which extends from the southwest corner of Vancouver Island to Ocean Station Papa (OSP, 50°N, 145°W) in the Gulf of Alaska, and many years of observations at station LB08 on the continental shelf of British Columbia. It extends previous analysis of surface ocean nutrient variability along Line P (Peña and Varela 2007; Di Lorenzo et al. 2009), and includes recent analysis of temporal changes in nutrient concentrations on the continental shelf of British Columbia. It also offers insight into future changes in these concentrations.

The Gulf of Alaska is a high-nutrient, low-chlorophyll (HNLC) region where iron limits phytoplankton growth. As a result of iron limitation, nitrate and silicate commonly remain abundant in summer. In contrast, continental shelf phytoplankton are not limited by iron but by nitrate supply. Due to frequent injections of nutrients from rivers, upwelling, estuarine circulation and tidal mixing, the continental shelf is very productive. Beyond the shelf, nutrient concentrations increase gradually offshore and are highest in late winter due to nutrient transport to the upper layer by wind-forced upwelling and mixing during winter storms. Between the HNLC region and continental shelf waters lies a transition area that does not experience coastal upwelling and where nitrate becomes depleted in summer. In addition to seasonal variability, large interannual and decadal variability in mixed layer nutrient concentration has been observed along Line P (Whitney et al. 1998; Peña and Varela 2007).

Climatic changes resulting in surface warming and/or freshening cause an increase in the density gradient between the surface layer and underlying nutrient-rich waters and thus could reduce the transport of nutrient-rich waters to the surface layer of the ocean. Also, increase in upper ocean stratification might increase the remineralization of organic matter (increasing the concentration of nutrients and consumption of oxygen) in waters just below the mixed layer, countering the effect of reduced water transport. Freeland et al. (1997) and Whitney et al. (1998) provided evidence of a long-term trend towards fresher, warmer, and less nutrient-rich waters at OSP based on observations over the 1956-1996 period. However, a later analysis of Line P surface layer nutrient concentrations for the years 1969-2005 (Peña and Varela 2007) showed significant interannual and decadal variations rather than a long-term trend. In the subarctic Pacific, Ono et al. (2008) found evidence of decline in summer surface nutrient concentrations during 1975 to 2005. Their analysis suggests that this nutrient trend is mainly due to recent stratification of the upper ocean rather than an alias generated by decadal or shorter term variation. In contrast, Whitney (2011) did not find significant linear trends in surface layer nutrients in the eastern subarctic Pacific in both winter and summer during the 1965-2009 period, despite evidence that the upper ocean is becoming more stratified (Freeland 2013). He suggested that nutrient enrichment of the shallow pycnocline might be countering the effects of strengthening upper ocean stratification in this region.

Open Ocean

Long time series of upper ocean nitrate and silicate concentration collected in the Gulf of Alaska along Line P have shown marked interannual and decadal variability. Nitrate anomalies (Figure 42a), computed by removing the long-term monthly means (1964-1981) along Line P, were positive beyond the continental shelf (west of 128°W), indicating higher concentrations of nitrate than the long-term average in 1971-1972, 1975-1978, 1988-1990, 2000-2002 and 2007-2009. During the 1990s, nutrient anomalies were mostly negative (i.e. lower concentrations of nutrients than the long-term average). This period coincides with the strong warming cycle observed in the NE subarctic Pacific. Di Lorenzo et al. (2009) showed evidence that these decadal variations in upper ocean nutrients (and also salinity) are linked to the North Pacific Gyre Oscillation (NPGO; Figure 42b); a climate mode of variability that tracks changes in strength of the central and eastern branches of the North Pacific Gyre and of the Kuroshio-Oyashio Extension. Their analysis included observations from years 1963-2004. In recent years, these relationships generally hold except for a brief period during 2009-2011 where nutrient anomalies present a different pattern of variability than the NPGO.

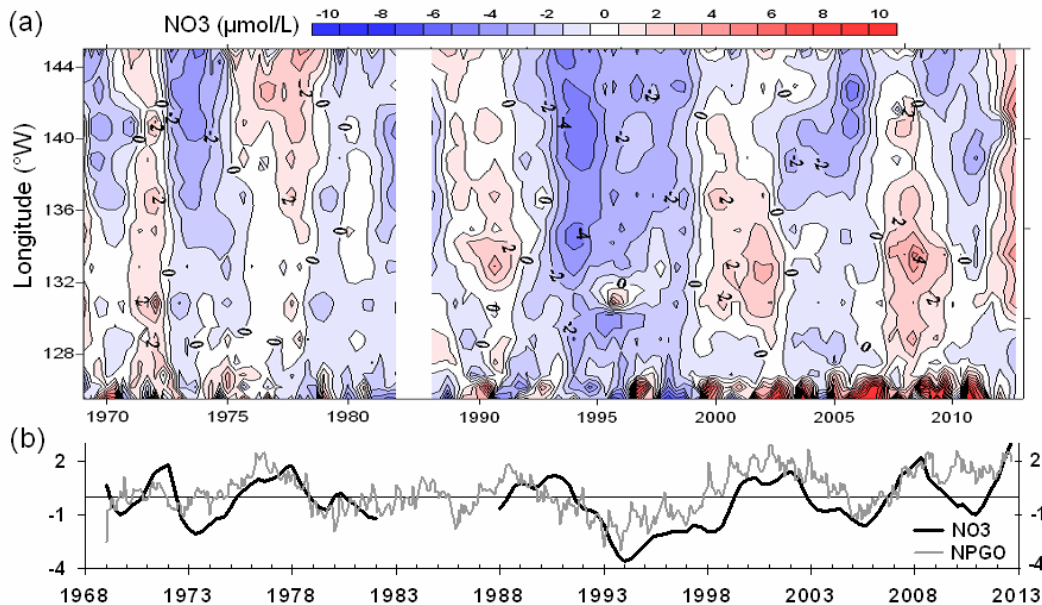


Figure 42: (a) Hovmöller plot of upper mixed-layer nitrate concentration anomalies ($\mu\text{mol/L}$) along Line P from 1969 to 1981 and from 1988 to 2012. (b) Comparison of upper mixed-layer nitrate concentration anomalies averaged along Line P (west of 128°W) with the NPGO climate index.

In the HNLC portion of Line P (Figure 43a), long-term fluctuations in upper layer nitrate concentration have little effect on phytoplankton nitrate utilization (Peña and Varela 2007) because iron availability rather than nitrate limits phytoplankton growth. Iron is transported to the northeast Pacific from continents either in the ocean as mesoscale eddies or off-shelf transport or in the atmosphere as volcanic ash and dust. Eastward, towards the shelf, fluctuations in the winter supply of nutrients to the surface layer results in variations in the size of the region where nitrate is depleted in summer. For example, during the summer following the 1997-98 El Niño nitrate was depleted eastward of 135°W along Line P. During 2010, nitrate depletion was also extensive but in nearshore stations nitrate was high. In contrast, in 2007 and 2008 (La Niña conditions) summer nitrate depletion occurred over a narrower region (from ~126° to 129°W). As shown in Figure 43c, variations in the extent of nitrate depletion are better linked to the Oceanic Niño Index (ONI; positive for El Niño, negative for La Niña) than to the NPGO, although both indices display some common variability. Whitney et al. (1998) suggested that variations in the

eastern boundary of the HNLC region were due to variable seasonal westward spreading of coastal waters which is related to El Niño effects.

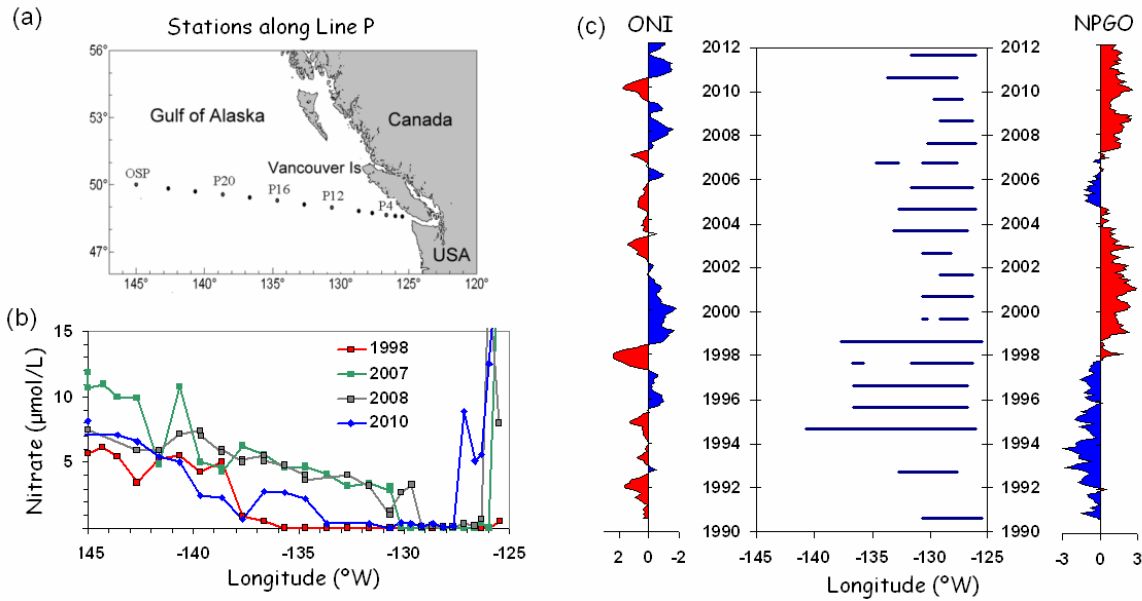


Figure 43: (a) Map of the NE subarctic Pacific showing the Line P transect and the location of the five main stations, (b) surface nitrate concentration along Line P during the summer in selected years, and (c) time-series of surface nitrate depletion (nitrate concentration $\leq 0.5 \mu\text{mol/L}$) during the summer and two climate indices (ONI and NPGO).

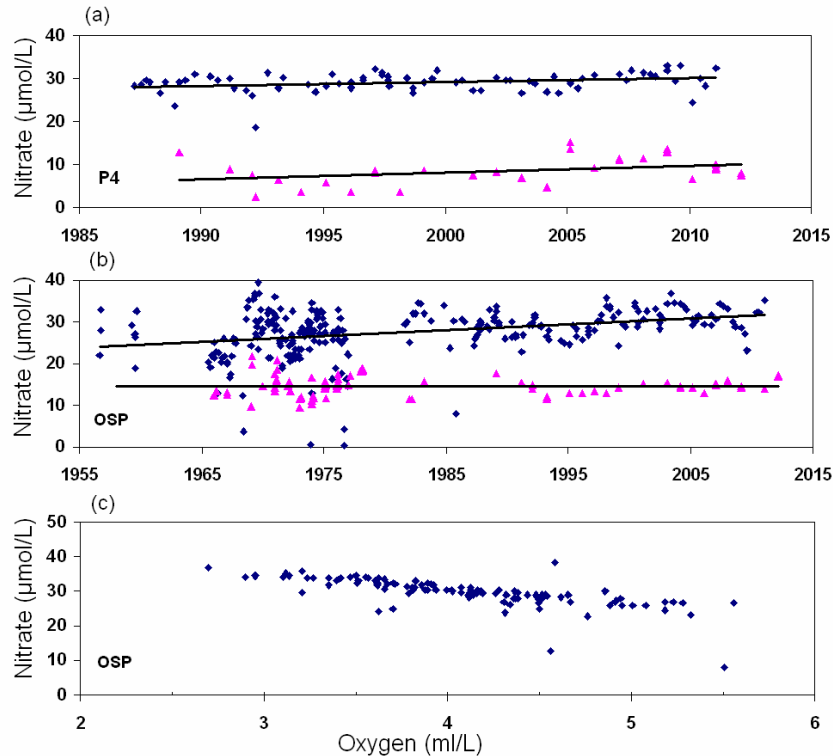


Figure 44: Time-series of nitrate concentration in the surface layer in winter (magenta triangles) and at 150 m (blue diamond) at (a) stations P4 and (b) OSP. (c) Comparison of nitrate and oxygen concentration at 150 m at OSP.

Given that significant decadal variations in nutrient concentrations are present in the northeast Pacific, long time series of observations are necessary to separate decadal oscillations and shorter-term variations from ‘linear’ long-term trends that may be resulting from increasing ocean stratification with anthropogenic climate change. Linear trends in nitrate concentration in the mixed-layer and below the surface layer (150 m) were carried out at the five main stations of Line P (Figure 43a). Only observations from winter were included in the analysis of upper layer nutrients. Contrary to expectation, significant ($P>0.95$) positive trends toward higher surface layer nitrate concentration were found at P4 and P12 but not at the other main stations (Figure 43). Below the surface layer, a significant trend towards higher nitrate concentration was found only at OSP. Similarly, a significant trend towards lower oxygen concentrations has been reported in subsurface water (100-300 m) at OSP (Whitney et al. 2007). Nutrient concentrations vary inversely with oxygen (Figure 44), as would be expected from the remineralization of organic particles.

British Columbia continental Shelf

Horizontal gradients in surface and sub-surface nutrient concentrations are significant along and across the continental shelf of British Columbia. In this region, surface layer nutrient concentrations are highest in late summer and early fall during the coastal upwelling season. The spatial distribution of surface layer and near-bottom nitrate concentrations during fall are shown in Figure 45. Nitrate concentrations are higher along the inner shelf of Vancouver Island and in Hecate Strait. At both depths, waters with high nitrate concentrations extend farther offshore off southwest Vancouver Island (SWVI) where there is a broad shelf between 100 and 200 m depth. The SWVI region is part of the northern California Current eastern boundary current system which is influenced by seasonal coastal upwelling. Upwelling winds along the west coast, especially in summer, advect nutrient-rich, oxygen-poor California Undercurrent waters across the slope and shelf. In addition, tidal mixing provides nutrients to the outflowing surface waters of Juan de Fuca Strait, which is a major source of surface nutrients on the continental shelf of the southwest coast of Vancouver Island

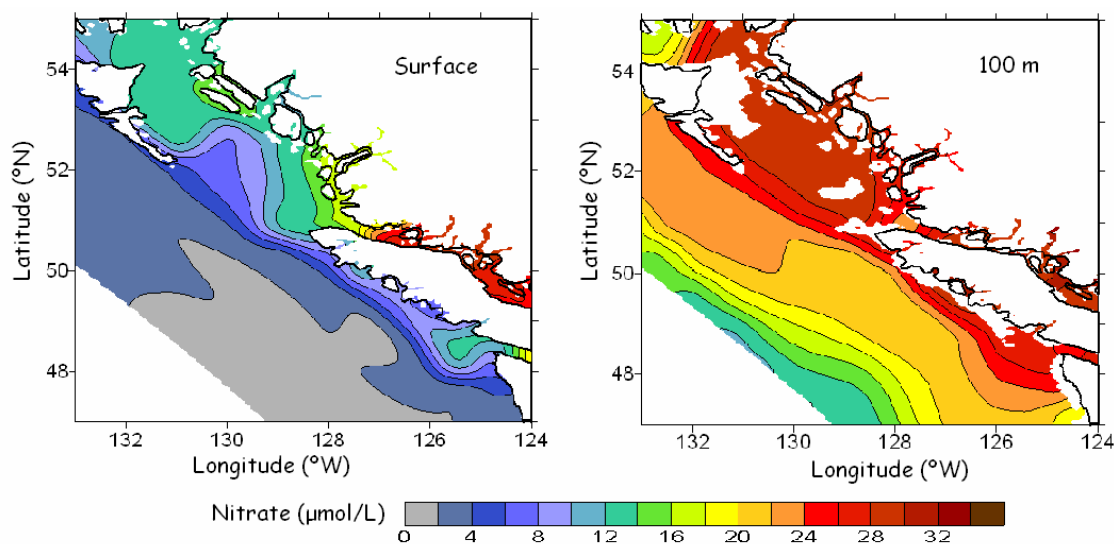


Figure 45: Composite contours of nitrate concentration at the surface and at 100m on the British Columbia shelf from historical observations at IOS and WOD05 data for the years 1960-2006.

In this region, nutrient observations are neither temporally nor spatially intense enough to resolve variations in surface layer nutrient concentrations during short-duration events such as tidal mixing or wind-driven upwelling. Therefore, to look at temporal changes, we focus on subsurface nutrient concentrations at a station on the southern British Columbia shelf, LB08 at 48° 25.3'N, 125° 28.66'W in

145 m of water, where sampling have been carried out in almost all summers for three decades. Figure 46 presents a summary of nitrate observations within 20 m of the ocean bottom for 1979-2010. Seasonally, nitrate concentrations range from 23 to 42 $\mu\text{mol/L}$ and are lowest in winter and highest at the end of summer (Figure 46a). More observations are available for oxygen concentrations (Figure 46b) which vary inversely with nitrate, as would be expected from the remineralization of organic particles (Figure 46c). In general, the highest nitrate (lowest oxygen) concentrations at LB08 have mostly occurred since 2005. One expects nitrate concentrations to increase in sub-surface waters as oxygen declines, because of the oxidation of organic matter. Thus, the increase in nitrate in recent years is compatible with oxidation in subsurface waters.

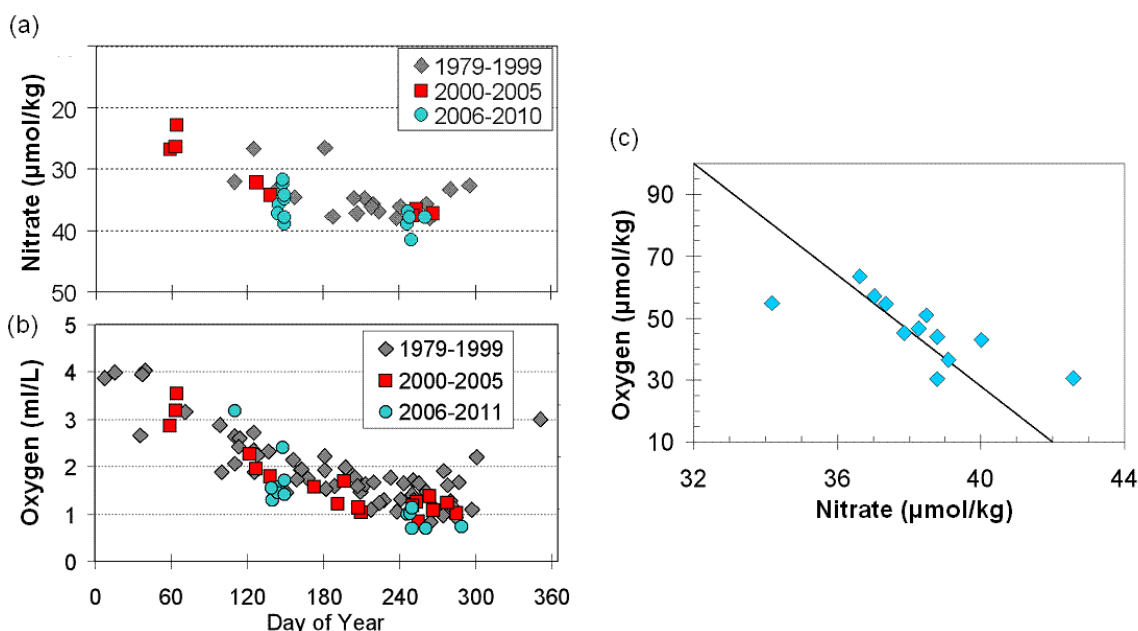


Figure 46: Near bottom nitrate (a) and oxygen (b) concentrations versus day of year at LB08 during 1979 to 2011. Comparison of nitrate and oxygen concentrations (c). The black line has a slope of 9.

THE INCREASE IN CARBON ALONG THE CANADIAN PACIFIC COAST

D. Ianson, Institute of Ocean Sciences, Fisheries and Oceans Canada

Introduction

This chapter deals with the increase in dissolved inorganic carbon along the Canadian Pacific coast and the risk that this increase may pose to marine organisms. The following text gives some brief background concerning the increase in carbon and associated ocean acidification. A biological indicator for ocean acidification is defined. Available data in the study region are discussed. The circulation in the study area is also discussed in detail, as this circulation plays a major role in setting the carbon state in our region. Finally the best evidence for the current carbon state in our region is presented and potential changes due to climate change are discussed.

Carbon in the Ocean: As atmospheric CO_2 increases due to anthropogenic greenhouse gas emissions, the oceans take up a significant portion of this carbon (about 25%, Le Quéré et al. 2010; 30% if land use changes are not included, Denman et al. 2007). The ocean has a great capacity to hold carbon due to the reaction of CO_2 with seawater (Revelle and Suess 1957). However, increasing the total amount of dissolved carbon in seawater changes the ratio of the chemical forms of that carbon, ultimately decreasing ocean pH. This issue has been termed 'ocean acidification' (e.g. Orr et al. 2005).

Biological impacts of ocean acidification: Biological impacts of ocean acidification on marine organisms are anticipated both through the decreased ability to calcify (for organisms that require calcification, Orr et al. 2005) and via hypercapnia (essentially the reduction of the blood's ability to carry oxygen when CO₂ concentrations become too high; e.g. Redfield and Goodkind 1929). Research into these biological effects is still in its infancy. However it is clear from the geological record that mass extinctions are possible. For example, about 55 million years ago, atmospheric CO₂ increased at the greatest rate in the Earth's history prior to human times (~10 times slower than the current rate of increase), many benthic calcifiers disappeared (Zachos et al. 2005). It is also possible that many organisms will adapt, although research into adaptation is only beginning (Kelly and Hoffmann 2012). Regardless, changes to marine ecosystems due to the increased carbon in the ocean are likely. These changes are anticipated to impact economies (e.g. Cooley and Doney 2009).

Defining a biologically relevant indicator - "Undersaturation": Many marine organisms (e.g. plankton such as coccolithophores and pteropods, and benthic molluscs such as oysters) build shells out of calcium carbonate, and from a thermodynamic standpoint, calcification becomes increasingly difficult as pH decreases (or as carbon concentrations increase). The shift in chemical speciation of carbon causes a decrease in the free concentration of carbonate ion with increased carbon (decreased pH). The two main mineral forms of calcium carbonate are aragonite and calcite. The form that is most susceptible to increased acidity is aragonite. Many organisms that are ecologically relevant along the Pacific Canadian coast use aragonite in their shells and structures e.g. pteropods, a staple food for juvenile salmon (Boldt and Haldorson 2003; Armstrong et al. 2005). For this reason, the aragonite saturation state (Ω_{arag}) will be used here as a biological indicator of ocean acidification. Specifically, the point at which aragonite dissolution occurs more rapidly than aragonite production ($\Omega_{\text{arag}}=1$) will be used. The depth in the water column at which this point is reached is termed the aragonite saturation horizon.

The aragonite saturation state decreases as the amount of dissolved carbon increases for a given temperature, salinity, pressure and alkalinity. Alkalinity changes occur when organisms precipitate calcium carbonate and when carbonate minerals dissolve. Lesser changes are associated with plankton uptake and remineralization of nutrients. In our region, alkalinity is affected most by dilution, i.e. inputs of fresh water with negligible alkalinity (Ianson et al. 2003). Because carbon (and pressure) generally increase with depth in the ocean, the saturation state almost always decreases with depth (e.g. Mucci 1983). As a result, at present surface waters are supersaturated with respect to aragonite at most times and places in the world's ocean and undersaturated (i.e. aragonite will dissolve) at depth. The exact depth of the transition from saturation to undersaturation (the saturation horizon) depends on the location and the time of year.

Our current knowledge of the carbon state: There are few places in the world's ocean where a time series of carbon state exists that is sufficient to examine trends in carbon, or acidity, with time. This lack of data is partially due to the fact that the ocean hasn't been sampled for carbon (or related parameters such as alkalinity, pH or the partial pressure of carbon dioxide, pCO₂) as extensively as it has for temperature, salinity or oxygen. In addition, to fully determine the carbon state, and aragonite undersaturation, at least two of the above carbon parameters must be measured, along with temperature, salinity and pressure.

A second barrier is the difficulty in making these carbon measurements well. Until the mid-late 1980s research groups were not able to get consistent results in their measurements because the techniques had not developed sufficiently. Now there are standard methods and well-developed inter-comparison projects (e.g. Dickson et al. 2007). This report only considers carbon data collected with well

established methods and in which the carbon state is defined (i.e. at least two of the carbon parameters have been measured, as described above).

On the outer coast in our study region the first carbon data were collected in July 1998 (Ianson et al. 2003). This year was not a typical year (strong El Niño in winter 1997-98 followed by strong La Niña in summer 1998). There have been three subsequent surveys along the outer coast: in 2004, 2007 (Feely et al. 2008) and in 2010. Carbon data are a regular part of the Line P surveys (data are collected at two stations over the shelf off the west coast of Vancouver Island, WCVI, on each of the 3 trips/year). DIC data have been collected along Line P since 1986 and alkalinity since 1992, but the quality of the alkalinity data is poor prior to 2000. Similarly 4 shelf locations are sampled on the LaPerouse cruises (DFO) (2 trips/year). In the inner waters of the Salish Sea, even fewer carbon data have been collected. There have been samples collected in the Strait of Georgia in fall and winter of 2003 and summers of 2010 and 2011. Similar to the WCVI, samples are now collected regularly at 4 stations as part of the Strait of Georgia monitoring programme. Thus, it is not possible at present to examine trends in carbon states and difficult to evaluate even the current state. This difficulty is in part due to the dynamic nature of the local circulation.

Physical circulation and its impact on carbon states

Outer British Columbian coast: The circulation off the WCVI is complex (e.g. Thomson 1981; Freeland et al. 1984). During all seasons, a strong buoyancy current flows northward over the inner-shelf, the Vancouver Island Coastal Current (VICC) (e.g. Hickey et al. 1991). During the summer, upwelling along the WCVI occurs along with equatorward flow along the shelf-break (adjacent to and seaward of the poleward VICC). During the winter, winds reverse direction, the shelf-break current flows poleward and downwelling occurs. Between these seasons are the spring and fall transitions. The northern tip of Vancouver Island forms the northern boundary for strong summer upwelling (Thomson 1981; Ware and Thomson 2005). North of Vancouver Island, in the Queen Charlotte Sound region, the summer is considered a time of relaxation (no consistent upwelling or downwelling) and winter downwelling is considerably stronger than off WCVI (e.g. Foreman et al. 2011).

Upwelling circulation causes dense, nutrient and carbon rich water from intermediate depths (~100 m) to be raised to the surface in sporadic bursts (e.g. Lentz 1992; Smith 1994). The upwelled water, rich in carbon, also has a considerably lower pH and saturation state (for both calcite and aragonite) than water usually found near the surface (e.g. Feely et al. 2008). Once at the surface this upwelled water sparks phytoplankton blooms, often so intense that they draw pCO_2 down well below atmospheric pressure (e.g. Ianson et al. 2003; Nemcek et al. 2008; Evans et al. 2012; Tortell et al. 2012). Under these conditions, surface waters are highly supersaturated with respect to aragonite. These changes happen rapidly, so that in a matter of days surface conditions at a given coastal location can change from saturated to under-saturated to highly super-saturated. Thus coastal upwelling regions have the most extreme spatial and temporal variability in carbon states of any oceanic region (e.g. Hales et al. 2007). These abrupt changes are much greater than the anthropogenic signal of increased carbon occurring in the atmosphere during the same period. Thus anticipated changes in carbon states along our coast over the next decades will be controlled primarily by physical wind forcing (responsible for upwelling) and changes in water column stratification (which affects the depth and density, hence carbon content, of upwelling).

Downwelling in winter is essentially the opposite of upwelling. Surface waters are forced onshore by the poleward winds (interacting with the Coriolis force, e.g. Smith 1994). Constant density surfaces are forced down further from the surface. In fact strong winter downwelling is likely to precondition the local shelf so that nutrient and carbon concentrations are lower in spring and summer following a strong

downwelling winter (e.g. Ianson et al. 2009; Tortell et al 2012) and potentially cause upwelled water to have lower carbon concentrations and fuel lower productivity, resulting in less variability (Ianson and Allen 2002).

Southern Strait of Georgia: In the southern Strait of Georgia the Fraser River plays a dominant role in setting circulation and chemical properties in the upper layer of the water column (e.g. Masson 2006). The Fraser River is the most important fresh water source (relative to other streams, inlets and tributaries). Its plume covers the south and central Strait and is usually 2-10 m thick with a strong density gradient beneath it (LeBlond 1983). Tides are strong, and open ocean connections at the south dominate the control of sea level in the Strait (LeBlond 1983). These ocean connections are relatively shallow and narrow and so are sites of intense tidal mixing, in which subsurface water, anticipated to be rich in carbon (therefore low Ω) is brought to the surface.

Thus, estuarine circulation (Hansen and Rattray 1966) and tidal flows play the key roles in setting the physical circulation. Briefly, over time scales larger than days, the upper layer flows seaward from the Fraser. In classical estuarine circulation (Hansen and Rattray 1966) there is a return flow in the sub-surface layer. In this case the return flow is modified in the shallow constricted areas where tidal energy mixes this flow into the surface. Most of the deeper water that flows into the Juan de Fuca Strait (the return flow) ends up flowing out (seaward) again as part of the overall estuarine circulation (e.g. Masson 2006). Some of this water enters the Strait of Georgia, primarily at intermediate depths (~100 m, Masson 2006). Only during summer are there occasional 'deep water renewal' events during which dense salty water from the return flow enters the deepest layer of the Strait. As a result, the deep Strait waters are relatively stagnant and mixing is minimal with only weak vertical gradients (Masson 2006). During winter the Fraser River flow is at a minimum, and during the summer its flow is strongest (due to snow melt). Thus, during winter the estuarine circulation is weakest. Winds are strongest in winter. As a result, wind mixing plays a more important role in the surface layer in the Strait during winter.

Annual carbon cycles

Outer Coast - Modelled: A model was developed to predict carbon states on the outer shelf and slope of the WCVI, not including the buoyancy current (Ianson and Allen 2002). This model shows the strong variability discussed above, particularly during the summer upwelling season (Figure 47). This variability is present despite averaging both surface and lower-layer concentrations. Fully resolved vertical profiles would be expected to show even greater extremes. A typical annual cycle in acidity (pH, Figure 48) shows that, as is the case with the other carbon parameters (pCO₂ and total inorganic carbon, Figure 47), the greatest variability occurs during the summer upwelling season. Surface acidity levels over the shelf range from well below 8 (~7.8) to just over 8.1, which is about the current average in the global surface ocean. Again these values represent average values in the upper layer and greater extremes are expected if results were vertically resolved. However, the lowest (or most acidic) intervals during summer are short lived. During winter and fall the average surface (both shelf and slope) pH is consistently low, i.e. less than ~7.9 (Figure 48). These results agree with a recent compilation of surface pCO₂ (Evans et al. 2012) given that pH generally decreases as pCO₂ increases (if alkalinity and T and S are constant). Where data are available results compare favourably (Figure 47).

In the lower layer pH and total inorganic carbon is less variable (Figure 48 and Figure 47 respectively) but still not constant, indicating that physical circulation and remineralization (decaying organic matter produced by phytoplankton blooms) play an important role (Ianson et al. 2009). These lower layer pH values (around 7.6) are generally indicative of undersaturated conditions. Thus, bottom-dwellers such as groundfish experience undersaturated conditions all, or most of, the time.

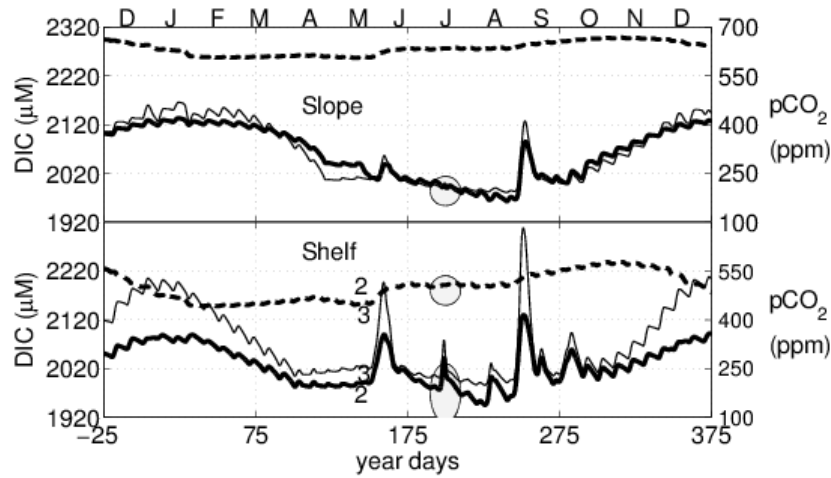


Figure 47: Modelled annual (bottom axis - Julian Day, top axis - months of the year) cycles of surface $p\text{CO}_2$ (thin solid line), surface average total inorganic carbon (DIC) concentrations (bold line) and lower layer average DIC (bold dashed line) over the outer shelf (bottom panel) and slope (top panel) of the WCVI for a typical year in upwelling and downwelling forcing. The range in DIC from several transects during the summer of 1998 (Ianson et al. 2003) is shown by grey ellipses. Average DIC data from two transects during spring 2007 (Feely et al. 2008) are also shown. Figure taken from Ianson et al. 2009.

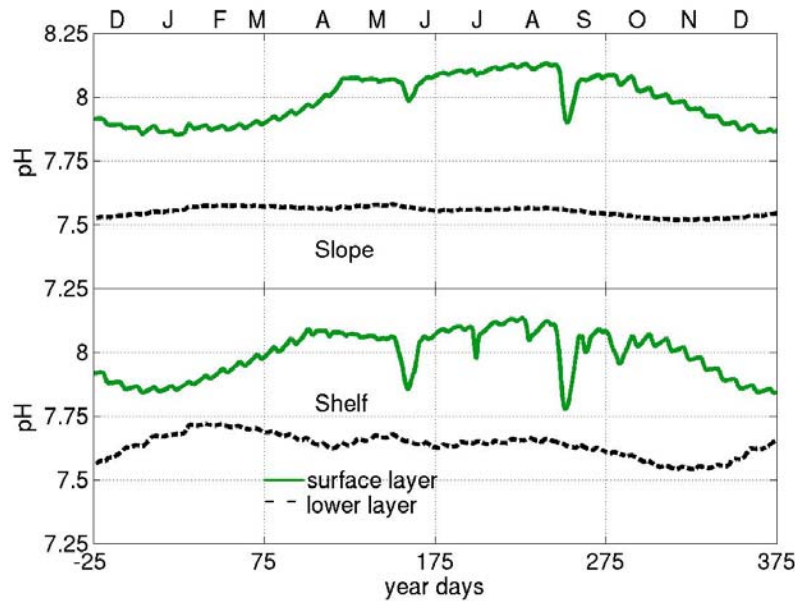


Figure 48: Modelled annual (bottom axis - Julian Day, top axis - months of the year) cycles of pH in the surface layer (bold green curve) and lower layer (black dashed curve) over the shelf (bottom panel) and slope (top panel) of the WCVI for a typical year in upwelling and downwelling forcing.

Year to year variability in wind forcing causes large changes in upwelling and downwelling, both in intensity, duration and timing (e.g. Thomson and Ware 1996; Foreman et al. 2011). These changes in wind-forcing will cause strong interannual variability in carbon states experienced on the shelf (e.g. Ianson and Allen 2002; Ianson et al. 2009). To generalize, strong downwelling will likely cause acidity to be lower throughout the year, while strong upwelling has the opposite effect. There are subtleties in

these generalizations as the ratio of upwelling to downwelling is important, as is shelf width (Ianson et al. 2009). Variation in buoyancy flux due to fresh water delivered through rain or terrigenous run-off, not addressed in the previous studies, will also play a role. Specifically, increased fresh water flux would cause stratification in the water column to increase so that more energy would be required to raise deep, carbon rich parcels of water to the surface. However, increased buoyancy fluxes themselves may play an important role in setting the carbon state (e.g. terrigenous run-off may contain ions that affect the alkalinity and acidity of the receiving waters).

The inner-shelf buoyancy current: The inner-shelf buoyancy current (VICC) is expected to play an important role in setting carbon concentrations along the WCVI. It is included in the model presented above (Ianson and Allen 2002) but not in a predictive sense. Its properties are prescribed based on data (Ianson et al. 2003). Similarly, a quasi 2-D vertically resolved model of the same region (that runs through spring and summer only, Bianucci et al. 2011) uses the same data set to prescribe conditions in the VICC.

Briefly, the VICC is a strong consistent current and forms a barrier to upwelled water, and other properties (Thomson et al. 1989; Bianucci et al. 2011). It also has exceptionally high nutrient and carbon content throughout the water column near its source at the south west tip of the island (e.g. Ianson et al. 2003). Thus surface waters of the VICC have generally high inorganic carbon concentrations, $p\text{CO}_2$ (Ianson et al. 2003; Nemcek et al. 2008) and so lower saturation states along the southwest of the WCVI. This excess carbon is a result of strong tidal mixing in the source waters of the VICC (the Juan de Fuca Strait) and is drawn down by biological productivity (in summer), mixed with outer shelf waters, and outgassed, so that by the time the VICC is roughly midway up the island its surface carbon content does not differ from the surrounding waters (e.g. Ianson et al. 2003). On the other hand the presence of the VICC stops upwelled water from penetrating the inner shelf, essentially protecting that region from the high carbon (low saturation state) water delivered by upwelling (e.g. Bianucci et al. 2011).

Reconstructed carbon states on the outer coast: An empirical method that allows estimation of Ω from Temperature (T) and O_2 observations was developed for the outer BC coast where the majority of the Pacific coast carbon data have been collected to date (Ianson, unpublished data). There are ~600 total carbon samples (for which DIC and alkalinity as well as T, S, O_2 and nutrients are available) collected mostly in summer (1998-2010). About 40% of these samples were collected in the surface. There are about 12 thousand concurrent observations of T and (bottle) O_2 available from the study region in the IOS data archive. These historical data (1979-1010) were collected at similar depths as the carbon data were, and are more evenly distributed about the seasons, with the majority still falling in summer (Ianson, unpublished data). For this study the oceanographic seasons are based on the shifts of winds that force upwelling and downwelling (Ianson, unpublished data) rather than calendar seasons were used. The (average) winter season is the longest, followed by summer and spring, while fall is the shortest; however interannual variability in season length is strong (Ianson, unpublished data).

Results show that some undersaturation of aragonite occurs in the deeper shelf waters much of the time throughout the year (the blue bars indicate probability of some undersaturation in the full water column, Figure 49). During winter most of the shelf is supersaturated with respect to aragonite most of the time, because downwelling forces offshore surface waters, which are relatively low in carbon, onto the shelf, and the subsurface carbon-rich waters are pushed off (Figure 49a). In contrast, the summer upwelling season shows that at least the bottom waters (water depths are always less than 200 m) of the shelf are undersaturated most of the time (over 80%) (Figure 49a). At the onset of this season, intermediate depth isopycnals (rich in carbon) are brought onto the shelf and periodically mix into the surface. The intense

blooms that result cause a secondary effect, remineralization of organic carbon over the shelf, which reduces the saturation state, especially in the lower layer during the fall (e.g. Ianson et al. 2009). As a result, the aragonite saturation horizon is found relatively high in the water column, above 60 m depth over 40% of the time during both summer and fall (green bars, Figure 49a). There are even rare occurrences of undersaturation in the upper mixed layer (upper 20 m) during summer (about 2% probability, yellow bar, Figure 49a) based on the historical data.

In addition, conditions are the most variable over the shelf, relative to the adjacent slope and offshore waters (Figure 49a and b, respectively). As discussed above, the greatest vertical displacement of isopycnals due to upwelling and downwelling occurs on the shelf (Figure 49a) so this result is not a surprise. It is unusual for undersaturation of aragonite to occur shallower than 60 m depth off the shelf ($< \sim 10\%$ chance, green bars, Figure 49a) and undersaturation never occurs in the surface, at least in these reconstructed data (there are no yellow bars in Figure 49b). Some undersaturation is always present in the water column adjacent to the shelf, simply because it is much deeper than the shelf (> 200 m at all locations) and the aragonite saturation horizon is always found above 200 m in these data (as expected in the Northeast Pacific, Feely et al. 2004; Feely et al. 2008).

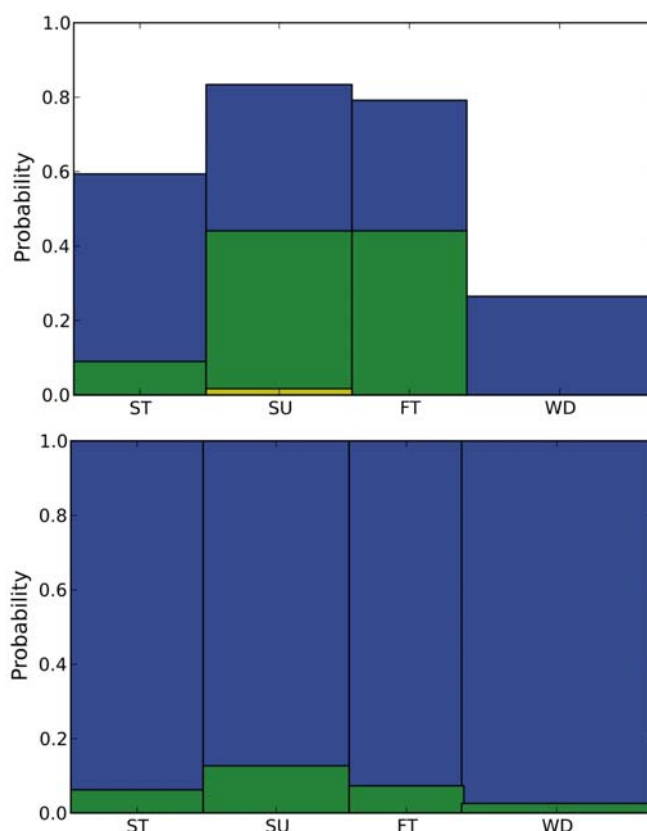


Figure 49: The probability of undersaturation with respect to aragonite along the BC coast as determined by an empirical model (A) over the shelf (inshore of the 200 m isobath) and (B) immediately adjacent to the shelf over the slope and offshore waters during the four oceanographic seasons. ST = spring transition (beginning on Julian day 65); SU = summer upwelling (beginning on Julian day 148); FT = fall transition (beginning on Julian day 239) and WD = winter downwelling (beginning on Julian day 311). The blue bars show the probability of undersaturation occurring at any depth in the water column. The green bars show the probability of undersaturation occurring between 20 and 60 m depth. Yellow shows the probability of undersaturation occurring in the upper 20 m of the water column (which only occurs over the shelf in the summer season). Undersaturation always occurs off the shelf because the water column is deeper than 200 m.

Modelled carbon states in the southern Strait of Georgia: A vertically resolved column model for the Southern Strait of Georgia (Collins et al. 2009; Allen and Wolfe 2012) is able to successfully predict the timing of the spring bloom. Although this model is only one-dimensional, it takes the flow of the Fraser into account (model fully described in Collins et al. 2009). The model captures only the upper 40 m of the water column, however many marine organisms of interest to DFO reside in this vertical zone (e.g. shellfish aquaculture). Carbon has been added to this model (Ianson, unpublished data) and the annual cycle of carbon analyzed for 10 years of local wind, cloud and freshwater forcing.

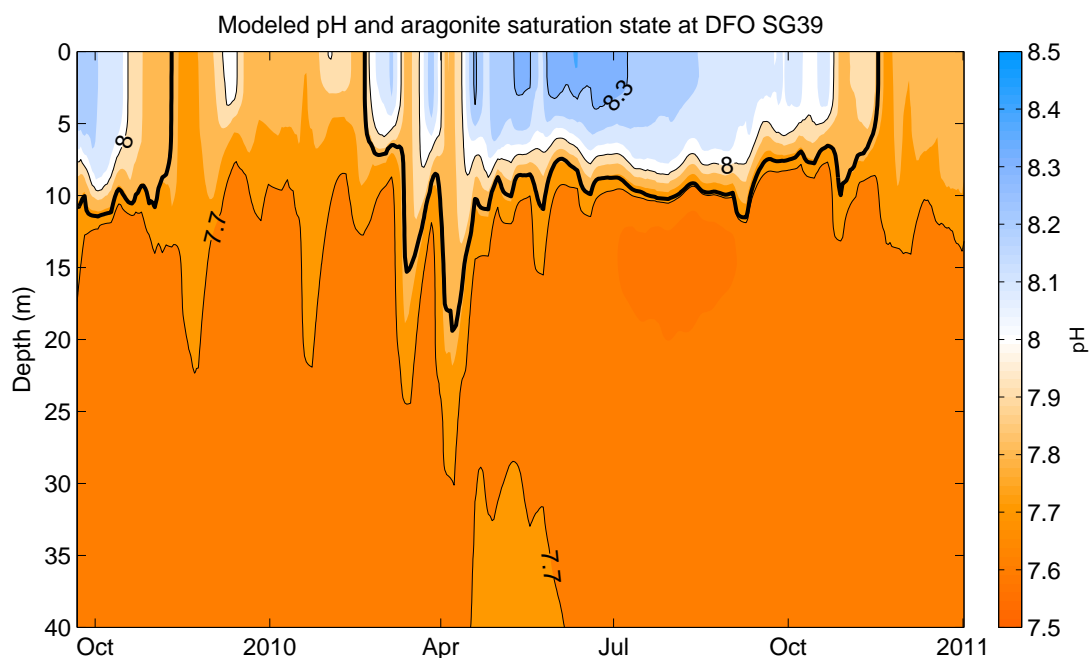


Figure 50: Modelled annual pH cycles in the Southern Strait of Georgia for 2010, which is a typical year, in the top 40 m of the water column. The bold dark line indicates the aragonite saturation horizon. The time series is smoothed using a 7-d window. Figure provided courtesy of B. Moore-Maley.

During the summer the Fraser River flow plays the dominant role in controlling surface pH (as expected). Increased stratification and light availability cause phytoplankton blooms and the resulting biological carbon uptake causes surface pH to increase, so that most of the time it is above 8, and greater than 8.3 for significant periods of time (Figure 50). There are however strong vertical gradients (again as expected) and as a result the saturation horizon remains relatively shallow (~ 10 m) in the water column as carbon increases rapidly below the upper mixed layer (Figure 50). The relaxation of strong winds in spring is a key feature in triggering the spring bloom (Collins 2009); however in summer winds mix nutrients (and carbon) into the surface to fuel the phytoplankton production.

A typical annual cycle (in this case 2010, Figure 48), validated by the few available data, shows that there is a period during winter in which pH is relatively low (~ 7.8, similar to surface values over the shelf on the outer coast at that time of year, Figure 48). Undersaturation with respect to aragonite occurs at the surface at this time. The dark solid line in Figure 50 indicates the aragonite saturation horizon. Sensitivity analyses show that the low surface pH is caused by wind mixing at this time, when light is limiting to phytoplankton growth. Subsurface waters, that are richer in carbon and lower in pH are mixed to the surface and because CO₂ air-sea gas exchange is relatively slow (an order of magnitude slower than O₂), the period of high surface carbon (low pH) persists.

Anticipated trends

Interannual variability throughout the Pacific coast (both the outer shelf and inner Strait of Georgia waters) is naturally high. Thus, it will take some time before any trends associated with climate change would be visible even if temporal sampling resolution were high (e.g. daily or monthly). For example, time series of only one to three decades may show a brief trend opposing the trend that would be visible in a time series that is much longer (*sensu* Easterling and Wehner 2009).

In fact, surface pCO₂ trends in the 'transition zone' between the outer WCVI and the Alaskan gyre (open ocean) from 1973--2005 do not show the expected positive trend (due to uptake of anthropogenic carbon) which is seen in the gyre itself (Wong et al. 2010). This data set has limited temporal resolution (~3 samples/yr) so natural variability could easily bias the result (recall the high variability possible within seasons, Figure 47 and Figure 48). In addition, changes in circulation, or biological processes, may play a role (Wong et al. 2010), highlighting the complexity of the processes upon which anthropogenic trends are superimposed.

Despite the fact that we know overall concentrations of carbon are increasing in the ocean due to oceanic uptake of anthropogenic carbon (Feely et al. 2004; Orr et al. 2005), this effect will be hard to observe for some time. Climate change is anticipated to bring stronger winds to the region, both during upwelling season and the downwelling season, although the predicted downwelling trend is not statistically significant (Merryfield et al. 2009). A positive trend in upwelling and downwelling strength has been observed in the past 50 years (Foreman et al. 2011). Either increased upwelling strength, or the incidence of isolated strong events, would serve to increase the chances of low Ω water on the outer shelf. Increased downwelling on the other hand would decrease surface carbon concentrations (and increase pH) and the annual carbon inventory on the shelf (Ianson and Allen 2002; Ianson et al. 2009). Decreased carbon inventories would in general reduce the potential for extremes in low Ω water being brought to the surface during the summer months and also decrease the carbon concentrations that benthic organisms experience. The balance between the impacts of the two, upwelling and downwelling, remains unknown. Regardless, in the next decades, natural variability in wind forcing is still expected to be greater than any climate-induced increase in winds in the Northeast Pacific region (Deser et al. 2012).

The Northeast Pacific Ocean has in general shown a trend to freshening (see chapter on "Trends in temperature, salinity, water column stability and mixing depth in the open Gulf of Alaska"). The resulting increased stratification would in general cause the depth of upwelled water for a given wind strength to decrease (e.g. Lentz and Chapman 2004) and so bring less carbon into or near the surface. However, dilution of surface DIC by buoyancy fluxes plays a dual role, as decreasing DIC increases Ω but decreasing alkalinity (again by dilution) decreases Ω . The net result of 'freshening' in the region can also depend on the ions present in the fresh water from rock weathering (e.g. additional terrestrial sources of alkalinity).

Conclusions

The ocean's carbon content is increasing due to uptake of anthropogenic carbon, i.e. ocean acidification (Orr et al. 2005). However trends associated with this increase have been determined primarily from global-scale models because in most locations of the ocean the data do not exist to determine a trend from observations. In addition it is difficult to identify trends given natural variability without relatively long time series (e.g. Easterling and Wehner 2009).

Relatively few carbon data have been collected on the Canadian Pacific coast that include enough information to define the carbon system. The first data were collected in 1998. Beginning in 2010, following an intensive carbon survey on the entire BC coast, some carbon data are collected as part of existing on-going monitoring programmes in the Strait of Georgia (16 profiles/yr) and on the WCVI (14 profiles/yr). This work is not formally funded. At this time it is not possible to determine any trend in carbon states along the BC coast. However some work has been done to assess the natural variability.

Modelling studies have allowed annual cycles of carbon and pH to be determined over the outer shelf and in the southern Strait of Georgia. These studies indicate high temporal variability, especially during summer, due to the dynamic circulation in the region, and the associated biological response (Figure 47, Figure 48 and Figure 50). In general the greatest extremes in low and high pH (and low and high omega) are found during the summer over the outer shelf (Figure 47 and Figure 48). However, during winter, when productivity is light-limited and wind-mixing is high, surface pH and omega are the lowest relative to the other seasons (Figure 48 and Figure 50). An empirical study that estimates omega from temperature and oxygen on the outer coast supports these model results, and shows that variability over the shelf is high, especially during summer (Figure 49). The aragonite saturation horizon over the outer shelf rarely reaches the surface, but undersaturated waters are usually present over the shelf. In the Strait of Georgia, model simulations show undersaturation at the surface in winter, and the saturation horizon is always relatively shallow, around 10 m (Figure 50).

In addition to increased carbon concentration due to ocean acidification, changes in ocean circulation due to climate change are expected to impact carbon states along the coast. Specifically increased upwelling intensity is expected (Merryfield et al. 2009) which will increase the likelihood of low omega states on the coast and likely cause extreme values to be lower. However, downwelling may also increase (Merryfield et al. 2009) and water column stratification may increase (see chapter on "Trends in temperature, salinity, water column stability and mixing depth in the open Gulf of Alaska") both of which would likely serve to modulate the negative impacts associated with increased upwelling. Regardless of these complex balances, natural interannual variability is expected to exceed any of these changes over the next several decades.

PROJECTIONS

PROJECTIONS FOR THE OPEN GULF OF ALASKA

J. R. Christian and O. Riche, Institute of Ocean Sciences, Fisheries and Oceans Canada

Introduction

Projection information from the CMIP5 (Taylor et al. 2012) models is available for the Gulf of Alaska subdomain. In the three coastal subdomains, this information is not usable without downscaling (see subsequent chapters on Canadian Regional Climate Model Projections Affecting British Columbia Coastal Waters and Results from Regional Climate Model Simulation for the British Columbia Continental Shelf). In the open ocean region, these models results can be used directly, with the understanding that they are simply model projections and therefore subject to model error and, for shorter time scales, aliasing of internal variability whose phase can never correspond exactly to the real world (Taylor 2001). It is well known in climate modelling that the mean of an ensemble of models frequently exhibits greater skill than any individual model (Lambert and Boer 2001). Different models have distinct biases, and if parameterizations are not common to many models (i.e. if the models are truly distinct and independent representations), these biases will more often than not partially offset each other.

Here we present physical and biogeochemical state information for the Gulf of Alaska from a suite of six CMIP5 models, for the present (2006-2025), the recent past (1966-1985), and projections for 2046-2065 for two distinct emission scenarios (“Representative Concentration Pathways”). This is far enough in the future that aliasing of internal variability should be a minor source of bias, especially for the mean of an ensemble of different models. The CMIP5 experimental design is described in detail in Taylor et al. 2012) and the Representative Concentration Pathways by Moss et al. (2010). The scenarios chosen are the “moderate mitigation scenario” (RCP4.5) and the “no mitigation scenario” (RCP8.5), which correspond to atmospheric CO₂ concentrations of about 500 and 600 ppm in 2050 respectively (Arora et al. 2011). However, it is important to note that the 2046-2065 time frame was not chosen for scientific reasons, and corresponds to the period where the two scenarios begin to diverge rapidly (i.e. by 2090 the difference between the two will be around 300 ppm). The models chosen were those that provide a broad range of ocean fields, and particularly those that provide information about the subsurface biogeochemical state (e.g., oxygen concentration and calcium carbonate saturation state). There are also logistical reasons, as these were the first models available that provided these fields; others have since been posted but have not yet been incorporated into the analysis. The six models used are CanESM2 (Arora et al. 2011), GFDL-ESM2M (Dunne et al. 2013), HadGEM2-ES (Martin et al. 2011), IPSL-CM5A-LR (Dufresne et al. 2013), MPI-ESM-LR (Giorgetta, unpublished data), and MIROC-ESM (Watanabe et al. 2011) (Table 9). These models collectively represent the state of the art in modelling Earth system responses to greenhouse gas forcing.

Table 9. List of global Earth System models used and their horizontal and vertical resolution (number of grid points in x/y/z directions).

	nx	ny	nz
CanESM2	256	192	40
GFDL-ESM2M	360	200	50
HadGEM2-ES	360	216	40
IPSL-CM5A-LR	182	149	31
MIROC-ESM	256	192	44
MPI-ESM-LR	256	220	40

Projections of ocean surface temperature, salinity, and stratification

The models collectively project increases in sea surface temperature (SST) and decreases in sea surface salinity (SSS) for the open Gulf of Alaska (Figure 51 and Figure 52). Note that these maps are means for 2046-2065 and therefore show only the beginning of the changes expected under a high-emission scenario. The overall trend in SST in the vicinity of Ocean Station Papa (OSP) is shown in Figure 53. This shows that the two scenarios are just beginning to diverge in 2046-2065 (mean temperature change from preindustrial of 2.35 and 2.85 °C respectively). The total increase in annual mean SST from 1850-2100 is projected to be about 2.7 °C under RCP4.5 and 5.1 °C under RCP8.5 for the ensemble of six models (Figure 53). Increasing SST and decreasing SSS leads to a more stable water column (see chapter on Trends in temperature, salinity, water column stability and mixing depth in the open Gulf of Alaska) and declines in convective mixing and therefore entrainment of nutrients that support plankton productivity. The CMIP5 definition of mixing depth is the deepest mixed layer within a given month of simulation; here we have averaged these monthly data into their annual mean (Figure 54). A slight downward trend is already apparent in the "present" (2006-2025) time compared to historical (1966-1985) values, and further declines are projected for 2046-2065. The multi-model mean projected decline in mixed-layer depth in the vicinity of OSP for 2046-2065 is 4.8 m for RCP4.5 and 6.4 m for RCP8.5. After 2065 the mixed layer stabilizes in the RCP4.5 simulation, while it declines further to 10.0 m by the 2090s under RCP8.5 (Figure 55).

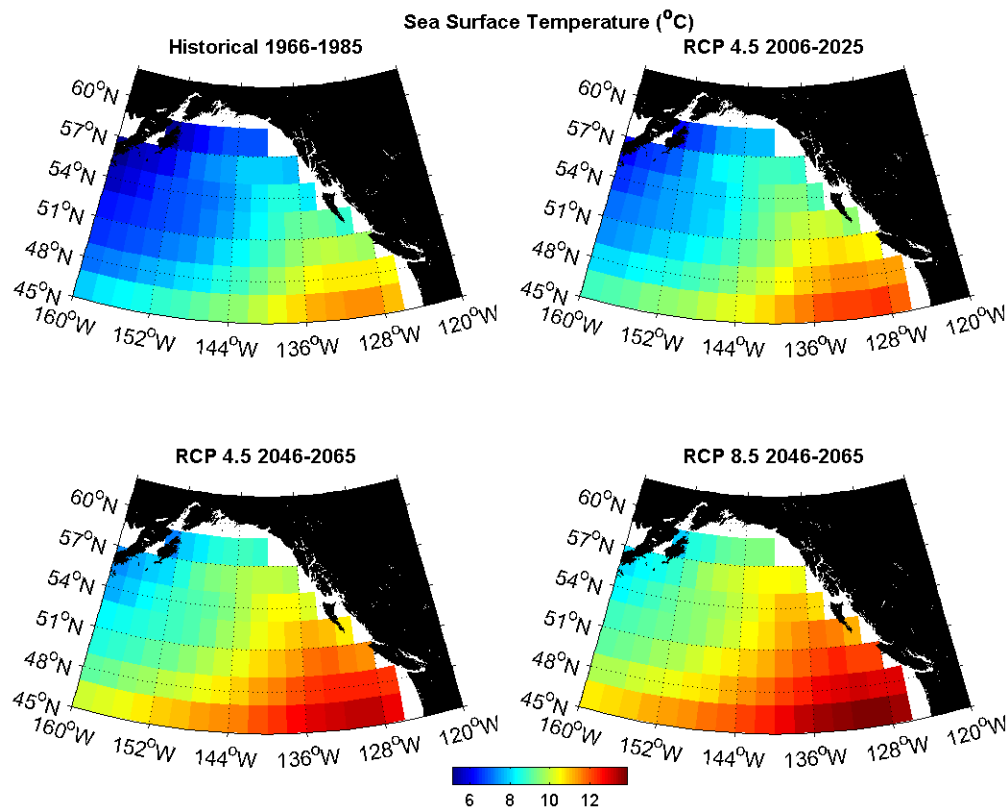


Figure 51: Maps of Gulf of Alaska sea surface temperature for 1966-1985, 2006-2025 (RCP 4.5) and 2046-2065 (RCPs 4.5 and 8.5). Ensemble mean of six models.

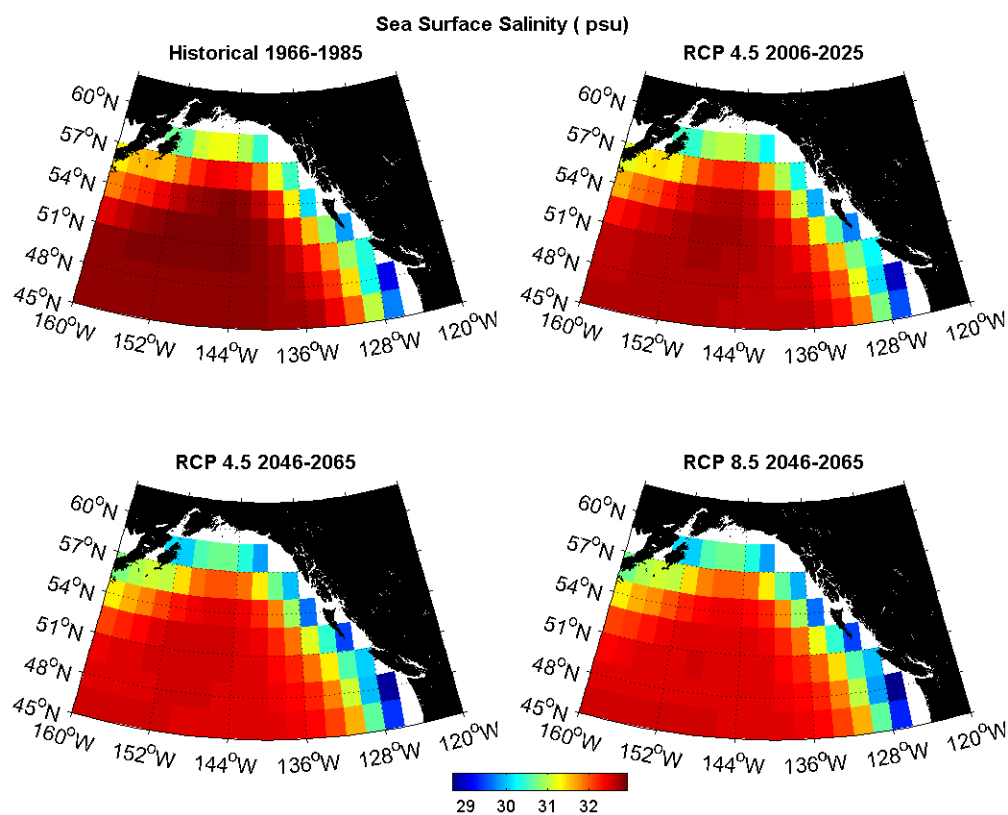


Figure 52: Maps of Gulf of Alaska sea surface salinity for 1966-1985, 2006-2025 (RCP 4.5) and 2046-2065 (RCPs 4.5 and 8.5). Ensemble mean of six models.

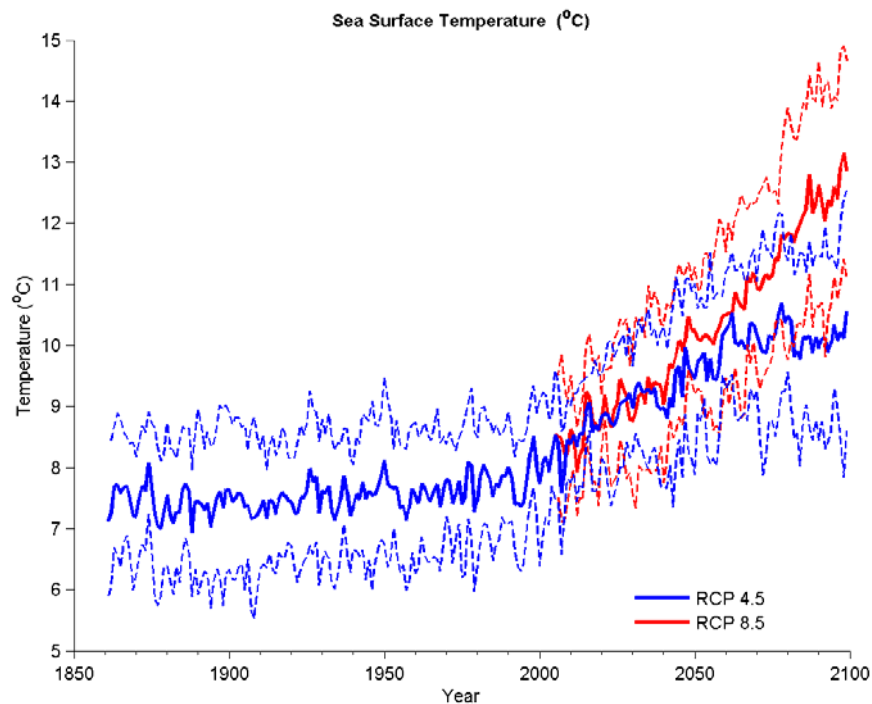


Figure 53: Time series of sea surface temperature in the vicinity of Ocean Station Papa (50°N, 145°W) from historical plus RCP 4.5 or 8.5 simulations. Ensemble mean \pm one standard deviation (dashed lines) of six models.

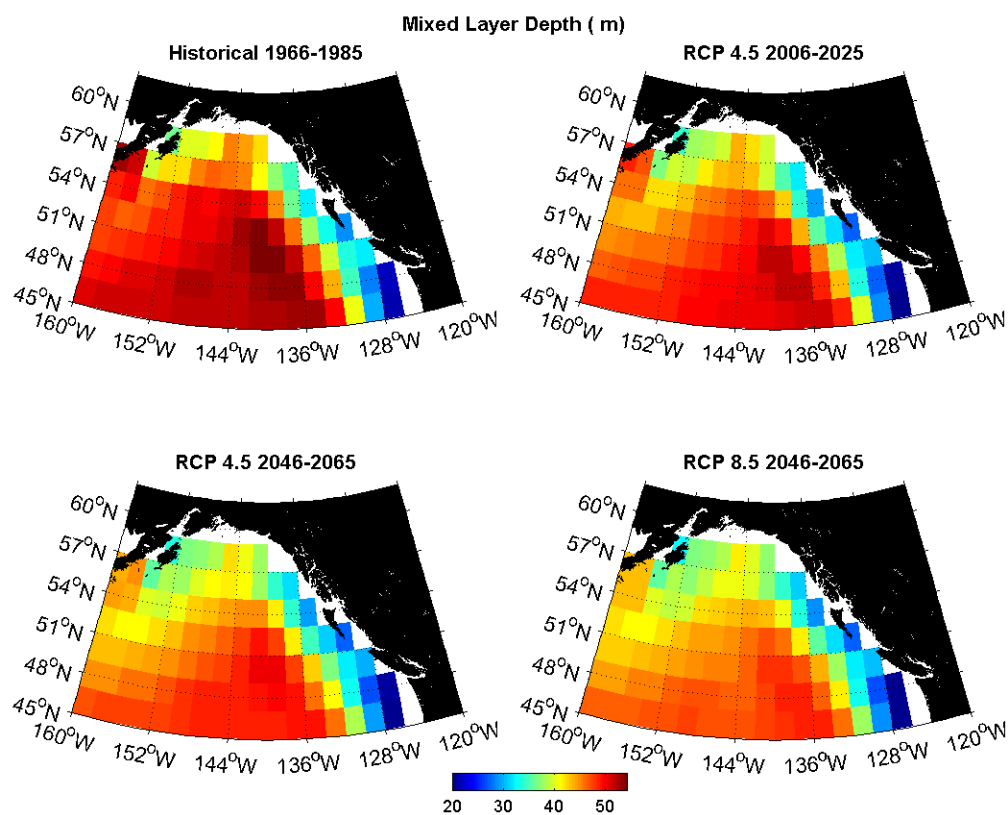


Figure 54: Maps of Gulf of Alaska mixed layer depth for 1966-1985, 2006-2025 (RCP 4.5) and 2046-2065 (RCPs 4.5 and 8.5). Ensemble mean of five models.

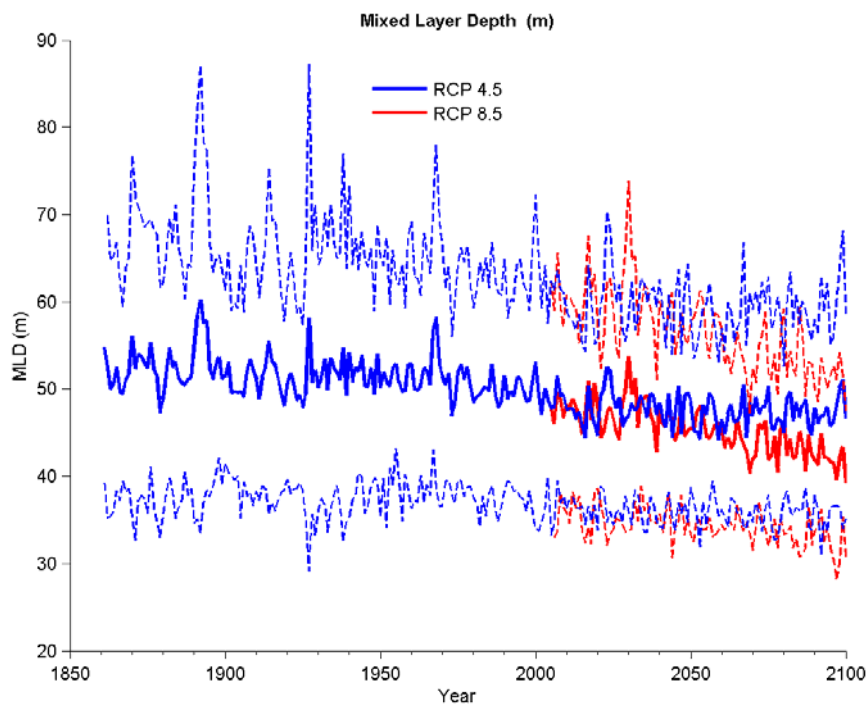


Figure 55: Time series of mixed layer depth in the vicinity of Ocean Station Papa (50°N, 145°W) from historical plus RCP 4.5 or 8.5 simulations. Ensemble mean \pm one standard deviation (dashed lines) of four models.

Changes in ocean carbon chemistry

The most obvious changes in ocean biogeochemistry are those forced directly by anthropogenic CO₂ (e.g., pH and calcium carbonate saturation state), i.e. the anthropogenic trend is much larger than the background spatial variability. Physical and biological changes associated with changing atmospheric forcing due to anthropogenic greenhouse gas radiative forcing are much more subtle and gradual. Surface ocean pH for the various time periods considered here shows almost no overlap on a common colour scale (Figure 56).

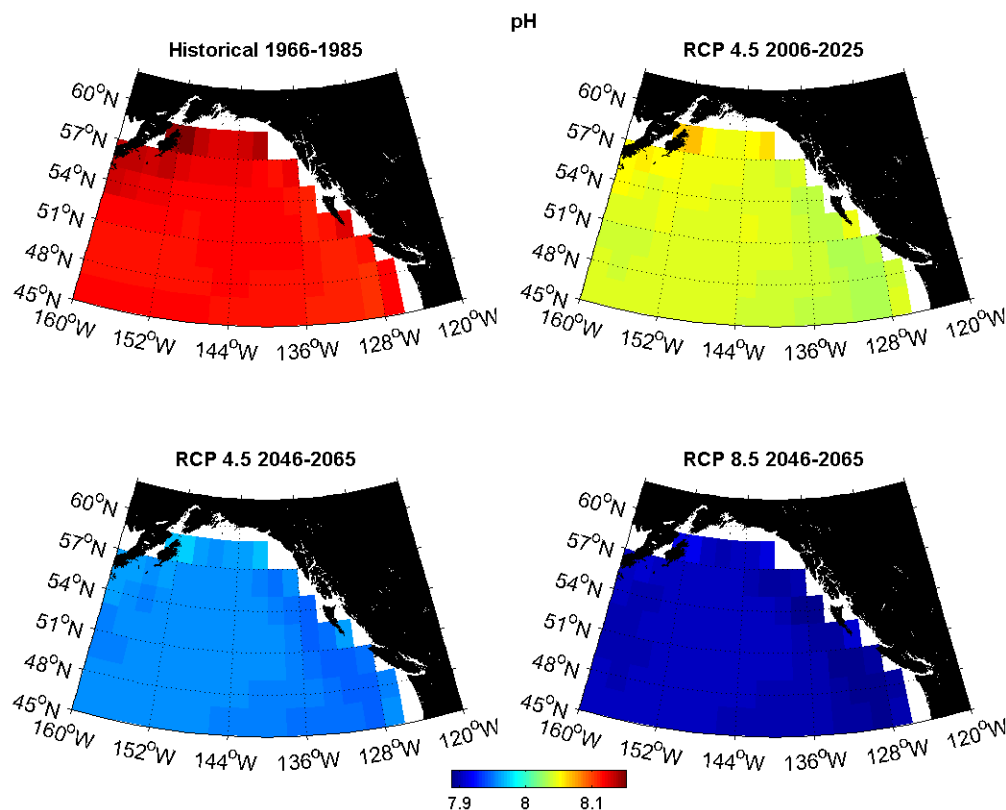


Figure 56: Maps of Gulf of Alaska surface pH for 1966-1985, 2006-2025 (RCP 4.5) and 2046-2065 (RCPs 4.5 and 8.5). Ensemble mean of six models.

Despite these apparently dramatic differences among time periods, changes in carbon chemistry at the surface are relatively minor because the surface ocean is always in contact with the atmosphere. The most significant biological impacts are in the subsurface ocean, where CO₂ from decomposition of organic matter has been accumulating for centuries. In the northeast Pacific, the calcium carbonate saturation state in the mesopelagic (200-800 m) ocean is as low as anywhere else on Earth: undersaturation was already encroaching on the euphotic zone before anthropogenic CO₂ invasion and is now moving inexorably upward with the rising atmospheric CO₂ concentration (Figure 57). At the 1026.6 kg m⁻³ density surface, there is already a marked decline between 1966-1985 and 2006-2025 (Figure 58). In 2046-2065, undersaturation is widespread, particularly near the continental margins, for the higher emission scenario (RCP8.5).

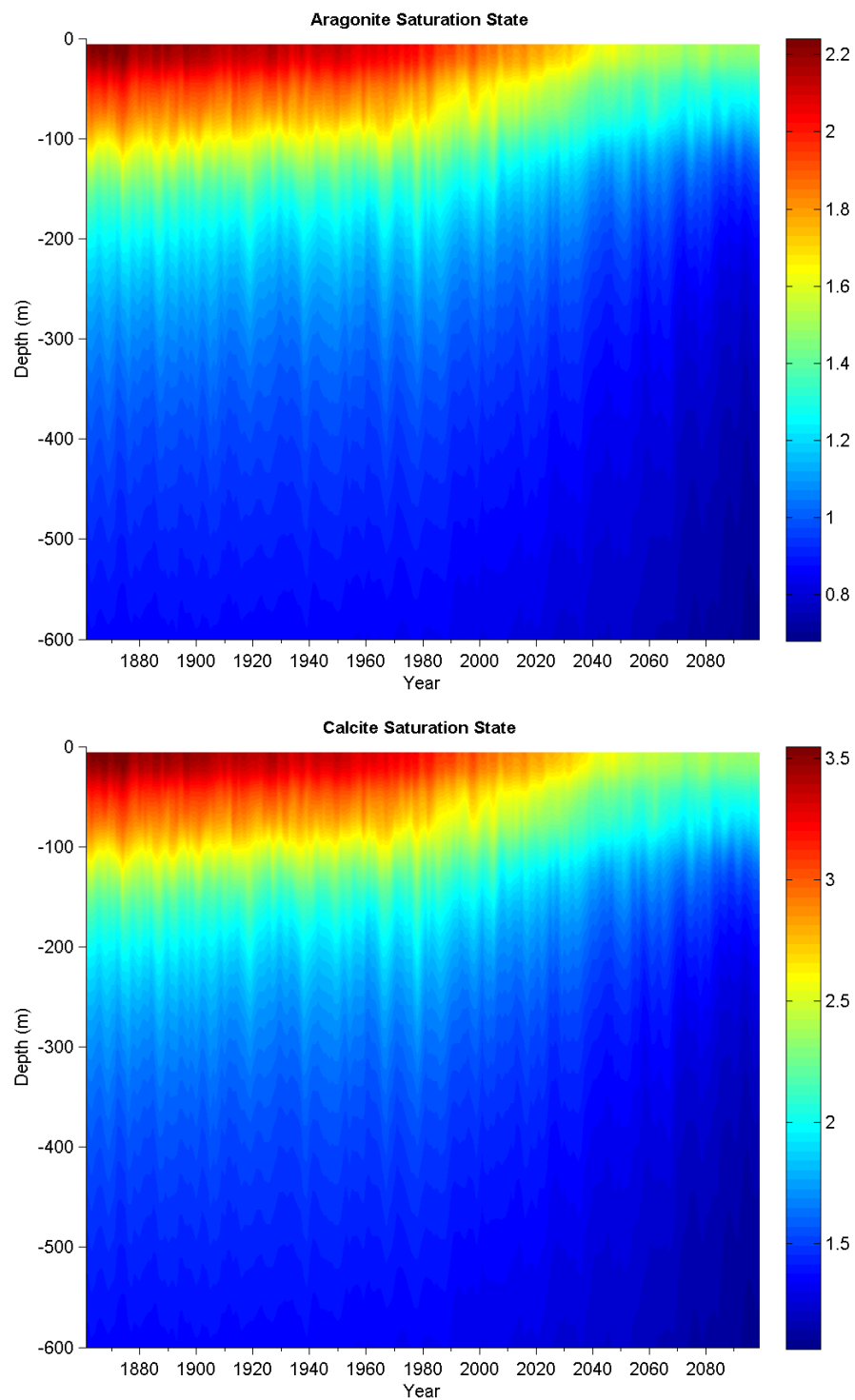


Figure 57: Depth-time plots of seawater saturation state with respect to aragonite (Ω_A) and calcite (Ω_C) in the vicinity of Ocean Station Papa (50°N, 145°W) using RCP 4.5.

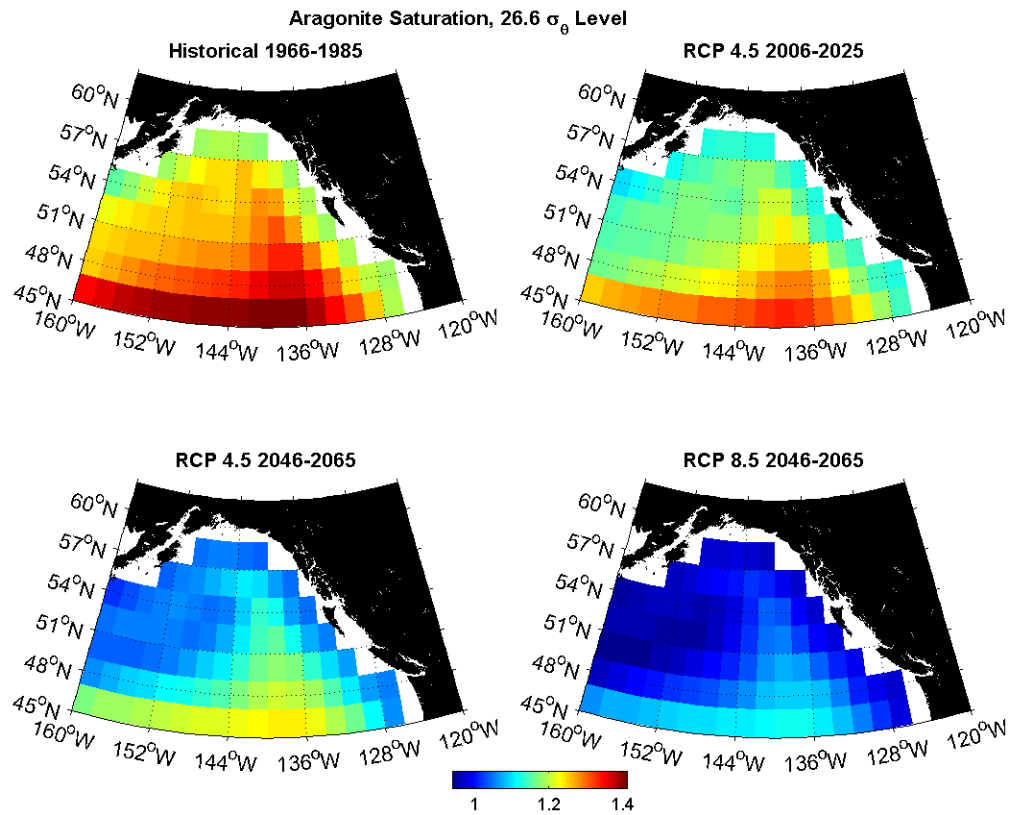


Figure 58: Maps of seawater saturation state with respect to aragonite (Ω_A) on the 1026.6 kg m^{-3} density surface for 1966-1985, 2006-2025 (RCP 4.5) and 2046-2065 (RCPs 4.5 and 8.5). Ensemble mean of six models.

Changes in ocean oxygen content

As with changes in carbonate chemistry, oxygen loss is a global phenomena with a nearly monotonic overall trend under anthropogenic forcing that primarily affects the subsurface ocean (e.g. Keeling et al. 2010). The North Pacific has most of the global volume of suboxic water and among the most intense oxygen minimum zones (OMZs), which sit at extremely shallow depths in the Canadian part of the northeast Pacific. Only four of the six models considered have oxygen as an output field, so the ensemble is slightly smaller than for other fields.

Model projections of oxygen concentration in the shallow subsurface ocean trend consistently downward (Figure 59). While it is important to consider that these projections are only valid for open ocean areas far from land, there is substantial advection of water from the OMZ onto the continental shelf, at depths too great for topographically induced mixing to affect the oxygen concentration. This will likely circumscribe the habitat available for commercially important groundfish species, as well as some midwater pelagic species as described by Koslow et al. (2011).

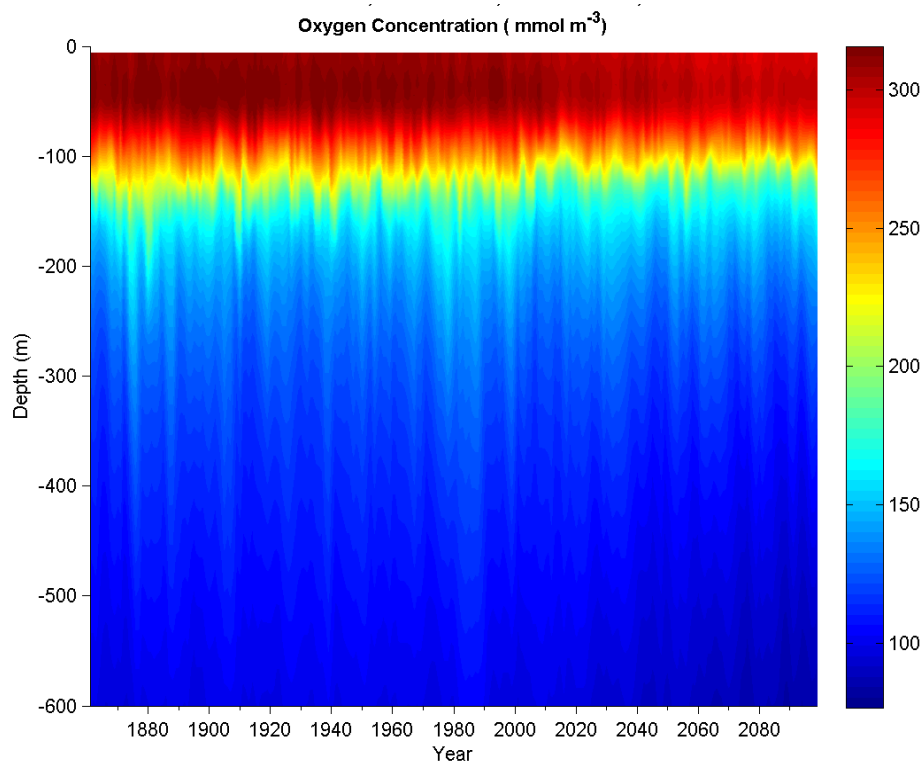


Figure 59: Depth-time plot of oxygen concentration in the vicinity of Ocean Station Papa (50°N, 145°W), for historical and RCP 4.5 simulations.

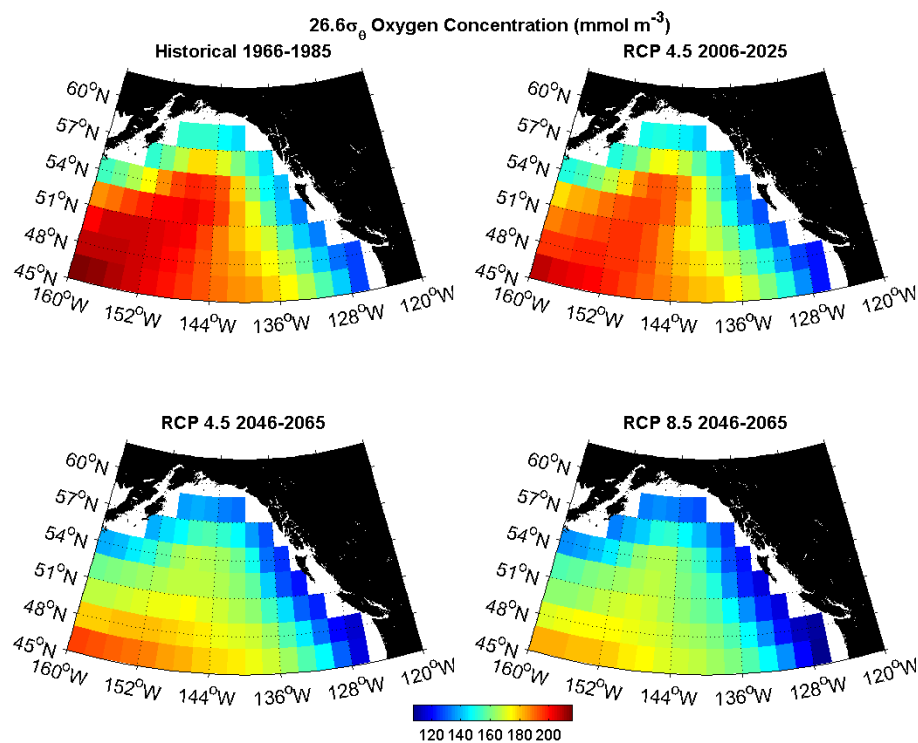


Figure 60: Maps of oxygen concentration on the 1026.6 kg m⁻³ density surface for 1966-1985, 2006-2025 (RCP 4.5) and 2046-2065 (RCPs 4.5 and 8.5). Ensemble mean of four models.

Projections indicate potential reductions of oxygen concentration at the 1026.6 kg m^{-3} density horizon (approximately representative of the main thermocline) of up to $100 \text{ }\mu\text{M}$ by 2100 (Figure 59, Figure 60 and Figure 61). Important points to note here are that (a) intermodel differences and therefore uncertainties attributable to model error are large, (b) there is substantial natural variability superimposed on the long-term anthropogenic trend, and therefore trends observed over shorter time scales (e.g. Pierce et al. 2012) can not be assumed to be representative of the long term trend, and (c) the projections using RCPs 4.5 and 8.5 diverge in the late 20th century, so ocean deoxygenation is potentially responsive to emissions mitigation.

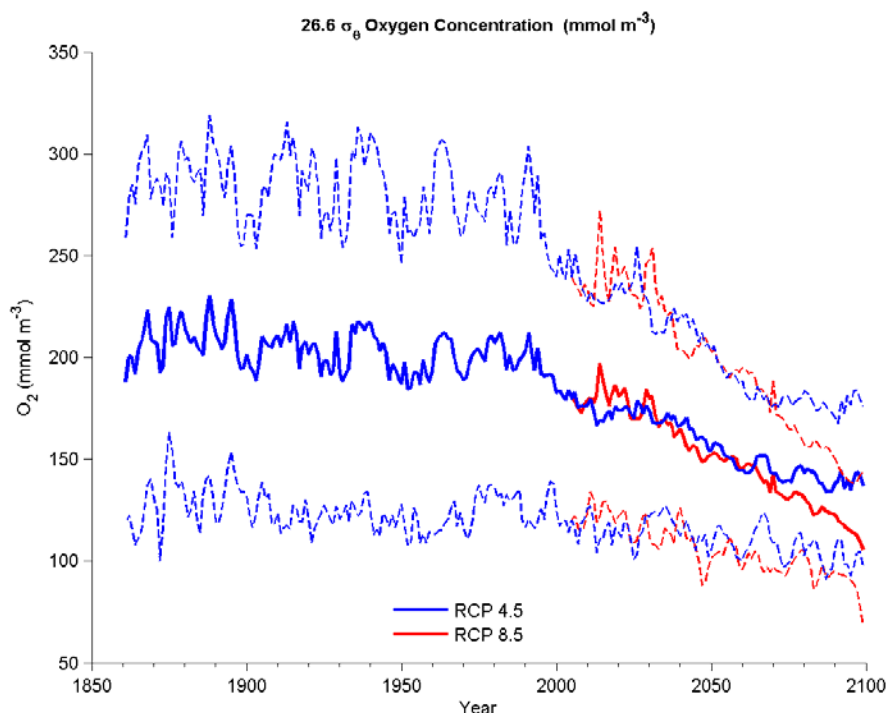


Figure 61: Time series of oxygen concentration at the 1026.6 kg m^{-3} density horizon in the vicinity of Ocean Station Papa (50°N , 145°W) from historical plus RCP 4.5 or 8.5 simulations. Ensemble mean \pm one standard deviation (dashed lines) of four models.

Changes in ocean productivity

Ocean productivity responds to changes in stratification and mixing, as well as other potential climate impacts like deposition of aeolian iron (Martin and Fitzwater 1988; Crusius et al. 2011). In the Gulf of Alaska the dominant influence on production under anthropogenic warming is expected to be greater upper ocean stability and stratification, with reduced depth of winter mixing (Figure 54 and Figure 55) and associated entrainment of nutrients. Primary production is therefore generally expected to decline (Figure 62). However, projected changes are small in the vicinity of OSP (Figure 63). The largest declines are in the regions of highest productivity in the northwestern Gulf of Alaska (Figure 62), potentially affecting availability of food for salmon and other wide-ranging species.

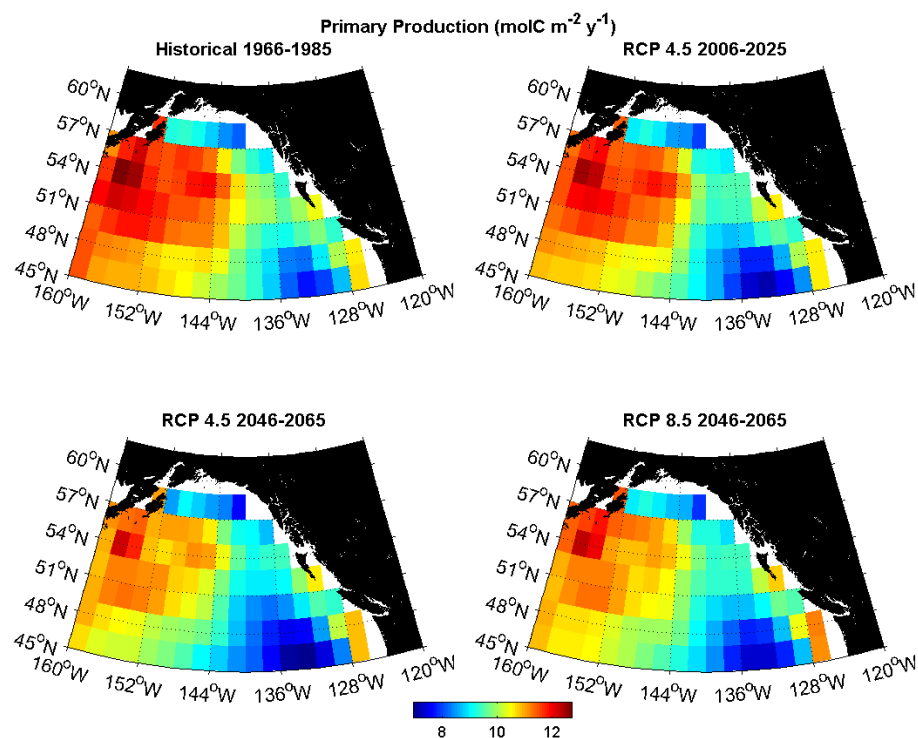


Figure 62: Maps of primary production for 1966-1985, 2006-2025 (RCP 4.5), and 2046-2065 (RCPs 4.5 and 8.5). Ensemble mean of five models.

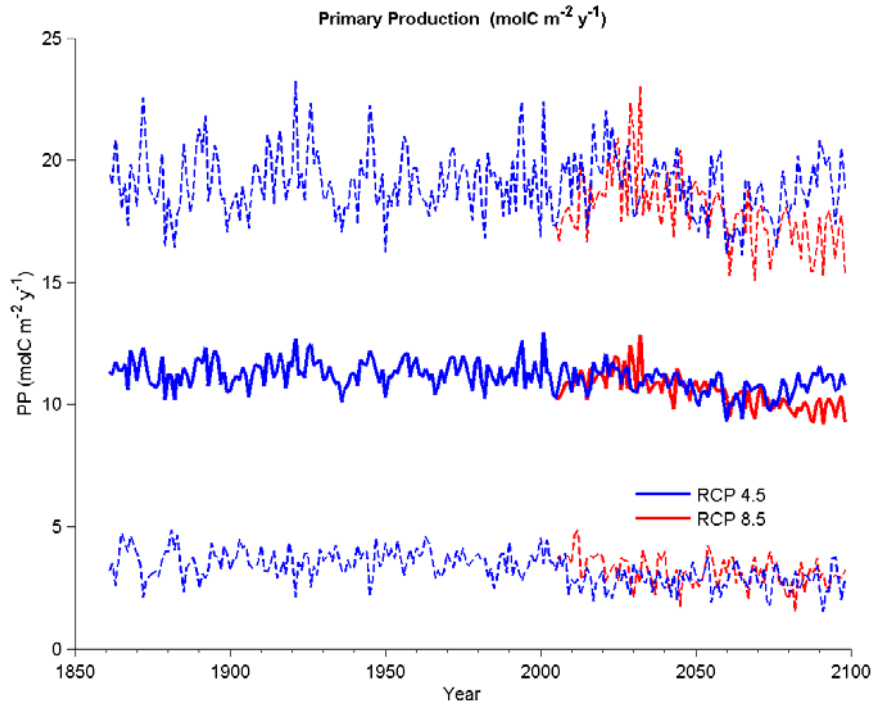


Figure 63: Time series of integrated primary production in the vicinity of Ocean Station Papa (50°N, 145°W) from historical plus RCP 4.5 or 8.5 simulations. Ensemble mean \pm one standard deviation (dashed lines) of five models.

Summary and Conclusion

Climate model projections show a consistent set of changes associated with a warming climate: increased upper ocean stratification, declining mixing depth, and reduced productivity. Interior ocean oxygen concentrations decline due to warming of the regions where the water masses are subducted, and calcium carbonate saturation state declines due to introduction of anthropogenic CO₂. All of these changes potentially affect both open ocean and coastal fisheries and ecosystems. Understanding the propagation of these effects into the coastal zone requires downscaling using high-resolution regional ocean models.

GLOBAL CLIMATE MODEL WIND PROJECTIONS ALONG THE BRITISH COLUMBIA CONTINENTAL SHELF

W.J. Merryfield¹, B. Pal¹, and M.G.G. Foreman². ¹Canadian Centre for Climate Modelling and Analysis, Environment Canada, University of Victoria, ²Institute of Ocean Sciences, Fisheries and Oceans Canada

Summary

As this section is largely a summary of Merryfield et al. (2009), the interested reader is referred to that publication for more details. Note that the analysis is based on projections from the set of IPCC AR4 global climate models. More recent AR5 projections have become available since this analysis and may provide somewhat different results than those discussed below.

Surface marine winds along the west coast of Canada have a pronounced influence on the oceanography and ecosystems of the region. Although other forcing influences like tides, the bifurcation of the eastward North Pacific Current into the south-ward California Current and the northward Alaska Current, and freshwater forcing from coastal rivers also contribute, marine winds dominate the seasonality of the coastal surface currents. In autumn and winter, the Aleutian Low pressure system generally gives rise to southerly winds and a northward-flowing, downwelling coastal current regime. In the spring and summer, a relatively stable offshore high pressure system produces northwesterly winds and a southward flowing, upwelling regime. This seasonal cycle strongly modulates primary production and is a major reason why the continental shelf off southern Vancouver Island supports such a large fishery (Ware and Thomson 2005).

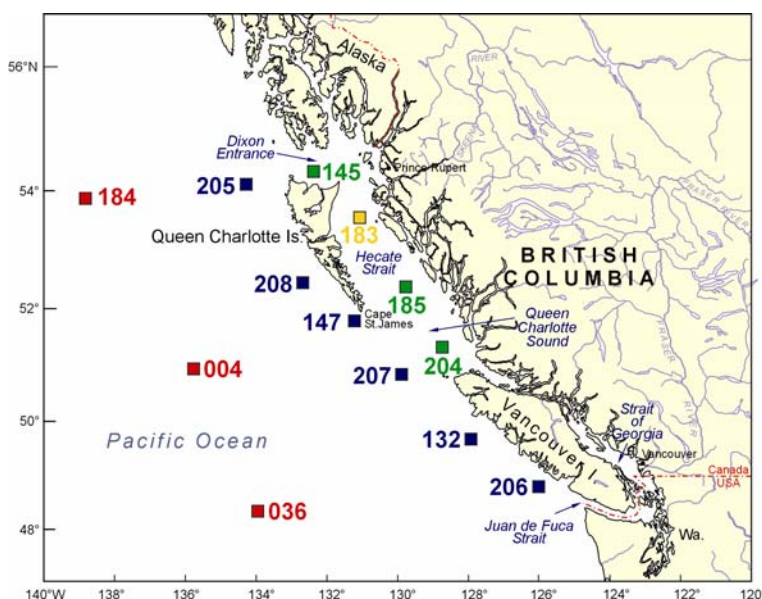


Figure 64: Locations of 13 weather buoys off the Canadian west coast. Colours denote the four categories described in Table 11.

Table 10: Climate Models Used in This Study and Their Atmospheric Resolutions.

Table 1: Climate models used in this study and their atmospheric resolutions

Symbol	Institution/Model	Atmospheric resolution*	Horiz grid dimensions lon × lat
a	BCCR/BCM2.0	T63L31	128 x 64
b	CCCMA/CGCM3.1(T47)	T47L31	96 x 48
c	CCCMA/CGCM3.1(T63)	T63L31	128 x 64
d	CCSR/MIROC3.2(med)	T42L20	128 x 64
e	CNRM/CM3	T63L45	128 x 64
f	CSIRO/Mk3.5	T63L18	192 x 96
g	GFDL/CM2.0	2.5° × 2°L24	144 x 90
h	GFDL/CM2.1	2.5° × 2°L24	144 x 90
i	GISS/AOM	4° × 3°L12	90 x 60
j	GISS/EH	5° × 4°L20	72 x 46
k	GISS/ER	5° × 4°L20	72 x 46
l	INM/CM3.0	5° × 4°L21	72 x 45
m	IPSL/CM4	2.5° × 3.75°L19	96 x 72
n	MIUB/ECHO-G	T30L19	96 x 48
o	MPI/ECHAM5	T63L31	192 x 96
p	MRI/CGCM2.3.2	T42L30	128 x 64
q	UKMO/HadCM3	3.75° × 2.5°L19	96 x 72
r	UKMO/HadGEM1	1.875° × 1.25°L38	192 x 144

*Horizontal resolution is described by spectral truncation or grid box dimensions as appropriate, and vertical resolution by the number of model levels, e.g. L31.

Long-term observations of the coastal winds in this region have been made via a network of coastal meteorological buoys (Figure 64) since the late 1980s (Cherniawsky and Crawford 1996). Faucher et al. (1999) extended these time series back another thirty years with an empirical-statistical downscaling procedure that was applied to large-scale predictors derived from the NCEP reanalysis. The resulting dataset consists of 6 hourly winds at 13 buoy sites for the period 1958-1997. This dataset provides an excellent basis for not only examining possible trends and shifts, but also for evaluating the winds produced by global climate models. The aim of this study was to examine projected changes in surface marine winds off the Canadian west coast, under the assumption they should have significant impacts on coastal ecosystems. This was done by interpolating winds from 18 Intergovernmental Panel for Climate

Change (IPCC) climate model simulations (Table 10) to the buoy locations and comparing contemporary and future decadal averages.

Table 11: List of Buoys and Their Positions.

Buoy	Lat	Lon	Classification
004	50.93N	136.10W	Far offshore
036	48.35N	133.94W	Far offshore
132	49.74N	127.93W	Near offshore
145	54.37N	132.42W	Inshore
147	51.83N	131.22W	Near offshore
183	53.62N	131.10W	Hecate Strait
184	53.91N	138.85W	Far offshore
185	52.42N	129.79W	Inshore
204	51.37N	128.75W	Inshore
205	54.16N	134.28W	Near offshore
206	48.84N	126.00W	Near offshore
207	50.87N	129.92W	Near offshore
208	52.52N	132.69W	Near offshore

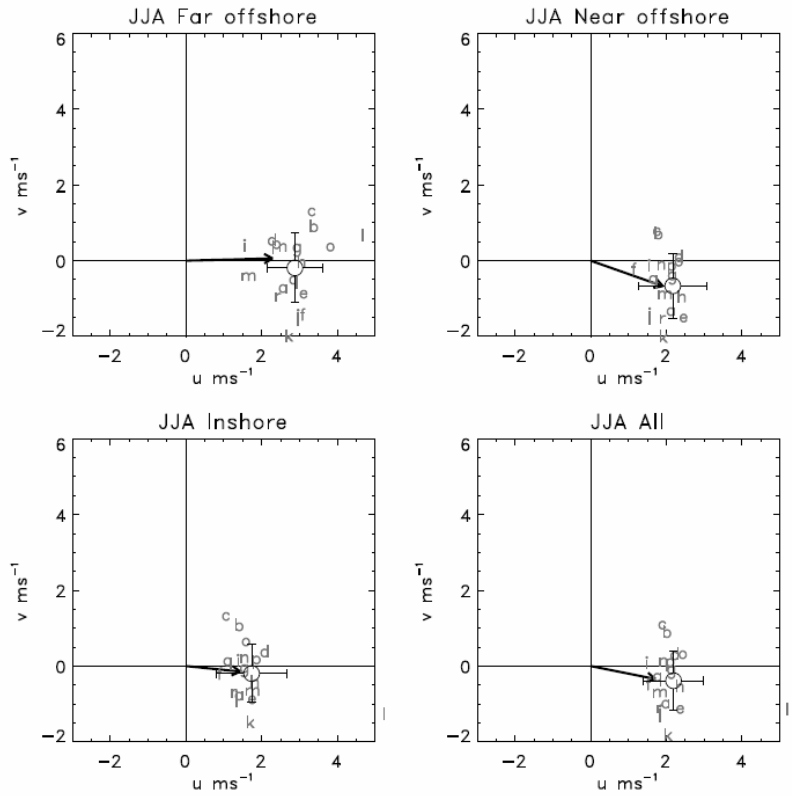


Figure 65: Summer (June-August) 1976-95 mean surface winds from buoy observations (vectors), individual GCMs (alphabetical codes from Table 10), and multi-model mean (large circles), for our regional groupings of the buoys. The error bars represent standard deviations of the multi-model ensemble.

To facilitate our analyses the buoys were grouped (Table 11) into four categories. The first step in the analysis was to assess the accuracy of the model winds through comparisons with buoy observations. Figure 65 summarizes results for summer (June-August) over the twenty-year period of 1976-95 and shows that despite the coarse resolution of the GCMs, there is relatively good agreement between the models and observations. Though there is scatter among the models, their ensemble averages display reasonably accurate upwelling winds at the near-offshore and inshore buoy locations. Merryfield et al. (2009) include a similar plot for the winter winds and note that although they are relatively accurate far offshore, they exhibit a northerly bias at nearshore and inshore locations, likely due to under-representation of the orographic influence of the southeast to northwest oriented coastline.

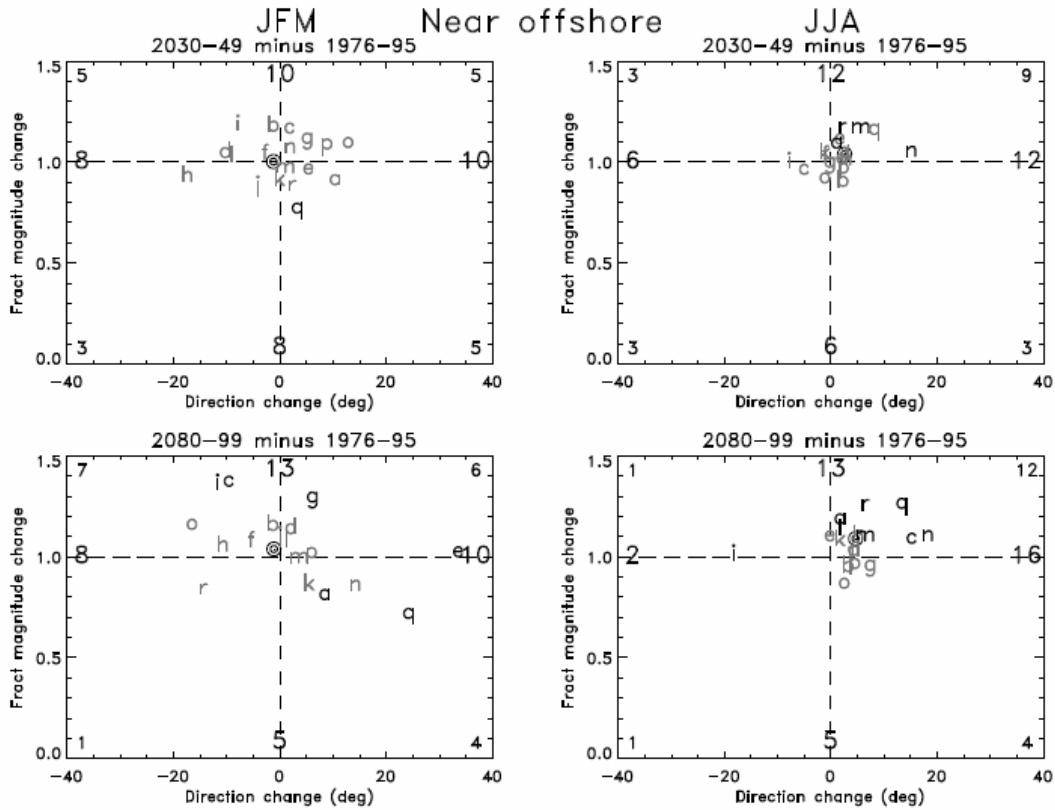


Figure 66: Future changes in January-March (left) and June-August (right) surface winds, averaged at the near-offshore buoy locations, between the 1976-95 base period and 2030-49 (upper panels) and 2080-99 (lower panels). The letters correspond to individual models as in Table 10, and the bulls-eyes to multi-model means. The larger numerals indicate the numbers of models residing in the corresponding half planes, and the smaller numerals denote the number of models in the corresponding quadrants. Bold letters indicate a probability that such a result would arise under the null hypothesis of no change is less than 0.05.

Figure 66 summarizes GCM projected wind changes, shown as fractional increases in magnitude and directional changes (degrees clockwise) over the periods 2030-49 and 2080-99 relative to 1976-95, at the near-offshore buoys. The winter (JFM) winds show sufficient scatter among the GCMs that no statistically significant pattern emerges, though the multi-model ensemble means suggest an approximately 5% intensification and slight counterclockwise rotation. However, a much clearer picture emerges for the summer (JJA) wind changes. Although only a few of the individual model changes between 1976-1995 and 2030-2049 are significant, the model ensemble mean wind speeds show increases of approximately 2-4% and clockwise rotations of about 2° that are statistically significant in

some cases. The JJA wind changes between 1976-1995 and 2080-2099 show similar though considerably stronger trends consisting of wind speed increases ranging from 4.5% to 9% and clockwise rotations between 4° and 5°. The strength of this signal is reflected in substantial inter-model consistency, with 16 models showing clockwise rotations.

Though the foregoing projected changes may have significant implications for marine ecosystems along the southern British Columbia continental shelf where summer upwelling winds bring nutrients to the surface and drive upper trophic level productivity (Ware and Thomson 2005), several other projected changes need to be considered before the complete picture is understood. Warmer air temperatures can be expected to heat the sea surface and contribute to a stronger stratification that will inhibit upwelling. Climate model analyses along the southern California shelf by Auad et al. (2006) showed that an increase in upwelling wind speed was sufficient to overcome stronger stratification. However, this result may not carry over to British Columbia where water column stratification is largely determined by salinity rather than temperature variations. Projected changes in precipitation and river discharge (Morrison et al. 2002), as well as the air-sea heat flux, will thus be needed to force a regional coastal ocean model in order to provide better estimates of physical changes to the coastal waters off British Columbia. Preliminary results of such a regional ocean-only climate model are described in the subsequent chapter on Results from Regional Climate Model Simulation for the British Columbia Continental Shelf.

CANADIAN REGIONAL CLIMATE MODEL PROJECTIONS AFFECTING BRITISH COLUMBIA COASTAL WATERS

J. Morrison, W. Callendar, M.G.G. Foreman, D. Masson and I. Fine. Institute of Ocean Sciences,
Fisheries and Oceans Canada

Introduction

The projections presented here have been dynamically downscaled from Canadian Global Climate Model results produced as part of the Inter-governmental Panel on Climate Change (IPCC) Fourth Assessment Report (AR4). More recent AR5 projections have become available since this analysis and may provide somewhat different results than those discussed below.

The recent development of an ocean circulation model for the British Columbia continental shelf (Masson and Fine 2012; henceforth MF12) and its application to hindcasting water properties and flow fields for the period of 1995 – 2008 has created a unique opportunity to investigate future conditions in this same region. Numerous global and regional projections of the future oceanic and atmospheric fields that would be needed to force and initialize such a simulation are available from archives storing the output from global and regional climate models associated with recent Assessment Reports of the IPCC. Consequently, it is a relatively straightforward exercise to set-up and run companion future simulations analogous to the MF12 hindcast. Here we describe a strategy for conducting such a future simulation and the downscaling and/or calculation of one set of fields that will be used to force it. Results from this simulation are summarized in the subsequent chapter on Results from Regional Climate Model Simulation for the British Columbia Continental Shelf.

In order to use the MF12 model for future projections, it need only be run with suitable future forcing and initial fields. Although the gravitational forcing that determines the tides could be easily calculated, the projection model was forced with the same tides as the contemporary model in order to facilitate comparison. The required atmospheric forcing can be obtained by applying downscaling techniques to output from global climate models (GCMs) and/or regional climate models (RCMs) that cover the

model domain (Figure 67). The outputs from several such models have been archived at the following sites

- the Coupled Model Intercomparison Project phase 3 (CMIP3) and phase 5 (CMIP5; http://cmip-pcmdi.llnl.gov/cmip5/data_description.html) multi-model data sets of the World Climate Research Programme (WCRP), assembled at the Program for Climate Model Diagnosis and Intercomparison (PCMDI, <http://www-pcmdi.llnl.gov/>) to inform the IPCC Fourth and Fifth Assessments, or
- the North American Regional Climate Change Assessment Program (NARCCAP, <http://www.narccap.ucar.edu/>),

and they will be the primary sources for this study.

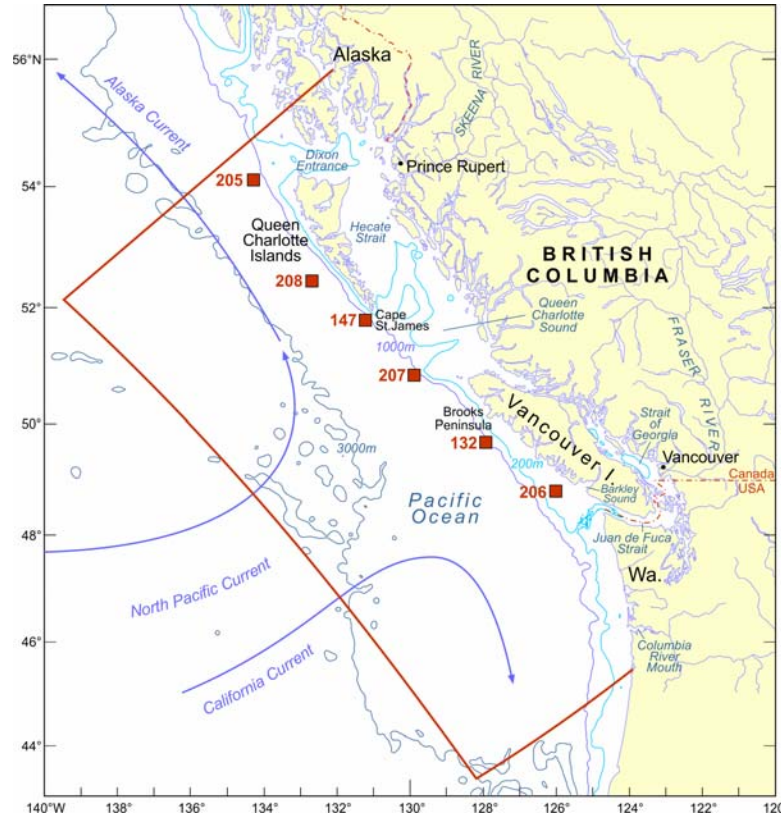


Figure 67: Map of the British Columbia continental shelf showing bathymetric contours, place names, and major offshore currents. Solid red lines denote the outer boundary of the regional shelf model and red boxes denote the Environment Canada (EC) buoys for which contemporary and projected winds are shown in Figure 68.

In particular, the NARCCAP RCM data have a finer horizontal resolution (approximately 50 km versus typically 1° or 2° for the GCMs) and thus should be better able to capture spatial variations in i) terrestrial precipitation (both rainfall and snowfall) and ii) oceanic winds and heat fluxes. Consequently, their fields were the preferable source of atmospheric forcing and our model simulations were restricted to the NARCCAP-defined ‘current’ and ‘future’ time periods of 1971-2000 and 2041-2070, respectively. Note that these NARCCAP future simulations only assume the A2 emissions scenario (no leveling off of greenhouse gases). Though NARCCAP offers output from six RCMs driven by up to four atmosphere-ocean general circulation models (AOGCMs), only results from the Canadian Regional Climate Model (CRCM) forced by the Canadian Global Climate Model (CGCM3) are presented here. Analogous simulations with other RCM/GCM combinations and the calculation of ensemble means and uncertainty estimates are planned. North American AR5 model output analogous to the NARCCAP AR4

results are just becoming available through the Coordinated Regional climate Downscaling Experiment (CORDEX, <http://www.meteo.unican.es/en/projects/CORDEX>) and may also be used in the future.

Strategy and Wind Stress Anomalies

Initial conditions, boundary conditions and atmospheric forcing values were generally constructed for the future simulation by calculating anomalies between future and current RCM/GCM downscaled values and adding them to the hindcast values. This approach was first justified and employed by Schär et al. (1996), and referred to as a “surrogate climate-change scenario” method, and more recently employed by several Japanese groups (e.g. Kimura and Kitoh 2007; Sato et al. 2007; Hara et al. 2008) who referred to it as the “pseudo-global-warming” (PGW) method. As described in Hara et al. (2008), the technique allows a comparison of the climate in present (control) and future PGW years, where the latter is similar to the former in terms of interannual variations but includes future climatology. The rationale for adopting the approach here is justified below.

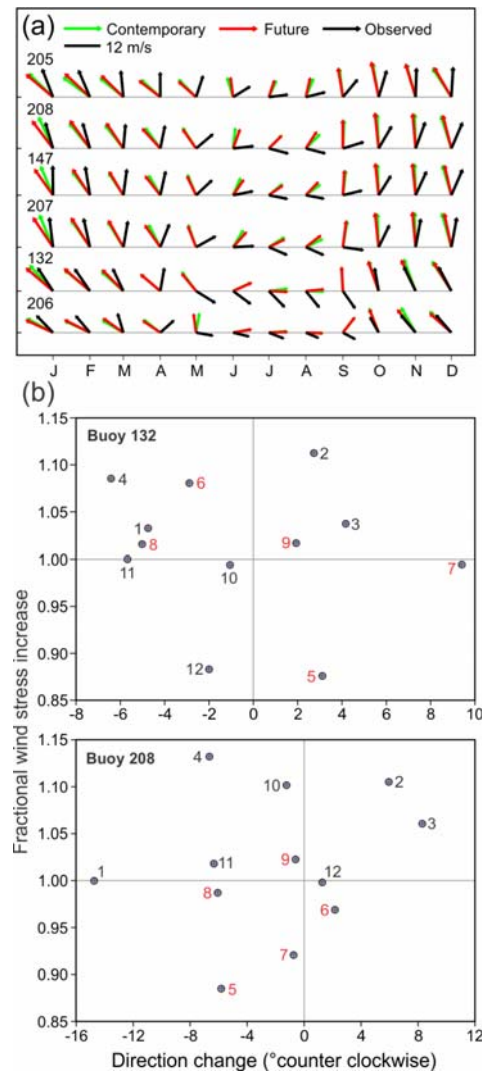


Figure 68: a) Mean monthly winds at the six EC buoys shown in Figure 67: observed and re-constructed (Foreman et al. 2011) means over the period of 1971-2000 (black), NARCCAP CRCM/CGCM means for the same period interpolated to these buoy locations (green), interpolated NARCCAP CRCM/CGCM means for 2041-2070 (red); b) monthly ratios of future versus contemporary wind stresses (red versus green in (a) for buoys 132 and 208. Numbers designate months with red (black) denoting those during the upwelling (downwelling) seasons.

Figure 68 shows observed and NARCCAP mean monthly winds at the six offshore weather buoy locations shown in Figure 67. The so-called observational time series is a combination of the 1971-1997 values that Faucher et al. (1999) regressed from 1990-95 observations and 1998-2000 observations whose gaps were filled with a technique described in Foreman et al. (2011). The monthly means show that winter winds along the BC shelf are typically toward the north or northwest and switch to being toward the east or southeast in summer. The spring and fall transitions in wind direction demarcate the start and end of the upwelling season and, together with cumulative wind intensity, largely determine annual marine ecosystem productivity along the BC shelf.

The magnitudes of the 1971-2000 monthly-averaged NARCCAP CRCM/CGCM3 winds show generally good agreement with their observed counterparts but there are notable differences in direction. In almost all instances, the observed winds are rotated clockwise from their CRCM counterparts and this discrepancy is seen to be largest in May and September, around the time of the spring and fall transitions. In particular, at the more southerly sites the CRCM transition to summer upwelling conditions is late and the switch back in fall is early. As future winds generally display this same behaviour (Figure 68), employing these CRCM/CGCM3 winds to force a future simulation could be expected to produce a late and short upwelling season that could generate misleading conclusions on future ecosystem impacts. So rather than employing these NARCCAP CRCM/CGCM3 winds to directly force our future simulations, instead we have chosen to force with wind stress fields that are the summation of those employed by MF12 and monthly future-minus-contemporary NARCCAP anomaly fields. With the exception of tides (as discussed above), this same anomaly approach has been applied consistently for all forcing and initial condition fields.

The monthly future and contemporary wind stress anomalies at buoys 132 and 208 reflect changes in both magnitude and direction (Figure 68b). During the downwelling months (October-April) the wind stress magnitudes are seen to be consistently larger at buoy 208 while with the exception of September, during the upwelling season they are consistently smaller. Although there is no apparent pattern to the directional changes, the range is relatively small so the projected changes can be considered minimal. Systematic changes in the upwelling and downwelling wind stresses at buoy 132 are less evident. Wind magnitudes are stronger in four of the seven downwelling months and three of the five upwelling months and again there is considerable scatter among the directional changes, albeit over a relatively small range. As similar patterns (or lack thereof) are found at the other four buoys, it seems that future downwelling (winter) winds are generally projected to be stronger while future upwelling (summer) winds will be weaker in the north and either about the same, or slightly stronger, over the southern BC shelf. These results are generally consistent with the increased cumulative upwelling and downwelling trends found by Foreman et al. (2011) at these same six locations over the period of 1959-2008.

However, based on Figure 68a and a similar plot (not shown) of weekly rather than monthly averages; it is difficult to make a definitive statement about changes in the timing of the spring and fall transitions. Both the April and May monthly-averaged future winds are seen to generally lag behind their contemporary counterparts in terms of rotating clockwise from a downwelling to upwelling favourable direction and this later onset of upwelling may explain the considerably smaller future wind stress at buoy 132 in May (Figure 68b). In June and July, the future winds have generally rotated further clockwise; however, by August they are further advanced than their contemporary counterparts in terms of rotating back to their winter downwelling directions. It would thus appear that the future upwelling season is projected to be both later in its start and shorter in duration, both results being consistent with the trends described in Foreman et al. (2011). However this conclusion should be taken cautiously as neither the contemporary nor future CRCM winds, even at the most southerly buoy locations, have substantial southward components. Thus they never truly become upwelling favourable.

Precipitation, Air Temperature, Short Wave Radiation and Cloud Cover Anomalies

Since the CRCM has significantly lower spatial resolution than our regional ocean model, there are regions that it has defined as land and the MF12 model has defined as water, and vice versa. As the values for air temperature, air pressure and humidity given by the CRCM in these regions are affected by being over land, new values for these coastal areas were calculated using Empirical Orthogonal Functions (EOFs). These EOFs were generated using North American Regional Re-analysis (Mesinger et al. 2006) data over a 15 year period between 1995 and 2009 where 14 years were used to generate the EOFs and the remaining year was used to test the ability of the EOFs to generate coastal data based on offshore data. Ten EOFs were used to approximate the data and the regeneration of the test year was accomplished with an average R-squared value of 0.95 and significance of the order of 10^{-5} . Dealing with the rest of the atmospheric forcing was less complex. As no land effects were noticeable in the CRCM precipitation output, these data were used as-is to calculate the necessary anomalies.

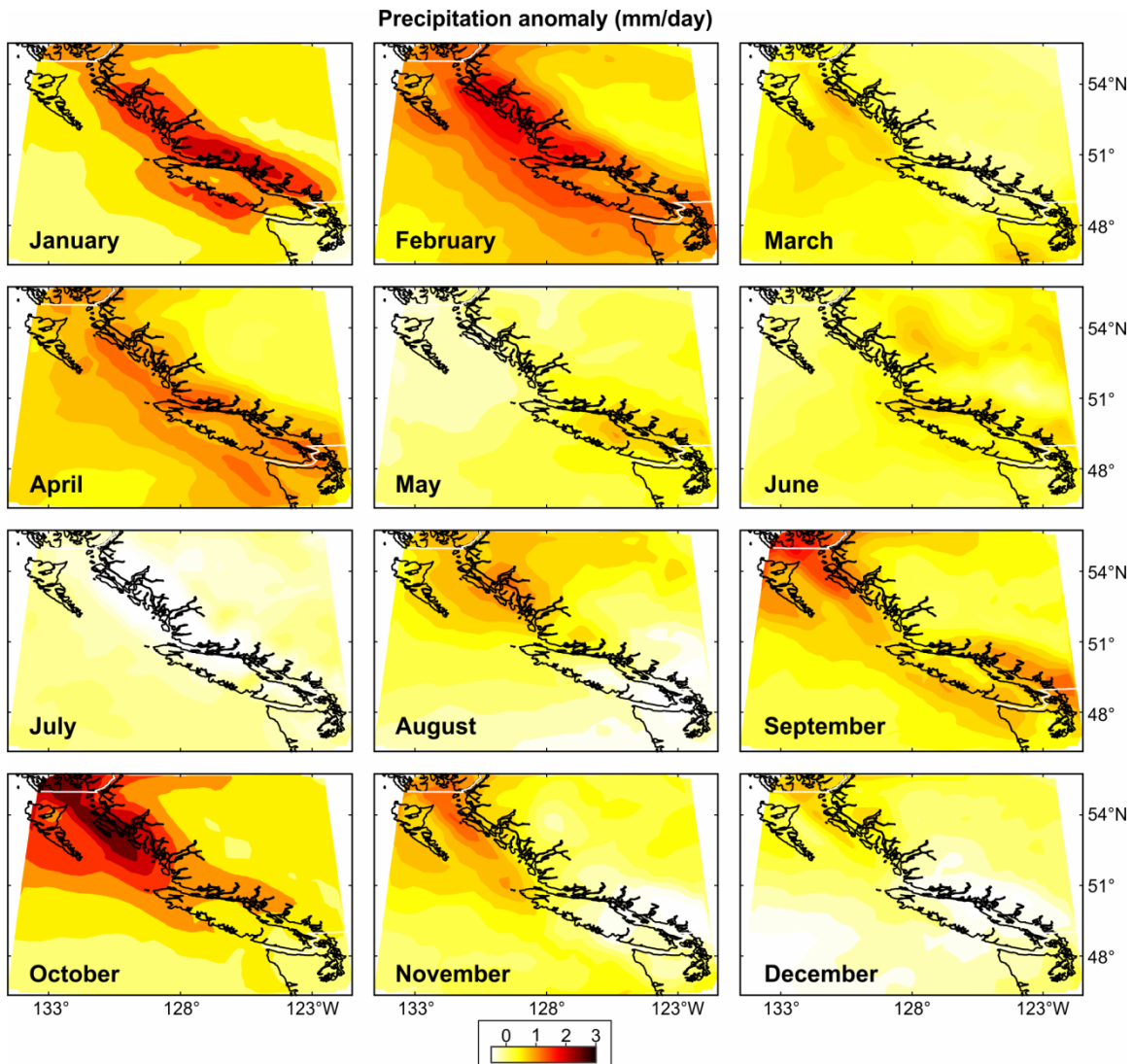


Figure 69: NARCCAP CRCM/CGCM3 monthly-averaged precipitation anomalies (mm/day) for the period of 2041-2070 minus 1971-2000.

Figure 69 shows monthly-averaged NARCCAP CRCM/CGCM3 precipitation anomalies over western British Columbia. January and February are seen to be notably wetter along the entire coast while October also shows significant increases along the north coast. The July anomaly is generally drier

along the entire coast while August, November and December are projected to be drier along the south coast. The average annual anomaly over the entire region is approximately 0.5 mm/day.

Figure 70 shows analogous monthly-averaged surface air temperature anomalies. For most months, with January being the most notable, temperature anomalies over land are larger than over the ocean. And though warming is seen throughout, there are distinct seasonal and regional differences. The wave-like pattern along the mainland coast for May – September suggests less warming over some of the major fjords, though an even-finer resolved grid than the CRCM would be needed to confirm this. (Typically these fjords are 4-5 km wide so the CRCM orography does not capture them accurately.) Slightly different patterns are seen when the averages are restricted to only day or night values, and interestingly, the night-time anomalies are generally larger than those for the day. As shown later, to some extent this may be due to more cloud cover.

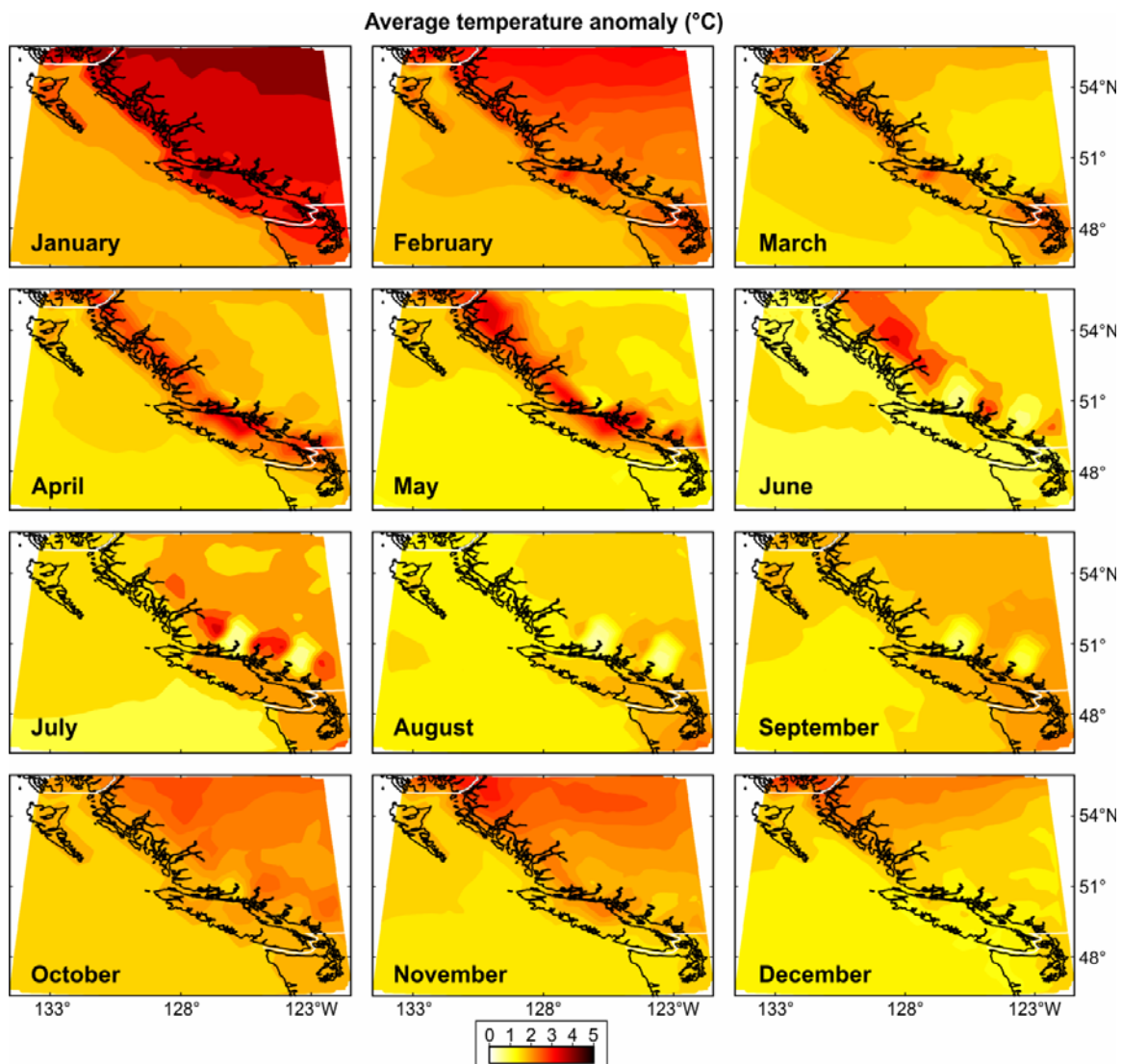


Figure 70: NARCCAP CRCM/CGCM3 monthly-averaged surface air temperature anomalies (°C) for the period of 2041-2070 minus 1971-2000.

Figure 71 shows monthly short wave radiation (SWR) anomalies. Though small increases are seen in some regions and months (e.g., July and August in southwestern BC), decreases are prevalent in many

months, with the most notable being in April and May. The high correlation between these SWR values and the associated daytime cloud cover values (not shown) reveals that these changes are primarily due to changes in cloud cover. Photosynthetically active radiation comprises about 50% of total incident solar radiation, so these April/May SWR decreases may be relevant to phytoplankton growth and could delay spring blooms. Note another wave-like pattern over the mainland coastal fjords in June, similar to what was seen in Figure 70.

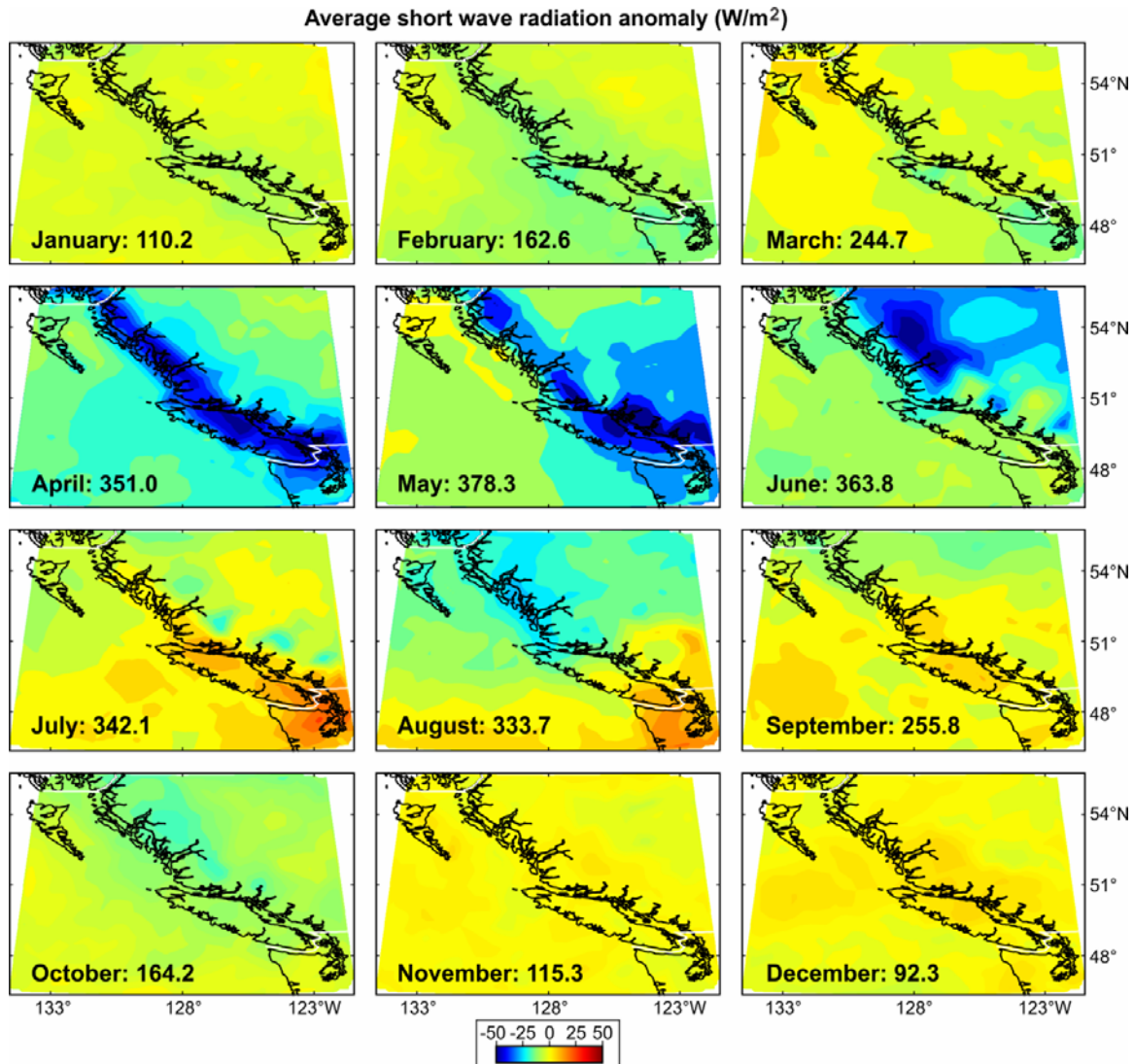


Figure 71: NARCCAP CRCM/CGCM3 monthly-averaged short wave radiation anomalies (W/m^2) for the period of 2041-2070 minus 1971-2000. Values following the month name within each panel are monthly average values (W/m^2) for the 1971-2000 period.

Freshwater Discharge

As baroclinic flows along the BC shelf are largely determined by salinity rather than temperature gradients, freshwater discharges along the coast are important. They not only have a direct role in generating coastal currents but an indirect role in transporting larvae and nutrients and acting as possible barriers to cross-shelf transport (Thomson et al. 1989). As seen in Figure 69, precipitation patterns near the BC coast are generally projected to become wetter in winter and drier in parts of the summer.

However, as a significant amount of the winter precipitation away from the coast is stored as snow-pack and released later in the year, drier summers do not necessarily mean less summer discharge.

The main problem in estimating both historical and future freshwater discharge affecting the BC coast is that approximately 20% is ungauged. Morrison et al. (2011) developed a technique for estimating ungauged runoff based on the precipitation, temperature, terrain characteristics, and storage capacity within twenty-two basins (Figure 72) whose freshwater discharges affect coastal BC waters. The technique has been verified with historical observations and used to reconstruct time series for each of the twenty-two watersheds back to 1970. Though there was considerable interannual variability, the total annual discharge averaged about 1000 km³ and no statistically significant trend was found over this time period.

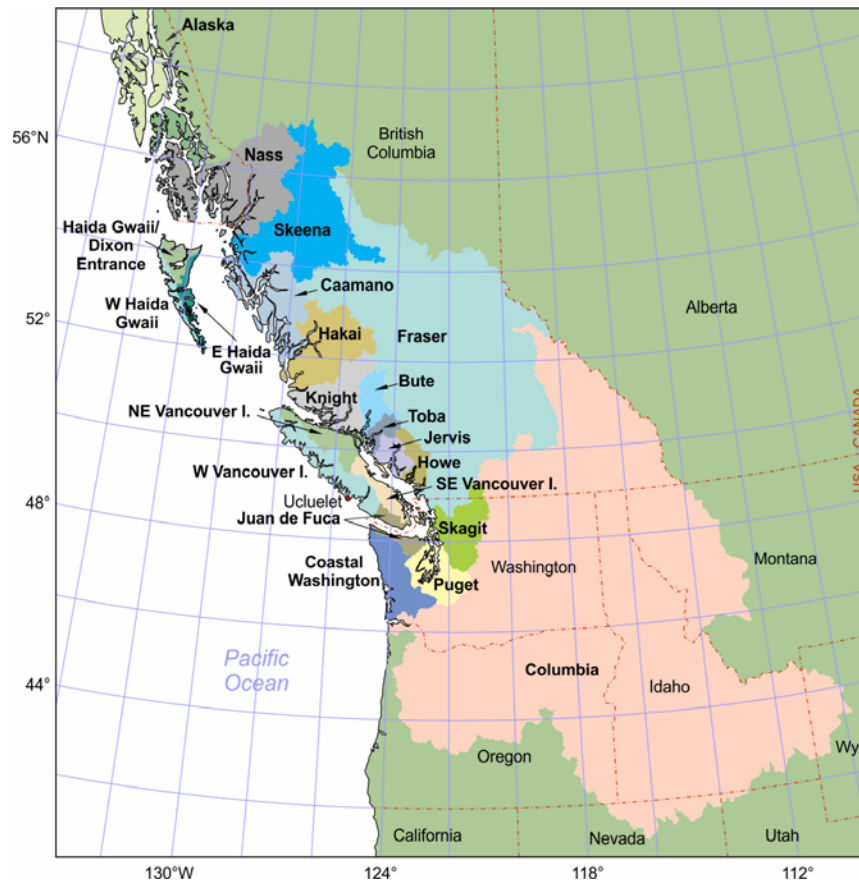


Figure 72: Drainage basins whose major rivers discharge into the model domain.

In order to employ the same technique to estimate future discharges, future precipitation, temperatures, and snowpack estimates were downscaled from NARCCAP CRCM/CGCM3 model output. An earlier study that was restricted to only the Fraser River watershed (Morrison et al. 2002) and projections from the CGCM1 (Flato et al. 2000) and HadCM2 (Johns et al. 1997) IPCC AR3 global models predicted only a modest (5%) increase in the average total annual discharge over 2070-2099. However the shape of the annual histogram was forecast to change with increased flow over the winter, an earlier (by 24 days) spring melt, and an 18% smaller peak discharge.

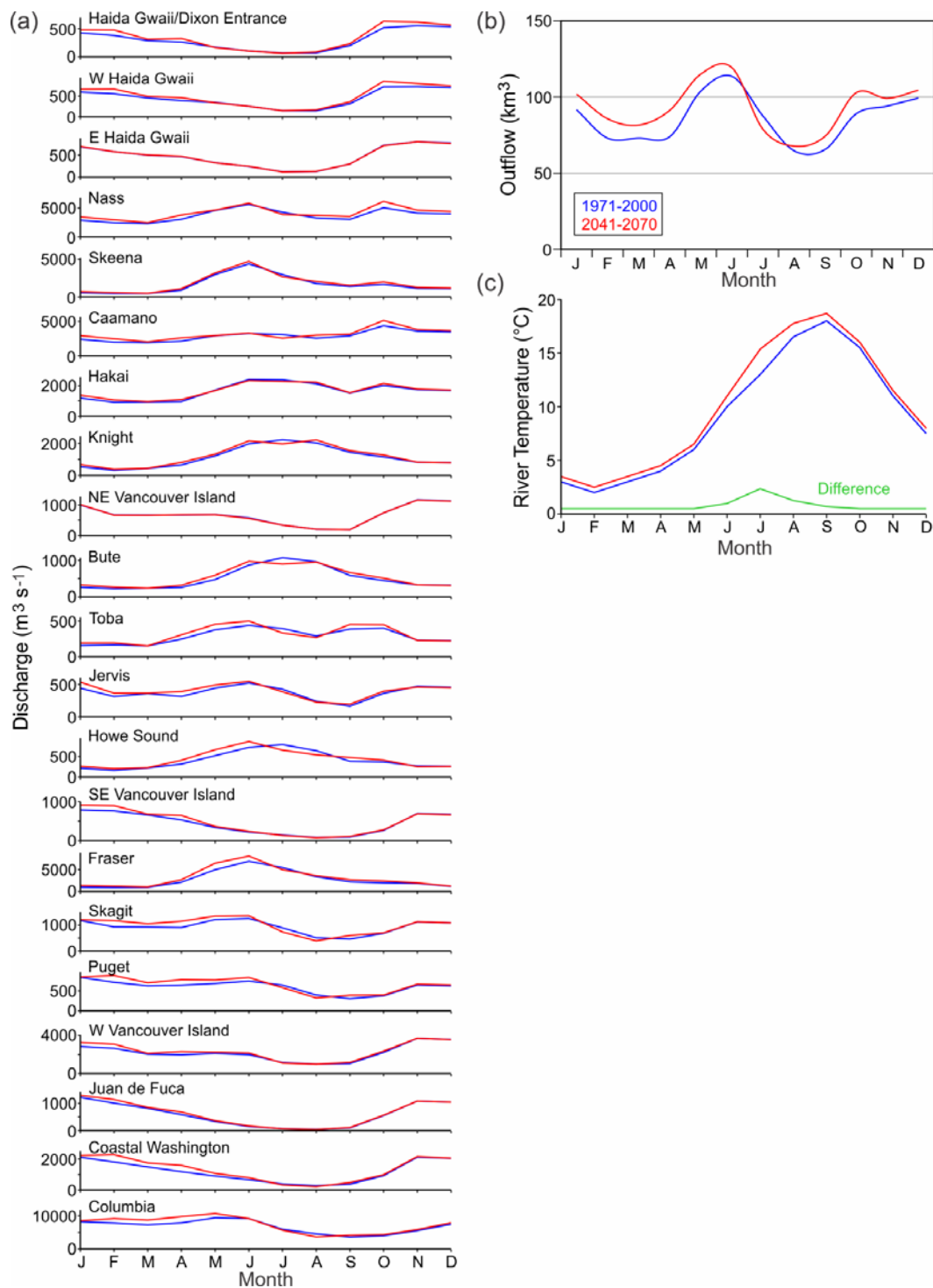


Figure 73: a) Monthly-average contemporary and future freshwater discharges for the twenty-one watersheds (Figure 73) impacting coastal BC waters as estimated by output from CRCM output, b) monthly-average total discharge for the entire coast, c) monthly-average discharge temperatures.

Figure 73a) shows the 1971-2000 and 2041-70 annual discharge curves for the twenty-one basins whose river discharges enter the MF12 model domain. (The most northerly Stikine watershed included in Morrison et al. (2011) is not included here because its river mouth lies outside the model domain.) Figure 73b) shows total discharges along the BC coast and consistent with the projections shown in Figure 69, only for July and parts of June and August are they projected to be less than present-day, for

the rest of the year they are larger. Although Morrison et al. (2002) predicted a future Fraser peak discharge that is slightly smaller and occurs earlier in the year, in this case the peak is larger and to the extent it can be determined from monthly values, occurs at the same time. Figure 73c shows the associated average monthly temperatures, which for now have been assumed to be the same for all rivers.

Ocean Conditions

As the CRCM is an atmosphere-only model, anomalies for the initial ocean temperature and salinity fields and forcing along the northern, western, and southern boundaries had to be calculated from CGCM3 output. As with the CRCM downscaling, the coarse CGCM3 resolution necessitated the use of special downscaling techniques. In this case, the dearth of GCM points contained within the bounds of the regional ocean model (ROMS, see next chapter) domain made using EOFs impractical. Monthly anomalies for the western boundary conditions were interpolated directly from the GCM output, and a latitudinal average was found from the GCM points available for the southern and northern boundaries as well as for the initial conditions.

Samples of the resulting anomaly fields that were applied to the boundaries are shown in Figure 74. In addition to salinity and temperature changes, changes to the normal velocities entering along these boundaries are also shown. Only the anomalies for the western boundary are shown here.

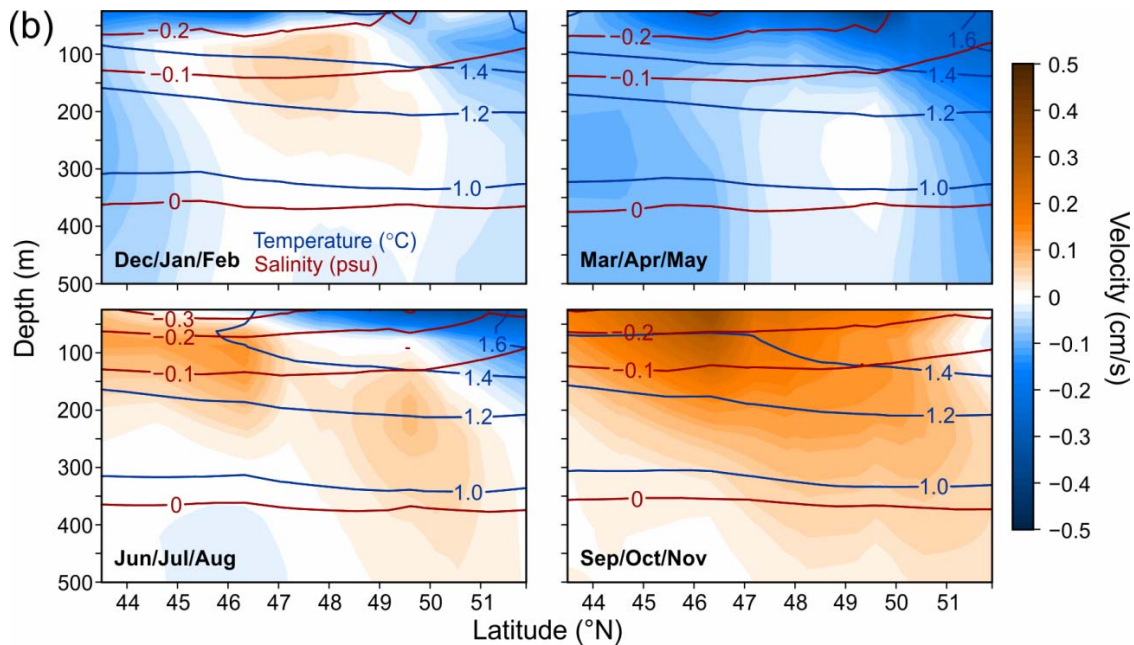


Figure 74: Seasonal temperature (blue lines), salinity (red lines) and perpendicular velocity anomalies (colour contours, difference of means for 2040-2070 and 1970-2000) for the western boundary as computed from CGCM3 (specifically CGCM3.1 T47 SRES A2 run #4). Positive velocities denote flow into the ROMS model domain.

Along the western boundary, the predominant current feature entering the ROMS model domain is the eastward flowing Kuroshio Extension or North Pacific Current (Dodimead et al. 1963). It enters around 45°N (Freeland, 2006) and bifurcates into the northwestward flowing Alaska Current and southward flowing California Current (Figure 67). The Sep-Nov panel of Figure 74 shows stronger northeastward (perpendicular) flows almost everywhere with notably stronger values near the core of the North Pacific

Current. In Mar-May, weaker eastward flows are seen everywhere with the largest reductions near the surface at around 50°N. Negative anomalies are seen near the surface and along the north portion of the boundary in Jun-Aug, consistent with an increasing Alaska Current. However, below and to the south of this region, the flow into the model domain is increasing. Finally, in Dec-Feb the subsurface part of the North Pacific Current is seen to be strengthening while everywhere else it is weakening. In all seasons, the salinity anomaly is seen to be about -0.2 near the surface, and become smaller with increasing depth, while maximum temperature anomaly is about 1.5°C near the surface. It is somewhat larger in the north and also decreases with depth.

Anomalies applied to the MF12 initial (January) temperature and salinity fields are shown in Figure 75. As mentioned above, the dearth of GCM points within the MF12 model domain meant that it was only practical to form latitudinally-averaged values. No anomalies were applied to the initial velocity fields and though this is admittedly inconsistent with the lateral boundary forcing, the model was spun up for a year so that internal dynamics would make the appropriate adjustments before the actual “projection run” was started.

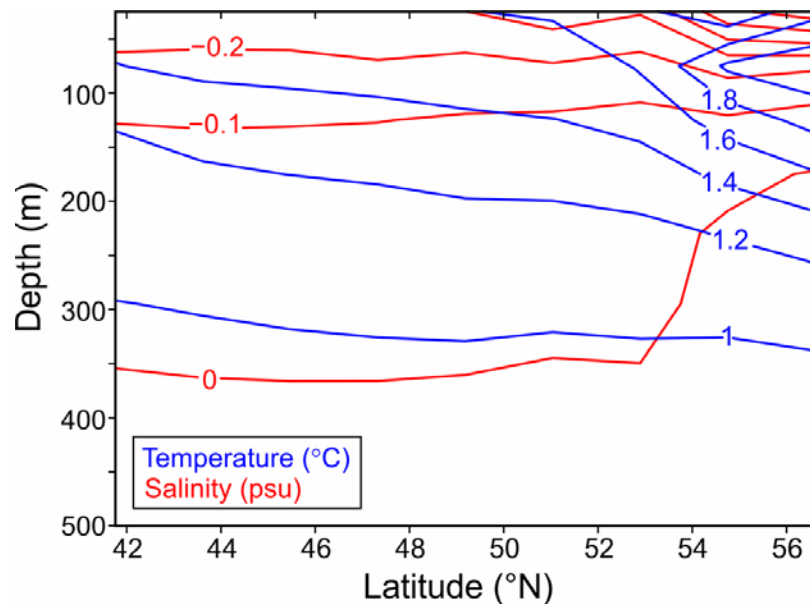


Figure 75: Temperature and salinity anomalies applied to the MF12 initial (January) conditions as functions of latitude and depth, and as computed from CGCM3.

Summary and Future Work

The preceding presentation has provided details on the calculation of forcing and initial fields for an ocean-only regional climate model for the BC continental shelf. The atmospheric and freshwater discharge forcing fields were downscaled and/or computed from CRCM/CGCM3 A2 scenario model output available on the NARCCAP archive (<http://www.narccap.ucar.edu/>) while the ocean initial conditions and lateral boundary conditions were downscaled from the associated CGCM3 run. As the CRCM winds were shown to poorly represent upwelling favourable conditions over the baseline period of 1971-2000, a strategy of computing anomalous forcing and initial fields and adding them to the analogous values used in MF12 was adopted.

Some of the atmospheric anomalies were consistent with the larger scale GCM findings of IPCC AR4 (Meehl et al. 2007), but CRCM did provide finer spatial resolution and some unanticipated results.

Average surface air temperatures were consistently warmer for all months with the January anomalies generally being the largest and those in June the smallest. Increases were larger over land than water, larger in the north for the winter months and generally larger over the coastal mountains in April through July. The monthly average precipitation was projected to increase along the entire coast in January, February, April, and along the northern coast in October and November. However drier conditions were projected along the entire coast in July and along the southern coast in August, November and December. As a consequence, the total freshwater discharge along the BC coast was projected to be about 10% larger in all months except for June-August when it was projected to decrease by up to 10%. Aside from parts of the southern coast in July-September and December and the north coast in January, the short wave radiation was projected to decrease. The largest reductions, seen along the coast in April and May, were correlated with increases in the daytime cloud cover and may have implications on the timing and magnitudes of spring phytoplankton blooms.

January salinity and temperature anomalies applied to the model initial conditions peaked at approximately -0.6 psu and 2.0°C and were generally largest near the surface and coast. Seasonal anomalies were applied to the salinity, temperature, and incoming/outgoing velocity fields along the northern, western, and southern boundaries, reflecting CGCM3 projected changes to the North Pacific, California, and Alaska Current system as well as to smaller scale features like the buoyancy-driven Alaska Stream and wind-driven Davison Current. Unfortunately, the CGCM3's relatively coarse grid did not allow adequate resolution of the California Undercurrent so it was not possible to project any changes to it.

Results arising from application of these forcing and initial conditions are summarized in the next section "Results from Regional Climate Model Simulation for the British Columbia Continental Shelf" of this report. Work has begun in computing analogous fields from other RCM/GCM combinations in the NARCCAP archive so they could be used to initialize and force other simulations, and ensemble averages and estimates of uncertainty could be computed.

RESULTS FROM REGIONAL OCEAN MODEL SIMULATION FOR THE BRITISH COLUMBIA CONTINENTAL SHELF

M.G.G. Foreman, W. Callendar, D. Masson, J. Morrison and I. Fine. Institute of Ocean Sciences, Fisheries and Oceans Canada.

Introduction

In the preceding chapter of this report, an approach was described for computing the initial and forcing conditions that would permit the simulation of future ocean conditions along the British Columbia continental shelf using a recently developed ocean circulation model (Masson and Fine 2012; henceforth MF12) that was used to hindcast conditions for the period 1995-2008. (Figure 76 shows the domain for this model.) The bases of these fields were regional and global climate model simulations archived as part of the North American Regional Climate Change Assessment Program (NARCCAP, <http://www.narccap.ucar.edu/>). Though NARCCAP offers several regional/global model combinations and thus the possibility of forming ensemble averages, only those from the Canadian Global Climate Model 3 (CGCM3) and Canadian Regional Climate Model (CRCM) coupling have been used here. However the NARCCAP projections were not used directly, as a comparison of winds over the contemporary period of 1971-2000 with the Faucher et al. (1999) and Foreman et al. (2011) re-constructed observations at buoys along the BC shelf revealed systematic biases in the timing of the spring and fall transitions and in particular, of the upwelling season. As the CRCM future winds generally displayed the same behaviour, employing them to directly force our future simulation would produce incorrect upwelling conditions and erroneous conclusions of their impact on marine

ecosystems. So instead, our future simulations were forced with fields that were the summation of those employed in the contemporary hindcast of MF12 and the future-minus-contemporary NARCCAP anomaly fields. Similar approaches for computing future projections have been used by Schär et al. (1996) and Hara et al. (2008)

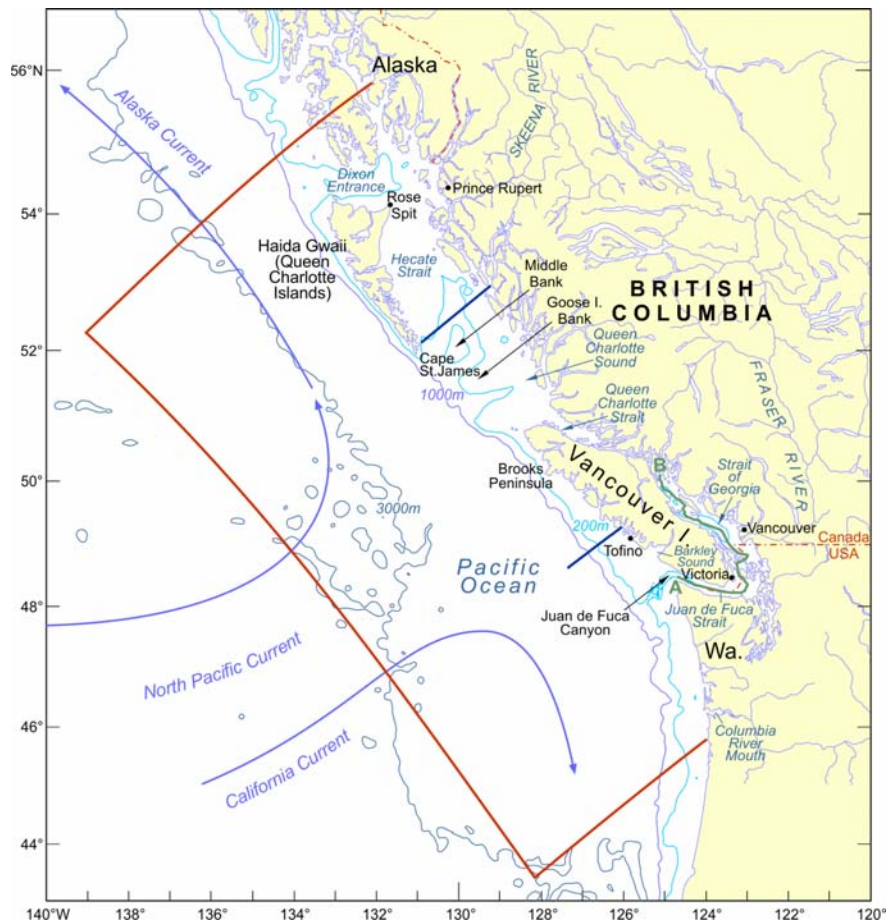


Figure 76: Map of the British Columbia continental shelf showing bathymetric contours, place names, and average positions of major offshore currents. Solid red lines denote the outer boundary of the regional shelf model and the solid dark blue line north of Tofino denotes the transect used in Figure 83.

In order to use the MF12 model for future projections, it need only be run with suitable future forcing and initial fields. In our case, the forcing anomalies are computed from the NARCCAP-defined ‘current’ and ‘future’ time periods of 1971-2000 and 2041-2070, respectively, with the future simulations assuming the A2 emissions scenario (no leveling off of greenhouse gases), the only scenario included in the NARCCAP archive. Though NARCCAP offers output from six regional climate models (RCMs) driven by up to four atmosphere-ocean general circulation models (AOGCMs), we chose to use the results from the Canadian Regional Climate Model (CRCM) forced by the Canadian Global Climate Model (CGCM3). This means that future water property and flow conditions along the BC shelf are essentially simulated by moving ahead the 1995-2008 sequence of events by seventy years. We acknowledge that our contemporary time period (1995-2008) only partially overlaps with the NARCCAP contemporary period of 1971-2000, thereby providing an inconsistency in this pseudo-projection. However until Masson and Fine extend their hindcast back to 1971 or another high resolution model is developed for the region and run over a period that includes a standard climate multi-decadal period, this is the best alternative approach.

Changes in Water Properties

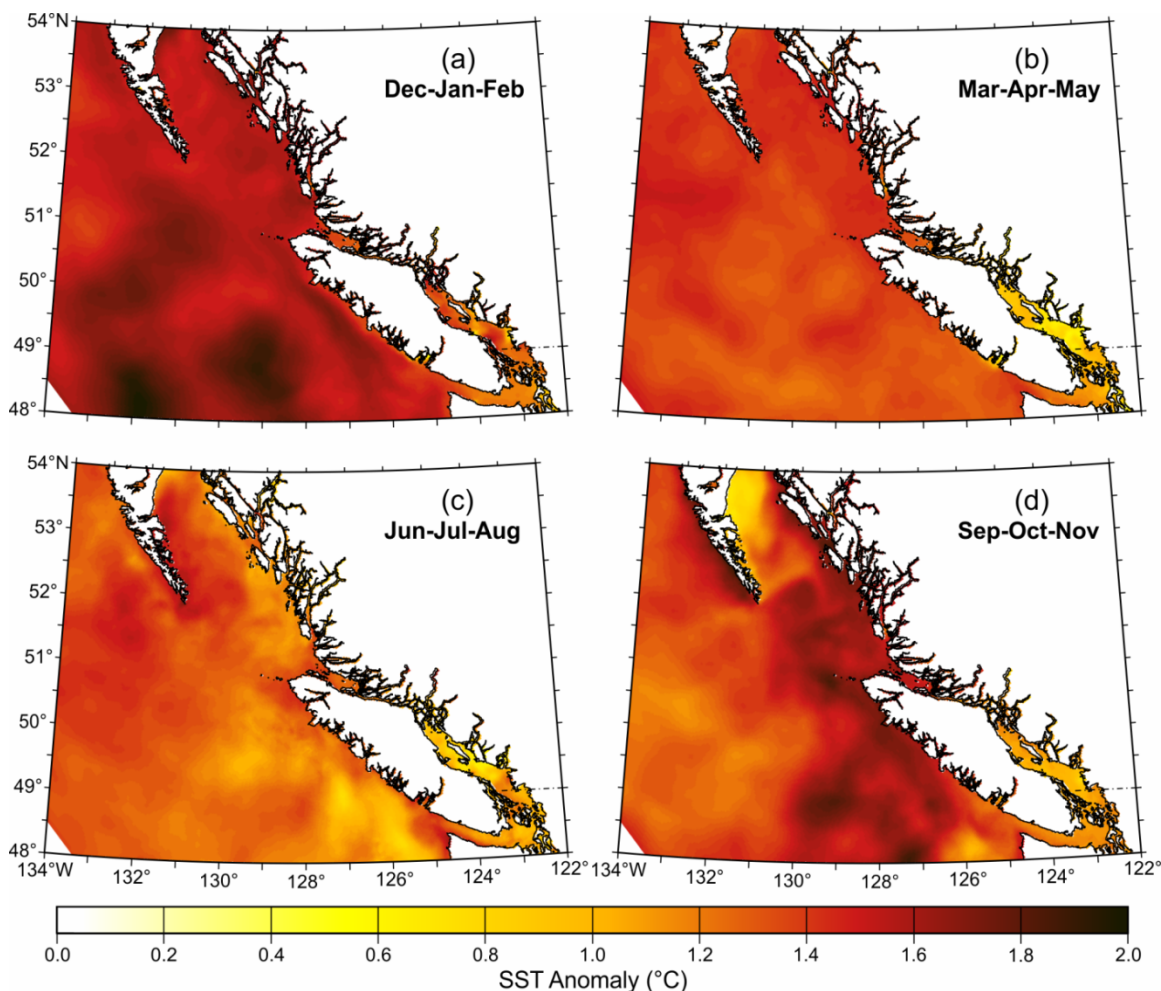


Figure 77: Seasonally-averaged sea surface temperature anomalies (°C).

Figure 77 shows seasonally-averaged sea surface temperature (SST) anomalies with respect to their MF12 counterparts. Though the model initial conditions were computed by adding latitude-dependent temperature anomalies that ranged from about 1.5°C in the south to 1.8°C in the north to the MF12 values in January 1995, the resultant 14-year average SST anomalies have a more complicated structure that reflects changes in the model forcing fields and circulation patterns (e.g., eddies). All SST anomalies are positive with those in the summer along the western Vancouver Island (VI) shelf being noteworthy in that they do not indicate a cooling due to an increase in the upwelling of colder subsurface water, at least not all the way to the surface. The Dec-Feb anomalies are generally largest and the Jun-Aug anomalies generally smallest, consistent with the surface air temperature anomalies seen in Figure 70. Even though the June-August river discharge temperatures have increased by a maximum of 2.5°C from those in MF12, there are relatively small SST increases (approximately 0.3°C) around the mouths of the Fraser and Columbia (not shown) Rivers because of decreases in the summer discharge (Figure 73).

Figure 78 shows seasonally-averaged sea surface salinity (SSS) anomalies with respect to the MF12 hindcast. Though here also, the model SSS initial condition anomalies were only latitude-dependent, ranging from -0.25 psu in the south to -0.6 psu in the north, changes in the winds and circulation patterns

arising from different monthly river discharges (Figure 73) have resulted in different seasonal SSS patterns. Though the generally smaller discharges from mid-June to mid-August have resulted in higher nearshore salinities at a few locations and seasons, SSS values are generally lower over most of the model domain, consistent with an overall increase in precipitation. Some of the local SSS anomalies, such as the winter positive anomaly emanating northwestward from Barkley Sound along the west coast of Vancouver Island and the positive winter anomaly in the Strait of Georgia, arise from changes in the spatial distribution of freshwater plumes under changing forcing.

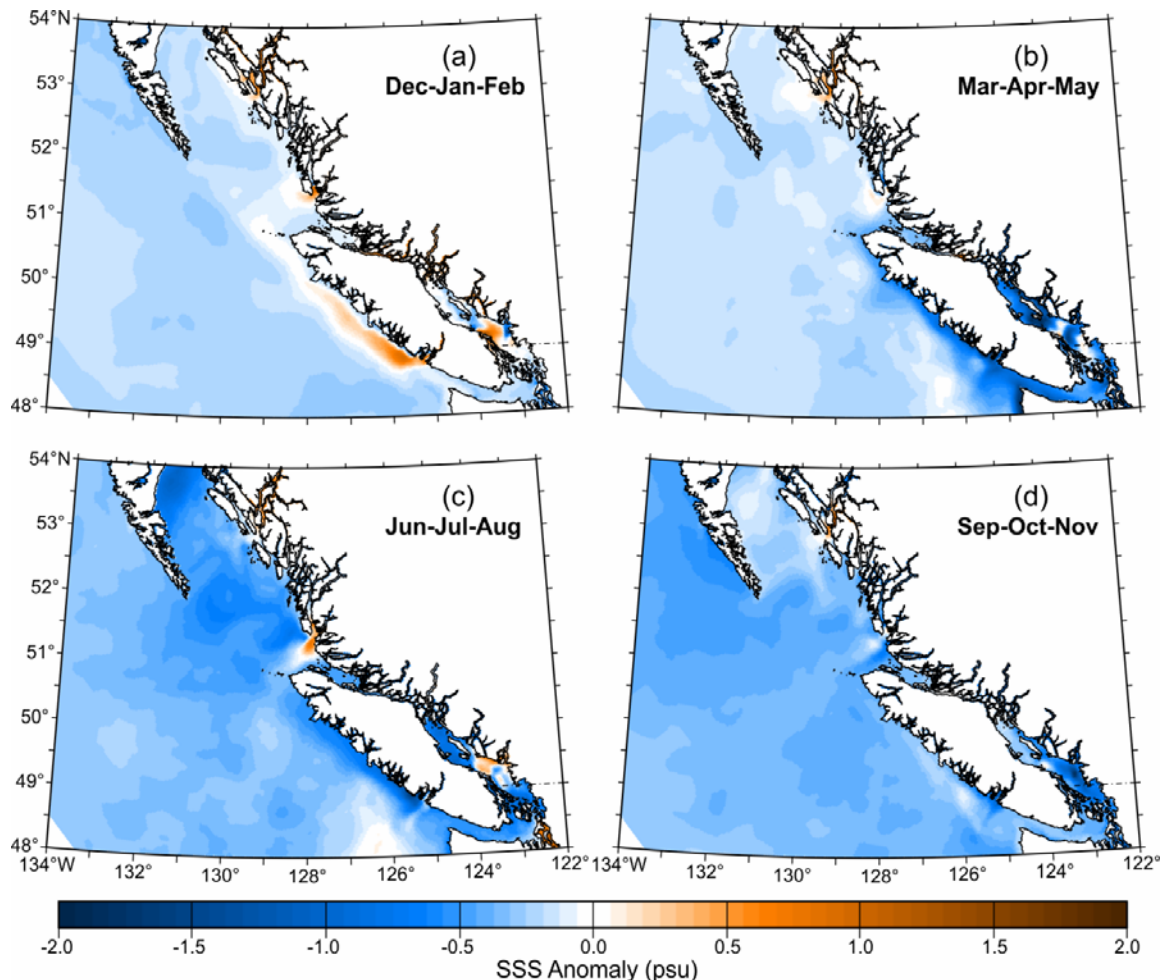


Figure 78: Seasonally-averaged sea surface salinity anomalies (psu).

Consistent with the predicted increase in the spring Fraser River discharge (Figure 73), the June surface salinity anomaly along the Salish Sea thalweg (not shown) decreases by about 0.75 psu and by up to 2.0 psu near the river mouth. Below the surface, the salinity in the Strait of Georgia is uniformly reduced by about 0.5 psu, with the general salinity signature of the estuarine circulation projected to remain practically unchanged.

Changes in Sea Surface Elevation

Figure 79 shows seasonally-averaged sea surface height (SSH) anomalies associated with changes in the regional ocean circulation. As described in the chapter on Trends in Sea Level, observed sea level rise also has contributions from: i) the melting of glaciers and continental ice sheets, ii) volume expansions (or contractions) arising from temperature and salinity effects, and iii) vertical land motions arising from glacial rebound, tectonic processes (e.g. subduction) and compaction (sinking) in delta regions. (The

interested reader is referred to Thomson et al. (2008) and the sea level rise chapter in this report for thorough descriptions of the factors affecting, information gaps associated with, and estimates of sea level rise along the BC coast.) Apart from the extent to which our future river discharges reflect changes in the melting of BC glaciers (Morrison et al. 2011), none of these additional contributions are included here. ROMS assumes the ocean fluid is incompressible and thus does not capture volume expansions that for example, would arise from warmer waters (Figure 77). Although models have been developed to include these expansions (e.g. Kim et al. 2011), the SSH anomalies computed here mostly arise from changes in the winds (set-up and set-down) and dynamic adjustments to changes in water density. In particular, most of these changes arise from forcing changes within the model domain rather than SSH signals entering via the lateral boundaries. (SSH anomalies were not directly included in the future lateral boundary forcing, though they can develop, via dynamical adjustments, to the new density fields.) As illustrated in the small portion of the western boundary shown in Figure 79, the CGCM3 SSH anomaly along the western boundary was generally negative, with only small areas showing positive anomalies in fall and winter.

The generally higher SSH values on the shelf in the winter and spring (Figure 79) are due to the stronger northwestward downwelling winds (set-up) and are projected to be as large as 4 cm in northern Hecate Strait in Dec-Feb. Analogously, the lower SSH anomalies in almost all regions in June-August are generally a result of stronger southeastward upwelling winds. The negative September-November anomalies seen in southern BC shelf waters seem to be a continuation of those in Jun-Aug and thus may be mainly explained by the winds, while the slightly positive anomalies seen in portions of Queen Charlotte Sound and Hecate Strait are probably due to dynamic height increases arising from changes in salinity and temperature and an earlier and/or larger set-up from the stronger winter northwestward winds.

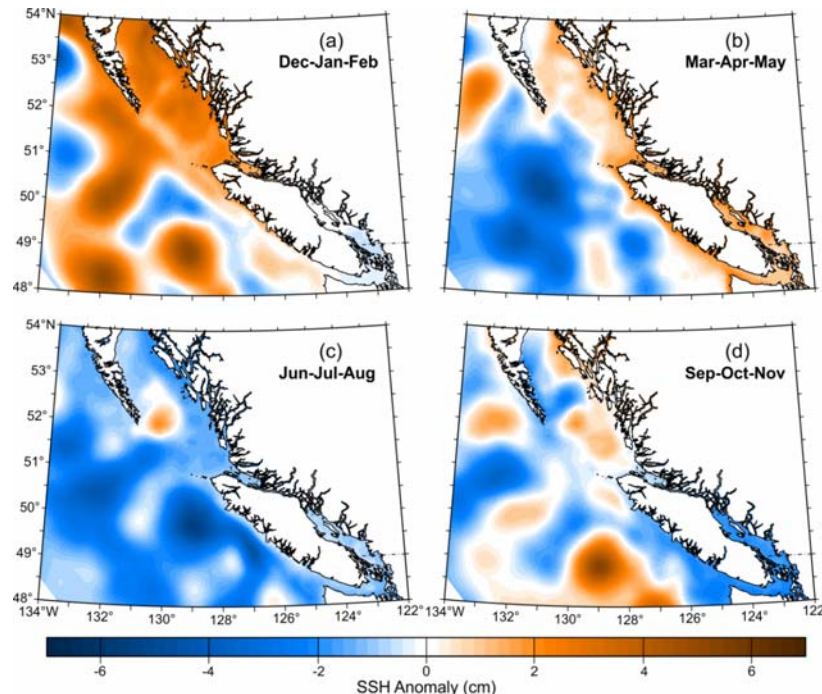


Figure 79: Seasonally-averaged sea surface height anomalies (cm).

Though ROMS has the ability to incorporate SSH changes arising from atmospheric pressure, ("the inverse barometer effect"), this was not done here nor in MF12. Therefore the SSH changes shown in Figure 79 do not include any changes arising from the inverse barometer effect. However gradients of

the monthly average atmospheric pressure anomaly fields (not shown) do explain many of the wind changes described in the previous section and shown in Figure 68. For example, a deepening of the Aleutian low pressure system in January combined with higher pressures over the continent is consistent with stronger northwestward winds over the BC shelf. Assuming a static inverse barometer correction to the sea levels associated with these pressures, the Prince Rupert January-July average range can be expected to increase by almost another 3cm. However these are only average SSH increases; storm events will certainly result in higher levels. Graham and Diaz (2001) showed that North Pacific winter storm intensity has increased over the last half of the 20th century while Abeyisirigunawardena (2010) showed an increase in storm frequency at Prince Rupert over the same time period. The implication is that the surges and surface wave heights associated with these events can be expected to further exacerbate the flooding consequences of mean sea level rise.

It should be noted that there can be significant interdecadal variations in sea level rise associated with patterns such as the Pacific Decadal Oscillation (PDO, Mantua et al. 1997) and they may over-ride those arising from greenhouse gas emissions (Overland and Wang 2007). In particular, though sea levels have been rising at approximately 3 mm yr⁻¹ globally (Cazenave and Nerem 2004) since 1992, SSHs along the western North American coast have remained approximately stationary since 1980. Bromirski et al. (2011) showed that this could be explained by the dynamical response to changes in the wind stress curl that arose when the PDO shifted from a cold to warm phase in the mid-1970s. They also cautioned that recent changes in wind stress along the Pacific eastern boundary “may be foreshadowing a persistent shift to the PDO cold phase” and a return to rates of sea level rise in the region that could approach or exceed the global mean. It is therefore important to place the SSH results for the MF12 and our present study in the context of these interdecadal variabilities. The average monthly value of the PDO over the 1995-2008 period of the MF12 hindcast (see <http://jisao.washington.edu/pdo/graphics.html> for a time series plot since 1900) is only slightly positive (+0.1). Consequently, SSH statistics arising from that hindcast and this subsequent future projection should not have been overly biased by the state of the PDO during these simulations.

Changes in the Flow Fields

Figure 80 shows contemporary and future eddy kinetic energy (EKE) along the BC continental shelf. Future higher EKE off the west coast of Haida Gwaii (Figure 76) and northwest VI are predominantly winter features that arise from stronger northwestward winds. Haida Eddies are generated when counterclockwise flows around Hecate Strait exit past Cape St James (Crawford et al. 2002; Di Lorenzo et al. 2005) while similar flow separation arises when the northwestward Davidson Current passes Brooks Peninsula. A simulation where only the future wind forcing was replaced with contemporary values (i.e., all other forcing fields included future anomalies) revealed this EKE increase was almost entirely due to increases in the winter winds. Animations further revealed that these future simulations do not produce more Haida Eddies, only that eddy size increases (not shown). However this result may be an artefact of our future wind forcing being formed by adding anomalies to the 1995-2008 winds. Were changes in storm frequency also included in the future winds, as suggested by the Abeyisirigunawardena (2010) analysis, the number of Haida Eddies generated might also change. The animations also showed that not all of the EKE off Haida Gwaii arose from Haida Eddies; some eddies were also generated further northward, perhaps from baroclinic instabilities similar to those described in Thomson and Gower (1998). Nevertheless, Haida Eddies do export coastal waters carrying nutrients and larvae offshore (Whitney and Robert 2002; Johnson et al. 2005) so changes in their magnitude may have important ecosystem consequences.

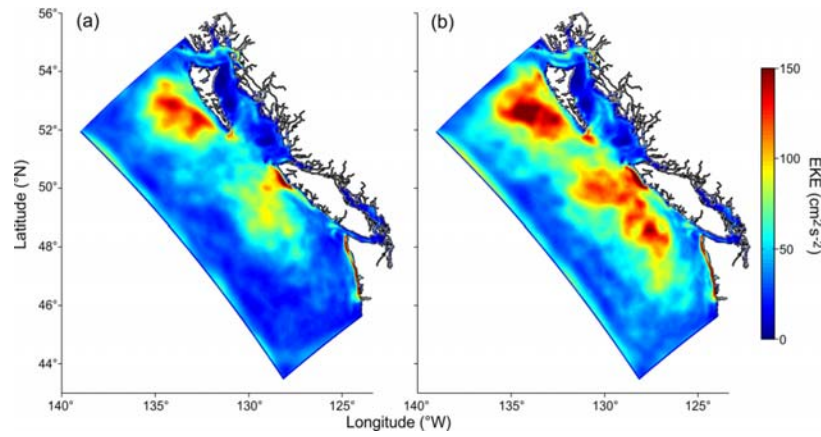


Figure 80: Annually-averaged eddy kinetic energy (cm^2/s^2) for the contemporary (from MF12) and future (2040-2070) simulations.

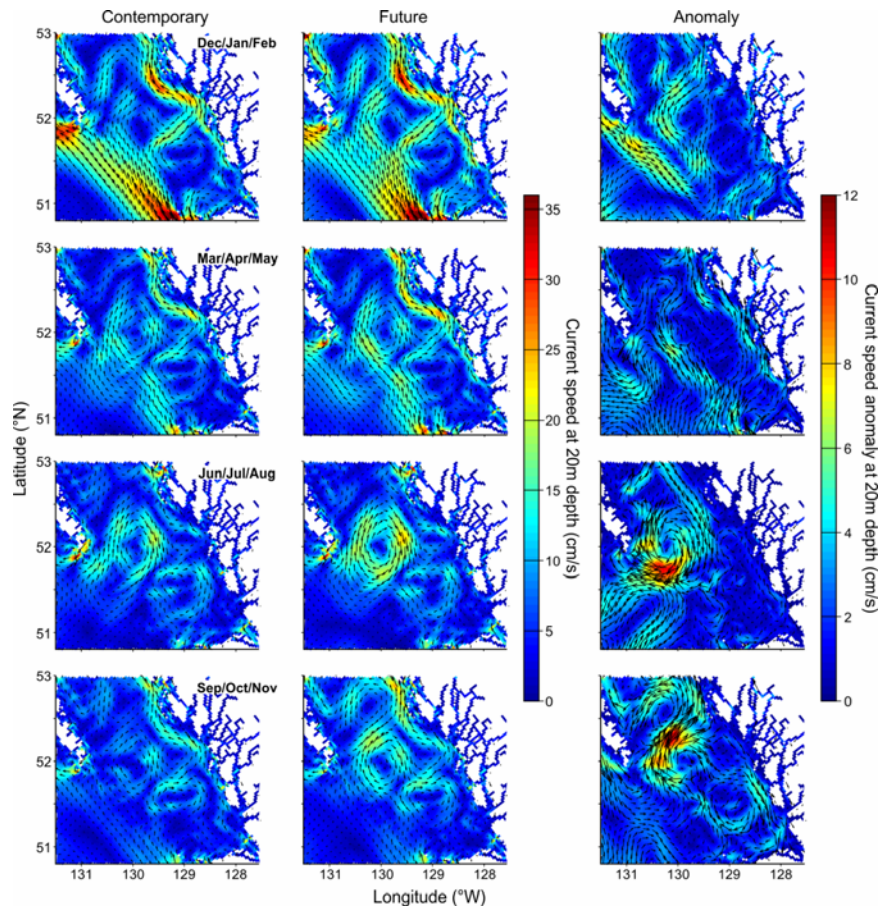


Figure 81: Contemporary, future and differences in seasonally-averaged currents at 20 m depth in Queen Charlotte Sound. Note the colour scale change for the anomaly column.

Flows crossing a transect in southern Hecate Strait (not shown) further illustrate the Haida Eddy generation mechanism and how it is projected to change in the future. Contemporary, future and differences in the seasonally-averaged, southern Hecate Strait flow fields at 20 m depth (Figure 81) illustrate some of these patterns from a different perspective. (20 m was chosen rather than the surface to reduce the effect of wind.) Stronger currents are seen along the western flank of Middle Bank in all seasons and in the summer and fall they are accompanied by stronger flows on the eastern side, thereby

strengthening the clockwise eddy. A similar but weaker eddy is also seen around Goose Island Bank and portions of its clockwise flows are also seen to change seasonally with larger scale patterns coming off northwestern Vancouver Island or along the eastern side of Hecate Strait. Though both these eddies are partially generated by tidal rectification, it is changes in the larger scale wind and buoyancy-driven flow patterns that are causing the strengthening projected here. The major summer features seen in Figure 81 have been observed and were described in Crawford et al. (1995).

The predominant features in analogous seasonally-averaged 20 m flows in northern Hecate Strait and Dixon Entrance (not shown) are the counter-clockwise Rose Spit Eddy (Crean 1967) in Dixon Entrance and the northward flows along the eastern side of Hecate Strait. Both are seen to intensify in all seasons except summer, with the eddy position also varying seasonally. The northern edge of the eddy is seen to be an extension of the northward Hecate flows, which in turn largely arise from river discharges and the wind

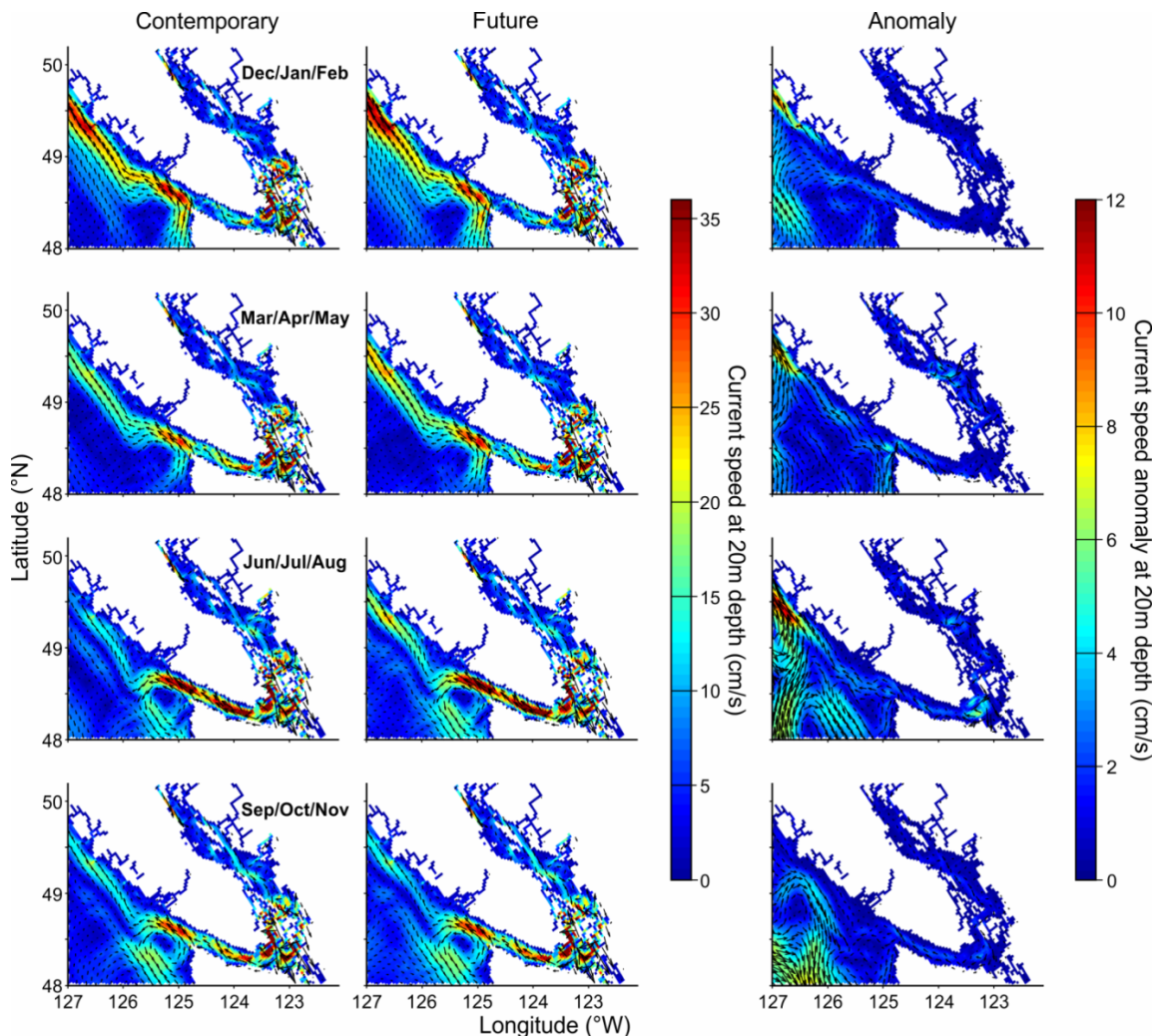


Figure 82: Contemporary, future and differences in seasonally-averaged currents at 20 m depth in the Salish Sea and southwest Vancouver Island shelf. Note the colour scale change for the anomaly column.

Figure 82 shows analogous seasonally-averaged 20 m flows in the Salish Sea and off southwest Vancouver Island shelf. Stronger winter winds have generally increased the northwestward component of all Dec-Feb surface flows and in particular, the Davidson Current (Freeland et al. 1984) off the west coast of VI. The Mar-May surface currents have a similar pattern and with the exception of stronger

flows along the western Washington coast, are generally weaker. These latter flows arise from stronger winds and larger Columbia River discharges and, either weaken the surface estuarine outflow in Juan de Fuca Strait, or are sufficiently strong to cause reversals (Thomson et al. 2007). A weak Juan de Fuca Eddy (Freeland and Denman 1982) is also seen off the entrance of Juan de Fuca Strait in the Mar-May contemporary and future panels and more fully formed versions are seen in the following two seasons. These eddies are formed by a combination of upwelling winds, tidal mixing off Cape Flattery, and estuarine flows in Juan de Fuca Canyon and Juan de Fuca Strait (Foreman et al. 2008; Macfadyen and Hickey 2010) and have important ecosystem impacts. However unlike the more northerly Haida Eddies which move offshore after their generation, Juan de Fuca Eddies are similar to the Middle and Goose Island Bank Eddies and largely remain locked in place by underlying bathymetric features. Though the Jun-Aug anomaly panel in the Figure 82 does suggest a small increase in the current magnitudes around the periphery of the Juan de Fuca Eddy, Figure 83 (and zoom-ins that are not shown) suggest very little difference in the future EKE in this region. Equally important to the magnitude of these eddies is the timing of their formation and disappearance, both of which are linked to the spring and fall transitions in alongshore winds. Attempts were made to determine if there was any change in these timings and none were found. So unlike the more northerly eddies described above, our future simulations do not suggest any significant changes to future Juan de Fuca Eddies.

However the Jun-Aug anomaly panel in Figure 82 does show a stronger Vancouver Island Coastal Current (VICC, Thomson et al. 1989) arising from the stronger surface estuarine flows in Juan de Fuca Strait. The Shelf Break Current (SBC, Freeland et al. 1984) arising from upwelling winds is also evident in the Jun-Aug and Sep-Nov contemporary and future panels, and though the associated anomalies suggest magnitude increases, the patterns are not sufficiently distinct from those of the Juan de Fuca and an offshore eddy, to permit definitive conclusions.

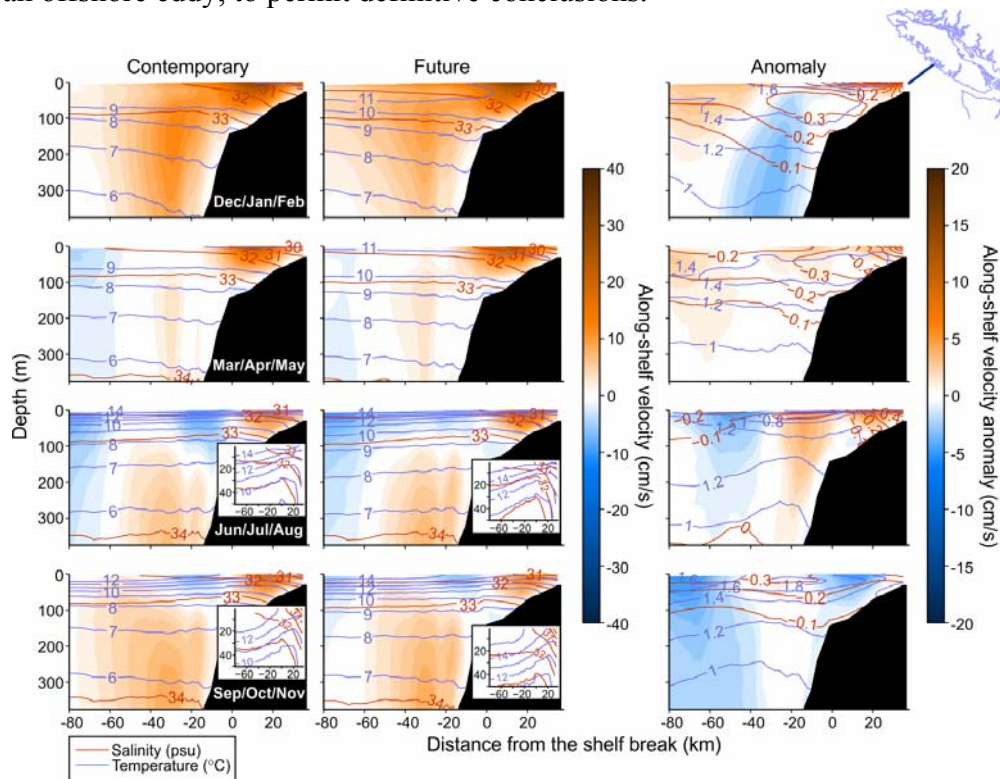


Figure 83: Along-shelf currents crossing, and temperature (blue) and salinity (red) contours along, a transect off the mid Vancouver Island shelf (see Figure 76). Redder (positive) shaded areas indicate greater flow to the northwest while darker blue regions indicate greater flow to the southeast.

Figure 83 shows contemporary and future seasonal alongshore currents, isotherms and isohalines along a transect crossing the mid VI shelf. There are five main currents in this region, four of which are seen in the Jun-Aug contemporary and future panels. They are the northwestward buoyancy-driven VICC; the southeastward SBC which is further offshore, primarily wind-driven, and extends down the water column to approximately 150m depth; the southeastward California Current that is even further offshore; and the northwestward California Undercurrent (CUC, Thomson and Krassovski 2010; Hickey 1979) which is centered at approximately 150-200m depth along the continental slope. The SBC disappears when the winds reverse in the fall and is replaced by the Davidson Current which, as can be seen in the Dec-Feb panels, merges with the CUC and VICC to provide northwestward flow over the entire shelf and slope.

The CUC is important for its roles in providing a conduit for the northward migration of fish species like hake (King et al. 2011) and being a source of nutrients and oxygen (Crawford and Peña 2012) that are upwelled onto the VI shelf in summer. Though our results on future CUC changes could thus have important ecosystem consequences, we need to be cautious in their interpretation because the CUC does not originate within the model domain and its magnitude is strongly influenced by our southern boundary forcing. In particular, as the anomaly component of this boundary forcing was interpolated from oceanic temperatures, salinities and currents in a model (CGCM3) that barely resolves the continental shelf, let alone slope, we do not have much confidence that these anomalies capture future changes accurately. Clearly, a global or regional climate model that has sufficient horizontal resolution (e.g. <10 km) to resolve the shelf and slope and that extends much further to the south (e.g., to Baja California) would be necessary to provide better estimates of changes to the CUC entering along the southern boundary of the model domain.

In that light, we must assign considerable uncertainty to the Dec-Feb projection that the CUC will be smaller in the future. On the other hand, the slight increases seen for the VICC and the off-shelf component of the Davidson Current are more credible as a future simulation wherein future wind forcing was replaced with contemporary values demonstrated that both were due to increases in the wind. As seen in the Mar-May anomaly panel, relatively minor changes to the alongshore currents are projected for this time period. The VICC is seen to strengthen slightly, consistent with the lower salinities along the coast. However the Jun-Aug changes are more notable. Though the VICC is also stronger (and salinities smaller), a stronger CUC seems to have weakened the SBC. Though this might be interpreted as a consequence of weaker upwelling winds, the 0-50 m depth insets in the contemporary and future panels of Figure 83 show isotherms (e.g. 10°C in contemporary vs 11°C in future) and isohalines (e.g., 32.5 psu) to be slightly steeper in the future case, suggesting more upwelling. And this would also be consistent with stronger southeastward winds and the stronger California Current. Finally, the Sep-Nov panels indicate a weakening of the VICC and perhaps not so much strengthening of the California Current, but rather an eastward movement of its core. The CUC is essentially unchanged and SBC is slightly weaker, possibly as a consequence of slight changes in the seasonally transitioning winds (Figure 68).

Summary and Future Work

The preceding presentation has described and interpreted results from a simulation for the BC continental shelf with an ocean-only regional climate model and the future forcing fields described in the previous section. In particular, the atmospheric and freshwater discharge forcing fields were downscaled and/or computed from CRCM/CGCM3 A2 scenario model output available on the NARCCAP archive (<http://www.narccap.ucar.edu/>) while the ocean initial conditions and lateral boundary conditions were downscaled from the associated CGCM3 run. As the CRCM winds were shown to poorly capture average upwelling favourable conditions over the baseline period of 1971-2000,

a strategy of computing anomalous forcing and initial fields and adding them to the analogous values used in MF12 was adopted.

Seasonally-averaged sea surface temperatures were projected to increase by between 0.5 and 2.0°C while the analogous sea surface salinities were projected to decrease by as much as 2.0 psu, though there were some regions and periods in which small increases were projected. Stronger winter winds were seen to result in larger Haida Eddies and this can be expected to have important ecosystem consequences given the nutrients and larvae that they export offshore (Whitney and Robert 2002; Johnson et al. 2005). Though there were indications of slightly stronger upwelling along the Vancouver Island shelf due to slightly stronger summer winds, no appreciable change was projected in the magnitude or formation timing of Juan de Fuca Eddies. However, increased flows were projected in some seasons for the Rose Spit, Middle Bank, and Goose Island Bank Eddies and these could also have important ecosystem impacts (e.g., Jamieson 1985). Although changes were also projected for the CUC, limitations associated with the calculation of oceanic anomalies along the southern boundary of the model domain meant they had considerable uncertainty. Consequently, it is difficult to make definitive statements on how oxygen and nutrients upwelled from the CUC onto the VI shelf might change in the future.

However, except in summer, more precipitation over the watersheds emptying into coastal waters produced larger freshwater input and in particular, a stronger estuarine flow in Juan de Fuca Strait and a stronger Vancouver Island Coastal Current. Similar discharge increases along the central and north coasts also contributed to stronger flows in Queen Charlotte Sound, Hecate Strait, and Dixon Entrance.

Finally, seasonal wind and freshwater discharge increases along most of the coast meant that the winter minus summer range of sea surface height was generally projected to increase. An average projected range increase of 10 cm at Prince Rupert, together with another 3 cm from average changes in the inverse barometer effect and event-specific storm surge and surface waves increases (Graham and Diaz 2001; Abeysirigunawardena 2010), certainly suggest a potential for increased flooding and damage to coastal structures.

Future work is planned to include the downscaling of forcing fields from other RCM/GCM combinations in the NARCCAP archive and from analogous IPCC AR5 models that are just becoming available through the Coordinated Regional climate Downscaling Experiment (CORDEX, <http://www.meteo.unican.es/en/projects/CORDEX>). These fields will be used to initialize and force other simulations so that ensemble averages and estimates of uncertainty can be computed. Work has also begun on coupling the present circulation model to a biogeochemical model in order to investigate the impacts that the aforementioned physical changes will have on future marine ecosystems.

ACKNOWLEDGEMENTS

We acknowledge the Climate Change Science Initiative (CCSI) and Ecosystem Research Initiative (ERI) within Fisheries and Oceans Canada for their financial support of this research. We thank the Centre for Ocean Model Development for Application within Fisheries and Oceans Canada for the funding to support the development of the BC shelf model and the Aquatic Climate Change Adaptation Services Program within Fisheries and Oceans for their financial support. We thank the CMIP5 data originators for their contributions, and the many Fisheries and Oceans Canada staff who have contributed to the collection of the data sets used in this report.

REFERENCES

- Abeysirigunawardena, D.S. 2010. Climate variability and change impacts on coastal environmental variables in British Columbia Canada. Ph.D. Thesis, Department of Geography, University of Victoria, Victoria, B.C. 322 p.
- Allen, S.E., and Wolfe, M.A. 2013. Hindcast of the timing of the spring phytoplankton bloom in the Strait of Georgia, 1968-2010. Prog. Oceanogr. In press.
- Arctic Monitoring and Assessment Programme. 2011. Snow, Water, Ice and Permafrost in the Arctic. International Arctic Science Committee, Oslo. 553 p.
- Ardizzone, J., Atlas, R., Hoffman, R.N., Jusem, J.C., Leidner, S.M. and Moroni, D.F. 2009. New multiplatform ocean surface wind product available. EOS. 90: 231.
- Armstrong, J.L., Boldt, J.L., Cross, A.D., Moss, J.H., David, N.D., Myers, K.W., Walker, R.V., Beauchamp, D.A. and Haldorson, L.J. 2005. Distribution, size and interannual, seasonal and diel food habits of northern Gulf of Alaska juvenile pink salmon *Oncorhynchus gorbuscha*. Deep-Sea Res. II. 52: 247-265.
- Arora, V.K., Scinocca, J.F., Boer, G.J., Christian, J.R., Denman, K.L., Flato, G.M., Kharin, V.V., Lee, W.G. and Merryfield, W.J. 2011. Carbon emission limits required to satisfy future representative concentration pathways of greenhouse gases. Geophys. Res. Lett. 38. doi:10.1029/2010GL046270.
- Auad, G., Miller, A.J., and Di Lorenzo, E. 2006. Long-term forecast of oceanic conditions off California and their biological implications. J. Geophys. Res. 111. doi:10.1029/2005JC003219.
- Bakun, A. 1973. Coastal upwelling indices, West Coast of North America, 1946-71. NOAA Tech. Rep., NMFS SSRF-671. 114 p.
- Barrie, J.V., and Conway, K. 2002. Rapid sea-level change and coastal evolution on the Pacific margin of Canada. Sedimentary Geology. 150: 171-183.
- Bianucci, L., Denman, K.L., and Ianson, D. 2011. Low oxygen and high inorganic carbon on the Vancouver Island shelf. J. Geophys. Res. 116. doi:10.1029/2010JC006720 .
- Bograd, S.J., Schroeder, I., Sarkar, N., Qiu, X., Sydeman, W.J., and Schwing, F.B. 2009. Phenology of coastal upwelling in the California Current. Geophys. Res. Lett. 36. doi:10.1029/2008GL035933.
- Boldt, J.L., and Haldorson, L.J. 2003. Seasonal and geographic variation in juvenile pink salmon diets in the northern Gulf of Alaska and Prince William Sound. Transactions of the American Fisheries Society. 132: 1035-1052.
- Bretherton, F. P., Davis, R.E., and Fandry, C.B. 1976. A technique for objective analysis and design of oceanic experiments. Deep-Sea Res. 23: 559-582.
- Bromirski, P.D., Miller, A.J., Flick, R.E., and Auad, G. 2011. Dynamical suppression of sea level rise along the Pacific coast of North America: Indications for imminent acceleration. J. Geophys. Res. 116. doi:10.1029/2010JC006759.

- Bromirski, P.D., Miller, A.J., and Flick, R.E. 2012. Understanding North Pacific sea level trends. *EOS*. 93: 249-250.
- Cazenave, A., and Nerem, R.S. 2004. Present-day sea level change: Observations and causes. *Rev. Geophys.* 42. doi:10.1029/2003RG000139.
- Chan, F., Barth, J.A., Lubchenco, J., Kirincich, A., Weeks, H., Peterson, W.T., and Menge, B.A. 2008. Emergence of anoxia in the California Current large marine ecosystem. *Science*. 319: 920. doi:10.1126/science.1149016.
- Cherniawsky, J.Y., and Crawford, W.R. 1996. Comparison between weather buoy and Comprehensive Ocean-Atmosphere Data Set wind data for the west coast of Canada. *J. Geophys. Res.* 101: 18,377-18,389.
- Collins, A.K., Allen, S.E., and Pawlowicz, R. 2009. The role of wind in determining the timing of the spring bloom in the Strait of Georgia. *Can. J. Aquat. Sci.* 66: 1597-1616.
- Connolly, T.P., Hickey, B.M., Geier, S.L., and Cochlan, W.P. 2010. Processes influencing seasonal hypoxia in the northern California Current System. *J. Geophys. Res.* 115. doi:10.1029/2009JC005283.
- Cooley, S.R., and Doney, S.C. 2009. Anticipating ocean acidification's economic consequences for commercial fisheries. *Environ. Res. Lett.* 4. doi:10.1088/1748-9326/4/2/024007.
- Crawford, W.R. 1991. Tidal mixing and nutrient flux in the waters of southwest British Columbia. *In* Tidal hydrodynamics. Edited by B.B. Parker. John Wiley and Sons, New York. pp. 855–869.
- Crawford, W.R., and Peña, M.A. 2013. Declining oxygen on the British Columbia continental shelf. *Atmos. Ocean*. 50. doi:10.1080/07055900.2012.753028.
- Crawford, W.R., Woodward, M.J., Foreman, M.G.G., and Thomson, R.E. 1995. Oceanographic features of Hecate Strait and Queen Charlotte Sound in summer. *Atmos. Ocean*. 33: 639-681.
- Crawford, W.R., Cherniawsky, J.Y., Foreman, M.G.G., and Gower, J.F.R. 2002. Formation of the Haida-1998 oceanic eddy. *J. Geophys. Res.* 107. 6.1–6.11.
- Crean, P.B. 1967. Physical oceanography of Dixon Entrance, British Columbia. *Bulletin of the Fisheries Research Board of Canada*. 156. 66 p.
- Crusius, J., Schroth, A.W., Gasso, S., Moy, C.M., Levy, R.C., and Gatica, M. 2011. Glacial flour dust storms in the Gulf of Alaska: Hydrologic and meteorological controls and their importance as a source of bioavailable iron. *Geophys. Res. Lett.* 38. doi:10.1029/2010GL046573.
- Denman, K.L., Brasseur, G., Chidthaisong, A., Ciais, P., Cox, P., Dickinson, R.E., Haugustaine, D., Heinze, C., Holland, E., Jacob, D., Lohmann, U., Ramachandran, S., daSilvaDias, P.L., Wofsy, S.C., and Zhang, X. 2007. Couplings between changes in the climate system and biogeochemistry. 2007. *In* *Climate Change 2007: The Physical Science Basis. Contribution of Working Group I to the Fourth Assessment Report of the Intergovernmental Panel on Climate Change*. Edited by Solomon, S., Qin, D., Manning, M., Chen, Z., Marquis, M., Averyt, K.B., Tignor M. and Miller, H.L. Cambridge University Press, Cambridge, United Kingdom and New York, NY, USA. pp. 499-587.

- Deser, C., Phillips, A.S., Bourdette, V., and Teng, H. 2012. Uncertainty in climate change projections: The role of internal variability. *Climate Dyn.* 38: 527-546. doi:10.1007/s00382-010-0977-x . http://www.cgd.ucar.edu/cas/cdeser/Docs/deser.internal_variab.climdyn10.pdf (accessed 27 March, 2013).
- Deutsch, C., Brix, H., Ito, T., Frenzel, H., and Thompson, L. 2011. Climate-forced variability of ocean hypoxia. *Science*. 333: 336-339. doi:10.1126/science.1202422.
- Di Lorenzo, E., Foreman, M.G.G., and Crawford, W.R. 2005. Modelling the generation of Haida Eddies. *Deep-Sea Res. II*. 52: 853-873.
- Di Lorenzo, E., Fiechter, J., Schneider, N., Bracco, A., Miller, A.J., Franks, P.J.S., Bograd, S.J., Moore, A.M., Thomas, A.C., Crawford, W., Peña, A., and Hermann, A.J. 2009. Nutrient and salinity decadal variations in the central and eastern North Pacific. *Geophys. Res. Lett.* 36. doi:10.1029/2009GL038261.
- Dickson, A.G., Sabine, C.L., and Christian, J.R. 2007. Guide to best practices for ocean CO₂ measurements. PICES Special publication 3.
- Dodimead, A.J., Favorite F., and Hirano, T. 1963. Salmon of the North Pacific Ocean: Part II. Review of oceanography of the subarctic Pacific region. *Int. N. Pacific Fisheries Commission Bulletin* 13, Vancouver B.C. 195 pp.
- Dufresne, J-L., Foujols, M-A., Denvil, S., Caubel, A., Marti, O., Aumont, O., Balkanski, Y., Bekki, S., Bellenger, H., Benshila, R., Bony, S., Bopp, L., Braconnot, P., Brockmann, P., Cadule, P., Cheruy, F., Codron, F., Cozic, A., Cugnet, D., de Noblet, N., Duvel, J.P., Ethé, C., Fairhead, L., Fichefet, T., Flavoni, S., Friedlingstein, P., Grandpeix, J.Y., Guez, L., Guilyardi, E., Hauglustaine, D., Hourdin, F., Idelkadi, A., Ghattas, J., Joussaume, S., Kageyama, M., Krinner, G., Labetoulle, S., Lahellec, A., Lefebvre, M.P., Lefevre, F., Levy, C., Li, Z.X., Lloyd, J., Lott, F., Madec, G., Mancip, M., Marchand, M., Masson, S., Meurdesoif, Y., Mignot, J., Musat, I., Parouty, S., Polcher, J., Rio, C., Schulz, M., Swingedouw, D., Szopa, S., Talandier, C., Terray, P., and Viovy, N. 2013. [Climate change projections using the IPSL-CM5 Earth System Model: from CMIP3 to CMIP5](#). *Climate Dyn.* Accepted. doi:10.1007/s00382-012-1636-1 (open access) [Manuscript](#).
- Dunne, J.P., John, J.G., Shevliakova, E., Stouffer, R.J., Krasting, J.P., Malyshev, S., Milly, P.C.D., Sentman, L.T., Adcroft, A., Cooke, W.F., Dunne, K.A., Griffies, S.M., Hallberg, R.W., Harrison, M.J., Levy II, H., Wittenberg, A.T., Philipps, P., and Zadeh, N. 2013. GFDL's ESM2 global coupled climate-carbon Earth System Models Part II: Carbon system formulation and baseline simulation characteristics. *J. Climate*. In press. doi:10.1175/JCLI-D-12-00150.1.
- Durack, P.J., and Wijffels, S.E. 2010. Fifty-year trends in global ocean salinities and their relationship to broad-scale warming. *J. Climate*. 23: 4342-4362. doi:10.1175/2010JCLI3377.1.
- Durack, P.J., Wijffels, S.E., and Matear, R.J. 2012. Ocean salinities reveal strong global water cycle intensification during 1950 to 2000. *Science*. 336: 455-458. doi:10.1126/science.1212222.
- Easterling, D.R., and Wehner, M.F. 2009. Is the climate warming or cooling? *Geophys. Res. Lett.* 36. doi:10.1029/2009GL037810.
- Evans, W., Hales, B., Strutton, P.G., and Ianson, D. 2012. Sea-air CO₂ fluxes in the western Canadian coastal ocean. *Prog. Oceanogr.* 101: 78–91. doi:10.1016/j.pocean.2012.01.003.

- Falkowski, P.G., Algeo, T., Codispoti, L., Deutsch, C., Emerson, S., Hales, B., Huey, R.B., Jenkins, W.J., Kump, L.R., Levin, L.A., Lyons, T.W., Nelson, N.B., Schofield, O.S., Summons, R., Talley, L.D., Thomas, E., Whitney, F., and Pilcher, C.B. 2011. Ocean deoxygenation: Past, present, and future. *EOS*. 92: 409–410.
- Faucher, M., Burrows, W.R., and Pandolfo, L. 1999. Empirical-statistical reconstruction of surface marine winds along the western coast of Canada. *Clim. Res.* 11: 173-190.
- Feely, R.A., Sabine, C.L., Lee, K., Berelson, W., Kleypas, J., Fabry, V.J., and Millero, F.J. 2004. Impact of anthropogenic CO₂ on the CaCO₃ system in the oceans. *Science*. 305: 362-366. doi: 10.1126/science.1097329.
- Feely, R.A., Sabine, C.L., Hernandez-Ayon, J.M., Ianson, D., and Hales, B. 2008. Evidence for upwelling of corrosive 'acidified' water onto the continental shelf. *Science*. 320: 1490-1492. doi: 10.1126/science.1155676.
- Flato, G.M., Boer, G.J., Lee, W.G., McFarlane, N.A., Ramsden, D., Reader, M.C., and Weaver, A.J. 2000. The Canadian Centre for Climate Modelling and Analysis global coupled model and its climate. *Climate Dyn.* 16: 451-467.
- Foreman, M.G.G., Callendar, W., MacFadyen, A., Hickey, B.M., Thomson, R.E., and Di Lorenzo, E. 2008. Modeling the generation of the Juan de Fuca Eddy. *J. Geophys. Res.* 113. doi:10.1029/2006JC004082.
- Foreman, M.G.G., Cherniawsky, J.Y., and Ballantyne, V.A. 2009. Versatile harmonic tidal analysis: improvements and applications. *J. Atmos. Oceanic Technol.* 26: 806–817.
- Foreman, M.G.G., Pal, B., and Merryfield, W.J. 2011. Trends in upwelling and downwelling winds along the British Columbia shelf. *J. Geophys. Res.* 116. doi:10.1029/2011JC006995
- Freeland, H.J. 1990. Sea surface temperatures along the coast of British Columbia: regional evidence for a warming trend. *Can. J. Fish. Aquat. Sci.* 47: 346-350.
- Freeland, H.J. 2006. What proportion of the North Pacific Current finds its way into the Gulf of Alaska? *Atmos. Ocean*. 44: 321-330.
- Freeland, H.J. 2013. Evidence of changes in winter mixed layer in the northeast Pacific Ocean: A problem revisited. *Atmos. Ocean*. 51: 126-133.
- Freeland, H.J., and Denman, K.L. 1982. A topographically controlled upwelling center of southern Vancouver Island. *J. Mar. Res.* 40: 1069-1093.
- Freeland, H.J., Crawford, W.R., and Thomson, R.E. 1984. Currents along the Pacific coast of Canada. *Atmos. Ocean*. 22: 151-172.
- Freeland, H.J., Denman, K., Wong, C.S., Whitney, F., and Jacques, R. 1997. Evidence of change in the winter mixed layer in the Northeast Pacific Ocean. *Deep-Sea Res.* 44: 2117-2129.

- Gill, A.E. 1982. Atmosphere-Ocean Dynamics. Academic Press, Orlando. 662 p.
- Gillett, N.P., Zwiers, F.W., Weaver, A.J., and Stott, P.A. 2003. Detection of human influence on sea-level pressure. *Nature*. 422: 292-294.
- Graham, N.E., and Diaz, H.F. 2001. Evidence for intensification of North Pacific winter cyclones since 1948. *Bull. Amer. Meteor. Soc.* 82: 1869-1893.
- Grantham, B.A., Chan, F., Nielsen, K.J., Fox, D.S., Barth, J.A., Huyer, A., Lubchenco, J., and Menge, B.A. 2004. Upwelling-driven nearshore hypoxia signals ecosystem and oceanographic changes in the northeast Pacific. *Nature*. 429: 749-754. doi:10.1038/nature02605.
- Hales, B., Gruber, N., Ianson, D., Chavez, F., and Hernandez-Ayon, J.M. 2008. North America's Pacific Coast. *In* North American Continental Margins: A Synthesis and Planning Workshop. Edited by Hales, B., Cai, W.-J., Mitchell, B.G., Sabine, C.L. and Schofield, O. Report of the North American Continental Margins Working Group for the U.S. Carbon Cycle Scientific Steering Group and Interagency Working Group. U.S. Carbon Cycle Science Program, Washington, DC, 110 pp.
- Hansen, D.V., and Rattray Jr., M. 1966. New dimension in estuary classification. *Limnol. Oceanog.* 11: 319-326.
- Hara, M., Yoshikane, T., Kawase, H., and Kimura, F. 2008. Estimation of the impact of global warming on snow depth in Japan by the pseudo-global-warming method. *Hydrological Research Letters*. 2: 61-64.
- Hickey, B.M. 1979. The California Current system - Hypotheses and facts. *Prog. Oceanogr.* 8: 191-279.
- Hickey, B., Thomson, R.E., Yih H., and LeBlond, P.H. 1991. Velocity and temperature fluctuations in a buoyancy-driven current off Vancouver Island. *J. Geophys. Res.* 96: 10507-10538.
- Hsieh, W.W., Ware, D.M., and Thomson, R.E. 1995. Wind-induced upwelling along the west coast of North America, 1899-1988. *Can., J. Fish. Aquat. Sci.* 52: 325-334.
- Hyndman, R.D., Currie, C., and Mazzotti, S. 2005. Subduction zone backarcs, mobile belts, and orogenic heat. *GSA Today*. 15. doi:10.1130/1052-5173.
- Ianson, D., and Allen, S.E. 2002. A two-dimensional nitrogen and carbon flux model in a coastal upwelling region. *Global Biogeochem. Cycles*. 16. 10.1029/2001GB001451, 2002.
- Ianson, D., Harris, S., Allen, S.E., Orians, K., Varela, D., and Wong, C.S. 2003. The inorganic carbon system in the coastal upwelling region west of Vancouver Island, Canada. *Deep Sea Res. I*. 50: 1023-1042.
- Ianson, D., Feely, R.A., Sabine, C.L., and Juranek, L. 2009. Features of coastal upwelling regions that determine net air-sea CO₂ flux. *J. Oceanography*. 65: 677-687.
- IPCC 2007. Climate Change 2007: The Physical Science Basis. Contribution of Working Group I to the Fourth Assessment Report of the Intergovernmental Panel on Climate Change. Edited by Solomon, S., Qin, D., Manning, M., Chen, Z., Marquis, M., Averyt, K.B., Tignor, M. and Miller, H.L. Cambridge University Press, Cambridge, United Kingdom and New York, NY, USA. 996 p.

- James, T., Gowan, E.J., Wada, I., and Wang, K. 2009. Viscosity of the asthenosphere from glacial isostatic adjustment and subduction dynamics at the northern Cascadia subduction zone, British Columbia, Canada. *J. Geophys. Res.* 114. doi:10.1029/2008JB006077.
- Jamieson, G.S. 1985. Dungeness crab, *Cancer magister*, fisheries of British Columbia. Alaska Sea Grant report 85-3. Alaska Sea Grant College Program, Fairbanks, Alaska, pp. 37-60.
- Jevrejeva, S., Moore, J.C., and Grinsted, A. 2010. How will sea level respond to changes in natural and anthropogenic forcing by 2100? *Geophys. Res. Lett.* 37. doi:10.1029/2010GL042947.
- Jevrejeva, S., Moore, J.C., and Grinsted, A. 2012. Sea level projections to AD2500 with a new generation of climate change scenarios. *Global and Planetary Change.* 80-81: 14-20.
- Johns T.C., Carnell, R.E., Crossley, J.F., Gregory, J.M., Michell, J.F.B., Senior, C.A., Teff, S.F.B., and Wood, R.A. 1997. The second Hadley Centre coupled Ocean-atmosphere GCM: model description, spinup and validation. *Climate Dyn.* 13: 103-134.
- Johnson, W.K., Miller, L.A., Sutherland, N.E., and Wong, C.S. 2005. Iron transport by mesoscale Haida eddies in the Gulf of Alaska. *Deep-Sea Res. II.* 52: 933-953.
- Kangasniemi, B. 2009. Climate Change Impacts for the Coastal BC. Available from http://www.corp.delta.bc.ca/assets/CPD/PDF/public_forum_presentation_moe.pdf [accessed 20 November 2012].
- Kara, A.B., Rochford, P.A., and Hurlburt, H.E. 2000. An optimal definition for ocean mixed layer depth. *J. Geophys. Res.* 105: 16,803–16,821.
- Keeling, R.F., Kortzinger, A., and Gruber, N. 2010. Ocean deoxygenation in a warming world. *Annu. Rev. Mar. Sci.* 2: 199–229.
- Kelly, M.W., and Hoffmann, G.E. 2012. Adaptation and the physiology of ocean acidification. *Functional Ecology.* doi:10.1111/j.1365-2435.2012.02061.x .
- Kim, D.-H., Woo, S.-B., and Lim, C.-W. 2011. Investigation on steric and nonsteric effect on sea level rise projections of the Northwestern Pacific Ocean. *In* Development and Application of Regional Climate Models, Oct 11-12, Seoul, Korea.
- Kimura, F., and Kitoh, A. 2007. Downscaling by pseudo global warming method. *In* The Final Report of the ICCAP. Research Institute for Humanity and Nature (RIHN), Kyoto, Japan.
- King, J.R., Agostini V.N., Harvey, C.J., McFarlane, G.A., Foreman, M.G.G., Overland, J.E., Di Lorenzo, E., Bond, N.A., and Aydin, K.Y. 2011. Climate Forcing and the California Current Ecosystem. *ICES J. Marine Science.* 68: 1199-1216.
- Koslow, J.A., Goericke, R., Lara-Lopez, A., and Watson, W. 2011. Impact of declining intermediate-water oxygen on deepwater fishes in the California Current. *Mar. Ecol. Prog. Ser.* 436: 207–218.
- Ladd, C., and Stabeno, P.J. 2012. Stratification on the eastern Bering Sea shelf revisited. *Deep-Sea Res. II.* 65-70: 72-83. doi:10.1016/j.dsr2.2012.02.009.

- LeBlond, P.H. 1983. The Strait of Georgia: functional anatomy of a coastal sea. *Can. J. Aquat. Sci.* 40: 1033-1063.
- Lentz, S.J. 1992. The surface boundary layer in coastal upwelling regions. *J. Phys. Oceanogr.* 22: 1517-1539.
- Lentz, S.J., and Chapman, D.C. 2004. The importance of nonlinear cross-shelf momentum flux during wind-driven coastal upwelling. *J. Phys. Oceanogr.* 34: 2444-2457.
- LeQuéré, C., Takahashi, T., Buitenhuis, E.T., Rodenbeck, C., and Sutherland, S.C. 2010. Impact of climate change and variability on the global oceanic sink of CO₂. *Global Biogeochem. Cycles*. 24: GB4007. doi:10.1029/2009GB003599.
- Li, M., Myers, P.G., and Freeland, H. 2005. An examination of historical mixed layer depths along Line-P in the Gulf of Alaska. *Geoph. Res. Lett.* 32. doi:10.1029/2004GL021911.
- MacFadyen, A., and Hickey, B.M. 2010. Generation and evolution of a topographically linked, mesoscale eddy under steady and variable wind-forcing. *Cont. Shelf Res.* 30: 1387-1402.
- Mantua, N.J., Hare, S.R. Zhang, Y., Wallace, J.M., and Francis, R.C. 1997. A Pacific interdecadal climate oscillation with impacts on salmon production. *Bull. Amer. Meteor. Soc.* 78: 1069-1079.
- Martin, J., and Fitzwater, S. 1988. Iron deficiency limits phytoplankton growth in the north-east Pacific subarctic. *Nature*. 331: 341-343.
- Martin, G.M., and the HadGEM2 Development Team. 2011. The HadGEM2 family of Met Office Unified Model climate configurations. *Geosci. Model Dev.* 4: 723-757.
- Masson, D. 2006. Seasonal water mass analysis for the Straits of Juan de Fuca and Georgia. *Atmos. Ocean*. 44: 1-15.
- Masson, D., and Cummins, P.F. 2007. Temperature trends and interannual variability in the Strait of Georgia, British Columbia. *Continental Shelf Res.* 27: 634-649.
- Masson, D., and Fine, I. 2013. Modeling seasonal to inter-annual ocean variability of coastal British Columbia. *J. Geophys. Res.* 117. doi:10.1029/2012JC008151.
- Mazzotti, S., Lambert, A., Van der Kooij, M., and Mainville, A. 2008a. Natural and anthropogenic subsidence of the Fraser River Delta. *Geology*. 37: 771-774. doi:10.1030/G25640A.1.
- Mazzotti, S., Jones, C., and Thomson, R.E. 2008b. Relative and absolute sea level rise in western Canada and northwestern United states from a combined tide gauge-GPS analysis. *J. Geophys. Res.* 113. doi:10.1029/2008JC004835.
- Meehl, G.A., Stocker, T.F., Collins, W.D., Friedlingstein, P., Gaye, A.T., Gregory, J.M., Kitoh, A., Knutti, R., Murphy, J.M., Noda, A., Raper, S.C.B., Watterson, I.G., Weaver, A.J., and Zhao, Z.-C. 2007: Global Climate Projections. *In* *Climate Change 2007: The Physical Science Basis*. Contribution of Working Group I to the Fourth Assessment Report of the Intergovernmental Panel on Climate Change. Edited by Solomon, S., Qin, D., Manning, M., Chen, Z., Marquis, M., Averyt, K.B., Tignor, M. and Miller, H.L. Cambridge University Press, Cambridge, United Kingdom and New York, NY, USA.

- Merryfield, W.J., Pal, B., and Foreman, M.G.G. 2009. Projected future changes in surface marine winds off the west coast of Canada. *J. Geophys. Res.* 114. doi:10.1029/2008JC005123.
- Mesinger, F., DiMego, G., Kalnay, E., Mitchell, K., Shafran, P.C., Ebisuzaki, W., Jovic, D., Wollen, J., Rogers, E., Berbery, E.H., Ek, M.B., Fan, Y., Grumbine, R., Higgins, W., Ki, H., Lin, Y., Mankin, G., Parrish, D., and Shi, W. 2006. North American Regional Reanalysis. *Bull. Amer. Meteor. Soc.* 87: 343-360.
- Mitrovica, J.X., Tamisiea, M.E., Davis, J.L., and Milne, G.A. 2001. Recent mass balance of polar ice sheets inferred from patterns of global sea-level change. *Nature*. 409: 1026-1029.
- Morrison, J., Quick, M.C., and Foreman, M.G.G. 2002. Climate change in the Fraser watershed: Flow and temperature predictions. *J. Hydrology*. 263: 230-244.
- Morrison, J., Foreman, M.G.G., and Masson, D. 2011. A method for estimating monthly freshwater discharge affecting British Columbia coastal waters. *Atmos. Ocean*. 50: 1-8. doi:10.1080/07055900.2011.637667.
- Moss, R.H., Edmonds, J.A., Hibbard, K.A., Manning, M.R., Rose, S.K., van Vuuren, D.P., Carter, T.R., Emori, S., Kainuma, M., Kram, T., Meehl, G.A., Mitchell, J.F.B., Nakicenovic, N., Riahi, K., Smith, S.J., Stouffer, R.J., Thomson, A.M., Weyant, J.P., and Wilbanks, T.J. 2010. The next generation of scenarios for climate change research and assessment. *Nature*. 463: 747-756.
- Mucci, A. 1983. The solubility of calcite and aragonite in seawater at various salinities, temperatures and one atmosphere total pressure. *Am. J. Sci.* 238: 780-799.
- Nemcek, N., Ianson, D., and Tortell, P.D. 2008. A high-resolution survey of DMS, CO₂ and O₂/Ar distributions in productive coastal waters. *Global Biogeochem. Cycles*. 22. doi:10.1029/2006GB002879.
- Ono, T., Shiimoto, A., and Saino, T. 2008. Recent decrease of summer nutrients concentrations and future possible shrinkage of the subarctic North Pacific high-nutrient low-chlorophyll region. *Global Biogeochem. Cycles*. 22. doi:10.1029/2007GB003092.
- Orr, J.C., Fabry, V.J., Aumont, O., Bopp, L., Doney, S.C., Feely, R.A., Gnanadesikan, A., Gruber, N., Ishida, A., Joos, F., Key, R.M., Lindsay, K., Maier-Reimer, E., Matear, R., Monfray, P., Mouchet, A., Najjar, R.G., Plattner, G.-K., Rodgers, K.B., Sabine, C.L., Sarmiento, J.L., Schlitzer, R., Slater, R.D., Totterdell, I.J., Weirig, M.-F., Yamanaka, Y., and Yool, A. 2005. Anthropogenic ocean acidification over the twenty-first century and its impact on calcifying organisms. *Nature*. 437: 681–686. doi 10.1038/nature04095.
- Overland, J.E. and Wang, M. 2007. Future climate of the North Pacific Ocean. *EOS*. 88: 178-182.
- Peña, M.A., and Varela, D.E. 2007. Seasonal and interannual variability in phytoplankton and nutrient dynamics along Line P in the NE subarctic Pacific. *Prog. Oceanogr.* 75: 200-222.
- Pierce, S.D., Barth, J.A., Shearman, R.K., and Erofeev, A.Y. 2012. Declining Oxygen in the Northeast Pacific. *J. Phys. Oceanogr.* 42: 495-501.
- Press, W.H., Teukolsky, S.A., Vetterling, W.T., and Flannery, B.P. 1992: Numerical Recipes in Fortran. 2nd Ed. Cambridge University Press. 963 pp.

- Rahmstorf, S. 2010. A new view on sea level rise. *Nature Reports Climate Change*. doi:1038/climate.2010.29.
- Rahmstorf, S. 2012. Sea-level rise: towards understanding local vulnerability. *Environmental Research Letters*. 7. doi:10.1088/1748-9326/7/2/021001.
- Redfield, A.C., and Goodkind, R. 1929. The significance of the Bohr effect on the respiration and asphyxiation of the squid, *Loligo pealei*. *J. Exp. Biol.* 6: 340-349.
- Revelle, R., and Suess, H.E. 1957. Carbon dioxide exchange between atmosphere and ocean and the question of an increase of atmospheric CO₂ during the past decades. *Tellus*. 9: 18-27.
- Riva, R.E.M., Bamber, J.L., Lavallée, D.A., and Wouters, B. 2010. Sea-level fingerprint of continental water and ice mass change from GRACE. *Geophys. Res. Lett.* 37. doi:10.1029/2010GL044770.
- Salathé Jr., E.P. 2006. Influences of a shift in North Pacific storm tracks on western North American precipitation under global warming. *Geophys. Res. Lett.* 33. doi:10.1029/2006GL026882.
- Sato, T., Kimura, F., and Kitoh, K. 2007. Projection of global warming onto regional precipitation over Mongolia using a regional climate model. *J. Hydrol.* 333: 144-154.
- Schär, C., Frei, C. Lüthi, D., and Davies, H.C. 1996. Surrogate climate-change scenarios for regional climate models. *Geophys. Res. Lett.* 23: 669-672.
- Schwing, F.B., Bond, N.A., Bograd, S.J., Mitchell, T., Alexander, M.A., and Mantua, N. 2006. Delayed coastal upwelling along the U.S. West Coast in 2005: A historical perspective. *Geophys. Res. Lett.* 33. doi:10/1029/2006GL026911.
- Scientific Committee on Antarctic Research. 2009. Antarctic Climate Change and the Environment. International Council of Scientific Unions, Scott Polar Research Institute, Cambridge. 555 p.
- Smith, R.L. 1995. The physical processes of coastal ocean upwelling systems. *In Upwelling in the ocean: Modern processes and ancient records*. Edited by Summerhayes, C. P., Emeis, K.-C., Angel, M.V., Smith, R.L. and Zeitzschel, B. Wiley and Sons Ltd, New York. pp 39-64.
- Taylor, K.E. 2001. Summarizing multiple aspects of model performance in a single diagram. *J. Geophys. Res.* 106: 7183–7192.
- Taylor, K.E., Stouffer, R.J., and Meehl, G.A. 2012. An Overview of CMIP5 and the experiment design. *Bull. Am. Meteorol. Soc.* 93: 485-498.
- Tebaldi, C., Strauss, B.H., and Zervas, C.E. 2012. Modelling sea level rise impacts on storm surges along US coasts. *Environ. Res. Lett.* 7. doi:10.1088/1748-9326/7/1/014032.
- Thomson, R.E. 1981. Oceanography of the British Columbia Coast. Canadian Special Publication of Fisheries and Aquatic Sciences 56. Department of Fisheries and Oceans, Ottawa. 291 p.
- Thomson, R.E., and Tabata, S. 1989. Steric sea level trends in the Northeast Pacific Ocean: Possible evidence of global sea level rise. *J. Climate*. 2: 542-553.

- Thomson, R.E., and Ware, D. 1996. A current velocity index of ocean variability. *J. Geophys. Res.* 101: 14297-14310.
- Thomson, R.E., and Gower, J.F.R. 1998. A basin-scale oceanic instability event in the Gulf of Alaska. *J. Geophys. Res.* 103: 3033-3040.
- Thomson, R.E., and Fine, I.V. 2003. Estimating mixed layer depth from oceanic profile data. *J. Atmos. Oceanic. Technol.* 20: 319-329.
- Thomson, R.E., and Krassovski, M.V. 2010. Poleward reach of the California Undercurrent extension. *J. Geophys. Res.* 115. doi:10.1029/2010JC006280.
- Thomson, R.E., Hickey, B.M., and LeBlond, P.H. 1989. The Vancouver Island Coastal Current: Fisheries barrier and conduit. *In* Effects of ocean variability on recruitment and an evaluation of parameters used in stock assessment models. Edited by Beamish, R. and McFarlane, G. Special Publication of Fisheries and Aquatic Sciences 108. pp.265-296.
- Thomson, R.E., Mihaly, S.F., and Kulikov, E.A. 2007. Estuarine versus transient flow regimes in Juan de Fuca Strait. *J. Geophys. Res.* 112. doi:10.1029/2006JC003925.
- Thomson, R.E., Bornhold, B.D., and Mazzotti, S. 2008. An examination of the factors affecting relative and absolute sea level in coastal British Columbia. *Can. Tech. Rep. Hydrogr.Ocean Sci.* 260: v + 49 p.
- Timmermann, A., Oberhuber, J., Bacher, A., Esch, M., Latif, M., and Roeckner, E. 1999. Increased El Niño frequency in a climate model forced by future greenhouse warming. *Nature.* 398: 694-697.
- Tortell, P.D., Merzouk, A., Ianson, D., Pawlowicz, R., and Yelland, D.R. 2012. Influence of regional climate forcing on surface water pCO₂, ΔO₂/Ar and dimethylsulfide (DMS) along the southern British Columbia coast. *Continental Shelf Research.* 47: 119-132. doi:10.1016/j.csr.2012.07.007 .
- Trenberth, K.E., and Hurrell, J.W. 1995. Decadal coupled atmospheric-ocean variations in the North Pacific Ocean. *In* Climate Change and Northern Fish Populations. Edited by R.J. Beamish. Canadian Special Publication Fisheries Aquatic Sciences.121: 15-24.
- U.S. Army Corps of Engineers. 2011. Sea-level change considerations for civil works programs. CECW-CE Circular No. 1165-2-212.
- U.S. National Research Council. 2012. Sea-level Rise for the Coasts of California, Oregon and Washington: Past, Present and Future. Committee on Sea Level Rise in California, Oregon and Washington; Board on Earth Sciences and Resources, National Research Council.
- Vecchi, G.A., and Wittenberg, A.T. 2010. El Niño and our future climate: where do we stand? *WIREs Clim. Change* 1: 260-270.
- Vellinga, P., Katsman, C.A., Sterl, A., Beersma, J.J., Hazeleger, W., Church, J., Kopp, R., Kroon, D., Oppenheimer, M., Plag, H.-P., Rahmstorf, S., Lowe, J., Ridley, J., von Storch, H., Vaughn, D., van de Wal, R., Weisse, R., Kwadijk, J., Lammersen, R., and Marinova, N. 2009. Exploring high-end climate scenarios for flood protection of the Netherlands. International Scientific Assessment carried out at the Request of the Delta Committee, De Bilt, The Netherlands.

- Von Storch, H., and Zwiers, F.W. 1999. Statistical analysis in climate research. Cambridge University Press, Cambridge, U.K. 21 p.
- Wada, Y., van Beek, L.P.H., Sperna Weiland, F.C., Chao, B.F., Wu, Y.-H., and Bierkens, M.F.P. 2012. Past and future contribution of global groundwater depletion to sea-level rise. *Geophys. Res. Lett.* 39. doi:10.1029/2012GL051230.
- Walker, I.J., Barrie, J.V., Dolan, A.H., Gedalof, Z., Manson, G. Smith, D., and Wolfe, S. 2007. Coastal Vulnerability to Climate Change and Sea-Level Rise, Northeast Graham Island, Haida Gwaii (Queen Charlotte Islands), British Columbia. Canada. Climate Impacts and Adaptations Program, Final Report Project A580.
- Ware, D.M., and Thomson, R.E. 2005. Bottom-up ecosystem trophic dynamics determine fish production in the northeast Pacific. *Science*. 308: 1280-1284.
- Watanabe, S., Hajima, T., Sudo, K., Nagashima, T., Takemura, T., Okajima, H., Nozawa, T., Kawase, H., Abe, M., Yokohata, T., Ise, T., Sato, H., Kato, E., Takata, K., Emori, S., and Kawamiya, M. 2011. MIROC-ESM 2010: model description and basic results of CMIP5-20c3m experiments. *Geosci. Model Dev.* 4: 845–872.
- Whitney, F.A. 2011. Nutrient variability in the mixed layer of the subarctic Pacific Ocean, 1987-2010. *J. Oceanogr.* 67: 481-492.
- Whitney, F., and Robert, M. 2002. Structure of Haida Eddies and their transport of nutrient from coastal margins into the NE Pacific Ocean. *J. Oceanogr.* 58: 715–723.
- Whitney, F.A., Wong, C.S., and Boyd, P.W. 1998. Interannual variability in nitrate supply to surface waters of the Northeast Pacific Ocean. *Mar. Ecol. Prog. Ser.* 170: 15-23.
- Whitney, F.A., Crawford, W.R., and Harrison, P.J. 2005. Physical processes that enhance nutrient transport and primary productivity in the coastal and open ocean of the subarctic NE Pacific. *Deep-Sea Res. II.* 52: 681-706.
- Whitney, F.A., Freeland, H.J., and Robert, M. 2007. Persistently declining oxygen levels in the interior waters of the eastern subarctic Pacific. *Prog. Oceanogr.* 75: 179–199. doi:10.1016/j.pocean.2007.08.007.
- Wong, C.S., Christian, J.R., Wong, S.-K.E., Page, J., Xie, L., and Johannessen, S. 2010. Carbon dioxide in surface seawater of the eastern North Pacific Ocean (Line P), 1973-2005. *Deep Sea Res. I.* 57: 687-695.
- Yin, J.H. 2005. A consistent poleward shift of the storm tracks in simulations of 21st century climate. *Geophys. Res. Lett.* 32. doi:10.1029/2005GL023684.
- Zachos, J.C., Röhl, U., Shellenberg, S.A., Sluijs, A., Hodell, D.A., Kelly, D.C., Thomas, E., Nicolo, M., Raffi, I., Lourens, L.J., McCarren, H., and Kroon, D. 2005. Rapid acidification of the ocean during the Paleocene-Eocene Thermal Maximum. *Science*. 308: 1611-1615.